# PRE-CRASH EXTRACTION OF THE CONSTELLATION OF A FRONTAL COLLISION BETWEEN TWO MOTOR VEHICLES

THOMAS KUEHBECK

A thesis submitted in partial fulfilment of the requirement of Staffordshire University for the degree of Doctor of Philosophy

In collaboration with BMW AG

September 2017

# Acknowledgements

This thesis was made possible with the help of many people. I am grateful to all of them.

First and foremost, I am grateful to Prof. Claude Chibelushi for his support and guidance throughout the years I worked on my thesis. Also, special thanks to Prof. Mansour Moniri for his valuable advice and encouragement.

It was a pleasure to work with the team of the Department of Vehicle Safety of the BMW Group. There I conducted research for my thesis.

I am grateful to Prof. Klaus Kompass who encouraged me by expressing confidence in my abilities and who gave me the possibility to research freely. His critiques were immensely valuable.

I am grateful to my colleagues Dr. Thomas Helmer and Dr. Michael Neubauer who shared their expertise with me. They also provided excellent working conditions and unending support.

I am grateful to Bernhard Seidl, Dr. Daniel Schwarz and Gor Hakobyan, their assistance was greatly appreciated.

I am grateful to have had Prof. Werner Huber as my supervisor at BMW. His wisdom and encouragement were invaluable. I am honoured to have had the opportunity to have worked with and for him.

I am particularly grateful to several friends who stood by me and who put up with my changing moods and emotional ups and downs and still remained friends. They are Xaver, Martin, Josef and Alex.

I am grateful to my parents Walter and Marianne who believed in me from the very beginning. Thanks also to my brother Bernhard and his wife Altai who contributed to my well-being.

Last but not least, I am grateful to Steffi who was always able to understand and motivate me; it would have been so much more difficult to reach my goal without her backing.

# Contents

# Abstract

One of the strategic objectives of the European Commission is to halve the number of road traffic fatalities by 2020. In addition, in 2010, the United Nations General Assembly initiated the "Decade of Action for Road Safety 2011-2020" to reduce the number of fatalities and decrease the number of road traffic injuries.

To address the scourge of road traffic accidents, this thesis presents a research study which has devised and evaluated a novel algorithm for extracting the constellation of an unavoidable frontal vehicle-to-vehicle accident. The primary research questions addressed in this work are:

- What are the most significant collision parameters which influence the injury severity for a frontal collision between two motor vehicles?
- How to extract the constellation of a crash before the accident occurs?

In addition, the secondary research questions given below were addressed:

- How to integrate physical constraints, imposed on the rate of acceleration of a real vehicle, together with data from vehicle-to-vehicle (V2V) communication, into the crash constellation extraction algorithm?
- How to integrate uncertainties, associated with the data captured by sensors of a real vehicle, into a simulation model devised for assessing the performance of crash constellation extraction algorithms?

Statistical analysis, conducted to determine significant collision parameters, has identified three significant crash constellation parameters: the point of collision on the vehicle body and the relative velocity between the vehicles; and the vehicle alignment offset (or vehicle overlap). The research reported in this thesis has also produced a novel algorithm for analysing the data captured by vehicle sensors, to extract the constellation of an unavoidable vehicle-to-vehicle frontal accident. The algorithm includes a model of physical constraints on the acceleration of a vehicle, cast as a gradual rise and eventual saturation of vehicle acceleration, together with the acceleration lag relative to the timing of information received from V2V communication. In addition, the research has delivered a simulation model to support the

evaluation of the performance of crash constellation extraction algorithms, including a technique for integrating (into the simulation model, so that the simulation can approach real-world behaviour) the uncertainties associated with the data captured by the sensors of a real vehicle.

The results of the assessment of the soundness of the simulation model show that the model produces the expected level of estimation errors, when simulation data is considered on its own or when it is compared to data from tests performed with a real vehicle.

Simulation experiments, for the performance evaluation of the crash constellation extraction algorithm, show that the uncertainty associated with the estimated time-to-collision decreases as vehicle velocity increases or as the actual time-to-collision decreases. The results also show that a decreasing time-to-collision leads to a decreasing uncertainty associated with the estimated position of the tracked vehicle, the estimated collision point on the ego vehicle, and the estimated relative velocity between the two vehicles about to collide. The results of the performance assessment of the crash constellation extraction algorithm also show that V2V information has a beneficial influence on the precision of the constellation extraction, with regards to the predicted time-to-collision, the predicted position and velocity of the oncoming vehicle against which a collision is possible; the predicted relative velocity between the two vehicles about to collide, and the predicted point of collision on the body of the ego vehicle.

It is envisaged that the techniques, developed in the research reported in this thesis, will be used in future integrated safety systems for motor vehicles. They could then strongly impact passenger safety by enabling optimal activation of safety measures to protect the vehicle occupants, as determined from the estimated constellation of the impending crash.

# Notation

## Abbreviations

| | |
|---|---|
| 2D | Two-dimensional |
| 3D | Three-dimensional |
| ABS | Antilock Brake System |
| ACC | Adaptive/Active Cruise Control |
| ACC S&G | Adaptive/Active Cruise Control Stop and Go |
| ADAS | Advanced Driver Assistance Systems |
| AHC | Automated Headlight Control |
| AHS | Automated Highway System |
| ALC | Automatic Level Control |
| ASC | Automatic Stability Control |
| BA | Brake Assist |
| C2C | Car-to-Car |
| CA | Collision Avoidance |
| CA | Constant acceleration |
| CCD | Charge coupled device |
| CMOS | Complementary metal oxide semiconductor |
| CV | Constant velocity |
| DSC | Dynamic Stability Control |
| DGPS | Differential Global Positioning System |
| EB | Emergency Brake |
| ESC | Electronic Stability Control |
| EKF | Extended Kalman filter |
| FMCW | Frequency-modulated continuous wave |
| FOV | Field of view |
| FSK | Frequency shift keying |
| GIDAS | German In-Depth Accident Studies |
| GPS | Global Positioning System |
| GT | Ground truth |
| GUI | Graphical User Interface |

| | |
|---|---|
| HC | Heading Control |
| HIL | Hardware-in-the-loop |
| HMI | Human Machine Interface |
| IBA | Intelligent Brake Assistant |
| ICS | Inevitable Collision State |
| IMF | Information Matrix Fusion |
| IR | Infrared |
| JPDA | Joint Probabilistic Data Association |
| LCA | Lane Change Assistant |
| LCW | Lane Change Warning |
| LDW | Lane Departure Warning |
| Lidar | LIght Detection And Ranging |
| MHT | Multiple-Hypothesis Testing |
| MTT | Multi-target tracking |
| NAVI | Navigation System |
| NN | Nearest Neighbor |
| NV | Night-Vision |
| OLC | Occupant Load Criterion |
| PA | Parking Assistant |
| PDC | Parking Distance Control |
| Radar | RAdio Detection And Ranging |
| SIL | Software-in-the-loop |
| TCS | Traction Control System |
| TTC | Time-to-collision |
| V2I | Vehicle-to-Infrastructure |
| V2V | Vehicle-to-Vehicle |
| V2X | Vehicle-to-X |

## Mathematical Notations

| | |
|---|---|
| $a$ | Scalar |
| $\boldsymbol{a}$ | Vector |
| $\boldsymbol{A}$ | Matrix |
| $\boldsymbol{A^T}$ | Transpose of matrix $\boldsymbol{A}$ |
| $\boldsymbol{A^{-1}}$ | Inverse of matrix $\boldsymbol{A}$ |

| | |
|---|---|
| $\boldsymbol{I}$ | Identity matrix |

## Latin Symbols

| | |
|---|---|
| $\boldsymbol{B}$ | Control-input model |
| $\boldsymbol{f}(.)$ | State transition function |
| $\boldsymbol{F}(.)$ | State transition matrix |
| $\boldsymbol{h}(.)$ | Measurement function |
| $\boldsymbol{H}$ | Measurement matrix |
| $\boldsymbol{J}$ | Jacobian |
| $k$ | Time instance |
| $\boldsymbol{K}$ | Kalman filter gain |
| $m$ | Dimension of the measurement vector |
| $m$ | Weight of a vehicle |
| $\boldsymbol{n}$ | Measurement noise |
| $P$ | Probability |
| $\boldsymbol{P}$ | Covariance matrix of the state |
| $\boldsymbol{Q}$ | Covariance matrix of the process noise |
| $\boldsymbol{Q}_d$ | Diagonal covariance matrix of the process noise |
| $\boldsymbol{R}$ | Rotation matrix |
| $\boldsymbol{R}$ | Measurement covariance matrix |
| $\boldsymbol{S}$ | Covariance matrix of the residual |
| $t$ | Time |
| $T$ | Time interval |
| $\boldsymbol{u}$ | Control-input vector |
| $v$ | Velocity |
| $v_x$ | x-component of the velocity vector |
| $v_y$ | y-component of the velocity vector |
| $\boldsymbol{w}$ | Process noise |
| $x$ | x-coordinate of a position in a Cartesian coordinate system |
| $\tilde{\boldsymbol{x}}$ | True state |
| $\hat{\boldsymbol{x}}$ | Estimated state |
| $y$ | y-coordinate of a position in a Cartesian coordinate system |
| $\tilde{\boldsymbol{y}}$ | Discrepancy between the measurement and prediction |
| $z$ | z-coordinate of a position in a Cartesian coordinate system |

| | |
|---|---|
| $\boldsymbol{z}$ | Measurement vector |

## Greek Symbols

| | |
|---|---|
| $\alpha$ | Azimuth angle |
| $\gamma$ | Angle in Kamm's circle defining a driving manoeuvre |
| $\boldsymbol{\Gamma}$ | Measurement gain matrix |
| $\theta$ | Pitch angle |
| $\mu$ | Mean value |
| $\mu_0$ | Static friction coefficient |
| $\sigma$ | Standard deviation |
| $\sigma^2$ | Variance |
| $\phi$ | Roll angle |
| $\psi$ | Yaw angle |

## Terminology

| | |
|---|---|
| Ego vehicle or host vehicle | A vehicle which is sensing its surrounding environment (which typically includes other vehicles) and activates driving manoeuvres or actions appropriate for the current or predicted driving situation. |
| Tracked vehicle or object vehicle | A vehicle which is tracked by the sensor system of the ego vehicle. |
| Vehicle state | The state of motion of a vehicle. |
| Tracked state | The state of motion of a tracked vehicle over time. |

# List of Figures

# List of Tables

# List of Algorithms

# 1 Introduction

## 1.1 Background and motivation

Mobility is the impulse of modern society. In Germany, the number of motor vehicles rose by a factor of 12.8 between 1954 and 2005, leading to an increasing combined mileage driven by all vehicles in Germany, as illustrated by Figure 1.1 (ADAC, 2008; Kunert et al., 2012). This increase resulted in a rise by a factor of 4.8 in the number of road accidents with badly injured people on German roadways. However, a decrease of 55% in the number of fatalities was observed during the same time period (Schamberger and Geduld, 2004; Schneider, 2006). That reduction is mainly to the credit of car manufacturers, as they steadily improved motor vehicle safety through the development of new protective features.

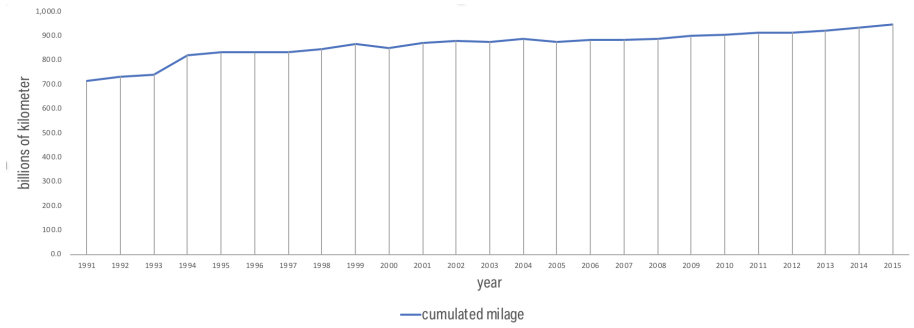


**Figure 1.1:** Cumulated mileage covered by motor vehicles in Germany (German Traffic Ministry, 2016)

According to the European Commission, road traffic accidents have become a major health problem, resulting in 1.5 million people injured in traffic accidents in 2010, in the European Union. The Commission's strategic objectives include halving the number of fatalities by 2020 (Figure 1.2) (European Commission, 2013).

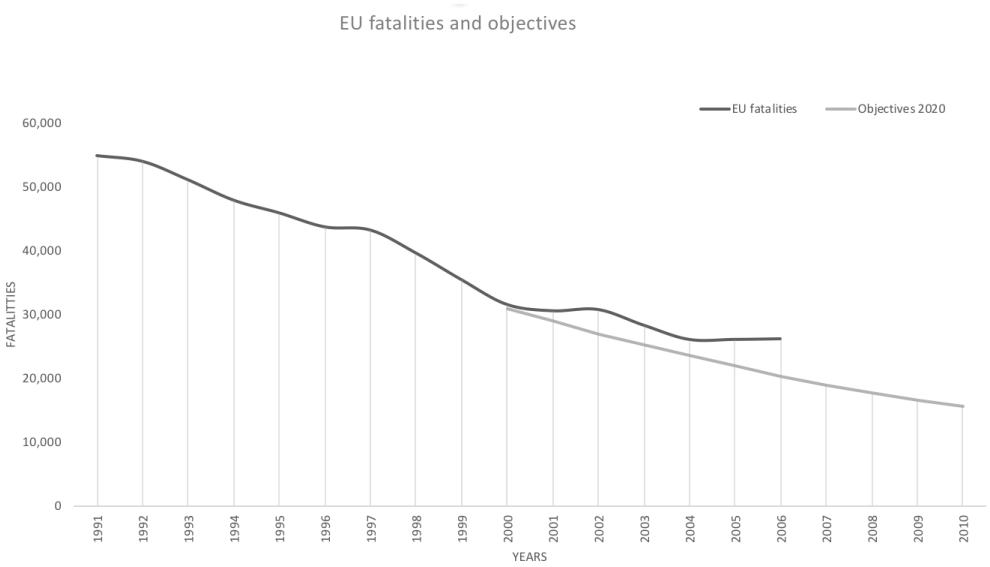


**Figure 1.2:** Road vehicle fatalities in the European Union, and extrapolation of the curve beyond 2016 to meet a key objective of the European Commission (European Commission, 2018)

The United Nations (UN) and the World Health Organization (WHO) also published a worrying statistic of nearly 1.3 million deaths caused each year by road traffic injuries, making accidents the leading cause of deaths for 15 to 29 year-old people in the world (Lozano et al., 2013). Immediate actions need to be taken to prevent the growing number of deaths from reaching, by 2030, the forecast figure of 2.4 million deaths worldwide each year (World Health Organisation, 2013). In 2010, the United Nations General Assembly initiated the "The Decade of Action for Road Safety 2011-2020" to reduce the number of fatalities and stabilize the increasing number of road traffic injuries (OECD, 2017; World Health Organisation, 2011; World Health Organization, 2017).

Analysis of the causes of today's traffic accidents can inform the development of future active safety systems. Figure 1.3 illustrates the most significant causes for road traffic accidents in 2012.

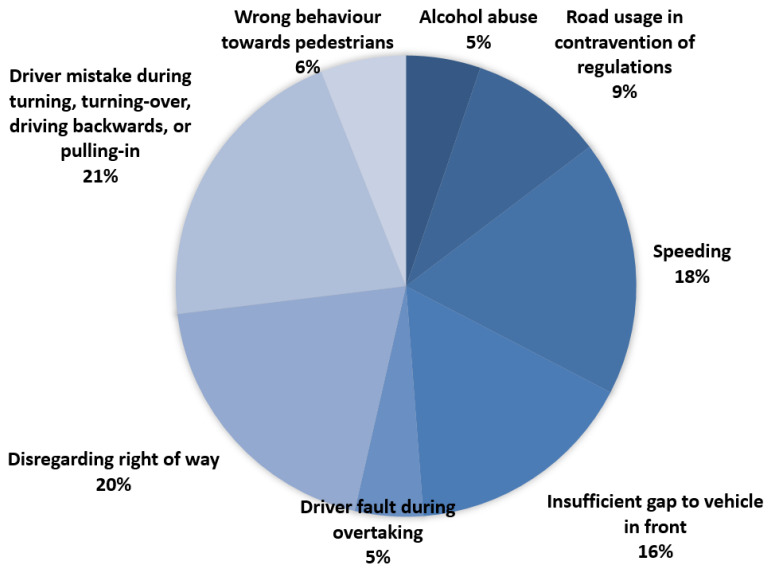


**Figure 1.3:** Traffic accidents categorised according to the type of human error (DeStatis, 2013)

The above mentioned errors have one fact in common: human error. Hence, advanced driver assistance systems (ADAS) are designed to (Ehmanns and Spannheimer, 2004; Neunzig, 2004)

- support the driver in critical situations
- take the complexity out of driving situations
- increase the comfort during drive time
- save fuel
- improve safety.

One of the first advanced driver assistance systems, the adaptive cruise control (ACC) introduced on the market in 1998, already supported the driver in their driving task. The system continuously controls the distance to the vehicle in front by interacting with the vehicle actuators (brakes and throttle). The radar sensors for the ACC enabled the first active safety systems by activating the brakes in critical situations.

As already mentioned, most accidents occur due to human error. Pre-crash safety systems assist the human driver in critical situations to avoid or mitigate a collision; they therefore act as life saving systems. The motivation for the doctoral

work presented in this thesis is to extract the crash constellation when a collision is inevitable, thus allowing safety systems to deploy more sophisticated counter measures tailored to the underlying crash constellation. The constellation of a collision can be described relation to different characteristics:

- Vehicle geometry properties, which can include for example the exact point of collision on the vehicle body or the impact angle between the vehicles.
- Applied safety measures to prepare the vehicle occupants ahead of an impending collision, namely airbags or belt pre-tensioner for example.
- Vehicle dynamics parameters, such as energies which prevail during the collision; including delta in velocities or absorbed energy, for example.

The research within this doctoral work is focused on the vehicle geometry parameters describing a collision which can be sensed before the collision occurs.

## 1.2 Aim and objectives

### 1.2.1 Aim

The aim of the doctoral work presented in this thesis is to produce novel techniques for extracting significant parameters of the constellation of an impending collision; these parameters can be used by a collision mitigation system. In this work, collision constellation is defined as a set of spatial and temporal parameters (e.g. velocity, alignment offset, point of collision etc.) describing the collision.

### 1.2.2 Objectives

To achieve the aim stated above, the objectives of this investigation are to

- conduct a systematic review of the state of the art in the areas of crash prediction and constellation extraction algorithms, automotive sensors, sensor data fusion, and trajectory planning.
- conduct statistical analyses on accident databases to identify the most significant crash parameters.

- define possible collision scenarios for the design, implementation, testing, and evaluation of the constellation extraction algorithm.
- devise a novel algorithm or combination of existing algorithms for extracting the constellation of a crash.
- conduct experiments to assess the devised constellation extraction algorithm.

## 1.3 Statement of the research questions

These days, passive safety measures activate based on the output of velocity sensors attached to the front bumper or elsewhere on the body of a motor vehicle; the sensors analyse the change in acceleration or deformation energy of the vehicle upon impact. This allows various passive safety measures to be fired, namely: airbags, active restraint systems, and more. However, the possibilities for the vehicle safety system to react pre-emptively to an impending collision are restricted by the limited foresight offered by these sensors. Firing countermeasures such as airbags requires a high guarantee of the timing of a crash, because a malfunction or incorrect activation can have a negative impact on the safety of the vehicle occupants.

Future active safety systems which act before a crash occurs, would be able to improve vehicle safety tremendously. In particular, knowing the crash constellation beforehand would enable the activation of active safety measures which are configured to match the crash severity corresponding to the specific constellation, and hence offer maximum protection to the people involved in the crash.

*However, no techniques have been reported in the literature for extracting the constellation of an accident, before it happens.* Hence, this work has addressed the following primary research questions:

- What are the most significant collision parameters which influence the injury severity for a frontal collision between two motor vehicles?
- How to extract the constellation of a crash before the accident occurs?

In addition, the secondary research questions given below were addressed:

- How to integrate physical constraints, imposed on the rate of acceleration of a real vehicle, together with data from vehicle-to-vehicle communication, into the crash constellation extraction algorithm?
- How to integrate uncertainties, associated with the data captured by sensors of a real vehicle, into a simulation model devised for assessing the performance of crash constellation extraction algorithms?

## 1.4 Contribution to knowledge

The work presented in this thesis has produced a novel algorithm for analysing the data captured by vehicle sensors, so as to extract the constellation of an unavoidable vehicle-to-vehicle accident. This work has also contributed to the field new findings from vehicle accident data to identify significant crash constellation parameters, and from the analysis of the performance of the crash constellation extraction algorithm. In addition, the work has produced a simulation model to support the evaluation of the performance of crash constellation extraction algorithms, including a technique for integrating (into the simulation model, so that the simulation can approach real-world behaviour) the uncertainties associated with the data captured by the sensors of a real vehicle.

With reference to real-world applications, it is envisaged that work will contribute to improvements of motor vehicle safety. The crash constellation extraction algorithm will allow future active safety systems to lower the impact of accidents on vehicle occupants by selective and balanced firing of active and passive safety measures tailored to the crash constellation.

## 1.5 Structure of the thesis

Chapter 1 gives an overall introduction to the vehicle safety domain within which the work is located. Furthermore, the aim and objectives are given, describing the scope of the work on extracting the constellation of an impending collision.

The methodology used in the thesis is detailed in Chapter 2 including the application of a logistic regression on accident databases, development of an offline simulation

model and its use for performance evaluation, and a further evaluation with a prototype vehicle which features a sensor fusion system.

This is followed by the summary of the current state of the art in motor vehicle safety, sensors for advanced driver assistance systems, as well as sensor data fusion architectures in Chapter 3.

Furthermore, filtering techniques for state estimation are investigated along with an assessment of current collision detection algorithms prevalent in the automotive and robotic domain in Chapter 4.

The literature regarding accident severity and related factors are reviewed in Chapter 5. In addition, an univariate binary logistic regression is used to identify the significant parameters influencing the severity of a collision.

Chapter 6 introduces the constellation extraction algorithm containing trajectory prediction based on driving dynamics, considering the velocity and position estimation, and predicting the state of the object vehicle.

A simulation model for crash constellation extraction is described in Chapter 7. The solution to get around the difficulty of conducting real pre-accident tests, which feature real-world sensor behaviour, is explained and thus simulated collision scenarios are proposed.

Chapter 8 presents and discusses the results for front-to-front and front-to-side collision scenarios, including the performance enhancement arising from the use of simulated vehicle-to-vehicle communication as additional source to the state estimation process. Furthermore, the soundness of the simulation model was assessed by comparing a real highway scenario with a similar simulated scenario.

The last chapter concludes the thesis by summarising the achievement of the aim and the contribution to knowledge regarding significant parameters influencing crash severity, the crash constellations algorithm, the simulation model, and the performance assessment of the extraction algorithm with or without a simulated V2V connection. This is followed by a discussion of the findings and their limitations, and proposal of further work emerging out of the thesis. The concluding chapter is followed by appendices.

# 2 Research Methodology

Different primary and secondary research methods, under the umbrella of a literature review and empirical evaluation using a simulation model, were used in this work which lies at the junction of two major areas: automotive safety and advanced driver assistance systems. The primary research used quantitative methods which include: collection of sensor and sensor-fusion data from a real motor vehicle driven under near-miss accident scenarios, analytical modelling, and software simulation. The research focusing on constellation extraction is broken into the following main tasks:

- Identifying the parameters which relate significantly to the severity of a motor vehicle crash, and which define the constellation of the collision.
- Reviewing and optimising state-of-the-art collision prediction algorithms for detecting an impending collision.
- Evaluating the uncertainties associated with an in-vehicle sensor fusion system for extracting the sensor measurement parameter values to be applied in an offline crash simulation model.
- Devising an algorithm for extracting the constellation of a crash.
- Extracting the crash constellation, and analysing its accuracy through a systematic performance assessment.

The tasks listed above fall into four pillars (illustrated in Figure 2.1) which supported the development of the simulation model for the extraction of the constellation of an unavoidable vehicle-to-vehicle frontal accident. Each pillar includes primary research which is underpinned by a review of the relevant literature. The four pillars are: (i) collection of real-world data for sensors and sensor-fusion behaviour, using sensors and a fusion system on-board a real prototype vehicle; (ii) identification of parameters which influence significantly the severity of a crash, using univariate binary logistic regression on crash databases; (iii) design and implementation of suitable algorithms for the extraction of a crash constellation; (iv) definition of

vehicle manoeuvres (i.e. test data) for evaluating the performance of the proposed constellation extraction solutions, using suitably designed driving scenarios.

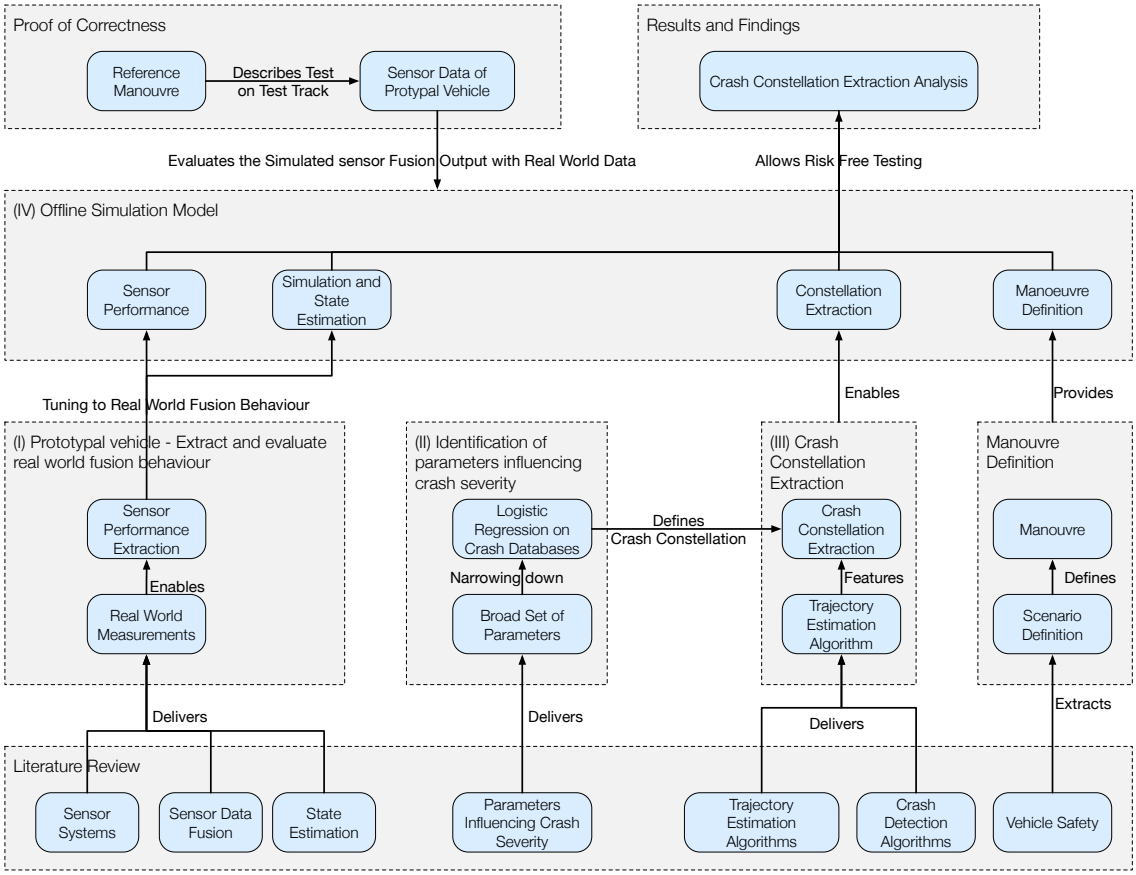


**Figure 2.1:** Layered structure of the work, which includes four pillars. The boxes represent the work completed for the fulfilment of the PhD.

## 2.1 Identifying the most significant crash parameters

In this work, two approaches were followed for identifying the parameters which influence significantly the severity of a crash:

- A literature review to identify the variables to be included in a subsequent analysis on accident databases, which used a univariate binary logistic regression analysis.
- A univariate binary logistic regression analysis on accident databases, to identify the most significant crash parameters by adopting the methodology of Helmer (2013) for vehicle-to-vehicle collisions.

## 2.2 Off-line simulation model reproducing real-world sensor and vehicle behaviour

The collision extraction algorithm developed in this work is for pre-crash scenarios, where protective countermeasures must be activated at least 500ms before a collision occurs. This very short time-to-collision limits the possibilities of performing a real-world evaluation of the algorithm, because of a lack of appropriate test equipment which can be used safely for these highly dynamic and destructive collision scenarios within such a narrow time window. Furthermore, real world tests are difficult to reproduce because they are associated with a complex set of parameters which influence the different components of a crash constellation extraction algorithm. In this doctoral research, the above constraints paved the way for the development of a simulation model which can enable the definition of arbitrary collision scenarios between two vehicles fitted with real world sensors, optionally enhanced with vehicle-to-vehicle (V2V) communication.

Furthermore, the solution proposed in this research includes algorithms for estimating the state of traffic objects, such as vehicles, to support the crash constellation extraction. All these components allow a performance analysis by comparing the precision of the crash parameter extraction for different collision scenarios. For example, they enable an assessment of the enhancement arising from V2V communication. Chapter 7 provides a more detailed description of the developed simulation model, including its main components.

## 2.3 Prototype vehicle featuring future ADAS sensors and a sensor data fusion system

Real-world testing of safety algorithms for pre-crash collision mitigation measures is dangerous for the test drivers and engineers involved in real crashes under testing, and it may result in costly damage to vehicles and other test infrastructure. Computer simulation offers the benefit of risk-free and relatively inexpensive testing. However, offline simulation of the crash constellation extraction algorithm requires a proof of correctness. In this research, this proof was done using a baseline computed from real-world sensor data. Data was collected while driving a prototype

vehicle, to allow the evaluation and tuning of the performance of the data fusion within the vehicle state estimation algorithm embedded in the simulation model, so that it can approach real-world behaviour. This real-world data forms the basis for offline simulation of diverse algorithms based on sensor data and vehicle state estimation, especially for crash constellation extraction.

The sensor signal routing and data integration architecture of the prototype car are presented in Appendix A.

## 2.4 Correctness of the simulation model

According to Murray-Smith (2015) a simulation model cannot be validated, but rather the error of the model must stay in the specified ranges of operation. This principle is followed in Section 8.1. Therefore, the assessment of the correctness was executed by comparing a cut in scenario recorded with a research vehicle to the output of the simulation model. The output of the in-vehicle sensor-fusion system and the simulation model was assessed afterwards confirming that the simulation model works within the same boundaries reproducing a real world system behaviour.

## 2.5 Performance assessment of the crash constellation extraction algorithm

For the assessment of the crash constellation extraction algorithm a front-to-front collision scenario is chosen. Furthermore, a simulated vehicle-to-vehicle communication was taken into account to assess the effectiveness of inter vehicle communication in providing accurate measurements to the sensor fusion model. Chapter 8 discusses the findings of the performance assessment with regards to the following:

- The estimation accuracy for the time-to-collision (TTC) is rated with or without a simulated vehicle-to-vehicle communication.
- Each collision is evaluated regarding the precision with which the crash constellation parameters can be extracted.

- The speeds are varied to evaluate the TTC estimates for different speeds of the collision partners.
- The estimate of the collision points also varies with different trajectories and uncertainties before collision. These estimates are assessed with respect to different speeds of the colliding vehicles.

## 2.6 Conclusion

The research was planned as a systematic investigation in search for answers to the research questions stated in Section 1.3. The main research methods, and key tools used in the primary research, are summarised below.

*Research methods:* This research used a number of primary and secondary research methods, beginning with a literature review to inform the primary research. The primary research used quantitative methods, including: (i) collection of numerical data from sensor and sensor-fusion modules of a real motor vehicle driven under near-miss accident scenarios; (ii) statistical analysis of data from a crash database, to identify significant parameters which influence the severity of a crash, and to define accident scenarios to be used in the performance evaluation of the crash constellation extraction algorithm proposed in this work; (iii) design and implementation of computer algorithms for crash constellation extraction; and (iv) empirical evaluation of the performance of the proposed algorithm, using software simulation.

*Key primary research tools:* A simulation model was produced, to allow risk-free testing of constellation extraction algorithms and assessment in customisable scenarios. These features are essential for developing future active safety applications through deriving the correct requirements for the sensor system to support the development of future vehicle models.

Based on an accident database the needed accident scenarios and the parameters describing a crash constellation were derived using univariate binary logistic regression analysis. As detailed in Chapter 5, the constellation parameters retained from the analysis were those associated with the more severe road accidents, whilst also capable to be derived from real-world sensors.

To evaluate the simulation model which is a core entity in this work, a prototype vehicle was used featuring a state-of-the-art sensor set up and sensor data fusion system. This allowed an assessment of the simulation outcome compared to real world vehicle data.

The next chapter presents some background material through an overview of motor vehicle safety systems. The background material is followed by a literature review in the subsequent chapter which focuses on techniques for predicting motor vehicle collisions.

# 3 Overview of Motor Vehicle Safety Systems

To provide some background knowledge for this investigation into crash constellation extraction, and to locate the investigation in its knowledge domain, the part of the literature review presented in this chapter covers important fields including:

- Vehicle safety, which is the frame and the research domain.
- Sensors for detecting the environment and the crash target.
- Sensor data fusion, which will deliver accurate object detection.

## 3.1 Motor vehicle safety

Over the past decade, vehicle safety innovation has focused increasingly on active approaches, in particular within the premium car brands. Significant progress in passive safety technology has already been achieved by optimizing the design and construction of vehicle safety structures and devices such as the bodywork, seat belts and systems, and many more. However, active safety still has enormous near-term potential due to the rapid pace of technological advancement in the electronic sector (Kompass, Gruber, and Domsch, 2010).

As modern electronics have enabled the early detection of hazardous situations, active safety systems are being designed to mitigate or even avoid accidents. This type of safety systems rely on advanced sensor systems which enable cars to see and interpret their environment. These sensor systems are described in more detail in Section 3.2.

In order to address a complex traffic context, intelligent algorithms are required. However, a prerequisite for intelligent algorithms is high-quality sensor data which will allow the system to interpret and accurately forecast the most important environmental features, especially pedestrian and vehicle motion, and the criticality of hazardous situations. With the help of a driving-situation evaluation of sufficiently

high quality, active systems will be capable to support the driver with adaptive strategies. This begins for example with making the driver aware of critical situations, and progressing to stronger interventions if required, and finally encompassing escape and crash mitigation strategies. These mitigation strategies can be intelligently combined with passive safety features (such as airbags and restraint systems). This "integral safety approach" is an important focus of development in automotive research and promises a very high potential to reduce the risk and consequences of severe accidents.

The crash constellation extraction techniques under development in this doctoral research project will enable the integrated safety system to adjust vehicle safety measures so as to match closely the crash situation, and therefore provide more protection for the occupants of the vehicle.

### 3.1.1 Crash phases

Different vehicle safety functions can be deployed along the time-line of a collision, which can be broken down into 3 sequential phases. These phases occur after normal drive time: pre-crash phase, crash phase, and post-crash phase.

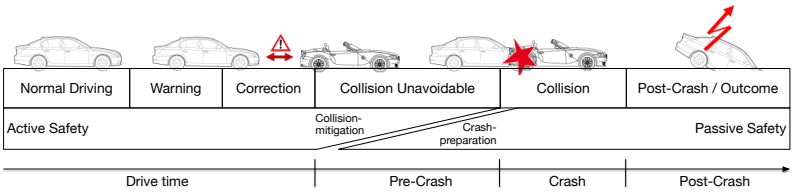


**Figure 3.1:** Vehicle safety and crash phases (Braess, 1996)

The **pre-crash phase** is defined as the time just before the actual crash. This phase represents the transition from the "drive time" to the actual vehicle collision. During this phase, safety counter-measures which can be deployed, include warning the driver or taking actions to correct the path of the vehicle. In addition, the severity of a crash can be reduced significantly by triggering active restraint systems before an impending collision. Reducing the speed of the vehicle, or restraining early the vehicle occupants to the seats using belt systems, can yield a better crash outcome. It is well known that a slight decrease of the vehicle speed can significantly improve the likelihood of survival (Karrenberg, 2008). The relationship between difference

in speed and the severity of the accident has been shown in numerous publications (Busch, 2004; Eichberger et al., 2009; Nitz, 2008).

The **crash phase** spans from the time of impact until all vehicles involved in the collision come to a complete standstill. During this time, airbags and vehicle occupant restraint systems are deployed to minimize the consequences of the crash.

The **post-crash** phase starts immediately after the crash phase. In this phase, the safety system can alert accident assistance services to take appropriate action, such as getting in touch with the vehicle occupants or sending life-saving emergency help immediately.

### 3.1.2 Active safety

Active safety systems mainly act during drive time and in the pre-crash phase, as illustrated in Figure 3.1. The safety systems can be grouped according to their type of interaction with the driver (Figure 3.2); the expansion of each acronym is given in the section titled "Abbreviations".

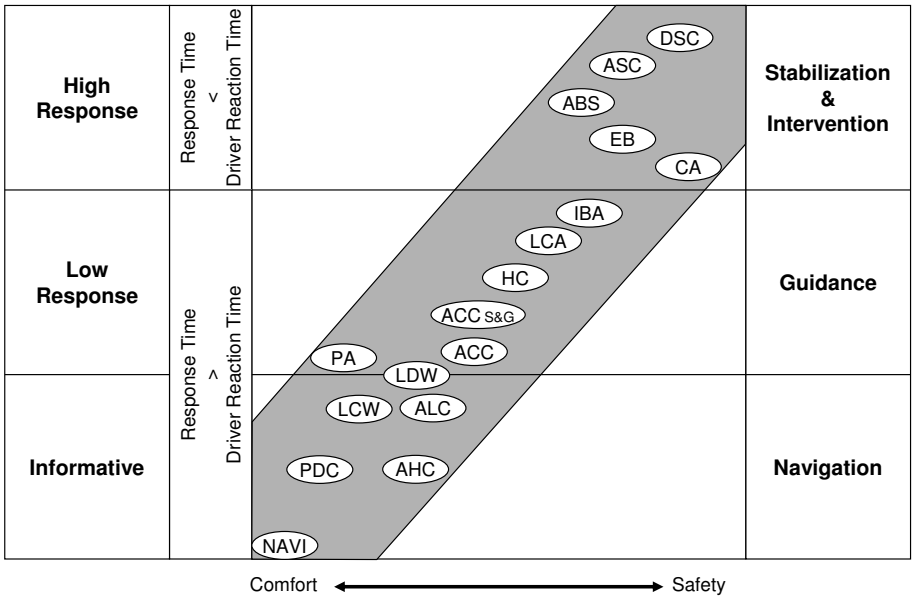


**Figure 3.2:** Classification of ADAS and active safety systems (Freymann, 2004)

The **informative** systems mainly support the driver during the normal driving phase with navigation information. The second group, comprising guidance systems, enhances the situation awareness of the driver by warning the driver of upcoming

situations. These systems (e.g lane departure warning) only need a slow response time. The last group of safety measures, comprising stabilization and intervention systems, act in critical driving situations and hence they need a fast response time, as they are active in a very dynamic environment. Additionally they have to be able to take control of the vehicle driving dynamics.

According to Figure 3.3, research in the field of active safety started to gain momentum at the start of the millennium with the introduction of 'Adaptive Cruise Control' and 'Brake Assist' to the markets (Winner, Hakuli, and Wolf, 2011). These two systems make use of radar to detect other traffic participants and thus offer adequate foresight about hazardous traffic situations.

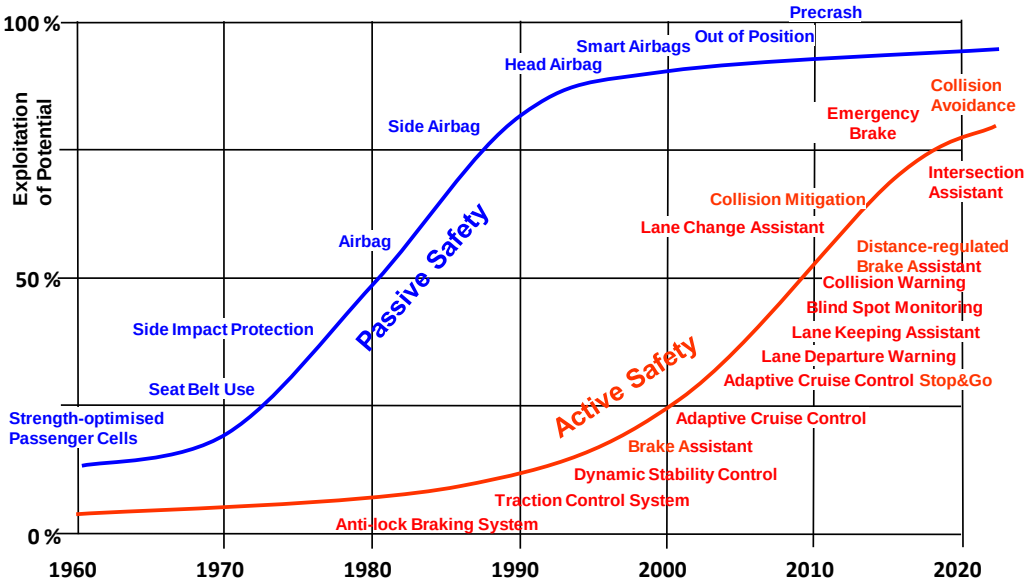


**Figure 3.3:** Exploitation potential of active and passive safety (Kompass, Domsch, and Kates, 2012)

A large part of today's innovations are based on the early brake assistant, lane departure warning, and collision warning systems. The first collision mitigation system to help the driver minimise the consequences of accidents was introduced by Kopischke (1999).

More recent research areas focus on road intersection assistants and add inter vehicle communication to exchange sufficient data about road zones where the visibility from a vehicle is restricted such as near a bend in the road (Aycard et al., 2011; Mages, Hopstock, and Klanner, 2012; Mangel et al., 2011).

For future safety systems, it is not only important for a vehicle to see other road users. These systems will also need to understand the traffic situation and estimate the risk of present and near-future situations. With reference to 3.1.1, each hazardous situation emerges from wrong driving decisions or environment changes during drive time. Fricke, Glaser, and De Filippis (2006) produced a generic fault tree which explains these circumstances including events and mistakes leading to a critical traffic situation. Therefore, new assistance systems, devised to help the driver master these situations, were proposed in Umemura (2004). The assistance systems highlight the following three aspects:

- Cognition: Providing information about the obstacles and traffic participants.
- Judgement: Helping to understand the traffic situation.
- Actions: Supporting the driver to master complex driving manoeuvres.

Merging the approaches of Umemura (2004) and Fricke, Glaser, and De Filippis (2006)) which cover the driver tasks the assistance system, and the situation itself, leads to the representation shown in Figure 3.4.

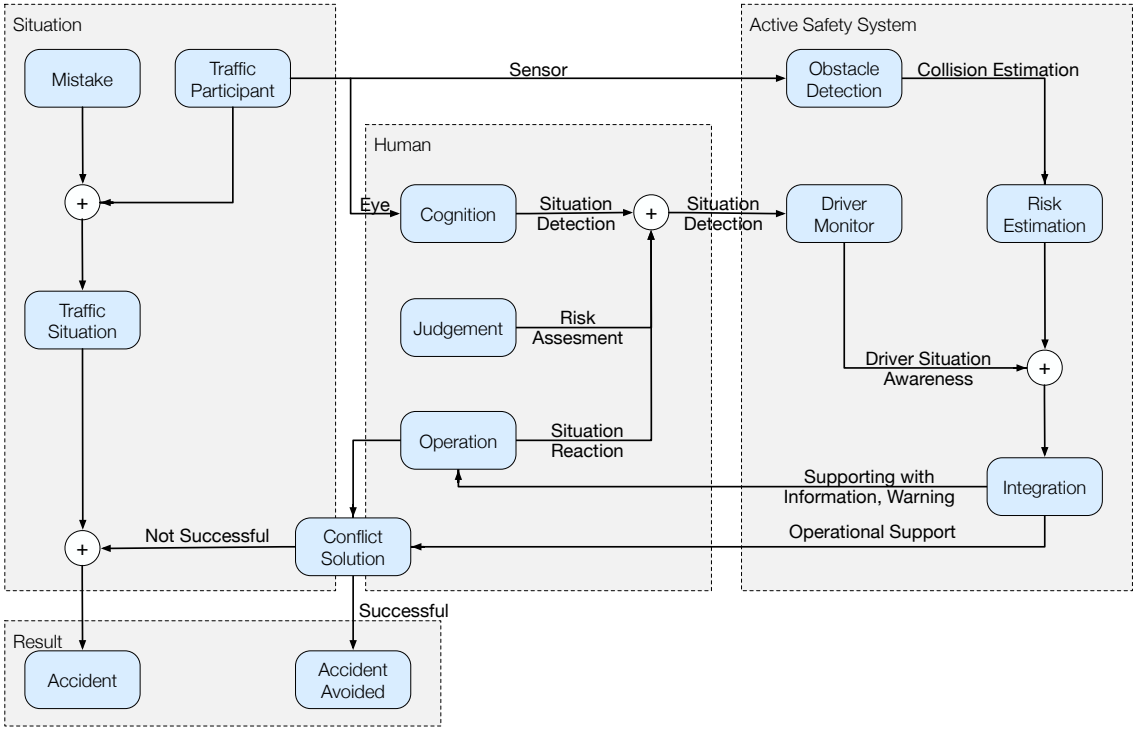


**Figure 3.4:** Merged generic fault tree for situations leading to an accident. The tree combines perspectives gleaned from Domsch and Huber (2008), Donges (1999), Kompass and Huber (2009), Reichardt et al. (2012), and Umemura (2004).

According to Umemura (2004), each traffic conflict is caused by a mistake or environment change of one or more traffic participants, as Figure 3.4 details. The consequence of not changing direction and/ or motion leads to a critical situation (Gstalter, 1983; Nitz, 2008). These situations can be detected by estimating the future movement of the traffic participants, which is explained in depth in Section 4.3 including various approaches for detecting an impending collision. Predicting critical situations early allows the driver, or active safety system, time to choose between different manoeuvres to avoid the impending accident. In detail, the active safety system detects its environment and forwards the different traffic objects to the risk estimation algorithm. In case driver inattention is detected by the driver monitor (which continuously observes the driver), the relevant information and warnings can be fired by the safety system using the Human Machine Interface (HMI). In addition, the active safety system is able to trigger the brake or steering, to support the driver in making the right decision and taking the correct action to avoid the accident, such as by breaking or circumventing the obstacle.

### 3.1.3 Point of no return and the dilemma of evading hazardous situations

Nitz (2008) stated that hazardous situations can be avoided mainly by breaking or circumventing the obstacle. The effectiveness of these two types of actions is limited by the amount of free space which each solution requires between the vehicle and the other body it might collide with, as dictated by the physical limitations of the vehicles' driving dynamics. This limitation directly leads to the dilemma of avoiding the collision using one of the stated solutions. A highly abstracted approximation is shown in the Appendix B.

Horst and Hogema (1993) determined a critical time-to-collision (TTC) value of 1.1 seconds for activating a collision avoidance system. Furthermore, Brown (2005) conducted several simulator studies resulting in 15 crashes with a mean value for the TTC of 0.65s, which is strengthened by the work of Braess and Seiffert (2011) stating the critical TTC to a value of 500ms. It is difficult to derive a fixed TTC in which a collision is inevitable, as it depends on the scenario and its individual circumstances. For the proposed doctoral work, the collision will be extracted at a step size of 100 milliseconds (ms) starting at 500ms before the actual crash occurs.

This allows a comparison of the various constellation extractions regarding their accuracy.

## 3.2 Sensors for automotive applications

This section describes different types of sensors and compares their individual strengths and weaknesses in relation to their use in future vehicles.

### 3.2.1 Radio detection and ranging (RADAR)

The Radio Detection And Ranging (RADAR) sensor emits electromagnetic waves in the radio frequency band and receives their reflection from metallic objects. The shift in the frequency band, the so called "Doppler shift" is processed to derive directly the velocity of the detected object. At the same time, this detection principle is the major strength of the radar sensor allowing direct velocity measurements of surrounding targets. The distance is calculated via the ToF (Time Of Flight) principle of the backscattered radar signal. According to Kaempchen (2007), the radars differ as follows:

- the waveform (pulse, Frequency Modulated Continuous Wave (FMCW), or Frequency Shift Keying (FSK)),
- the frequency (24GHz, 77GHzm, 79GHz),
- And the antenna characteristics (fixed (multi) beam, scanning electrically or mechanically).

The main advantages are the robustness against weather conditions (fog, rain, or snow) and non-constrained usage in dark environments or by night (Karrenberg, 2008). The disadvantages are a bad resolution of angle and object dimensions, as the RADAR is rather about tracking a single point than detecting the contour or outline of an object. Therefore, it is difficult to track pedestrians or distinguish between a motorcyclist and a bicyclist (Naab, 2004). The accuracy and characteristics of todays sensors, such as the Continental ARS-301, are shown in Table 3.1.

**Table 3.1:** Sensor characteristics of an ARS-301 radar (Continental, 2016)

| Sensor | Radar (77GHz) |
|---|---|
| Range | 60m/200m |
| Opening angle (horizontal, azimuth) | 56 deg / 16 ° |
| Opening angle (vertical, elevation) | 4.3 ° |
| Resolution (horizontal, Azimuth) | 2-3 ° |
| Resolution (vertical, Elevation) | not known |
| Update frequency | 15Hz |

### 3.2.2 Light detection and ranging (LIDAR)

The LIght Detection And Ranging (LIDAR) sensor follows the ToF principle related to the radar described in section 3.2.1 to measure the distance to a reflection point. Its wavelength spectrum differs from the spectrum for radar, as lidar uses optical sensors featuring a laser pulse in the infra-red spectrum (Kaempchen, 2007). The velocity of objects is derived from the distance over time, resulting in a reduced precision in the objects velocity measurement. The measurements of the environment are taken by using two different techniques:

- Multi-beam lidar featuring multiple diodes allowing the lidar sensor to process the scanning area in a single evaluation.
- A laser scanner utilising a prism to manually scan the acquisition area.

The concentrated light pulse and the sequential scans offer a high resolution in the angle estimation, which allows contour measurements of objects in 'L'-shape form (Winner, Hakuli, and Wolf, 2011). Due to the sensitivity to water droplets, the accuracy decreases in bad weather conditions such as fog, rain, or snow (Nitz, 2008). As lidar uses an active sensor, the scans are not influenced by the surrounding illumination or night. Characteristics of a state of the art sensor is given in Table 3.2 below.

### 3.2.3 Vision based systems

The importance of using vision based-systems for automotive applications is growing due to the relatively low cost of the required cameras. Their future potential to

**Table 3.2:** Sensor characteristics for a IBEO Lux Lidar (Ibeo, 2010)

| Sensor | Lidar (905nm) |
|---|---|
| Range | 180m |
| Opening angle (horizontal, azimuth) | 110° |
| Opening angle (vertical, elevation) | 3.2° |
| Resolution (horizontal, azimuth) | 0.25° |
| Resolution(vertical, elevation) | 0.8° |
| Update frequency | 25Hz |

extract rich visual information about the perceived environment from the image stream demands high computational power.

Vision based systems which detect visible light feature Charged-Coupled-Device (CCD) and Complementary Metal Oxide Semiconductor (CMOS) chips. These can perceive a range of wavelengths including the infra-red and visible spectrum (Schneider, 2006). The cameras can deliver high resolution images similar to the human eye and therefore the data produced need tremendous computational power to extract the information out of the image using pattern recognition and image processing algorithms. Distance relative to the viewpoint can be calculated by scaling (for mono cameras) or using basic trigonometry (for two or more cameras (software-based stereo fusion)). Therefore, the measurement quality of the distance is directly dependent on the number of cameras used. A huge advantage of vision-based systems is the opportunity to classify objects (such as: cyclist, vehicle, truck, etc.) based on the pattern of their corresponding pixels. This classification allows subsequent measurement of width, height and thickness of objects (Winner, Hakuli, and Wolf, 2011). Thus, cameras are able to detect lanes, traffic signs, and other road features to extract relevant information as input into ADAS algorithms. Vision-based systems mainly use passive sensors and are strongly influenced by weather conditions, overexposed sunlight, or darkness. These factors may lead to operational restrictions. Table 3.3 shows a comparison between state of the art low and high resolution mono cameras and a stereo camera. The data provided in the table is derived of a data sheet of the Mobileye camera system.

**Table 3.3:** Example sensor characteristics for mono and stereo camera

| Sensor | Mono camera (low resolution) | Mono camera (high resolution) | Stereo camera |
|---|---|---|---|
| Range | 30m/70m | 60m/120m | 50m/80m |
| Opening angle (horizontal, azimuth) | 38° | 40° | 38° |
| Opening angle (vertical, azimuth) | 25° | 30° | 30° |
| Resolution (horizontal, azimuth) | 20 pixel/° | 32 pixel/° | 20 pixel/° |
| Resolution (vertical, elevation) | 20 pixel/° | 32 pixel/° | 20 pixel/° |
| Update frequency | 13.7Hz | 36 Hz | 16.7Hz |

### 3.2.4 Ultra sonic sensors

Ultra sonic sensors are applied in today's parking assistance systems due to their limited range of 0.5m to 4m (Winner, Hakuli, and Wolf, 2011). The ultrasound pulses are clocked at 40kHz and sent at the speed of sound (340m/s) to its environment. The reflection from the first object which is hit by the pulses is directly measured and calculated. Although the sensor is robust in a variety of weather conditions, it is too limited to find usage in sophisticated active safety systems (Winner, Hakuli, and Wolf, 2011).

### 3.2.5 Vehicle to Vehicle (V2V) communication

Vehicle-to-Vehicle (V2V) communication can increase automotive safety due to additional information provided through inter-vehicular communication. In 2014, the U.S. National Highway Traffic Safety Administration announced that it was working towards enabling V2V communication technology for light vehicles to exchange basic safety data at a frequency of 10Hz. The technology will allow various safety measures for collision avoidance to take advantage of the transmission of vehicle data such as position, acceleration, or velocity (Harding et al., 2014; NHTSA, 2014). Vehicle-to-Infrastructure (V2I) communication additionally allows the vehicle to communicate with traffic lights, highway roadwork sites, and more.

The major advantage of V2V communication, compared to physical sensors covered in the previous section, arises from its impact on the fusion process. Data from physical sensors are generally more afflicted with variances which influence the quality of the vehicle state detection by the system. V2V directly distributes the vehicle's own state (acceleration, deceleration, size, etc.) measured by in-vehicle sensors and sent over the air to the surrounding vehicles. Therefore, the state estimation is less error prone, as the variance is only tied to the latency produced by the communication channel (Kuehbeck et al., 2014a; Nitz, 2008). In most cases, this latency is constant and easy to be modelled in a fusion process allowing a highly accurate estimation of the state of vehicles during the environment perception process. Röckl, Gacnik, and Schomerus (2008) analysed the benefits for a fusion process using a virtual V2V sensor providing complementary and redundant information about the vehicles' state to the particle filter. Their findings showed that V2V data increased the reliability, robustness and accuracy of the state estimation.

Furthermore, most sensors have a field of view which limits their detection capability to objects which are within the field of view. V2V communication can reveal hidden objects by transmitting their position and state directly to the traffic participants, enabling the detection of occluded objects in blind spots for instance at crossings (Huber, 2007). With V2V communication, the field of view is therefore not limited to a specific distance, as vehicles are able to transmit their state to others at a distance of couple of hundred meters, adding new vehicle detection features to future ADAS systems (Klanner, Ehmanns, and Winner, 2006). The original V2V is limited to Wireless Local Area Network (WLAN) standards but it is enhanced by V2X (vehicle-to-infrastructure) networks which can span a network over several nodes covering hundreds of metres. A huge set of additional information can be distributed to traffic participants.

The effectiveness of V2V and V2X directly depends on the level of market penetration by the technology, because the functionality mentioned above needs a high number of vehicles providing V2V communication. Achieving an appropriate level of market penetration will take time (Röckl, Gacnik, and Schomerus, 2008).

### 3.2.6 (Differential) global positioning service ((D)GPS)

The common Global Positioning System (GPS) is based on a simple sender and receiver technique using the World Geodetic System WGS84 standard (The Defense Mapping Agency, 1987). Satellites surrounding the earth send, at the speed of light, cyclic data containing the current time and position of the vehicle. The receiver part calculates its position via multilateration using the data of at least 4 satellites. The accuracy of 7.8m (concerns 95% of measured data) (Department of Defense, 2014) is not suitable for highly dynamic ADAS applications. Furthermore, GPS has no functionality at all in enclosed built structures such as tunnels. The accuracy of GPS strongly depends on the environment surrounding the receiver, e.g. signal distortion due to reflections in dense urban areas. The accuracy is also influenced by the number of visible satellites, the atmosphere, and clock drifts between the receiver and satellites.

The differential global positioning system (dGPS) calculates local correction data for the data received using a stationary base station. This correction data is sent to the receivers to calculate position with higher accuracy by taking the correction data into consideration. These services offer a position accuracy within 0.01m - 0.02m.

At the time of writing, the costs for dGPS are tremendous and therefore not suitable for series production vehicles, so that dGPS is only used for prototypal vehicles to generate ground truth data for test drives.

## 3.3 Automotive sensor data fusion

Advanced driver assistance systems directly rely on the underlying quality and quantity of information about the environment surrounding the vehicle (Naab, 2004). To master the challenges of tomorrow, it is essential to improve the robustness, reliability, accuracy, and field of view of the environment perception module. Single sensor systems are prone to fail or to misinterpret the environment. Hence, active safety systems built around a single sensor are very vulnerable. This is a serious concern as safety systems are required to act in critical situations and facilitate demanding robustness and accuracy requirements (Randler, Wilhelm, and Lucas, 2003). In the past, many researchers acknowledged the additional benefits of fusing sensor data to achieve sophisticated environment perception for ADAS applications (Dietmayer,

Kirchner, and Kämpchen, 2005; Kaempchen and Dietmayer, 2003; Niehsen et al., 2005; Vukotich and Kirchner, 2001; Wisselmann et al., 2004).

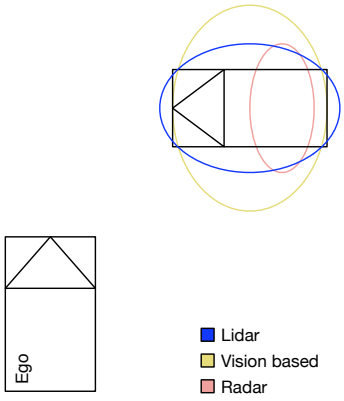


**Figure 3.5:** Target detection performance of sensors (illustration for a road junction scenario). The ego vehicle is approaching a road intersection, and the other vehicle is in the field of view of all sensors on the ego vehicle.

To illustrate this problem, Figure 3.5 describes a road junction scenario in which the ego vehicle is approaching a road intersection. The tracked vehicle is passing from the right to the left, crossing the field of view of all sensors on the ego vehicle. The different sensors with different detection principles sense the azimuth, the velocity, and the distance with a different precision. The fusion of the different sensors strengthens the classification of the vehicle and the robustness of its tracking. The following benefits result from the fusion:

- The **vision based** system classifies the object (truck, car, motor cycle, pedestrian, etc.).
- The **lidar** tracks the angle and distance with high precision, as well as the contour of the object.
- The **radar** delivers the velocity by relying on the Doppler shift.

Sensor fusion combines the different sensors, exploiting their positive properties to generate a more precise environment for the safety system.

The sensor data and its corresponding output of the sensor data fusion are afflicted with noise and hence with variances in the position and velocity estimation. Therefore, the design of a model which simulates real-world state estimation behaviour

requires a good understanding of the complete processing chain of sensor data, including the impact of measurement noise.

### 3.3.1 Sensor data fusion in the context of ADAS

Steinberg, Bowman, and White (1999) define the fusion process as

*"data fusion is the process of combining data or information to estimate or predict the entity states."*

The entity state in the context of ADAS refers to an abstract element in the environment surrounding the vehicle. The element is either a real object (vehicle, tree, etc.) or a value such as a pitch angle (Winner, Hakuli, and Wolf, 2011).

The fusion process combines the diverse and redundant measurements of the different sensors to produce a consistent view of the driving environment. In the design concept of a multi-sensor system, the information acquisition process needs to be decoupled from the ADAS function, as no sensor is tied to a specific application. Therefore, information management and acquisition should be designed as an atomic process which distributes the environment-perception function to one or more ADAS applications (Naab, 2004). A possible solution for the sensor framework integration with ADAS functions is illustrated in Figure 3.6.

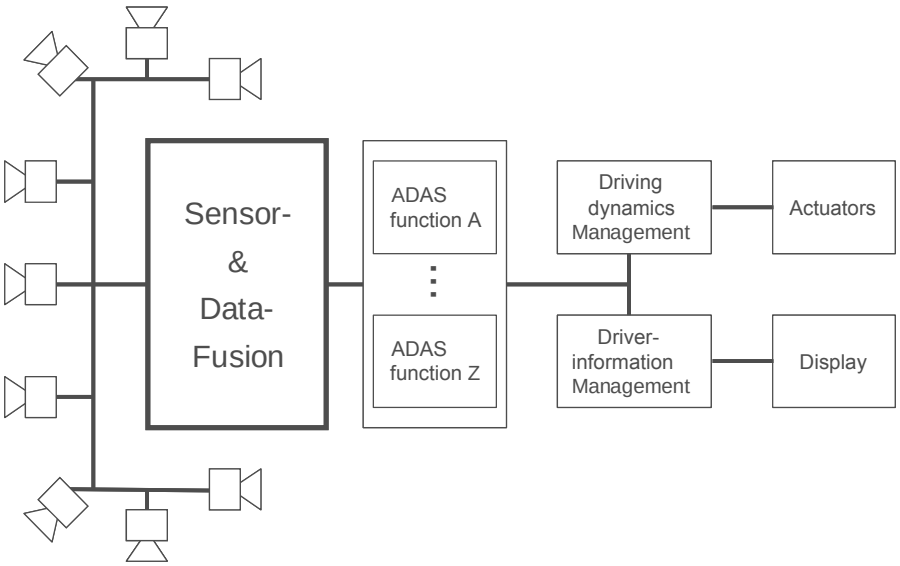


**Figure 3.6:** Sensor data fusion as an integration platform between sensors and ADAS applications (Naab, 2004)

Figure 3.6 above shows, that modularisation is required for future system integration. The sensor and data fusion unit provides the ADAS applications with information about the environment. The ADAS functions directly send motion commands to the actuators, or display information to the driver.

### 3.3.2 Main goals of data fusion

The main focus of sensor fusion is to combine the strengths of different sensors and minimising their weaknesses. Ruser and Puente León (2007) give a mathematical description for the combination of sensors ($S_1$, $S_2$) with different working principles and the resulting performance gain $L(S_1 U S_2)$ of the multi-sensor fusion:

$$L(S_1 U S_2) > L(S_1) + L(S_2) \tag{3.1}$$

or at least

$$L(S_1 U S_2) > max[L(S_1),L(S_2)] \tag{3.2}$$

The benefit of a multi-sensor fusion architecture is mentioned in a large number of publications and can be summarised based on Winner, Hakuli, and Wolf (2011) as follows:

#### Redundancy

- Availability:

  The system tolerance against failures is improved. A sensor blackout can be avoided by using sensors sharing parts of their field of view. In this special case the fusion is responsible for delivering suitable data quality for the ADAS.

- Detection:

  Redundant sensors deliver the properties and state of one object in a redundant manner to enhance the quality of the measurements. The measurement variance is considered in the state estimation algorithm (Bar-Shalom, 1990).

- Ambiguity:

  The influence on the complete system of failures originating from the measurement principle of a single sensor is reduced and the accuracy of the system improved by sensor fusion (Kato, Ninomiya, and Masaki, 2002; Shimomura et al., 2002; Steux et al., 2002; Takahama et al., 2003).

### Complementarity

- Measurement variance:

  Complementary sensors featuring different measurement principles are able to detect additional properties of tracked objects, thereby feeding the fusion process with enhanced information about the sensed entity. The different sensing technologies decrease the measurement noise and variance of the sensed environment (Klaus, 2006).

- Field of view:

  In addition to the improvement in sensing the state of objects, multi-sensor fusion allows the tracking of objects beyond the sensing boundaries of each individual sensor. Therefore, it enlarges the field of view as illustrated in Figure 3.7.

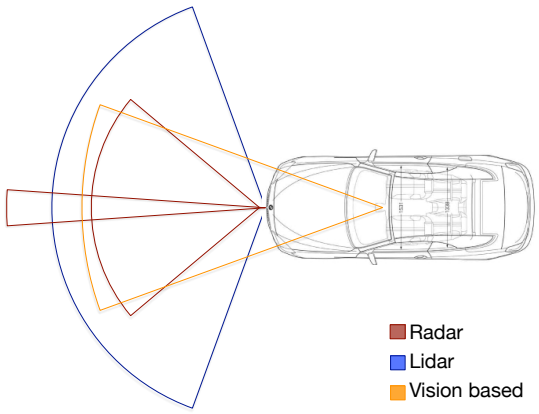


**Figure 3.7:** Sensor configuration for a BMW 6 Series test vehicle

- Robustness:

  The overall robustness of the complete system is enhanced by the usage of different sensor techniques (Winner, Hakuli, and Wolf, 2011).

#### Temporal aspects

- Measurement rate:

  Different sensing principles imply unequal update rates, as it can be seen in the different characteristic tables of Section 3.2. This allows sensing the environment at a higher frequency (Klaus, 2006).

- Processing time:

  The environment is sensed through each sensor individually and in parallel leading to an increased processing time.

#### Cost efficiency

According to (Naab, 2004) the fusion unit provides the environment information to several ADAS applications instead of linking one sensor with one ADAS application. This lowers the cost for future ADAS applications (Winner, Hakuli, and Wolf, 2011).

### 3.3.3 The data fusion process

In general, the following components are executed recursively during the sensor data fusion process (Kaempchen, 2007; Schneider, 2006):

- Data preprocessing
- Data synchronisation
- Data alignment
- Data association
- State estimation

- Object classification

The **preprocessing** can take place in the sensor unit itself generating sensor based object lists out of the raw values.

The **data synchronisation** task labels each data with the system wide timebase to order the measurements temporally (Bar-Shalom, 1990; Blackrnan and House, 1999).

The different sensors in the car are mounted at specific places, e.g. the radar in the front bumper and the camera behind the wind screen. The objects detected in each individual coordinate system during the pre-processing step need to be transformed within the **data alignment** process into a common vehicular coordinate system. Not only the different mounting positions are a problem, also the varying sensing technologies. For example, when the ego vehicle is following the tracked vehicle, the radar measures the distance to the rear axis of the tracked object, the camera detects the rear end of a vehicle. In this case the sensor calibration methods are very important and explained in more detail in (Kaempchen, 2007; Putzinger, 2005)

During the **association** phase the various objects distributed by the sensors are referenced and combined to tracks (multi-target tracking)(Bar-Shalom, 1990). This process is directly related to the quality of the following state estimation process (Bar-Shalom, 1990; Holt, 2004; Stüker, 2004; Winner, Hakuli, and Wolf, 2011). Different techniques for the association are proposed in the literature: Nearest Neighbour (NN), Multiple-Hypothesis Testing (MHT), Joint Probabilistic Data Association(JPDA), and more (Herpel et al., 2008; Schneider, 2006; Steinberg, Bowman, and White, 1999). Assigning the wrong objects to tracks results in an information error in the state estimation. In reality, for example, sensors detect trucks sometimes as two individual objects resulting in fragmented tracks.

The **state estimation** process fuses newly gained information about objects to the existing track information. The estimated states are used as starting points for the next iteration as Figure 3.8 illustrates. The different state estimation methods are explained more detailed in Section 4.2.

At the end each track is classified into the probability of existence or if known into different classes (pedestrian, motor cyclist, car, truck, ...) (Aeberhard et al., 2012; Kaempchen, 2007). Furthermore, the states of the tracked vehicles are afflicted with variances and therefore, it is important to forward these to the ADAS and active

safety systems. This work uses the variances of the position and velocity estimation to benchmark the accuracy of extracting a crash constellation.

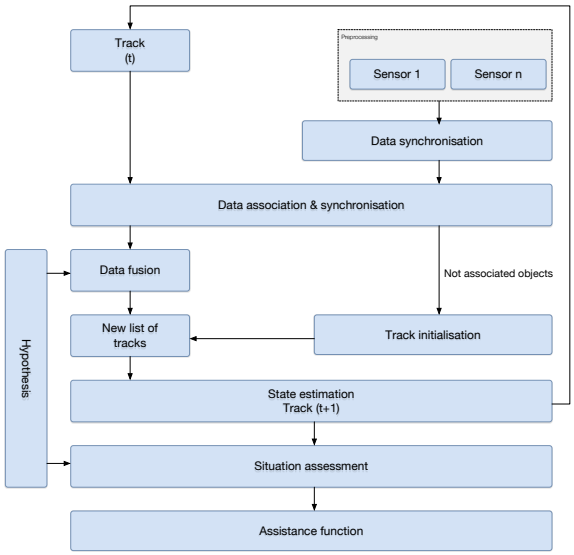


**Figure 3.8:** Schema for sensor data fusion, reproduced from Naab (2004)

The tracks and states make up the interface to various ADAS applications, each potentially with different requirements for state estimation. For example, an emergency braking system analyses the environment with regards to object properties. Therefore, the algorithm decides whether the tracked vehicle is an agile motorcycle or a heavy truck with limited evasion possibilities (Naab, 2004), for example.

### 3.3.4 Architectures for sensor data fusion

In general, there is no right or wrong architecture for the concept of fusing sensor data, it is chosen according to the targeted problem to be solved. Low-level fusion uses the raw sensor data, whereas high-level fusion processes the data already preprocessed by the sensor or other components. It is also possible to fuse the data at several levels of abstraction, as in the approach introduced by (Kaempchen, 2007). This section provides a summary of advantages and disadvantages for different fusion architectures, according to the level of abstraction of the data used in the fusion.

#### 3.3.4.1 Low-level fusion

Low-level fusion uses the data at the lowest possible layer, by processing the raw sensor data (Aeberhard and Kaempchen, 2011); for pictorial data, it is also called *pixel-level* fusion. At the first step the sensor delivers the raw data to the fusion unit where the information is extracted out of the measurements. After aligning the measurements spatio-temporally, the fused data is forwarded to the tracking and classification module. The data is mainly processed in a central unit, the architecture is therefore often called the centralised tracking architecture (Aeberhard and Kaempchen, 2011). Figure 3.9 illustrates the structure of the low-level fusion architecture.

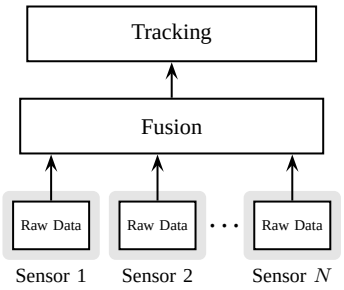


**Figure 3.9:** Architecture for low-level fusion (Aeberhard and Kaempchen, 2011)

This architecture provides the fusion algorithm with the maximum information about the environment and theoretically features optimal tracking which considers all information of the various sensors (Kaempchen, 2007). The objects resulting from low-level fusion can have a high probability of existence, as the entity is measured by several sensors simultaneously (Aeberhard and Kaempchen, 2011), which enables good tracking of a detected object. The main drawback of this fusion methodology is the huge amount of information provided by the sensor, which claims tremendous computational power. Furthermore, the centralisation hinders the scalability and modularity of the system, as the fusion algorithm needs to be adjusted to the measuring properties of each sensor. Lidar as mentioned in Section 3.2.2 for example, delivers data about the rear end of a vehicle, whereas radar produces data about the rear axle of a vehicle. These two pieces of information about the tracked object now need to be fused in a meaningful manner. Another limitation is that extending the fusion with a new sensor sometimes requires a redesign of the fusion algorithm; in contrast, high-level fusion features a standardised object list, as interface to the fusion unit, thereby facilitating the enhancement through the addition of sensors.

#### 3.3.4.2 High-level fusion

The *high-level* or *decision-level* fusion approach merges data already pre-processed by the sensor. Objects and object lists (corresponding to decisions made by the sensor) are exchanged between the sensors and the fusion layer. The objects are aligned and merged in the fusion block. This allows an easy extension of the architecture (illustrated in Figure 3.10) through additional sensors, as a result of defined interfaces, which enable high modularity and scalability.

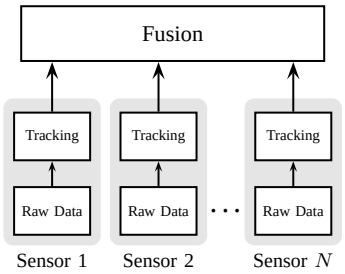


**Figure 3.10:** Architecture for high-level fusion (Aeberhard and Kaempchen, 2011)

ADAS applications which demand simplicity and modularity prefer this methodology for interpreting and merging the measurements from sensors. Furthermore, adding multiple sensors with different measurement principles does not imply a fusion concept redesign, as the interface between sensors and the fusion unit is generic (Floudas et al., 2007; Takizawa, Yamada, and Ito, 2004).

#### 3.3.4.3 Feature-level fusion

Feature-level fusion aims to combine the advantages of both the low (or raw) level fusion and the high (or decision) level fusion, by limiting the disadvantages to a minimum (Kaempchen, 2007). The architecture for feature-level fusion can be seen in Figure 3.11.

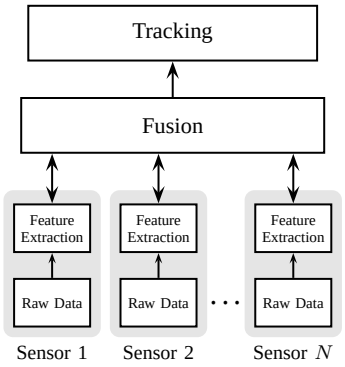


**Figure 3.11:** Architecture for feature-level fusion (Aeberhard and Kaempchen, 2011)

The architecture borrows from the high-level fusion the principle of keeping generic interfaces to the fusion unit. Therefore, each sensor uses its specific measurement principle to extract the features of a detected object. The detected objects, enhanced with the sensor specific features gained about the object, are forwarded to the fusion unit. Due to the generic interface, the fusion unit can be extended by several sensors without touching the algorithm of every sensor in the system, in contrast to a low-level fusion architecture (Kaempchen, 2007). In this way, the system is scalable and the interfaces to the sensors are reusable. Feature-level fusion is suitable for various applications in the field of advanced driver assistance systems (Kaempchen, Buehler, and Dietmayer, 2005; Mählisch et al., 2006).

## 3.4 Conclusion

The survey of the literature has revealed that the automotive sector is moving towards a future where integrated vehicle safety systems will support the driver in a wide range of traffic contexts, from warning the driver about potential dangers through to autonomous deployment of crash mitigation or avoidance mechanisms. Such integrated vehicle safety systems will combine data from several sensors and intelligent algorithms, to predict accidents and their associated collision parameters, and to take appropriate safety-enhancing decisions and actions. This chapter presents an overview of advanced safety systems, comprising active safety systems and passive safety systems. Key points from the overview are summarised below

*Accident phases:* The main phases associated with motor vehicle accidents are presented in the literature as: pre-crash phase, crash phase, and post-crash phase.

*Automotive sensors and data fusion:* Common automotive sensors presented are RADAR, LIDAR, GPS, and ultrasonic sensors. Some publications have also reported research on additional information provided by vehicle-to-vehicle communication about vehicles, drivers and the surrounding environment, to support predictions by an intelligent vehicle and its actions in relation to accidents. Other research has investigated sensor data fusion, geared towards improving the accuracy and resilience of the perception by the vehicle of the environment around it.

*Critical time for activating collision avoidance mechanisms:* An important finding from the overview presented in this chapter is that it has been reported in the literature that the critical time for activating collision avoidance mechanisms should be at least 500 ms before the collision occurs. Hence, the doctoral work reported in this document has adopted 500 ms as the total time for extracting the crash constellation and for the ensuing deployment of the relevant collision mitigation mechanism(s).

The background material presented in this chapter is followed, in the next chapter, by a literature review which focuses on techniques for predicting motor vehicle collisions.

# 4 Review of Prediction Techniques for Collisions Between Motor Vehicles

To be able to extract the constellation of a crash, the active safety system of the ego vehicle will be required to predict the prospective collision and then compute vehicle parameters deemed to influence significantly the severity of a collision.

This chapter reviews collision prediction techniques for motor vehicles. The prediction of a collision requires the estimation of the movement of other vehicles relative to the ego vehicle. Thus, this chapter also presents a review of the literature on trajectory prediction techniques, and on the state estimation filters which are typically included in techniques used for predicting collisions. As crash severity is an important consideration for this thesis, this chapter also reviews the literature on the prediction of the severity of a collision and on vehicle collision parameters associated with crash severity. Finally, the chapter presents the outstanding research questions addressed by the thesis.

## 4.1 Taxonomy of collision prediction techniques

The process of extracting a crash constellation consists of two main steps: (i) the estimation of the trajectory of each of the vehicles which are about to collide, followed by (ii) the estimation of the possible points where the collision could occur along the vehicle paths or estimation of collision probabilities. Collision detection techniques repeatedly search for trajectories, of the object vehicle relative to the ego vehicle, which would lead to a possible collision.

Collision avoidance and trajectory planning techniques have been excluded from this review. The reason for considering them to be outside the scope of this thesis is as follows. The planning of the trajectory of the ego vehicle is a key element of driver assistance systems for highly automated vehicles; it takes many factors into

account (Rathgeber et al., 2015), including collision avoidance. Collision avoidance techniques continuously search for collision-free trajectories, and evaluate a set of evasive driving manoeuvres if a collision is possible (Söntges and Althoff, 2015). Thus, the problem space of collision avoidance techniques, and of the associated trajectory planning techniques, is (to borrow terminology from set theory) the complement of the focal area of collision detection as addressed in this thesis.

Figure 4.1 displays a taxonomy of collision prediction techniques for motor vehicles. As explained above, collision prediction techniques work in concert with trajectory estimation techniques. Hence, a classification of the associated trajectory prediction techniques and motor vehicle motion models are shown in Figure 4.2 and Figure 4.3, respectively. Often, in the manoeuvre-based trajectory prediction approach, the manoeuvre intention is detected in the early stage of the manoeuvre, such that knowledge of the manoeuvre can be used to predict its subsequent physical states. Hence, Figure 4.4 shows a classification of techniques for detecting driving manoeuvre intentions. The family of techniques included in the crash constellation algorithm proposed in Chapter 6 of this thesis are the shaded boxes shown in the classification diagrams, to position them in the context of the domain knowledge relevant to the thesis. Harvard System referencing indices corresponding to the reference numbers shown in the classification diagrams are given in Table C.1.

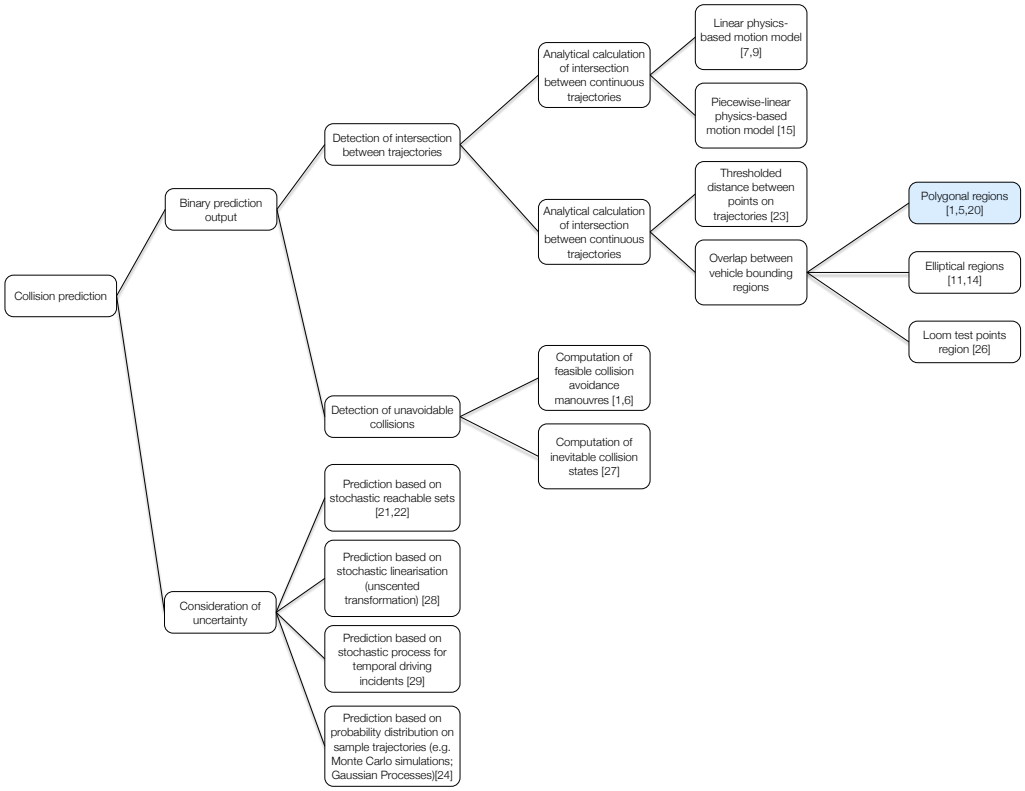


**Figure 4.1:** Classification of techniques for predicting a collision between motor vehicles. (The classification was synthesised based on the structure and content of (Lefèvre, Vasquez, and Laugier, 2014))

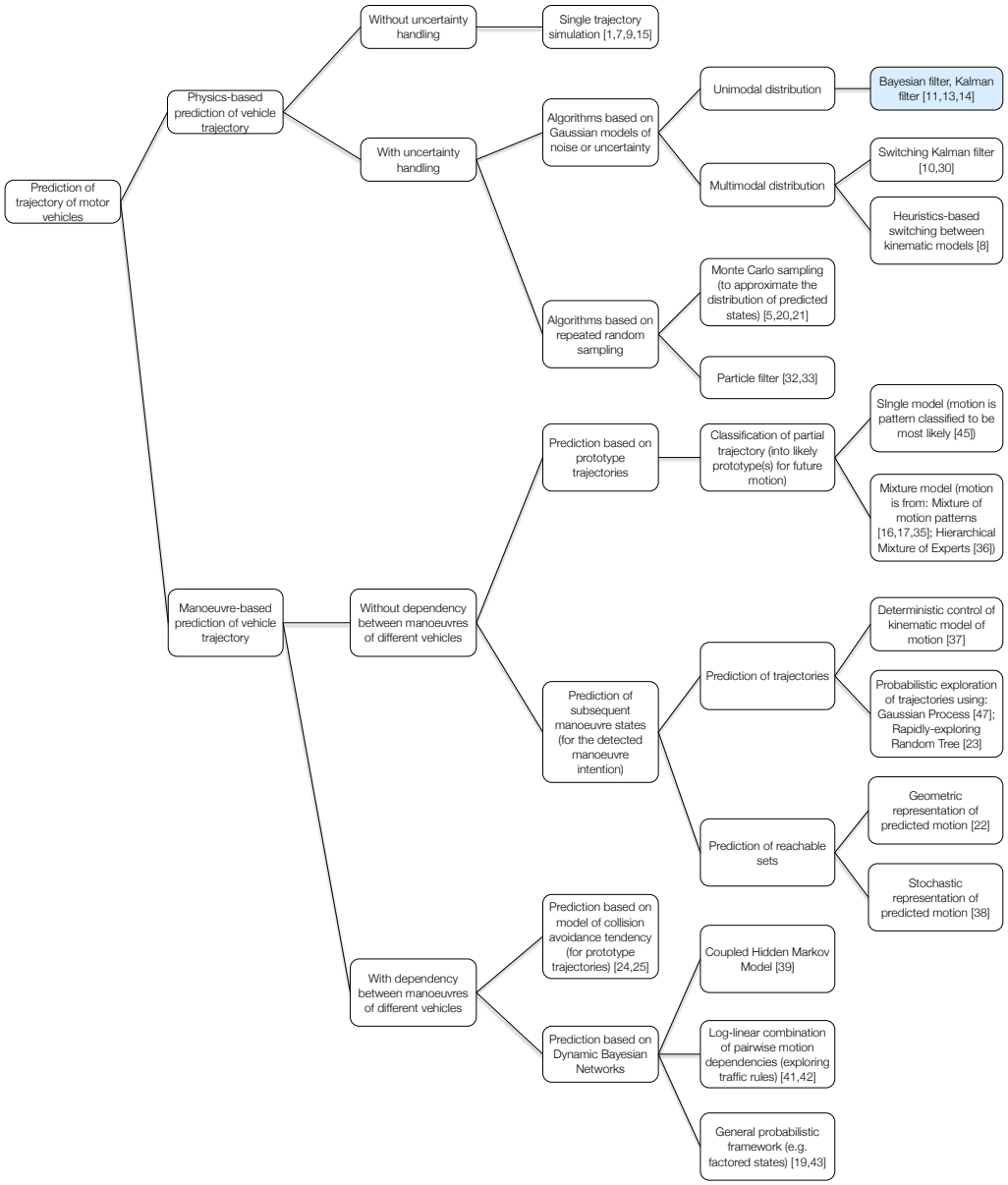


**Figure 4.2:** Classification of techniques for predicting the trajectory of a tracked motor vehicle. (The classification was synthesised based on the structure and content of (Lefèvre, Vasquez, and Laugier, 2014))

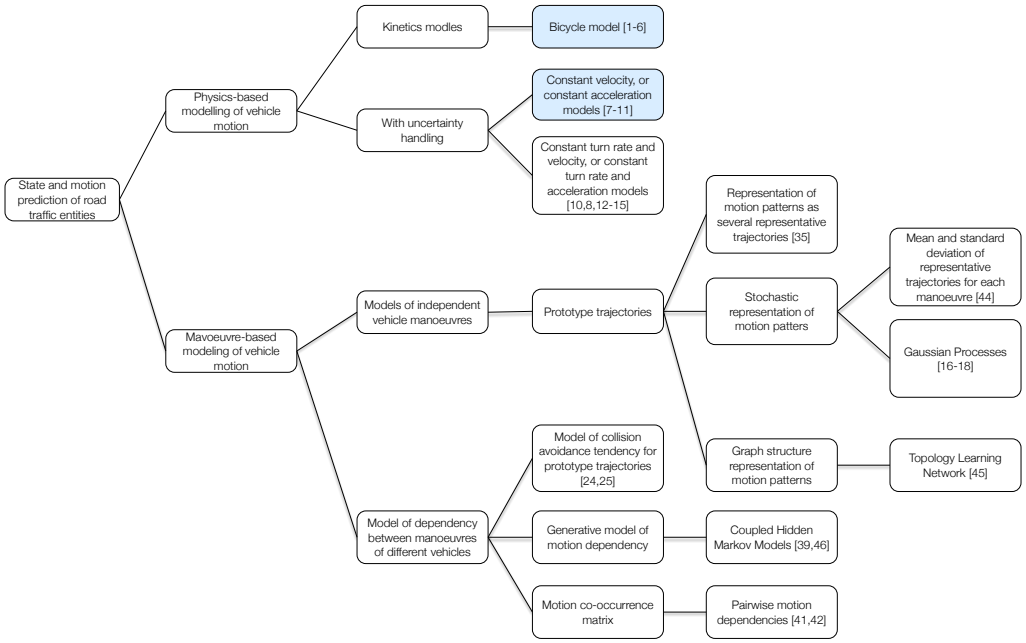


**Figure 4.3:** Classification of motor vehicle motion models which are embedded in trajectory prediction techniques. (The classification was synthesised based on the structure and content of (Lefèvre, Vasquez, and Laugier, 2014)

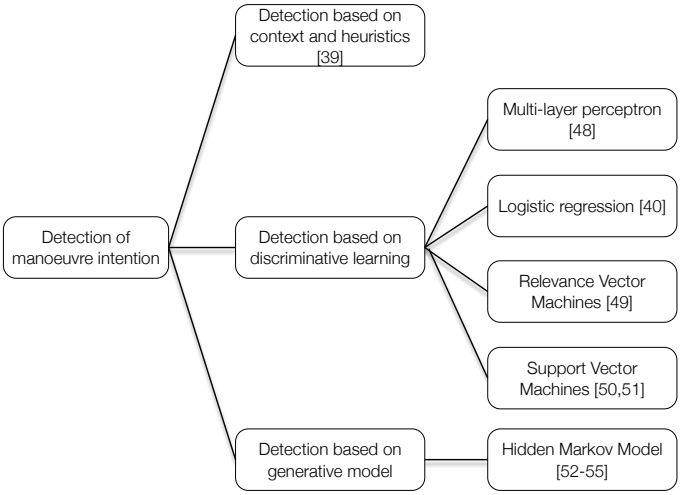


**Figure 4.4:** Classification of techniques for detecting driving manoeuvre intentions for motor vehicles. (The classification was synthesised based on the structure and content of (Lefèvre, Vasquez, and Laugier, 2014))

## 4.2 Filtering techniques for state estimation

Active safety systems respond to a dynamic environment, around the ego vehicle, which may include bikes, pedestrians, and other vehicles. To enable active safety systems to act according to the present situation, the position and movements of these traffic participants need to be tracked over time, during the so-called "tracking" process. The aim of the state estimation process is to estimate the state of participants (generically called "objects", in this chapter); object state includes their relative position, speed, heading and dimensions. The properties of a state (represented by hidden variables) cannot be measured directly by a sensor and need to be estimated recursively over time by processing noisy and possibly incomplete measurements (Arulampalam et al., 2002). Different estimation techniques are described in (Bar-Shalom, 1987, 1990; Bishop, 1995; Blackrnan and House, 1999; Ristic, Arulampalm, and Gordon, 2004). This section describes different approaches for the state estimation process.

### 4.2.1 Kalman filter

Introduced by Kalman (1960), the Kalman filtering technique offers a recursive solution for the state estimation problem, with low computational expense. The Kalman filter considers the control input of the ego system, the measurement update, and the motion model for the tracked target. Based on its slim recursive operation for processing the present and future measurements, the filter is used in numerous real-time applications (Barrios, Motai, and Huston, 2016). However, due to the assumption that the process and measurement noise vectors are mutually uncorrelated (based on a white Gaussian distribution), and zero-mean, the field of application is restricted to linear systems.

For many real world applications, a tracking algorithm needs to cope with a highly dynamic environment; therefore, the extended Kalman filter (EKF) is designed for non-linear functions. The extended Kalman filter uses a first- or higher-order Taylor series to linearise the non-linear function to a Gaussian distribution before handing it to the recursive Kalman filter. Despite the high error rates which the extended Kalman filter produces for highly non-linear functions, it is widely used in the automotive area for object tracking with range sensors (Kaempchen, 2007). Over the years, different approaches have emerged from the initial idea according to their

field of application supporting non-linear systems. These approaches include the unscented Kalman filter (UKF) and the emerging group of sigma point Kalman filters (SPKF).

To overcome the limitations of the extended Kalman filter in highly non-linear functions and its implementation difficulties associated with the use of Jacobi matrices (substituting the linearisation part of the Kalman filter), the unscented Kalman filter utilises non-linear transformations which propagate means and covariance information (Julier and Uhlmann, 2004). The sigma points representing the Gaussian probability density function are transformed using a non-linear function. These points form the basis for estimating the mean and covariance representing the non-linearity.

The extended Kalman filter is still the most widely used filter for non-linear systems in the automotive area combining computational complexity and representational flexibility (Julier and Uhlmann, 2004). To simulate real-world behaviour, it is important to work with filters which are used in state-of-the art state estimation and sensor fusion systems, for their modelling capabilities and behaviour including their strengths and weaknesses. Therefore, the extended Kalman filter has been chosen for the core of the state estimation module in the simulation model. It is described in detail in Section G.1.

### 4.2.2 Bayesian filter

The main goal of the state estimation, as already mentioned is to predict recursively the objects states. The optimal solution for this task is the recursive Bayesian estimation technique, which uses the available statistical information about the system and model state in each recursion cycle, including the accuracy of the estimate (Arulampalam et al., 2002). Some researchers try to lower the computational demands of Bayesian filtering techniques for multi-target tracking, to meet the requirements of automotive standards (Coué et al., 2006; Shao, Huang, and Lee, 2010). However, the lack of general analytical solutions and computational demands hinder the use of the Bayesian filtering method for real-time systems (Kaempchen, 2007).

### 4.2.3 Particle filter

A further approach, to estimate the state of the environment around a vehicle uses particle filters (He et al., 2016; Liu, Fang, and Chen, 2017). In this method the dynamics of a complex system (such as the environment perception module) is modelled accurately with non-linear and non-Gaussian elements. It is stated in the literature, that particle filters are based on sequential Monte Carlo simulated samples representing the probability densities with point masses, the "particles" (Arulampalam et al., 2002; Eidehall, Schon, and Gustafsson, 2005). Particle filters feature two models, the system model describing the development of a state and the measurement model relating the noise to the state. This leads to a recursive update of the tracked state at each measurement update. Having this in mind allows the testing of several hypothesis in parallel about states of tracked objects, featuring a fast adaptation to measurement noise and incompleteness (Arulampalam et al., 2002; Gordon, Salmond, and Smith, 1993; Röckl, Gacnik, and Schomerus, 2008). The number of samples per cycle directly influences the computational expenses, and approaches the Bayesian filtering technique as more particles are used.

## 4.3 Collision prediction

Active safety systems, as mentioned in Section 3.1, use different algorithms to interpret and sense the vehicle surroundings. To anticipate a potential accident, trajectory estimation algorithms are used for diagnosing the relative movement of the other vehicles and objects around the ego vehicle. Different approaches for detecting hazardous situations in the area of vehicle safety, have been proposed in various publications (Ameling, 2002; Busch, 2005; Kaempchen, 2007; Karrenberg, 2008, 2000; Lages, 2001).

This section assesses different approaches reported in the literature, for detecting an impending collision. The main focus of recent activities can be grouped into two main groups:

- Trajectories based on physical constraints a vehicle is limited by (Section 4.3.1, 4.4.1, 4.4.2)

- Statistical assumptions leading to inevitable collision states based on probability functions (Section 4.3.2)

### 4.3.1 Vehicle collision detection using dynamics-based trajectory prediction

In the literature different approaches are described using driving dynamics to derive an algorithm for detecting impending collisions. Lages, 2001 defines a circular trajectory based on the velocity relative to the tracked object, which allows the ego vehicle to escape the collision (see Figure 4.5). If steering would not prevent a collision, additional braking manoeuvres are verified before the unavoidable collision is detected and the emergency brake is triggered. A drawback of this approach is, that a circular trajectory does not account for the effect of the steadily increasing brake and steering forces upon the movement of a vehicle. The change in the heading of a vehicle which diverges from the straight-on movement into a circular path needs to also be described. Furthermore, the steering velocity is limited by human constraints and it is not considered in this algorithm.

Kopischke (1999) and Ameling (2002) follow a similar approach which assesses the impending collision by checking the braking and steering options, as illustrated by Figure 4.5. Instead of representing the escapes trajectories by a circle, different splines or clothoids are used for representing the maximum trajectories which the vehicle can take.

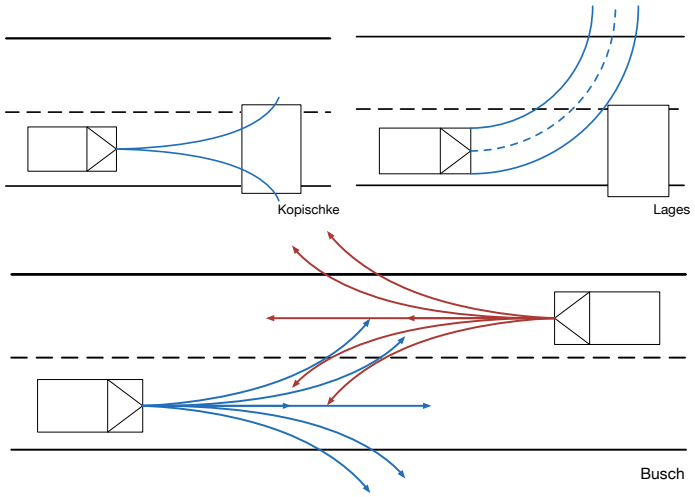


**Figure 4.5:** Collision prediction algorithms by Kopischke (2000) (top left), Busch (2005) (bottom), and Lages (2001) (top right)

Both approaches are only suitable for scenarios which include static objects or vehicles moving at a lateral or longitudinal constant velocity.

Busch (2005) refined these algorithms by using a simulation tool which generated realistic trajectories based on statistical analysis on accident databases. These trajectories of the colliding vehicles consider the vehicle driving dynamics. In the pre-crash phase, at every time step $t$ for each vehicle six possible trajectories are computed followed by a check for colliding trajectories $n_{collisions}$. The collision index $p_{col}$ is defined by

$$p_{col}(t) = \frac{n_{collisions}(t)}{36} \tag{4.1}$$

The collision is inevitable, if the index equals 1, assuming that no escape trajectory is given (Figure 4.5). For extracting the crash constellation, these algorithms need to be extended by:

- considering physical limitations in the computation of the trajectories
- letting sensor variances influence the outcome of object tracking
- increasing the numbers of trajectories calculated at a time

### 4.3.2 Inevitable collision states and crash probability

An Inevitable Collision State (ICS) for a robotic system is a state for which, a collision with an obstacle eventually occurs, no matter what the future trajectory followed by the system is (Fraichard and Asama, 2003). In the paper of Parthasarathi and Fraichard (2007) a collision state-checker which assumes a car-like behaviour is described, and a generic approach is presented by Martinez-Gomez and Fraichard (2008). Bautin, Martinez-Gomez, and Fraichard (2010) strengthened the probabilistic perspective on ICS by modelling the future behaviour of the robots in the workspace. ICSs are widely researched in the robotic domain and have been mapped to automotive applications which support overtaking manoeuvres or safety applications.

The ICS method considers numerous static and movable objects $\mathcal{B}_i$ for $i = 1....n_b$ provided with a possible set of trajectories acting in a workspace $\mathcal{W}$ of a robot $\mathcal{A}$. These trajectories or dynamics are described as a differential equation

$$\dot{s} = f\,(s,u) \tag{4.2}$$

with $u \in \mathcal{U}$ representing a control input and $\dot{s}$ the derivative of the state $s \in \mathcal{S}$; $s$ and $u$ respectively define the *state space* $\mathcal{S}$ and *control space* $\mathcal{U}$ of a robot. The union of all dynamic and non-dynamic objects is described as follows:

$$\mathcal{B} = \bigcup_{i=1}^{n_b} (\mathcal{B}_i) \tag{4.3}$$

Martinez-Gomez and Fraichard (2008) define a set of control trajectories $\tilde{\mathcal{U}}$ of objects which can be represented by controls $u$ over time $t$ with

$$\tilde{u} : [0,\infty( \rightarrow U \tag{4.4}$$

A robot $\mathcal{B}_i$ will occupy a subset of the workspace $\mathcal{B}_i(t)$ in the future. A state trajectory is therefore a derived control trajectory containing states $\tilde{u}(s(0),t)$ at different time steps $t$.

Based on the formulas 4.2 to 4.4 a definition of a state $s$ representing an ICS can be given by:

$$ICS(\mathcal{B}) = \{\forall \tilde{u} \in \tilde{\mathcal{U}}, \exists t, \exists \mathcal{B}, \mathcal{A}(\tilde{u}(s,t)) \cup \mathcal{B}(t) \neq \emptyset\} \tag{4.5}$$

and for a collision with a particular object $\mathcal{B}_i$, it is as follows (Bautin, Martinez-Gomez, and Fraichard, 2010):

$$ICS(\mathcal{B}_i) = \{\forall \tilde{u} \in \tilde{\mathcal{U}}, \exists t, \exists \mathcal{B}_i, \mathcal{A}(\tilde{u}(s,t)) \cup \mathcal{B}_i(t) \neq \emptyset\} \tag{4.6}$$

The computational demands are rather high due to the infinite number of possible control inputs needed to be calculated. To gain a performance enhancement, a

subset of the possible trajectories and therefore, an ICS approximation is processed (Martinez-Gomez and Fraichard, 2008):

$$ICS(\mathcal{B}) \subseteq \bigcap_{\tilde{u}\in\mathcal{I}} ICS(\mathcal{B}_i,\tilde{u}) \tag{4.7}$$

with $\mathcal{I}$ representing a subset of the control space $\tilde{\mathcal{U}}$.

Althoff et al. (2011) developed two improvements for computing unions of inevitable collision states, as the computational problem is very demanding due to the fact that inevitable collision states cannot be computed for each obstacle individually. For every new obstacle entering the workspace, the inevitable collision states need to be recalculated by the following formula which state that the computation of the ICS for all objects is not equal to processing the union of ICS calculations:

$$ICS(\mathcal{B}) \neq \bigcup_{i=1}^{n_b} ICS(\mathcal{B}_i) \tag{4.8}$$

Althoff et al. (2011) calculated the ICS in a sequential manner, by forwarding the collision free trajectories relative to the start obstacle to the ICS calculation for subsequent obstacles. Bautin, Martinez-Gomez, and Fraichard (2010) extended the algorithm to support probabilistic collision state checks by assigning a probability measure to the control input of the obstacle which would result in the trajectories that the obstacle might take in the future. Taking into account the peculiarities of motorcycles, the investigation reported in

## 4.4 Vehicle trajectory estimation

### 4.4.1 Representative trajectories

Karrenberg (2008) presented in his work an approach of using representative trajectories to avoid an impending collision. For his approach 20 participants circumnavigated an obstacle resulting in various trajectories (Figure 4.6).

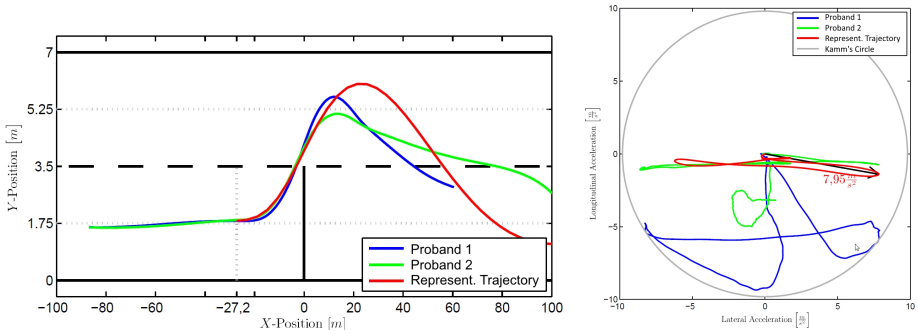


**Figure 4.6:** (a) Trajectories circumnavigating an obstacle at point $x(0)$, and (b) the resulting tire forces shown on the Kamm's circle (Karrenberg, 2008)

The trajectories compared to each other by considering the Kamm's circle[1], as illustrated in Figure 4.6, lead to an optimised trajectory (red) which is characterised by the following points:

- the trajectory minimises the required friction force.
- the trajectory is calculated ideally around the obstacle.
- the trajectory is optimised for collision avoidance.

This approach is not considered for use in the work presented in this thesis, because its output is a single trajectory and is thus not applicable for collision prediction, as the driver may take several actions before a collision occurs, resulting in a different crash constellation extraction.

Trajectory planning used for applications in the ADAS highly automated driving domain are implemented with the aim deriving a comfortable and collision free trajectory for the motion of the vehicle based on the vehicles physics (Li et al., 2016, 2017). In theory these algorithms are taking the navigation goals also often called as reference trajectories to a motion level and are searching for an optimum in the local space for trajectories. An example implementation is shown in (Li et al., 2017).

1 Explained in more detail in section 4.4.2

### 4.4.2 Techniques which include tire-road friction in the dynamics model for predicting colliding trajectories

The approach reported in (Kaempchen, Schiele, and Dietmayer, 2009) considers physical constraints which limit the manoeuvres of vehicles. The constraints are directly dependent on the friction between the tires and the road surface (Aaltonen, 1979; Gustafsson, 1998; Lee, Hedrick, and Yi, 2004), whereby the friction force is depicted as $F_f$ in Figure 4.7. Figure 4.7 illustrates the forces applied in a system vehicle during an acceleration phase. Böhmländer et al. (2014) also used the vehicle dynamics when predicting trajectories for estimating the risk of a collision.

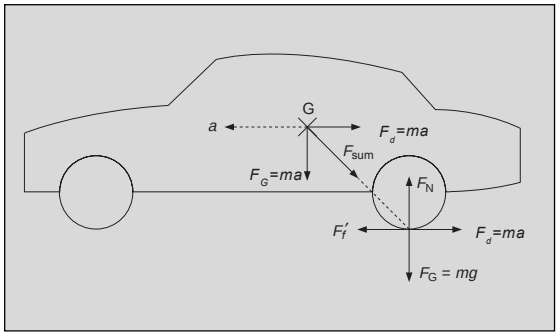


**Figure 4.7:** Simplified representation of forces which influence a vehicle during acceleration (Risch, 2002)

The acceleration force $F_d$ defined by the vehicle mass $m$ and acceleration $a$,

$$F_d = ma \tag{4.9}$$

applies at the centre of gravity ($G$) and is directly linked to the force of inertia $F_d$. According to (Risch, 2002), the sum of the forces $F_{sum}$ is the addition of the forces of inertia $F_d$, gravity $F_G$ and friction. Furthermore, the gravity force is equal to the normal force representing the reaction force of the ground onto the tyres,

$$F_N = mg \tag{4.10}$$

where m is the vehicle mass and g the gravity coefficient. In addition, the inertia force $F_d$ is equal to the friction force $F_f$ resulting from static friction between the tyres and the ground.

$$F_f = \mu' mg \tag{4.11}$$

where $\mu'$ is the static friction coefficient. Therefore, combining equations 4.9 and 4.11 leads to the maximal acceleration

$$a_{max} = \mu' g \tag{4.12}$$

The friction coefficient due to the surface of the road and the tire is limited to $\mu' \in [0; 1]$. Equation 4.12 is only an estimate resulting from a theoretical derivation; today's sport vehicles can reach under ideal conditions (extremely sticky tires) a maximum deceleration of 11 m/s$^2$ (Jansson, 2004; Risch, 2002).

The magnitude of the acceleration vector $a$ is split into a longitudinal $a_l$[1] and a lateral (cross) component $a_c$[2] (Kaempchen, Schiele, and Dietmayer, 2009). Combined with an angle $\boldsymbol{\gamma}$ representing the orientation of the driving wheels, the acceleration (see Figure 4.8) allows different possible turning manoeuvres of a vehicle.

$$a_l = a \cos(\boldsymbol{\gamma}) \tag{4.13}$$

$$a_c = a \sin(\boldsymbol{\gamma}) \tag{4.14}$$

Representing the acceleration magnitude $a$ and the angle $\boldsymbol{\gamma}$ according to the Kamm's circle, presented in Figure 4.8 (a), leads to the trajectories illustrated in Figure 4.8 (b). Figure 4.8 (b) depicts the case of a vehicle moving towards the positive x-axis. Hence, the x-axis corresponds to the longitudinal direction shown on the Kamm's circle. The acceleration is either positive (the vehicle is accelerating) or negative (the vehicle is braking).

1 In the driving direction
2 Representing the orthogonal acceleration

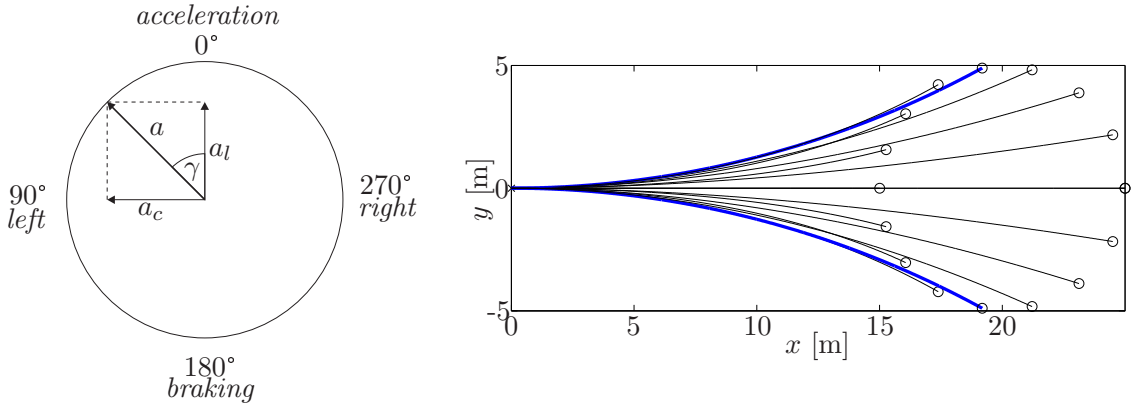


(a) (b)

**Figure 4.8:** (a) Kamm's circle. (b) Possible trajectories for $a$=10 m/s$^2$ and $v_0$=20 m/s, predicted over a drive lasting 1s and a range of driving-wheel orientations. (Kaempchen, Schiele, and Dietmayer, 2009)

The following equations (Kaempchen, Schiele, and Dietmayer, 2009) summarise the trajectories, shown in Figure 4.8 (b), describing the motion of a vehicle subject to the constraints (see Equation 4.12, 4.13 and 4.14) depicted by a Kamm's circle.

$$\dot{\boldsymbol{v}}(t) = a_{max}\cos(\boldsymbol{\gamma}) \tag{4.15}$$

$$\dot{\boldsymbol{\psi}}(t) = \frac{a_{max}\sin(\boldsymbol{\gamma})}{\boldsymbol{v}(t)} \tag{4.16}$$

$$\dot{\boldsymbol{x}}(t) = \boldsymbol{v}(t)\cos(\boldsymbol{\psi}(t)) \tag{4.17}$$

$$\dot{\boldsymbol{y}}(t) = \boldsymbol{v}(t)\sin(\boldsymbol{\psi}(t)) \tag{4.18}$$

The motion model, and therefore the underlying vehicle dynamics, used for the calculated trajectories in this approach are similar to a coordinated turn model (Kaempchen, Schiele, and Dietmayer, 2009). The resulting equations are

$$\boldsymbol{v}_n = \boldsymbol{v}_{n-1} + a_{max}\cos(\boldsymbol{\gamma})\Delta t \tag{4.19}$$

$$\boldsymbol{\psi}_n = \boldsymbol{\psi}_{n-1} + \min\left(\frac{a_{max}\sin(\boldsymbol{\gamma})}{\boldsymbol{v}_{n-1}}, \frac{\boldsymbol{v}_n}{\boldsymbol{r}_{min}}\right)\Delta t \tag{4.20}$$

$$\boldsymbol{x}_n = \boldsymbol{x}_{n-1} + \left(\boldsymbol{v}_{n-1}\Delta t + \frac{a_{max}\Delta t^2}{2}\right)\cos(\boldsymbol{\psi}_n) \tag{4.21}$$

$$\boldsymbol{y}_n = \boldsymbol{y}_{n-1} + \left(\boldsymbol{v}_{n-1}\Delta t + \frac{a_{max}\Delta t^2}{2}\right)\sin(\boldsymbol{\psi}_n) \tag{4.22}$$

with $v$ for the velocity, $[x; y]$ for the position, and $\psi$ for the yaw angle. For cases of low velocities the turn radius $\boldsymbol{r}_{min}$ limits the vehicles turn rate. These trajectories are calculated iteratively at each $\Delta t$ time step, spanning a fan of trajectories. A simplified version was introduced by Kopischke (2000) assuming that a collision is inevitable if the maximal possible trajectories lead to an object.
The motion model described above has limitations with regards to reproducing real-world behaviour because the acceleration in both lateral and longitudinal directions depends on the current speed of the vehicle; acceleration is limited particularly at high speeds. For instance, evasive steering manoeuvres are not possible in higher speed ranges. This needs to be considered, if this algorithm is used as basis for the extraction of the crash constellation. The Kamm's circle needs to be adjusted such that it is not represented with a perfect circle as shown in Figure 4.8 (a).

## 4.5 Prediction of crash severity and associated vehicle collision parameters

Road safety and inherently injury severity can be addressed at different levels of abstraction. Schlögl and Stütz (2017) gives an overview of different data sources and the corresponding uncertainties with regards to data quality for road safety analysis. The separation is proposed as follows:

- Accident databases featuring information about the accident participants (for example trucks, vehicles, pedestrians), the occupants (including severity scores), weather conditions, roadway lighting, and many more.
- Road geometry and road conditions. These can be obtained by transportation administrations through so called Graph Integration Platforms (GIP).
- Weather data influencing the accident occurrence are issued by institutions such as the World Meteorological Organization (WMO) who provide standardised measuring procedures.
- Traffic volume influences accident occurrences; it is measured by national highway administration offices in an automatic manner using camera systems.

These sources provide an immense amount of data supporting road safety analysis. Different researchers are analysed the road geometry and its impact on accident

occurrences. Elvik (2017) illustrates the effect of roundabouts on traffic incidents. This study showed that change in road geometry would decrease fatal accidents by 65% and reduce injury rates by 45%. Other factors, such as the impact of human factors (for example aggressive behaviour or sleeping), were investigated by Bener et al. (2017). These road safety analyses were mostly conducted to find out root causes of accidents. For example, a study of traffic volumes on motorways in England using a logistic regression model was conducted in (Michalaki et al., 2015). The focus of the doctoral work presented in this thesis is on cases where the accident is not avoidable, to support the deployment of appropriate safety mechanisms. Generally speaking a head-on collision with a delta in velocity of 50km/h can have different root causes (for example driver drowsiness or distraction) but the injury risk is determined by physical constraints, for example the structure of the colliding vehicles (e.g. truck versus van), differences in vehicle velocities, crash angles, and more. These parameters which relate to the severity of a collision need to be determined

### 4.5.1 Approaches for predicting the severity of a crash

Müller et al. (2016) tries to detect an unavoidable collision during the pre-crash phase at a time to collision of 512ms using a trained neural net estimating the severity of a collision. The paper uses crash severity measures as Occupant Loan Criterion (OLC) which measures the crash impulse an occupant would suffer during a crash. This criterion is mainly used for application of active seat belt restraint systems.

Furthermore, a mass spring model is applied to model the crash behaviour of a collision. The functionality of such models is explained in more detail in (Appel, Krabbel, and Vetter, 2013).

To simulate various collision scenarios Müller et al. (2016) implemented a simulation chain of different tools allowing to generate multiple crash scenarios. Their work focused mainly on the severity outcome of a collision and it generated a crash severity distribution over collision scenarios.

### 4.5.2 Vehicle collision parameters linked to road traffic injuries

Haddon Jr (1980) grouped risk factors for road traffic injuries into three categories, respectively linked to the human, the vehicle and the environment. He further divided the factors into sub-categories related to accident phases corresponding to before, during, and after a collision. A number of studies have assessed the complex interactions between crash-injury severity and these factors (Boufous et al., 2008; Conroy et al., 2008). In particular, a variety of statistical analysis techniques have been applied to crash-severity data (Savolainen et al., 2011). A small sample of available sources is listed in Table 4.1 below. For analyses on crash databases the

**Table 4.1:** Available data sources for accident analyses using statistical methods

| Data Source | Database parameters available |
|---|---|
| US Fatality Analysis Reporting System | - Accident, Vehicle and Causality<br>- No detailed description of the collision parameters<br>- No injury severity score |
| UK Road Safety Data | - Accident, Vehicle and Casuality<br>- No detailled description of the collision parameters<br>- No injury severity score |
| National Automotive Sampling System Crashworthiness Data System (NASS/ CDS) | - Passenger vehicle crash worthiness reports<br>- Sophisticated injury reports of passengers<br>- Detailled description of vehicle design<br>- Detailled collision constellation description |
| German In-Depth Accident Study GIDAS database | - Passenger vehicle crash worthiness reports<br>- Sophisticated injury reports of passengers<br>- Detailled description of vehicle design<br>- Detailled collision constellation description |

quality of the inherited data is of high importance as described by (Imprialou and Quddus, 2017) with the "garbage in garbage out" (GIGO) principle. This principle describes the direct link between the processed data and the quality of the output from the analysis (Oliveira, Rodrigues, and Henriques, 2005). Therefore, the data source is an important factor which influences the credibility of the analysis outcome. Schlögl and Stütz (2017) states that the overall increasing availability of data does not imply that the data has also improved alongside. (Schlögl and Stütz, 2017) gives a well described guidelines for different data sources and methodological considerations to be taken into account when working with numerous data sources and the

associated uncertainty for road safety analysis.The open literature has been searched to identify the significant pre-crash vehicle parameters relevant to the research reported herein, towards adaptive pre-crash active safety mechanisms. However, the search has been fruitless. Hitherto, researchers have devoted their attention mostly to: (i) factors which cause a collision. This information has been used to devise or deploy (in the pre-crash phase) countermeasures to prevent crashes from occurring. (ii) factors which influence crash severity. This information has been used to devise or activate (in the crash phase) passive-safety countermeasures to prevent injury during a crash or reduce its severity. (iii) factors which influence the outcomes of injuries which have been sustained in an accident. This information has been used to devise or deploy (in the post-crash phase) life-sustaining actions to reduce the adverse outcomes of a collision which has occurred.

There is a knowledge gap about what are the significant collision parameters for vehicles in a frontal collision. The answer to this question will feed into the development or activation of vehicle-based countermeasures, tuned to match the measured parameters, so as to prevent injury or reduce its severity. The vehicle parameters sought in this project must be measurable with automotive sensors in the pre-crash phase, and they are not linked to humans or the environment.

## 4.6 Outstanding research questions addressed by this doctoral research

Two focal research questions, which are addressed by the doctoral research presented in this thesis, emerge from the literature review presented in the previous sections which cover the state of the art in the underlying research domain. They are:

- What are the most significant collision parameters which influence the injury severity for a frontal collision between two motor vehicles? This set of parameters is called "collision constellation", in this thesis.
- How to extract the constellation of a crash before the accident occurs?

Furthermore, the secondary research questions given below are addressed:

- How to integrate physical constraints, imposed on the rate of acceleration of a real vehicle, together with data from vehicle-to-vehicle communication, into the crash constellation extraction algorithm?
- How to integrate uncertainties, associated with the data captured by sensors of a real vehicle, into a simulation model devised for assessing the performance of crash constellation extraction algorithms?

A number of issues need to be addressed when investigating solutions towards answering these questions. As presented in Section 3.1 a key limitation of current safety systems is linked to the limited foresight which current sensors provide for predicting an impending collision. Future safety systems for activating safety measures are required to gain sufficient and reliable information about an impending collision and therefore need active sensing devices such as radars, lidars, and vision based systems. These sensors are already used for various mitigation and collision avoidance systems. For safety applications nevertheless the demands on the detection accuracy are higher due to the critical nature of the tasks (i.e. accident prevention or damage limitation) for which the information gathered by these sensors is used. Therefore, the level of accuracy for detecting an impending collision needs to be assessed and maximised.

As mentioned in Section 3.1 future automotive safety applications rely on various sensors with different sensing capabilities. A sensor fusion system as described in Section 3.3 combined with an estimation of the state of surrounding objects which is detailed in Section 4.2, can allow a reliable extraction of the state of objects over time. The sensing of these objects is afflicted with measurement variances. Hence, another quest in this research is the investigation of a solution which enhances current collision detection algorithms with sensor variances. Section 4.3 gives an overview of current collision detection and trajectory planning algorithms. These support the prediction of impending collisions.

Referring to Section 2.1 a set of parameters need to be identified using stochastic analysis to form a collision constellation.

## 4.7 Conclusion

Given the changing nature of the state of vehicle dynamics and of its surroundings, the survey of the literature has revealed that state estimation techniques and collision prediction algorithms have received significant attention from researchers.

Furthermore, risk factors for road traffic injuries are grouped in the literature into three categories, respectively linked to the human, the vehicle and the environment. The factors are further divided into sub-categories related to the pre-crash, crash and post-crash phases.

*Knowledge gap:* A number of studies have assessed the complex interactions between crash-injury severity and the risk factors summarised above. However, the literature search conducted in this work has not found any previous systematic research which identifies the significant pre-crash vehicle parameters relevant to this research towards adaptive pre-crash active safety mechanisms.

To guide the primary research conducted in this project, the focal research questions which have emerged from the survey of the literature are:

- What are the most significant collision parameters which influence the injury severity for a frontal collision between two motor vehicles?
- How to extract the constellation of a crash before the accident occurs?

In addition, the secondary research questions given below were addressed:

- How to integrate physical constraints, imposed on the rate of acceleration of a real vehicle, together with data from vehicle-to-vehicle communication, into the crash constellation extraction algorithm?
- How to integrate uncertainties, associated with the data captured by sensors of a real vehicle, into a simulation model devised for assessing the performance of crash constellation extraction algorithms?

The collision parameters sought in this project must be measurable with automotive sensors in the pre-crash phase, and they are not linked to human or environmental factors.

*Practical relevance and anticipated impact outside academia:* The answers to the above research questions will feed into the development or activation of vehicle-based integrated-safety countermeasures, tuned to match the measured collision parameters, so as to prevent injury or reduce its severity. The outcomes of this research will primarily benefit road users and the automotive equipment and vehicle manufacturing industries.

The research provides important information in relation to significant collision parameters (which can be extracted in the pre-crash phase), and it has produced a computing algorithm for extracting these parameters. These two research contributions will enable automotive equipment and vehicle manufacturers to improve vehicle safety through active safety systems or driver assistance systems which prevent accidents or minimise the severity of injury in an unavoidable accident.

Improved motor vehicle safety, through the development of better protective mechanisms, will in turn reduce the number of road accidents with severe injuries or fatalities. It will thus contribute to world-wide efforts (such as those by the United Nations or the European Commission) towards safer road traffic. The reduced number of road accidents and associated fatalities and severity of injuries will also have an impact on society in general, and on the economy in particular. The latter will result from a reduction of costs and reduction of loss of potential contribution to economic activities by the affected individuals, where the said costs and losses are associated with hospitalisation, incapacitating injury or loss of human life, for example.

The next chapter presents the research conducted to identify the most significant crash parameters which impact on injury severity, and to identify collision scenarios with a high rate of severe accidents.

# 5 Identification of Significant Crash Constellation Parameters

A major step towards the extraction of the crash constellation is the identification of parameters which influence the severity of an accident. In this work, the identification is conducted as a two-stage approach. The first stage consists of secondary research to narrow down the set of considered parameters and the second stage is a regression analysis on a crash database to assess the significance of each parameter with regards to the severity of a collision.

## 5.1 Relevant literature on vehicle accident severity and related factors

### 5.1.1 Injury severity scales

Analysis of accident databases, such as the GIDAS, 2014 (GIDAS) database, are essential for identifying key parameters defining the severity of a collision (Al-Ghamdi, 2002; GIDAS, 2014; Kononen, Flannagan, and Wang, 2011; Sobhani et al., 2011; Wood et al., 2007). Most literature uses injury severity scores as an indicator for the severity of a collision, as it enables the assessment of the outcome of a crash, with reference to the injuries sustained by vehicle occupants. An overview of the recent analyses on accident databases according to the method used in the literature is given in (Sobhani et al., 2011). The majority of the researchers use the severity score as a dependent variable. Understanding the different approaches is important, in order to apply the appropriate method to the underlying database.

In the literature, parameters such as the road and its surrounding environment, human factors, and vehicle constitute the independent variables. A variety of scales are used for the dependent variable which represents the severity of a crash, to support objective interpretation. Often, the Abbreviated Injury Scale (AIS), the maximum abbreviated injury scale (MAIS), or the Injury Severity Score (ISS) are

used for the dependent variable. The use of such scales allows the identification of significant crash parameters based on comparative assessment guided by an objective measurement of injury.

The Abbreviated Injury Scale is an injury severity scoring system that classifies, on a six-point ordinal scale (1 Minor; 2 Moderate; 3 Serious; 4 Severe; 5 Critical; 6 Maximum), the severity of each injury sustained in nine body regions (Head, Face, Neck, Thorax, Abdomen, Spine, Upper Extremity, Lower Extremity, External and other). Table 5.1 shows the different AIS codes and the corresponding injury severity. The AIS code is estimated immediately after a collision. A detailed catalogue of the AIS score provides a comprehensive list of injuries and their corresponding lethality rate and category. When a collision occurs, it is most likely that an occupant would suffer more than one injury. When multiple injuries have been sustained by an individual, the highest AIS is known as the maximum AIS (MAIS). It has been used to describe overall severity given that the MAIS score highlights the highest AIS score a person received.

**Table 5.1:** Abbreviated injury scale classification (Kramer, 2008)

| AIS | Severity description | Lethality rate [%] |
|---|---|---|
| 0 | not injured | 0.00 |
| 1 | minor injury | 0.00 |
| 2 | moderate injury | 0.07 |
| 3 | serious injury | 2.91 |
| 4 | severe injury | 6.88 |
| 5 | critical injury | 32.32 |
| 6 | maximum (untreatable) injury | 100.00 |

The ISS determines not only one or the most severe injury received by a vehicle occupant, it is calculated based on the three most severe injuries suffered by a person, over all body regions. The ISS is based on six body regions (Head; Face; Chest; Abdomen; Extremities or pelvic girdle; External). The ISS is calculated as the sum of the squared values of the highest AIS severity code in each of the three most severely injured body regions. Squaring the values enables the ISS to correlate more with the lethality rate than the AIS score. The ISS score is superior to the AIS, respectively the MAIS score, but it is not suitable for the work reported herein, in which the primary collision is of interest. The prediction model for the ISS used within the GIDAS database contemplates instead the major three injuries

of multiple collisions. Due to this fact that only primary collisions are extracted out of the GIDAS database, the ISS distorts the correlation between the injury severity and the severity of the accident itself. In this case, the MAIS score is more appropriate for the injury severity.

In general it is difficult to derive the degree of injury of occupants by the severity of the collision itself. Therefore different injury models are defined and investigated forming risk curves estimating the severity outcome of an injury by chosen parameters (Helmer, 2013; Kononen, Flannagan, and Wang, 2011). The parameters guiding these risk curves are based on the abbreviated injury scale (AIS)(CIVIL and SCHWAB, 1988; Otte, Haasper, and Krettek, 2006), the injury severity score (ISS)(Baker and O'neill, 1976; Baker et al., 1974), or the MAIS (Otte, Haasper, and Krettek, 2006; Stevenson et al., 2001) score. As in this work it is important to determine whether a variable is significant with regards to the severity outcome of a collision, no risk curves need to be modelled.

Furthermore, evaluation of advanced safety systems such as anti-lock braking system (ABS), electronic stability programme (ESP), or airbags requires restricting the data set and therefore the analysis to modern vehicles (Segui-Gomez and Baker, 2002). This restriction is complied with when selecting the sample used in the primary research presented in this chapter.

### 5.1.2 Factors known to influence injury severity

As described in Section 4.5 different root causes can lead to an accident. Mannering (2018) explains two different approaches for analysing crash injury:

- The first approach focuses on the likelihood of a collision with a specified injury scale. These models focus on the frequency at which collisions occur; they are reviewed in (Lord and Mannering, 2010).
- The second approach uses detailed in-depth accident data studies for analysing the injury scale for specific accident constellations. A good list of current models for analysing highly detailed in-depth accident data studies is given by Savolainen et al. (2011).

An update of the accessible analytical methods regarding the analysis of crash data was given by Mannering and Bhat (2014). The factors of interest in this thesis are

those which can be estimated using data acquired by sensors within the pre-crash phase of an accident. Hence, detailed in-depth studies of accident data are of interest, with respect to injuries associated with specific collision constellations. Different studies on databases have been reported in the literature; for example, Behnood and Mannering (2017) investigated the impact of gender and age on driver injury-severity outcome in single-vehicle collisions, is studied by Conroy et al. (2008). The study showed a direct dependency between vehicle damage across the front plane and occupant injury. An overview of past research regarding collision constellation characteristics and occupant injury was given by Boufous et al. (2008). They grouped the characteristics into:

- Driver characteristics, including gender, age, driver fatigue, alcohol level, number of occupants, and further.
- Road and environmental conditions, including location, rurality, road surface, intersection configuration, natural light conditions, etc.
- The characteristics of an accident and its vehicles, including type and age of the vehicles, and their maneuver during the collision phase.

The following factors have been identified in various literature as being significant for the occurrence of an accident or for the severity of injuries sustained in a motor vehicle accident.

1. Age of the people.
2. Vehicle change in velocity at the time of impact.
3. The duration of the collision phase.
4. Intrusion at drivers side.
5. Proper belt usage.
6. Vehicle weight.

## 5.2 Regression analysis

### 5.2.1 Aim

The primary aim of the study is to identify the most significant factors (which can be estimated using data acquired by sensors in the pre-crash phase) which contribute to the severity of a frontal collision between two motor vehicles. The secondary aim is to identify collision scenarios which are associated with a high rate of severe accidents.

### 5.2.2 Methods and results

The primary study reported in this section is a systematic analysis of crash data, to identify the contributory factors of injury severity by using binary logistic regression. A secondary investigation is conducted to identify collision scenarios with a high rate of severe accidents. The primary study focuses on vehicle-related pre-crash factors which aggravate the effect of a collision and thus contribute to injury severity.

#### 5.2.2.1 Input parameters for the logistic regression

It is important to point out that some of the seven factors, listed in Section 5.1.2, cannot be measured or calculated from sensor data at drive time; they thus cannot be extracted in the pre-crash phase. However, capitalising on the findings from the literature (given in Section 5.1.2), the seven factors were used as an initial guide for the selection of relevant parameters, from the extensive parameter list provided in the GIDAS database. The retained GIDAS parameters are shown in Table E.3 and Table E.4. For use as input variables in the linear regression, these parameters were filtered to retain only those which can be obtained from sensor data. Linear regression on accident databases is an accepted method in the accident research domain (Al-Ghamdi, 2002; Yan, Radwan, and Abdel-Aty, 2005). Linear regression on the GIDAS database was carried out to find parameters that are significant for the severity outcome of a vehicle-to-vehicle collision.

#### 5.2.2.2 The GIDAS database

The data for the regression analysis was provided by the GIDAS database. It consists of accidents recorded in the metropolitan areas of Hamburg and Dresden. GIDAS constitutes the largest in-depth accident study in Germany organised by the Automotive Research Association (FAT) and the Federal Highway Research Institute (BASt). The recording of the accidents was conducted by the Technical University of Dresden in cooperation with the Medical University of Hannover. The project was initiated in July 1999 and since then the database has been growing by approximately 2,000 accidents involving personal damage each year. Detailed reports conducted by the investigation teams are inserted in the database including:

- Vehicle equipment
- Vehicle damage
- Various injuries sustained by those involved in the accident
- The rescue chain
- Accident conditions
- Etc.

A full list complete with the description of the available variables is provided at the GIDAS (2014) website. Each accident is accurately recorded and also contains interviews of the people involved. Each collision, including the entire course of the accident, is reconstructed with the help of the simulation program PC-crash (Wagner, Hannawald, and Liers, 2015). Due to the high number (3000) of encoded parameters per accident a pruning of the variable set is indispensable (GIDAS, 2014).

Before the different variables were characterised and chosen, the scenarios of interest were identified, as described in the next section.

#### 5.2.2.3 Definition of reference scenarios

Reference scenarios in the domain of active safety systems are commonly extracted out of accident research analysis as illustrated in Figure 5.1. The development of active safety systems begins with the identification of scenarios with a high rate of severe accidents from which use cases for active safety systems are derived. Analysing the chain of misconduct for these cases allows the implementation of appropriate counter measures for avoiding or mitigating each scenario.

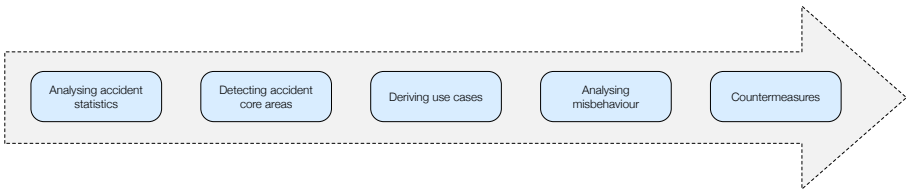


**Figure 5.1:** Development process for active safety systems

In his work, Ebner (2014) defined reference scenarios for active safety systems using a similar approach deriving the various use cases from accidents extracted out of the GIDAS database. Figure 5.2 describes the location of the damage and the direction of the deformation energy that the vehicle absorbed in the various accidents. The GIDAS specification uses codes allocated to directions, in clockwise order around the vehicle, as detailed in Appendix D.3.1. For the analysis, however, the directions are grouped by Ebner (2014) as follows:

- **Front:** Force in direction from 10 - 2 o'clock
- **Side right:** Force in direction from 1 - 5 o'clock
- **Side left:** Force in direction from 7 - 11 o'clock
- **Rear:** Force in direction from 4 - 8 o'clock

Considering Figure 5.2, 54% of vehicle-to-vehicle collisions are caused by frontal vehicle collisions, followed by side collisions (left and right) and rear end collisions. For the definition of the scenario, frontal collisions are therefore explored below in more detail.

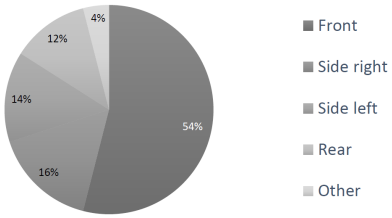


**Figure 5.2:** Location and direction of the vehicle damage and deformation energy (Ebner, 2014)

These frontal collisions can be separated further and grouped by:

- A collision of the front of a vehicle with the front of another
- A collision of the front of a vehicle with the rear of another
- A collision of the front of a vehicle with the (left or right) side of another

These different collisions types are illustrated in Figure 5.3, which depicts that the front-to-front and side collisions amount to a total of 35% of the overall frontal vehicle-to-vehicle collisions. These are the most relevant scenarios for frontal sensor systems, which are described in Section 3.2, as these scenarios challenge the full range of the sensing and fusion aspects of a sensor set-up. Vehicle data for the front-to-front scenario is simpler to capture by sensors, as the longitudinal aspect is considered in state-of-the art sensor systems. In comparison the front-to-side collision scenario focuses on the lateral velocity estimation.

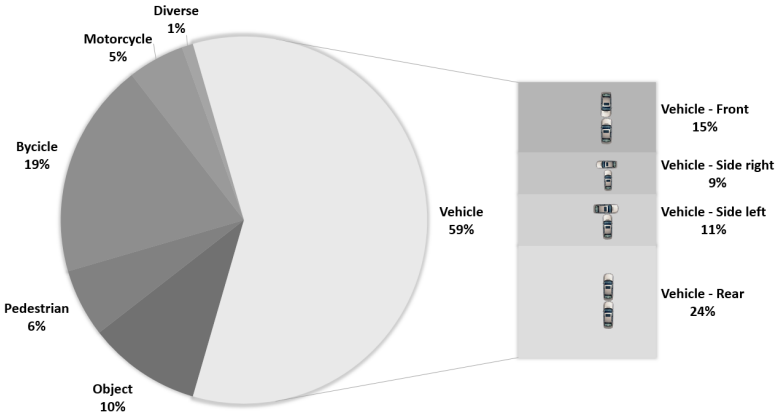


**Figure 5.3:** Distribution of the collision type in 8182 frontal collisions (Ebner, 2014)

As detailed in Section 5.2.2.4.2 the filtered dataset extracted out of the accident database is also used for the definition of the reference scenario suitable for the field of application of the proposed system.

Section 5.1 reiterated the well-known fact that the relative velocity is a parameter with a significant influence on the severity of a collision. Generally, for the analysis of vehicle safety however, the Energy Equivalent Speed (EES) is often taken as measure. The EES estimates the amount of energy absorbed by the vehicle in a real world collision by comparing it to an equivalent amount of energy which a vehicle would absorb by colliding into a rigid barrier. It means the deformation energy would be the same, if the vehicle collides with a full overlap into a non-deformable, and non-moveable barrier (Burg and Zeidler, 1980; Niessen, 2011) matching for example the US NCAP frontal test (National Highway Traffic Safety Administration, 2012).

Figure 5.4 shows a histogram of the EES for 9051 frontal collisions ranging between 0 and 100 km/h. In fact, 95% of the accidents occur for EES up to 56 km/h. The US NCAP test performs a crash test at a speed of 56 km/h representing the majority of real world collisions. For an active safety system the EES speed is an indicator for deformation energy and therefore, for occupant injuries. Therefore, the velocities for the different scenarios of interest in this doctoral research will range between 30 and 60 km/h. Collisions with EES lower than 30 km/h are not relevant due to the low kinetic energy being absorbed.

Figure 5.5 shows a histogram of the EES for collisions in which occupants suffered an injury score higher than three on the MAIS scale, which is described in Table 5.1. This histogram reinforces the decision to set the velocity for the simulation scenarios between 30 and 60 km/h, as the most severe accidents occur according to GIDAS at speeds of 30 - 50 km/h.

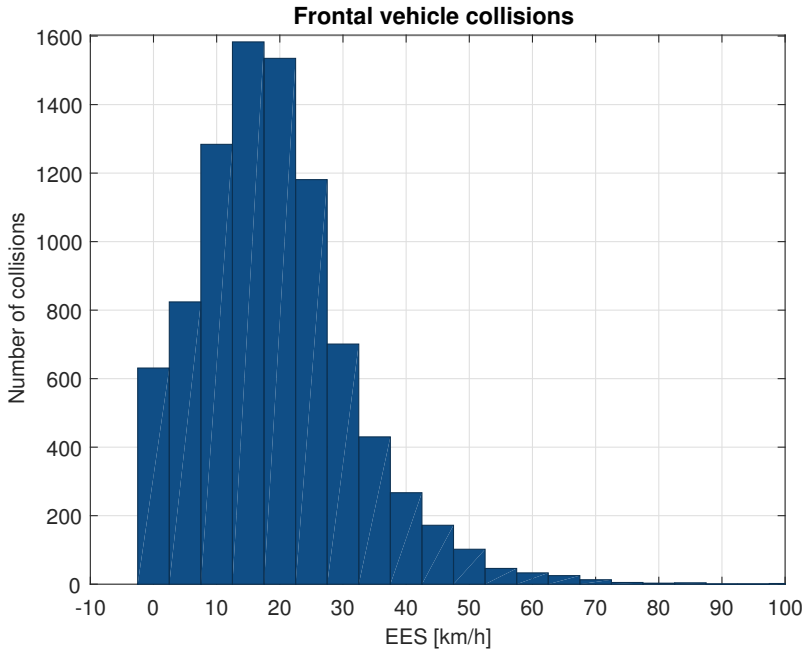


**Figure 5.4:** EES distribution for 9051 frontal vehicle collisions calculated from the GIDAS database

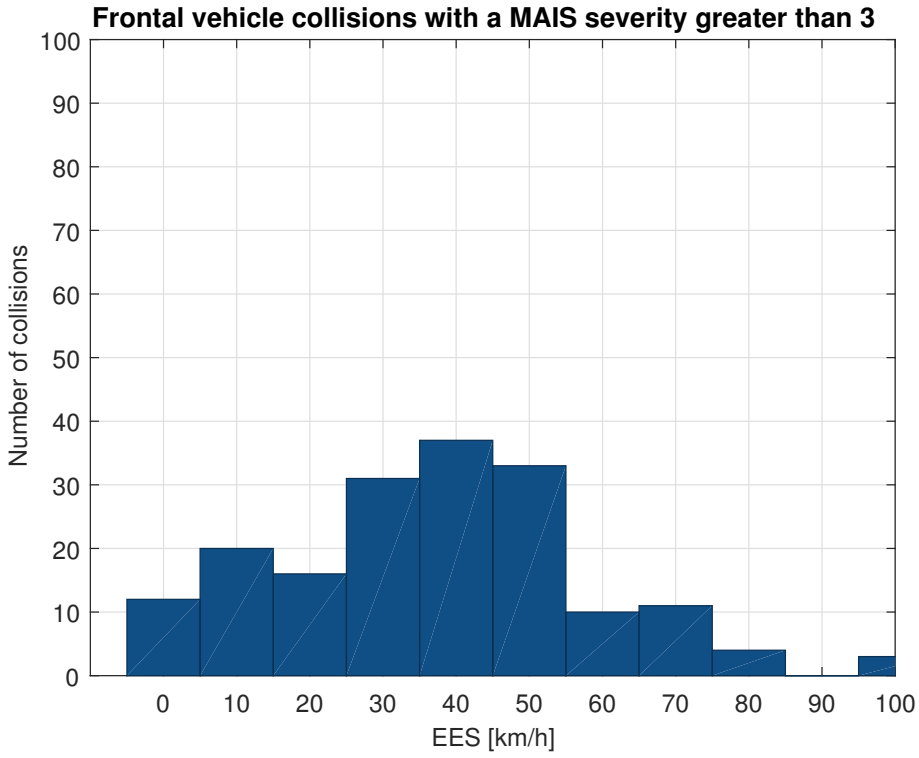


**Figure 5.5:** EES distribution for frontal vehicle collisions with MAIS3+ injuries calculated from the GIDAS database

The EES distribution for city, urban and freeway areas are attached in Appendix D.1. Furthermore, the EES distribution for collisions in which occupants suffered injuries with an MAIS score higher than three in city, urban, and freeway environments are attached in Appendix D.2.

#### 5.2.2.4 Binary logistic regression for crash parameter identification

This section addresses the use of univariate analysis to identify the most significant parameters which influence crash severity. The method is based on a univariate analysis using binary logistic regression on accident databases, which is an accepted method in the accident research domain (Al-Ghamdi, 2002; Yan, Radwan, and Abdel-Aty, 2005). Due to the fact that the aim of the regression analysis was to provide the parameters influencing the severity outcome of a collision, an univariate analysis was chosen as one dependent variable was existent the MAIS score. The choice of using the MAIS score was due to the fact that the MAIS was available within almost every collision dataset. The GIDAS database offers a very sophisticated view on each accident providing a set of 3000 parameters describing each collision. Therefore, the data need to be reviewed and prepared for the regression analysis, which is detailed in Section 5.2.2.4.2 and Section 5.2.2.4.3.

##### 5.2.2.4.1 Binary logistic regression

Logistic regression is an accepted mathematical method in the field of advanced driver assistance and active safety systems; it is used for generating models to rate the potential of proposed systems. In the current field of active safety there are only a few models for vehicle-to-vehicle collisions. Neubauer (2014) introduced a method for deriving injury risk models for vehicle-to-vehicle collisions using a modified version of the approach described in Helmer (2013), which focuses on frontal collision with a pedestrian. It is also stated, that linear regression models are not appropriate for defining injury probability models, as this approach delivers values outside 0 and 1 (Backhaus et al., 2006). The focus of this part of the doctoral work documented in this thesis is to identify the most significant parameters for a collision and therefore, no injury risk models are developed for a later analysis of the potential of a proposed system. For this case, binary logistic regression is suitable as it calculates the probability of a variable being part of a group considering the influence of one or more parameters in the data set. Univariate binary logistic regression directly outputs the

significance of a single parameter regarding the dependent variable, namely crash severity. Various

Logistic regression is grouped into two main approaches, the binary (binomial) logistic regression, and the multinomial logistic regression. The binary logistic regression deals with events occurring or not occurring (e.g. success versus failure) and the probability of this observed outcome. The multinomial regression observes outcomes with different possible types (e.g. "not injured", "slightly injured", "heavily injured"). For the binary logistic regression the parameters are commonly coded as "1", if the event occurs, e.g. "success", and "0" for the absence of an event or e.g. "failure". Furthermore, logistic regression allows to predict the "odds" for an event of "success" considering one or more independent variables. The variables are allowed to be nominal or other scales. The function to represent the occurrence probability of an event $y = 1$ is described using the following formula (Backhaus et al., 2006):

$$p(y = 1) = \frac{\exp(k)}{\exp(k) + 1} = \frac{1}{1 + \exp(-k)} \tag{5.1}$$

with the logit $k$ conveying the influence of the independent variable (Backhaus et al., 2006; Neubauer, 2014). A univariate binary logistic regression considers one independent variable $x$ in the function whereas the multivariate logistic regression features at least two independent variables. In multivariate logistic regression involving M predictor variables, the formula for $k$ is given in Equation 5.2.

$$k = \beta_0 + \sum_{m=1}^{M} \beta_m x_m \tag{5.2}$$

Assuming a binary logistic regression with one independent variable the equation for the function is solved by using Equation 5.1 combined with Equation 5.2 for one variable $M = 1$ resulting in:

$$p(y = 1) = \frac{1}{1 + \exp(-\beta_0 + \beta_1 x)} \tag{5.3}$$

Figure 5.6 shows the graph for Equation 5.3 with

$$\beta_0 = 0 \tag{5.4}$$

$$\beta_1 = [0.5; 1.5] \tag{5.5}$$

$$x = [-12; 12] \tag{5.6}$$

In general the output for logistic regression ranges between zero and one being symmetric relative to the probability of 0.5 as illustrated in the figure below. In the analysis conducted in this chapter, the input variables, as described later, are for example collision speed, offset of the colliding vehicles, or the point of contact between the vehicles. A dataset is therefore constructed of the independent variables (input) and the severity of the collision. The logistic regression predicts the probability of a severe collision (represented by a MAIS value above three) based on the input set of parameters. The study reported in this chapter deployed a univariate binary logistic regression; hence, each input parameter was considered on its own.

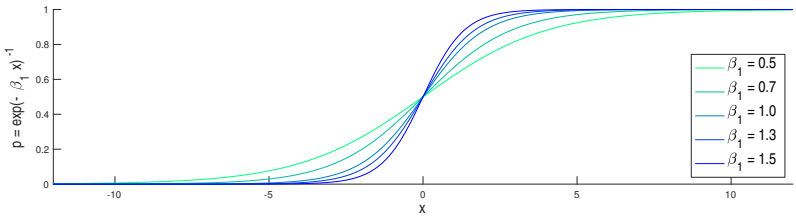


**Figure 5.6:** Example of the logistic regression function with outputs ranging from "0" to "1"

The logistic regression aims to predict the probability of an event being in a group (binary "1") based on the independent variables in the equation. This divided by the probability of not being in the group, defines the odds (for being in the group) and is described in Equation 5.7 (for a single independent variable).

$$odds = \exp(\beta_0 + \beta_1 x) \tag{5.7}$$

Furthermore, the odds ratio (OR) identifies the increase of the odds, if $x$ is increased by one unit based on the ratio of the quotients for the occurrence of an event divided by the quotient of failure.

$$OR = \frac{odds(x+1)}{odds(x)} \tag{5.8}$$

Stating that for every $x$ increasing by one unit the odds are multiplied with $\exp(\beta_1)$.

#### 5.2.2.4.2 Extraction of a data subset from GIDAS

The data for the statistical analysis is based on an export of the GIDAS database gathered from 07/1999 till 06/2014 featuring a dataset for various collision types including vehicles, pedestrians, objects, and more. To allow a reliable work on the dataset different filters were applied to the data during the extraction process. The various filters reduced the total number of analysable data. This is an important step as mentioned in Section 5.1 and the following filters were used:

- Occupants with an age of 18 and older.
- Restricted to cases with only cars involved.
- Focusing on collisions with the front of the vehicle.
- Considering only left steered vehicles.
- People who sustained injuries are restricted to driver and co-driver ignoring passengers in the rear seats.
- Omitting vehicles not equipped with airbags.
- The MAIS field is filled, which is the dependent variable.
- Only considering single collisions, as multiple collisions cannot be mapped onto injuries.
- Limiting the data set to collisions with occupants wearing a seat belt.

Applying these filters to the dataset yielded 4323 collisions for analysing the significant parameters influencing the crash outcome. All data are fully reconstructed by GIDAS researchers, which is an additional flag in the dataset. This yields a higher quality of the various cases and allows analysis on comparable objective data. Furthermore, the number of collisions allows a representative analysis with statistical methods.

After studying the characteristics of the data set, the data was prepared for the binary regression analysis and therefore, the variables were split into binary groups. The dependent variable MAIS score representing the injury severity of an accident was scaled as illustrated in Table 5.1. These variables were grouped into so called

"dummy variables" which can be associated with the presence or absence of an event. For example MAIS3+ represents the group of accidents featuring a severity score greater than three. The next sections describe the coding of the dependent and independent variables into dummy variables to allow the application of a binary logistic regression.

As mentioned in Section 5.2.2.4.1 the variables were coded into binary events supporting a binary logistic regression. For the coding the parameters were imported into SPSS (IBM, 2012), which is used for logistic regression. For automated grouping of the variables into value ranges MS Excel was used for generating the necessary SPSS code for a faster coding. An example of how the SPSS inputs were generated using MS Excel is attached in Appendix E.1.

#### 5.2.2.4.3 Coding the dependent variable

The MAIS score is the dependent variable for the analysis. Therefore, only primary collisions with no multiple collisions are considered to guarantee that no injuries from subsequent collisions distort the analysis. Due to the fact that only the significance of parameters is analysed regarding a severity outcome of MAIS3+ and no risk curves are modelled, as mentioned in Section 5.1 the univariate logistic regression was processed with collisions featuring a severity outcome greater than a MAIS score of three. This approach is based on the methods used by Helmer (2013) and Neubauer (2014) but reduced in its complexity due to the analysis regarding only one injury severity group.

#### 5.2.2.4.4 Coding the independent variables

The independent variables describe the accident and were therefore split into different groups for a better understanding.

##### Parameters which describe the severity of an accident

The severity of an accident is linked to four different parameters:

- Relative speed at the time of collision
- The EES (described in more detail in Section 5.2.2.3)
- The acceleration applied on the occupants

- The deviation of the speed vectors

Neubauer (2014) compared the four parameters and found a sophisticated representation of the severity of a collision. The deviation of the speed vectors is used in the work of Neubauer (2014) and is explained as follows.

The relative speed of two motor vehicles is represented by the vector difference between the speeds of two vehicles at the time of collision. The magnitude of this parameter has an impact on the severity of a collision, but considering it alone does not account for important information such as the type of colliding vehicles (for example, a truck colliding with a light weighted motor vehicle).

The EES, which is used in Section 5.2.2.3 for the definition of the scenario, accounts for the deformation energy absorbed by the vehicles and therefore it is suitable for the collision phase as well. A limitation of the EES measure is illustrated by the following example. A small light-weight vehicle with a very stiff architecture collides with a heavy truck featuring a soft bodywork, the heavy truck absorbs more deformation energy, but the EES ignores the resulting impulse on the small vehicle and on the occupants. The small EES for that case does not capture the high change in velocity for the occupants and therefore it is not suitable.

The acceleration of the occupants inside a vehicle is a very accurate measure for predicting the resulting injury severity. This measure is reconstructed and documented in accident databases, but it does not have high data quality for all accidents. There is currently no possibility to accurately monitor the change in the velocity of occupants. Sensor systems are not able to track occupant motion at a suitable measurement resolution.

The deviation of the relative speed vectors $\Delta v$ is relevant in the collision phase and indirectly takes the change in velocity of the occupants into account. This parameter is used in various papers published previously (Bahouth et al., 2004; Gabauer and Gabler, 2008; Johnson and Gabler, 2012; Kononen, Flannagan, and Wang, 2011).

The relative speed at time of collision is the only parameter, out of the four mentioned, which can be measured by current state-of-the-art sensor systems.

#### Parameters which describe dynamic properties relevant to a collision

For the direction of the impulse, different values are considered, which differ in resolution and data quality. The direction of the first impact (VDI) parameters

of the GIDAS database describe the vector of the impulse directed towards the vehicle, the overlap over the deformed area, and the height of the target area of the impulse, as illustrated in Appendix D.3.1. For the analysis carried out in the work reported herein, the impulse directions between nine and three o'clock were considered because the analysis is focused on frontal vehicle collisions as mentioned in Section 5.2.2.3. The different parameters describe the direction in an abstract and a very detailed way. For example an abstract value indicating that the front of the vehicle is hit, or a more precise value stating the collision point calculated in centimetres. The parameters and dummy variables for the various directions are listed in Appendix E.2. The impulse angle between the colliding vehicles was used for the underlying analysis as a further parameter. Furthermore, the collision point is defined and explained.

#### Parameters which describe static properties relevant to a collision

The following static parameters were included in the binary regression analysis:

- Length, width, and weight of the vehicle
- Architecture and class of the vehicle
- Left or right steered vehicle
- Belt usage
- Type and class of the street
- Gender of each occupant

The above mentioned parameters are known to be significant for describing a collision outcome. A list of all parameters considered in the analysis are detailed in Appendix E.2. A correlation to the dynamic parameters is conceivable, as (for example) the weight of a vehicle directly contributes to its resulting EES.

#### 5.2.2.4.5 Findings of the binary logistic regression

This section presents the results of the univariate binary logistic regression. The dependent variable as mentioned in Section 5.2.2.4.3 is the injury severity score of the occupants with a value higher than three indicating severe injury. The full set of 140 predictor parameters are listed in Appendix E.2. The categories in which the findings are grouped are as follows:

- **Parameters for safety measures** describing the status of the safety systems of a vehicle
- **Parameters describing the geometrical properties of a collision** with collision points, offsets, and impulse directions
- **Dynamic parameters and energies** including speeds just before the collision and the post collision speeds of the vehicles, as well as forces applied on the vehicles

A Hosmer-Lemeshow test was applied for validating the binary logistic regression model. The test allows an estimation of how well the model fits the data (Canary et al., 2017; Fagerland and Hosmer, 2016). The produced probability value indicates the quality of the model. If the p-value (produced by the goodness of fit test) falls below 0.05 the model does not fit the data and it would therefore be rejected. Vice versa, if the value is high the model passes the test. (Hosmer and Lemeshow, 1980) recommend to group the data regarding their predicted value into 10 groups equally sized. For each of these 10 groups the observed number of occurrence and non-occurrence is compared to the expected number of events. To calculate the expected number of events the sum of the predicted probabilities of each record in the group is taken. Hence, subtracting the expected number of events from the group size results in the number of non-events. Afterwards the observed counts are compared with the expected counts with the help of the chi-square function. The results of the Hosmer-Lemeshow test is attached for each parameter in Appendix E.7.

Table 5.2 depicts the most significant parameters for accidents with severe injuries. The detailed list (including not significant parameters) of results which arose from the univariate binary logistic regression analysis are attached in Appendix F.1 to Appendix F.6.

**Table 5.2:** Binary logistic regression results for severe accidents with a MAIS score higher than three

| Variable | VDI description | Number of cases | Significance (p value) | Odds ratio | 95% Confidence interval Lower value | Upper value |
|---|---|---|---|---|---|---|
| **Parameters for safety measures** | | | | | | |
| RHSBEN | Belt status | 4125 | 0.017 | 1.934 | 1.124 | 3.325 |
| airbfb_1 | Airbag activated | 4323 | <0.001 | 7.628 | 4.216 | 13.79 |
| airbfb_2 | Airbag not activated | 4323 | <0.001 | 0.131 | 0.072 | 0.237 |
| RHSBEN_not_activated | Belt not activated | 4323 | 0.019 | 1.929 | 1.113 | 3.343 |
| **Parameters describing the geometrical properties of a collision** | | | | | | |
| VDI1 | Direction of impulse | 4323 | <0.001 | 1.089 | 1.035 | 1.145 |
| VDI4 | Point of collision vertically | 4323 | <0.001 | 0.477 | 0.402 | 0.565 |
| VDI5 | Abstracted kind of collision | 4323 | 0.025 | 1.427 | 1.045 | 1.947 |
| VDI6 | Degree of deformation | 4322 | <0.001 | 1.942 | 1.782 | 2.116 |
| STOSSPX | Point of Contact (x) | 4302 | <0.001 | 1.019 | 1.015 | 1.023 |
| STOSSPY | Point of Contact (y) | 4302 | 0.019 | 0.996 | 0.992 | 0.999 |
| VDI1_tewlve | Collision at 12 o'clock | 4323 | <0.001 | 1.955 | 1.384 | 2.762 |
| VDI1_one | Collision at 1 o'clock | 4323 | 0.004 | 0.439 | 0.252 | 0.765 |
| VDI3_30 | Part of the vehicle hit | 4323 | <0.001 | 3.212 | 1.768 | 5.837 |
| VDI3_80 | Part of the vehicle hit | 4323 | 0.027 | 1.688 | 1.062 | 2.685 |
| STOSSPX_trans | Transcoded point of contact | 4302 | <0.001 | 1.696 | 1.529 | 1.881 |
| STOSSPY_trans | Transcoded point of contact | 4302 | 0.019 | 0.820 | 0.695 | 0.967 |
| **Dynamic parameters and energies** | | | | | | |
| DV | Delta in velocity | 4273 | <0.001 | 1.078 | 1.068 | 1.088 |
| EES | Energy equivalent speed | 4298 | 0.002 | 1.002 | 1.001 | 1.003 |
| V0 | Initial Speed | 3966 | <0.001 | 1.019 | 1.014 | 1.023 |
| VK | Outlet speed | 4245 | <0.001 | 1.020 | 1.015 | 1.024 |

The significance of each parameter is indicated by the significance or p value in the fourth column. For values below 0.05, the parameter influences the outcome significantly. In this study, a cut-off point for p-values is set at 0.001. Values below this point indicate that the corresponding accident parameter strongly influences the severity of the accident outcome. The results show that the dynamic factors (such as velocity, EES, and others) are a strong indicator for the severity of an accident outcome. The odds ratio describes, as in Equation 5.8 the change in the probability that a parameter influences the occurrence of an MAIS score above three. For instance, a change in the initial speed by one km/h results in an increasing probability of an injury above MAIS three by 1.019.

A detailed look at the parameters describing the geometrical properties of a collision reveals that frontal collisions in the direction of from twelve and one o'clock are more significant than others. Regarding Section 5.2.2.3 the investigation into the scenario showed already a strong presence of front-to-front collisions compared to all types of collisions. VDI3_30 and VDI3_80 indicate, that the degree of overlap is also a strong parameter influencing the severity outcome of a collision. VDI5 is a more abstract view on the overlap and is roughly separated into

- A counterpart the vehicle is colliding being broader than 40cm
- Slim collision counterpart with a diameter smaller than 40cm
- Sliding along the collision counterpart
- Rollover and tip over

VDI4 represents the collision regions along the z axis and is illustrated in Figure D.8. VDI6 is the degree of deformation. This parameter cannot be detected before a collision occurs and therefore not further investigated.

The above mentioned parameters are the most significant parameters related to the severity outcome of a vehicle-to-vehicle collision. For pre-crash safety countermeasures, it is important to identify parameters which can be measured with the help of sensors, to enable the extraction of the constellation of the upcoming collision.

Given that this research project focuses on delivering an enhancement in the field of extracting the collision constellations out of sensor data, the parameters need to be detected by active sensors. This practical constraint reduces the set of significant parameters in combination with its GIDAS parameter, to the subset listed in

**Table 5.3:** Reduced set of significant parameters which can be detected by active automotive sensors

| Significant parameter | GIDAS parameter |
|---|---|
| Relative velocity | DV |
| Collision point | STOSSPX, STOSSPY |

Table 5.3. Table 5.3 shows the different parameters which can be measured with different sensors directly or derived out of sensor data.

## 5.3 Conclusion

This chapter reports a study, which is cast as a systematic analysis of crash data (from the GIDAS database), to identify the contributory factors for injury severity by using binary logistic regression. A secondary investigation is also reported; it was conducted to identify collision scenarios which have a high rate of severe accidents.

*Crash constellation:* To answer the research question about what collision parameters strongly influence the severity of injuries for frontal collisions between two motor vehicles, a binary logistic regression was applied to data from the GIDAS database. The regression analysis, performed in this doctoral research, produced a set of significant parameters which fall into three broad categories:

- parameters describing the status of safety devices or safety mechanisms of a vehicle (such as airbag activation), when the collision occurred.
- parameters describing the geometrical properties of the collision, such as the directions of the colliding vehicles and the part of the vehicle body which was hit.
- parameters describing the dynamics of the collision, such as speeds before and after collision, and impact forces.

The set of significant parameters was then trimmed, to retain only those which can be measured with automotive sensors in the pre-crash phase, and which are not linked to human or environmental factors. This subset of significant parameters constitutes the crash constellation which will be extracted by the algorithm devised in this research. The crash constellation is made of three collision parameters:

- relative velocity between the vehicles;
- point of collision on the vehicle body;
- vehicle alignment offset (or vehicle overlap);

*Collision scenarios for the performance assessment:* Another statistical analysis discussed in the chapter offers two collision scenarios, for the performance assessment of the constellation extraction algorithm proposed in this research. The chosen scenarios are for collisions in which vehicle occupants suffered injuries with an MAIS score of 3 or higher. The scenarios are:

- Front-to-front collision of two vehicles travelling at speeds ranging from 30 km/h to 130 km/h.
- Front-to-side collision of two vehicles travelling at speeds ranging from 30 km/h to 60 km/h.

The next chapter proposes an algorithm for extracting the crash constellation.

# 6 Crash Constellation Extraction Algorithm

This chapter describes the proposed crash constellation extraction algorithm. Referring to the outstanding research questions stated in Section 4.6, the proposed crash constellation extraction algorithm considers uncertainties in the signal processing chain and adapts different existing algorithms as mentioned in Section 4.3 to extract the constellation of an impending collision. Figure 6.1 displays the overall system design containing the different steps towards extracting the collision parameter set which was determined in Chapter 5.

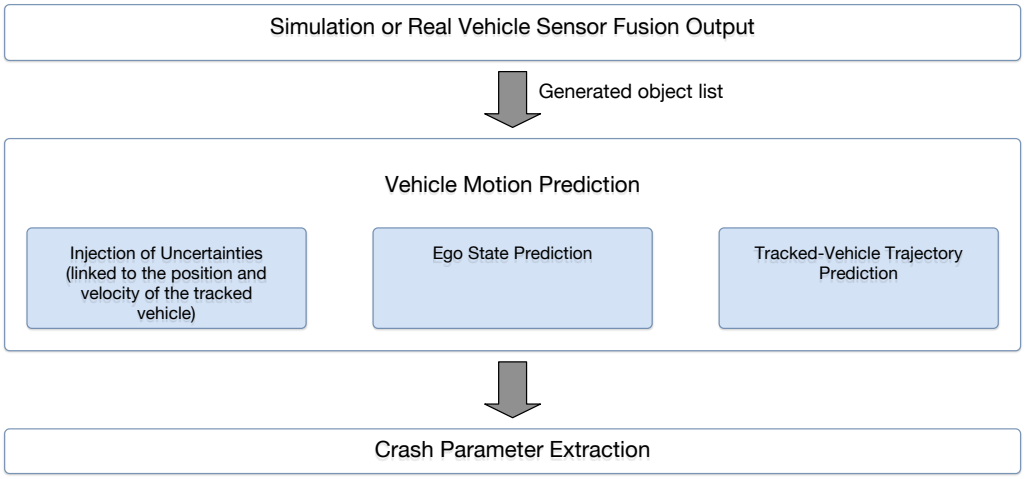


**Figure 6.1:** System design for the proposed crash constellation extraction algorithm

As illustrated in Figure 6.1, the object list produced by the sensor fusion module, which also contains the covariances associated with the predicted state are forwarded to the constellation extraction algorithm. The object list in the simulation reported herein is produced by an offline simulation model, which is explained in Chapter 7. Data captured from a real vehicle was used to extract the behaviour (with regards to uncertainties) of real-world sensors, and to evaluate the simulation model.

The constellation extraction algorithm contains a prediction module (consisting of three main pre-processing instances) and a crash parameter extraction module. The prediction module is divided as follows:

- Trajectory prediction: Trajectory estimation includes Kamm's circle and trajectory calculation allowing (based on the algorithm by Kaempchen, Schiele, and Dietmayer (2009) explained in Section 4.4.2) the prediction of the future paths of objects such as other vehicles in the vicinity of the reference vehicle.
- Inclusion of position and velocity uncertainties: The uncertainties in the measured position and velocity of the tracked-vehicle are injected into the aforementioned trajectory space by using estimates of standard deviations obtained from the covariances provided by the state estimation (detailed in Chapter 7).
- The ego state prediction: The motion of the ego vehicle is predicted using a constant-acceleration model. The predicted paths of the ego and tracked vehicles will be compared to detect possible collisions, for each of which the corresponding crash constellation will be extracted by the crash parameter extraction module.

The crash parameter extraction module extracts the constellation for the predicted collision, and also estimates the accuracy of the parameters, within a time-to-collision smaller than 500ms in the pre-crash phase.

An off-line simulation method is needed for the implementation and evaluation of the constellation extraction algorithm, as mentioned in Section 2.2, due to the lack of testing equipment for destructive manoeuvres. The simulation model is described in the next chapter.

## 6.1 Definition of the extracted crash constellation

Chapter 5 identified parameters which influence the severity of a collision, and can be extracted out of sensory data during the pre-crash phase. The following section addresses some aspects of the implementation relevant for the extraction of some of these parameters.

The GIDAS specification defines the collision point as a distance to the front middle point of the vehicle. Furthermore, the collision point along the side of the vehicle is calculated from the foremost point of the vehicle. Thus, the collision point parameter is implemented as illustrated in Figure 6.2:

- The value is positive for distances to the right and negative to the left of the centre of the vehicle front.
- The value is positive along each side of the vehicle measured from the top point.

The vehicles overlap parameter is only possible to be calculated for front-to-front collisions, or front-to-side collisions at 90°. For the case of a collision featuring an overlap the value is given in percentage, as shown in Figure 6.2.

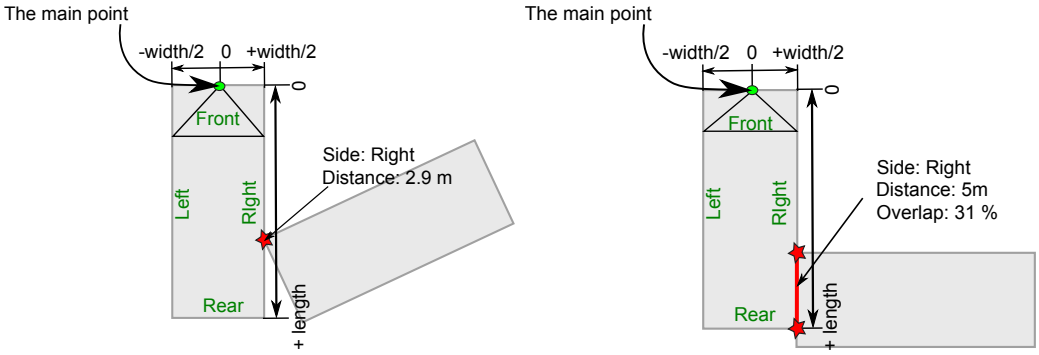


**Figure 6.2:** Definition of the collision point (left) and collision overlap (right)

## 6.2 Pre-processing stages of the collision constellation extraction algorithm

### 6.2.1 Estimation of the tracked-vehicle trajectory based on driving dynamics

To address the drawbacks (mentioned in Section 4.4.2) for the technique proposed in (Kaempchen, Schiele, and Dietmayer, 2009), this section proposes an extension of the technique, to improve the estimation of the possible trajectories of a tracked vehicle. The extension addresses the limitation mentioned in Section 4.4.2 by considering current dynamics properties affecting the vehicle. Furthermore, the turn rate is limited by a minimum turn radius $\boldsymbol{r}_{min}$, as illustrated in Equation 4.20. Using the equations from 4.19 to 4.22 the processed fan of trajectories will be calculated iteratively at each $\Delta t$ time step chosen to be

$$\Delta t = 0.002s \tag{6.1}$$

This value for the iteration time step allows a high update rate for the calculation of feasible trajectories which a vehicle is able to take under current driving dynamics. Due to computational demands the time steps need to be adjusted for real-time systems fitting the update rate of the ego vehicle dynamics at 10ms. For simulation purposes the update rate is increased to have a smoother signal.

#### 6.2.1.1 Modelling the effect of non-instantaneous change of acceleration

The model described in Section 4.4.2 assumes that maximal acceleration or deceleration can be reached instantly. In reality, vehicles develop the magnitude of positive and negative acceleration over time. Referring to the literature a rough time estimate of 200 ms is mentioned by Nitz (2008) but it is neglected by many driver assistance systems. For active safety applications targeted at a pre-crash phase of less than 500 ms, this physical constraint is of importance. Furthermore, the trajectory calculation based on the Kamm's circle needs to also be adjusted to account for the fact that vehicles can reach a higher magnitude of deceleration than acceleration. Within a time step of 200 ms, current cars can reach a maximal deceleration of about 10 m/s$^2$ during braking or a maximal acceleration of about 10 m/s$^2$ during a turn; however, their maximal acceleration is only about 2 m/s$^2$ under other manoeuvres (Mehar, Chandra, and Velmurugan, 2013). Hence, a linear rise of the acceleration during braking or steering manoeuvres up to a maximum of 1g has been adopted for the prediction algorithm as illustrated in Figure 6.3.

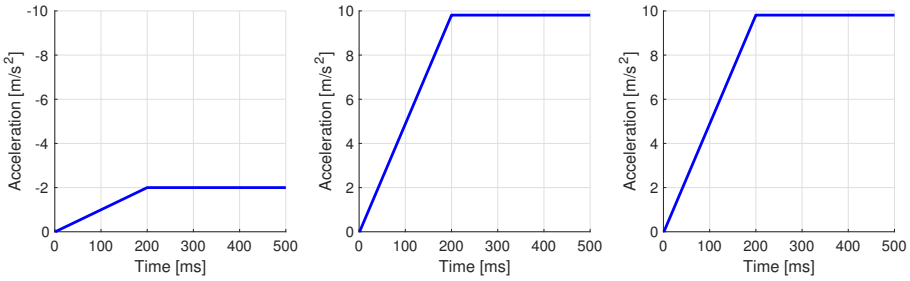


**Figure 6.3:** Limiting the magnitude of forces applied to the vehicle (left – deceleration, middle – acceleration, right – steering)

The trajectories are calculated for the front middle point of the object vehicle spanning a range of possible trajectories. These reachable trajectories are described by the maximum feasible acceleration as dictated by the aforementioned restrictions on the physics and dynamics of a motorcar. As illustrated in Figure 6.4, for each time

step, a modified[1] Kamm's circle for the object vehicle is predicted, representing its possible manoeuvres, assuming that the vehicle remains under control throughout a manoeuvre - skidding does not occur, for example. According to Schmidt, Oechsle, and Branz (2005) most accidents are not prevented by maximum steering or deceleration but through a combination of manoeuvres. In the simulations conducted as part of this thesis (see Chapter 8), a large number of trajectories (200 at a time step) are simulated to represent a variety of manoeuvres during the pre-crash phase.

An example for the prediction and trajectory calculation is illustrated in Figure 6.4 for an impending collision of two vehicles each travelling at a speed of 10 m/s without acceleration. The trajectory calculation starts at 500ms before the collision occurs; the position bounding regions for the object vehicle are shown every 30ms. These bounding regions correspond to forces that not only lie within the Kamm's circle but are also further constrained as depicted in Figure 6.3.

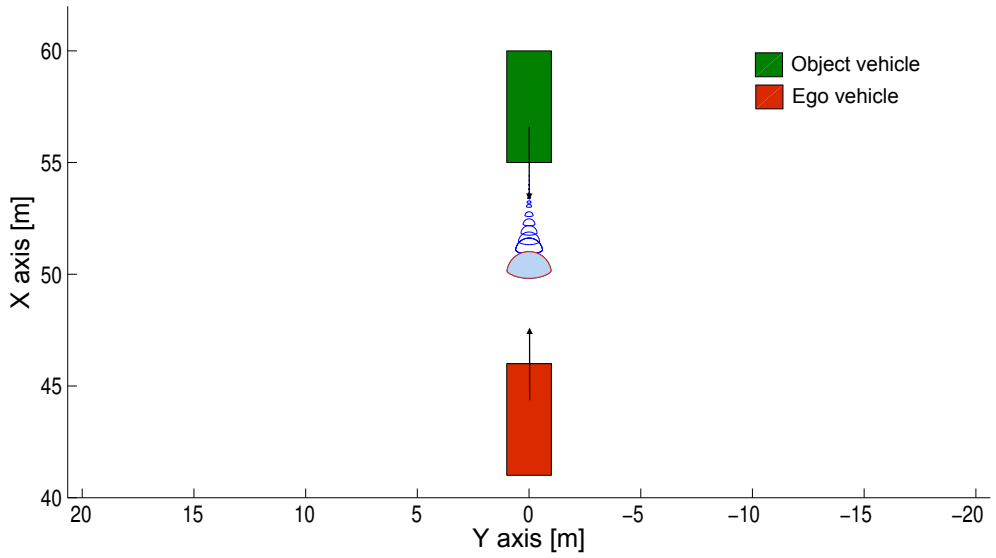


**Figure 6.4:** Example showing the predicted bounding regions for possible positions of the object vehicle every 30ms illustrating the modified Kamm's circle. The position estimation begins 500ms before collision.

1 This term is used in subsquent text in the thesis, because the calculation relating to the current acceleration does not give a perfect circle.

#### 6.2.1.2 Modelling movement actuation lag relative to V2V communication

As stated in Section 3.2.5 V2V communication adds additional information about the environment to the fusion process and can be modelled as a virtual sensor. The V2V-communication is integrated in the sensor data fusion system, thereby enhancing its performance. Apart from delivering the velocity with a higher accuracy, the acceleration is also obtained via the V2V-communication. As mentioned in Section 3.2, no state-of-the-art sensor is able to measure acceleration directly and deliver acceleration information with an acceptable precision. V2V otherwise, is able to sense and transmit in-vehicle data of the opponents motorcar directly over the air to the ego vehicle. Moreover, the additional information obtained via V2V (driver's intention) is considered during the pre-crash phase. In the following V2V-communication enhancement is discussed for both sensor fusion and driver intention.

As mentioned above the integration of the V2V communication into the framework is implemented by including a more precise estimation of the velocity ($\sigma_v$ =0.1 m/s) and acceleration ($\sigma_a$ =0.1 m/s$^2$) of the tracked object. These values rely on the work of Khairnar and Kotecha (2013) who analysed the performance of the IEEE 802.11p standard for vehicle-to-vehicle ad-hoc communications. Furthermore, the cooperative awareness messages require an update rate of 10Hz and a maximum latency of 100ms (ETSI, 2009, 2011; Shi and Sung, 2014). This latency is therefore our uncertainty for the velocity and acceleration estimation in the Jacobian matrix (Equation 7.31). As the acceleration component is also considered, V2V enhancement demands the utilization of the constant acceleration model. The velocity and acceleration of the opponent vehicle is directly extracted out of the vehicle inertia and sent over an active V2V communication link.

Furthermore, an earlier and more accurate update of information about the vehicles movement would increase the precision of the constellation extraction. Nitz (2008) stated that after the drivers steering manoeuvre 100ms elapse until the vehicle changes its movement, which then can be measured by an active sensor such as a radar. The V2V communication though is able to deliver information about this change in movement earlier in time. Another 200ms pass until a maximal acceleration is reached. Figure 6.5 depicts the model of the non-instantaneous change of acceleration with V2V-communication.

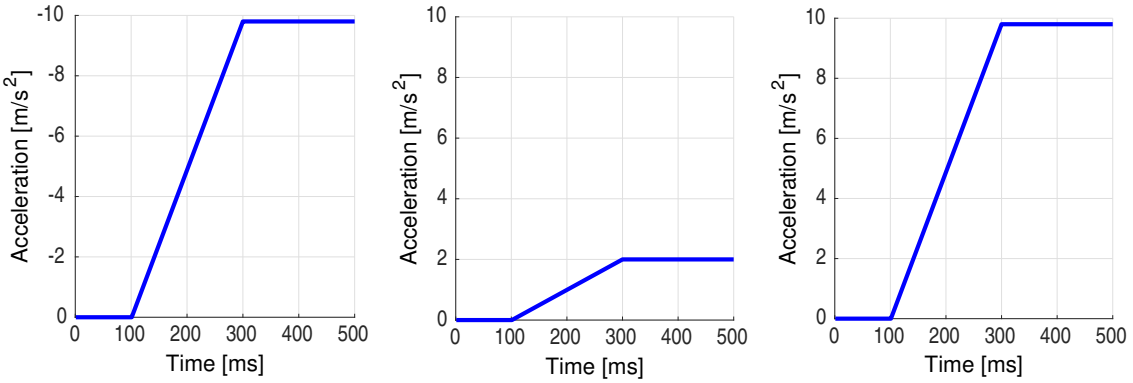


**Figure 6.5:** Modelling the vehicle acceleration lag relative to the timing of information from a virtual V2V sensor (left – deceleration, middle – acceleration, right – steering)

Due to the availability of high precise acceleration measurements of the object vehicle, this information gathered is included in the crash extraction algorithm. Although the dynamic data of the object vehicle is measured accurately, position data is less precise than the information provided by the in-vehicle sensor system of the ego vehicle. This leads to a similar performance of the position measurement with or without V2V-communication. Nevertheless, the accuracy enhancement of velocity and acceleration measurements is expected to increase the precision of the filtered position data.

The trajectories of tracked vehicles are calculated based on the front middle point of the object. The crash constellation algorithm also considers sensor fusion inaccuracies. The prediction uncertainties of the sensor fusion system are applied to the Kamm's circle in Section 6.2.2.

### 6.2.2 Injection of state-estimation uncertainties into trajectory calculations for the tracked vehicle

As described in Section 4.2 the sensor fusion output is afflicted with uncertainties which will affect the result from the state estimation process which is described in Section 7.4. This process estimates the position and velocity of the tracked vehicle. For the prediction of the state of the tracked vehicle, the following three properties are considered:

- Driver's intention

- Position estimation error
- Velocity estimation error

For the collision extraction algorithm, the state estimation uncertainty is assumed to stay within three standard deviations from the mean ($P(\mu - 3\sigma \leqslant x \leqslant \mu + 3\sigma) \approx 99.73\%$ assuming a normal distribution) disregarding the marginal opportunity of object state parameters being outliers. Measurements outside the 3-sigma interval are considered to be outliers (Saxena and Zawodniok, 2014; Theiler and Schindler, 2012). The driver's intention and state estimation uncertainties are considered to be independent; hence, there is an uncertainty of about 0.27% that the driver and vehicle take a maximum acceleration manoeuvre (e.g steering and decelerating) and match the error of state estimation in position and velocity.

A first design of the collision extraction algorithm considered four maximal manoeuvres for the tracked vehicle (maximal acceleration, deceleration, or steering left or right). The resulting uncertainty in velocity and position was cumulated to the estimated bounding region of the possible positions of the tracked vehicle. The second design features trajectories estimated for vehicle acceleration constrained within the modified Kamm's circle combined with an uncertainty bounding region. Each trajectory was estimated for the maximal possible acceleration of the object vehicle, increased by $3\sigma$ along its trajectory. The size of the bounding region, in which the tracked vehicle is predicted to be, increases with the uncertainty provided by the state estimation. Figure 6.6 illustrates the prediction of the maximal manoeuvres of the object vehicle.

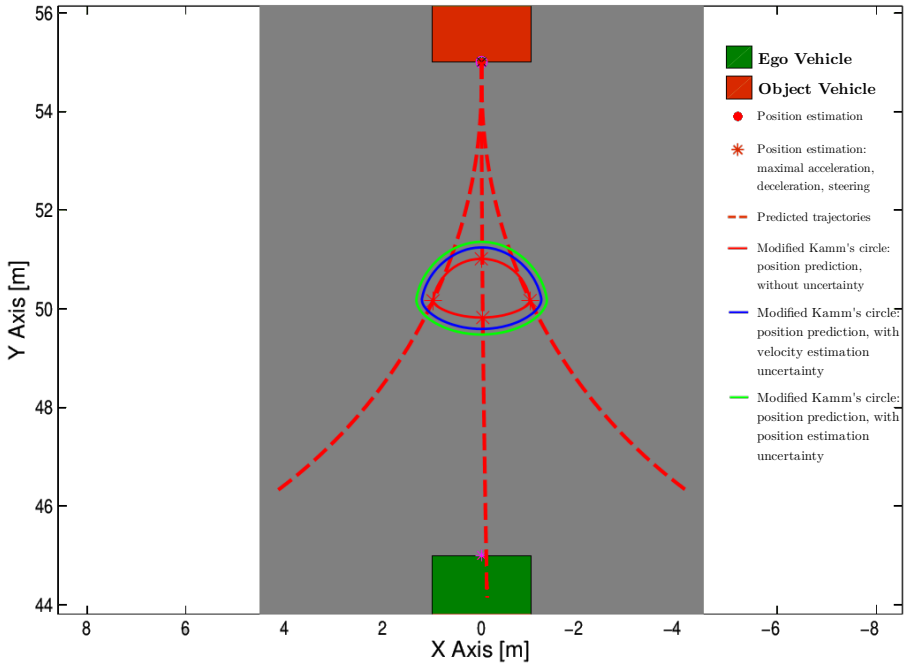


**Figure 6.6:** The predicted bounding regions for the position of the object vehicle, estimated based on a modified Kamm's circle and with or without vehicle state estimation uncertainty, for $v_{ego} = v_{obj} = 10$ m/s, $a_{ego} = a_{obj} = 0$, and a start of the prediction at 500 ms TTC (GT)

The crash constellation extraction requires the calculation of the intersection point between the trajectories of the ego and object vehicle. This requires a prediction of the ego vehicle motion along its current path.

### 6.2.3 Ego state prediction

The algorithm for predicting the motion of the ego vehicle is given below (see Algorithm 1). The time span for the ego motion prediction has been chosen to be double the duration of the time-to-collision. This allows the calculation of the ego vehicle trajectory into the crash and post-crash phase. The ego motion prediction algorithm is invoked at discrete moments in time $t$. At each time t, the algorithm produces a number of predicted points ($n_{predpoints}$) representing the predicted ego motion path. The ego state $ego_{state}(t)$ and its history need to be known.

Predicting the motion of the ego vehicle after time $t$, over a time span which produces a number ($n_{predpoints}$) of predicted points. The time step separating each pair of adjacent predicted points is $\Delta T_{pred}$

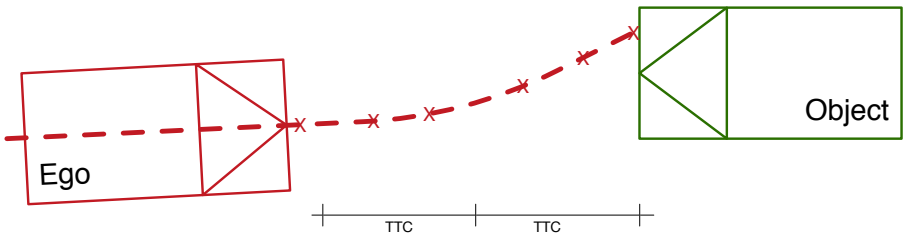


**Figure 6.7:** Calculating the ego vehicle motion for time span $\Delta T_{pred}$ with time steps $\Delta t$ for $n_{predpoints}$ points

**Algorithm 1** Predicting the motion of the ego vehicle after time $t$, over a time span which produces a number ($n_{predpoints}$) of predicted points. The time step separating each pair of adjacent predicted points is $\Delta T_{pred}$

**Require:** $n_{predpoints}$, $\Delta T_{pred}$, $ego_{state}$, $t$
**Ensure:** Path of ego vehicle for $n_{predpoints}$ points
1: Initialising $ego_{state}(t)$ {Including position$(x, y)$, velocity$(v)$, acceleration $(a)$, and velocity direction $(\vec{v})$}
2: $\Delta\vec{v} = \vec{v}(t) - \vec{v}(t-1)$ {Calculating the change in velocity direction}
3: **for** $j < n_{predpoints}$ **do**
4: $\quad v_{ego}(j) = v_{ego}(j-1) + a_{ego}(j) * \Delta T_{pred}$
5: $\quad \vec{v}_{ego}(j) = \vec{v}_{ego}(j-1) + \Delta\vec{v}$
6: $\quad \Delta s = v_{ego}(j-1) * \Delta T_{pred} + a_{ego} * \frac{\Delta T_{pred}^2}{2}$
7: $\quad x_{ego}(j) = x_{ego}(j-1) + \Delta s * \cos(v_{dir\,ego}(j))$
8: $\quad y_{ego}(j) = y_{ego}(j-1) + \Delta s * \sin(v_{dir\,ego}(j))$
9: $\quad j = j + 1$
10: **end for**

The increasing sophistication of advanced driver assistance systems supporting the driver in his/her driving task leads to a decrease of situation awareness by the driver and therefore an increase in reaction time (Knapp and Vardaman, 1991). According to Ward, Fairclough, and Humphreys (1995) drivers with ADAS equipped vehicles tend to be inattentive more frequently. Inattentiveness in this context is due to the driver's increased reliance on automation systems. This reduction of situation awareness leads to the decision not to include (in the ego state prediction) driver interaction within the short time (500ms pre-crash phase) which has been assumed. Funkhouser and Drews (2016) found a strong relation between the duration of automated driving and the increase of reaction time which accompanies it.

## 6.3 Calculating the crash constellation

The combination of the aforementioned algorithms allow the calculation of the crash constellation. At each time step $\Delta t_{coll}$ a collision detection algorithm compares the possible object vehicle trajectories (200 trajectories within the constraints of the modified Kamm's circle) to the predicted trajectory of the ego vehicle. Figure 6.8 depicts the bounding region for the position of the object vehicle, estimated using a modified Kamm's circle afflicted by velocity and position uncertainties, as mentioned in Section 6.2.2.

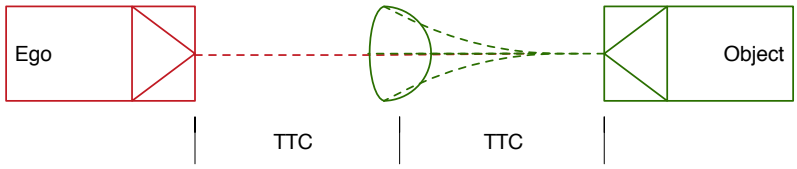


**Figure 6.8:** Bounding region for the position of the object vehicle, estimated using a modified Kamm's circle together with prediction uncertainties

The ego motion trajectory, as well as each predicted trajectory of the object vehicle is represented at each discrete time by a bounding box which has the dimensions of a vehicle. An example for this representation form is illustrated in Figure 6.9 which forms the basis for the calculation of the crash constellation parameters. For every occurrence of a collision between bounding boxes, the crash constellation parameters are calculated and stored.

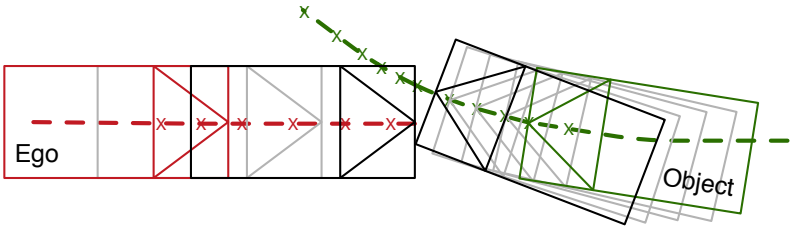


**Figure 6.9:** Trajectory of the object vehicle corresponding to one point within the constraints of the modified Kamm's circle for the object vehicle

The following algorithm shows how the collision constellation is calculated for each single trajectory of the object vehicle intersecting the predicted trajectory of the ego vehicle motion. The inputs to the algorithm are:

- Prediction of the object vehicle $pred_{obj}$ represented by the points along the modified Kamm's circle for $2 * n_{pred}$ predicted points.

- Prediction of the path of the ego vehicle $pred_{ego}$ (as calculated in Algorithm 1).
- The number of predicted points $n_{pred}$ which is the TTC (here 500ms) multiplied by the prediction rate.
- The dimensions of the car.

**Algorithm 2** Calculating the crash constellation parameters

**Require:** $pred_{obj}$, $pred_{ego}$, $n_{pred}$
**Ensure:** Collision parameters for all collisions between $pred_{ego}$, $pred_{obj}$

```
{Iterate through the points constituting the Kamm's circle}
for j < sizeof(kamm) do
    Calculate the path for one point of the Kamm's circle over time for pred_obj
    (path = [pred_obj.x_kamm(:,j), pred_obj.y_kamm(:,j)])
    Calculate the rectangles representing the object car for every point along the
    current path.
    {Iterate through the doubled amount of predicted points (2 * TTC)}
    for k < 2 * n_pred do
        {Check if the rectangles of pred_obj and pred_ego intersect}
        if (intersect(pred_obj, pred_ego)) then
            Extract the collision constellation.
        else
            No collision occured.
        end if
        k = k + 1
    end for
    j = j + 1
end for
```

For each extracted collision the five parameter values are stored for a later assessment of the extracted collision constellations and the associated uncertainties.

## 6.4 Conclusion

This chapter describes the algorithm developed for crash constellation extraction which is executed 500ms before collision. The extraction algorithm takes into account the estimation uncertainties of the estimated state of the tracked vehicle. The algorithm proposed for extracting the crash constellation comprises a vehicle motion prediction module and a crash parameter extraction module. The vehicle motion prediction module consists of three main pre-processing instances: trajectory

prediction for the tracked vehicle, calculation of the acceleration, and ego-state prediction. Further details for these pre-processing instances are given below, together with those for the collision detection and collision parameter extraction processes.

**Trajectory calculation** was designed for the tracked vehicle, taking into account vehicle dynamics constraints represented by the Kamm's circle modified according to physical constraints imposed on the rate of acceleration of a real vehicle. The modification includes two aspects: (i) a model of the effect of non-instantaneous change of acceleration; (ii) a model of the vehicle movement actuation lag relative to V2V communication. This modified Kamm's circle allows the calculation of the maximal manoeuvres that the tracked vehicle is able to make. All manoeuvres are represented by trajectories corresponding to acceleration vectors represented by points along the modified Kamm's circle. Knowledge of the trajectories corresponding to these maximal manoeuvres allows the prediction of the bounding region for all possible positions of the tracked vehicle at a given time. These possible positions of the vehicle at a given time define the position estimation uncertainty at that time.

**Inclusion of position and velocity uncertainties** computed by the state estimation module, which includes parameters of uncertainties measured for real world sensor fusion behaviour. These uncertainties are injected into the trajectory calculation for the tracked vehicle, effectively resulting in enlarging the modified Kamm's circle by an amount related to the standard deviation associated with the state estimation uncertainties.

**Predicting the ego state** by computing the position and velocity of the ego vehicle using a constant-acceleration model over a time span equal to twice the time to collision of 500ms.

**The constellation extraction** module attaches a bounding box corresponding to the vehicle dimensions to the trajectories estimated for the object and ego vehicles. The trajectories are scanned for intersections between vehicle bounding boxes. The intersections correspond to a collision of the ego and object vehicles. A detected collision is the trigger point for extracting the collision parameters.

The next chapter presents the simulation model developed for evaluating the crash constellation extraction algorithm. Among other things, the simulation model includes a state estimation module for the tracked vehicle, and a real-word emulation component which measures vehicle state estimation parameters to capture uncertainties associated with the behaviour of real-world sensor fusion.

# 7 Simulation Model

The simulation model is the platform for the development and analysis of the accuracy of the crash constellation extraction algorithm, and for the extraction of uncertainty parameters associated with the sensor fusion system incorporated in the work reported in this thesis. The sensor and fusion model built into the simulation model emulates the real-world sensor behaviour of an in-vehicle sensor fusion and tracking system. Real-world collisions and tests are not feasible due to financial, technical and safety restrictions. Therefore, an offline simulation model which includes support for sensor fusion and crash scenario simulation is required to mimic real-world behaviour while offering the following functionality:

- Ability to define and simulate scenarios for vehicle-to-vehicle collisions.
- A single track model is utilised, for simulating the ego vehicle dynamics.
- Vehicle state estimation featuring a system and object motion model, within an extended Kalman filter for predicting the state of objects, specifically vehicles, in the context of the work reported herein.

## 7.1 Architecture of the simulation model

The offline simulation model provides different modules allowing arbitrary pre-crash simulations which feature a sensor fusion system including state estimation, object tracking, crash prediction, and collision constellation extraction.

Figure 7.1 depicts the architecture and data flow of the simulation model. The simulation model allows the definition and execution of crash simulations to support the analysis of crash constellation extraction. A key requirement placed on the implementation of the simulation is the ability to replicate the sensor fusion output produced by a real test vehicle. Furthermore, a number of constraints are placed on the simulation. The driving dynamics are implemented with a single track model, as roll and pitch angles are not considered, due to the simplification to a 2D space representing a top-down viewpoint from above the road vehicle. These constraints

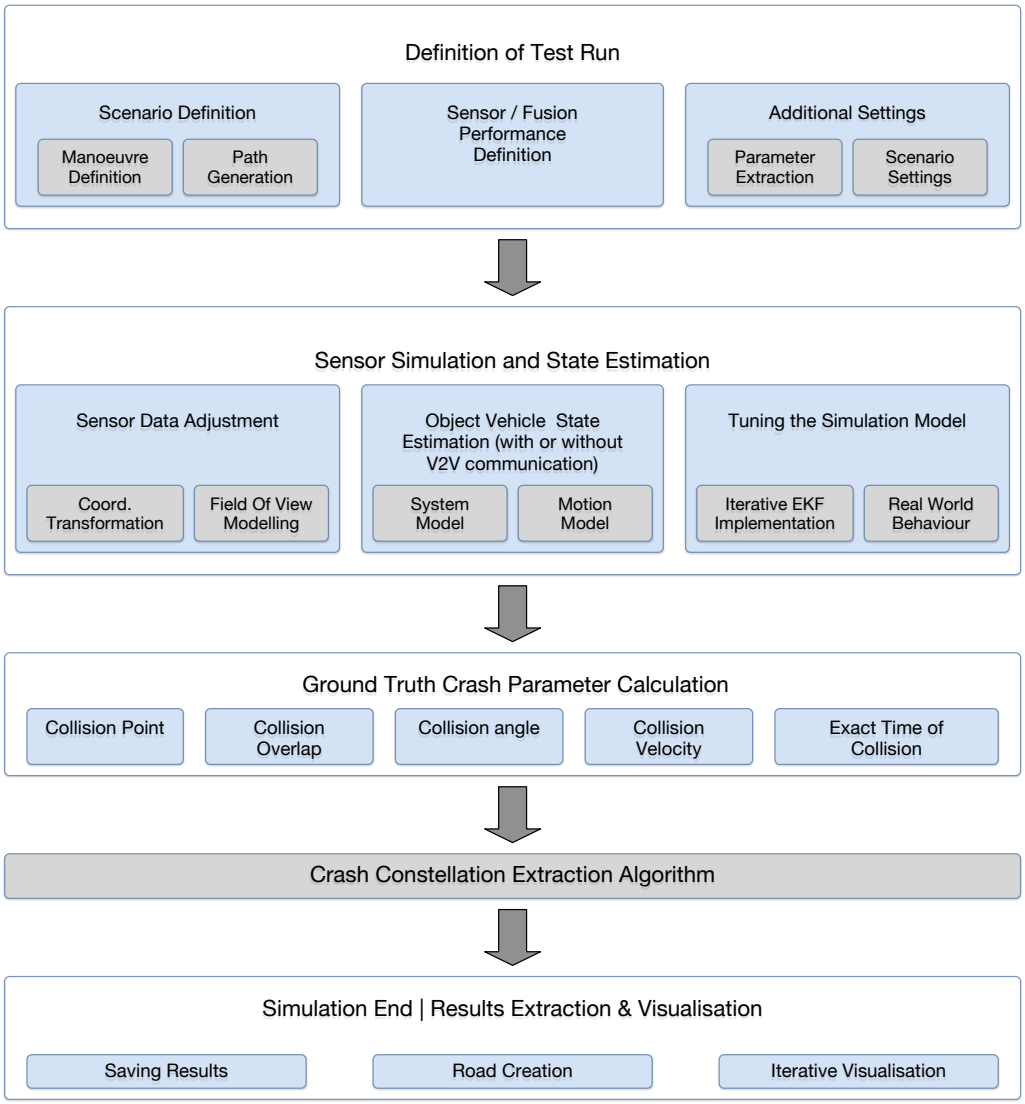


**Figure 7.1:** Architecture of the simulation

do not affect the simulation outcome, as the focus is on the evaluation of the crash constellation extraction, which can be computed in a 2D space. The model of the driving dynamics is sufficient for the calculation of vehicle trajectories.

## 7.2 Definition of collision scenarios

The simulation allows the definition of frontal collision scenarios involving two vehicles. The paths generated by the scenario definition component constitute the ground truth for the fusion and tracking simulation. Each path is generated freely

by combining straight and curved paths along which vehicle movements during simulation time.

### 7.2.1 Additional settings for a test run

The simulation framework provides additional settings to configure each test run. Different parameters can be chosen for the ground truth calculation and the later analysis for the constellation extraction. This gives the ability to pre-define the values calculated during runtime to allow the analysis and evaluation of the crash constellation extraction algorithm. The **scenario settings** provide an option for the user to distinguish between three different approaches for defining a scenario:

- Custom manoeuvre definition
- Collision based manoeuvre definition
- Crash parameter based manoeuvre definition

These different approaches are explained in more detail in the following section.

### 7.2.2 Manoeuvre definition and arrangement

#### Custom manoeuvre definition

A simulation run depends on various freely definable manoeuvres which are grouped as follows:

- Straight motion
- Left turn
- Right turn

The radius of the turn is defined by the radius of the path and the turn angle. These are cross checked against physical limitations, which arise from the driving dynamics for constant speeds $v$, by defining a minimal radius $R_{min}$ of

$$R_{min} = \frac{v^2}{a_{lat_{max}}} \tag{7.1}$$

with respect to the maximal lateral acceleration $a_{lat_{max}}$

$$a_{lat_{max}} = \mu_0 \cdot g \tag{7.2}$$

with the gravitational acceleration $g$ and the static friction coefficient $\mu_0$.

The simulation allows the design of various manoeuvres for collision or near-miss scenarios, thereby constituting a flexible platform for analysing the crash constellation extraction.

#### Collision based manoeuvre definition

The collision-based manoeuvre definition follows an approach similar to the custom manoeuvre definition. The only difference is that in addition to the user-defined path parameters, the starting points of the vehicles are calculated by the simulator such that the manoeuvre results in a collision. The paths of the vehicles defined freely by the user are anchored to vehicle starting points calculated to guarantee a collision.

#### Crash parameter based manoeuvre definition

This implementation offers the opportunity to look at specific collision constellations by specifying the collision parameters before the test run. The current implementation allows only straight motions which lead to the specified constellation parameters.

### 7.2.3 Performance settings for sensors or sensor fusion

The settings for the sensor fusion performance are stored aligned with the additional parameters in a settings file and they can be preloaded for a faster scenario definition. The main parameters which are adjusted by the user are the model noise, sensor fusion covariance matrix, the field of view and the sensor range. This gives the ability to adjust the fusion performance of the ego vehicle to compare different sensor settings; this is important to find the right sensor set up for future active safety systems.

### 7.2.4 Path generation and driving dynamics

The generation of the initial paths describing vehicle movements are constrained by physical limitations. The needed simulation time $t$ is calculated by solving Equation 7.3 for $t$, over the length of each of the path segments $S$ which are joined into a simulation manoeuvre. $v_0$ represents the initial velocity, and $a$ the acceleration, for the path segment $S$. The total simulation time is the sum of the individual segment times.

$$S = v_0 t + \frac{at^2}{2} \tag{7.3}$$

The number of points simulated throughout a simulation run is the total time $t$ for the manoeuvre, divided by the sensor update time step $T$. This allows the calculation of the change of vehicle position at each time step, taking into account the manoeuvre type and chosen angle, followed by the path calculation respectively with

$$x_i = x_{i-1} + (v_{i-1}T + \frac{aT^2}{2}) \cos(\psi_{v_i}) \tag{7.4}$$

$$y_i = y_{i-1} + (v_{i-1}T + \frac{aT^2}{2}) \sin(\psi_{v_i}) \tag{7.5}$$

where $x$ and $y$ represent the two components of the path vectors, $v$ is the magnitude of the velocity vector, $\psi_v$ is the angle for the orientation vector, and $a$ is the magnitude of the acceleration. The corresponding data is saved for each generated path, allowing free scenario generation with multiple manoeuvres. The paths of the vehicles serve as ground truth data for later analysis, and they provide the input measurements to the vehicle state estimation by the EKF.

The model for the position change is calculated for the single-track model.

## 7.3 Sensor coordinate system and field of view

### 7.3.1 Transforming coordinate systems

The vehicle paths and manoeuvres are created in the global world coordinate system. However, the tracking of objects occurs in the local coordinate system of the vehicle to which the modelled sensor and data fusion is attached. Therefore, a coordinate transformation is applied to obtain orientation and position measurements in the local sensor coordinate system.

To transform into the local coordinate system, the position is compensated by subtracting the ego vehicle coordinates from the coordinates of the object vehicle which is also referred to in this thesis as 'tracked vehicle'. Furthermore, the rotation matrix $\boldsymbol{R}$ transforms the orientation change into the local coordinate system. Its transpose is used for both ego-motion compensation and inverse transformation.

$$\boldsymbol{R} = \begin{bmatrix} \cos\psi & -\sin\psi \\ \sin\psi & \cos\psi \end{bmatrix} \tag{7.6}$$

The complete transformation is done by

$$\begin{bmatrix} x_{obj_{local}} \\ y_{obj_{local}} \end{bmatrix} = \boldsymbol{R} \cdot \left( \begin{bmatrix} x_{obj} \\ y_{obj} \end{bmatrix} - \begin{bmatrix} x_{ego} \\ y_{ego} \end{bmatrix} \right) \tag{7.7}$$

It is not enough to convert only the point representing the position of the vehicle, the whole vehicle bounding box is transformed because this is required for the collision detection; the transformation is thus applied to the field of view of the modelled sensors. Additionally, the rotation matrix is applied to the velocity and accelerations of objects. This is so as to obtain the relative velocity (for example), which is sensed by the environment perception system in the case of a real vehicle

The ego-motion compensation is explained in more detail in section 7.4.3.

For the visualisation, the inverse transformation provides the graphical user interfaces (GUI) with the correct transformations to the global coordinate system.

### 7.3.2 Model of the field of view for the virtual sensor

For the later analysis, it is important to have a field of view implementation to enable the fusion system to analyse more complex scenarios, such as crossing scenarios. The ego vehicle therefore features an adjustable sensor field of view with initially an horizontal opening angle of 120° and an operating range of 200m. These values were chosen due to the fact that the sensor fusion in the real vehicle produces stable data in this field of view (Aeberhard et al., 2012; Rauch et al., 2012).

The tracking starts, as soon the other vehicle enters the field of view. In reality, the system is more complex, as each sensor has its own detection principle. For example, the laser scanner detects objects in "L-shapes" representing two sides and a corner of the object. Furthermore, a monochrome camera for instance needs its image processing algorithm to classify the object for tracking. The radar also needs an initial phase to distinguish between an object and an erring target. Due to the fact that this work is for analyses performed in the pre-crash phase, scenarios with objects entering the FOV of the ego-vehicle within a TTC less than 500ms are addressed in this thesis. These scenarios are very complex and they cannot be verified due to the lack of adequate sensor models. A possible solution would be to use a Monte-Carlo simulation, as presented by Helmer (2013) featuring a virtual test bed for system testing, but this solution is outside the scope of this project.

The field of view implementation of the virtual sensor is computed in the local coordinate system of the vehicle. For reasons of simplicity a polar coordinate system is used to define the field of view of the sensor. Therefore, the points of the tracked vehicle are transformed from the global system (Cartesian) to the local system using the following transformations:

$$\Theta = atan2(y,x) \tag{7.8}$$

$$\rho = \sqrt{x^2 + y^2} \tag{7.9}$$

## 7.4 Estimation of the state of the object vehicle

In the following, the basis of the simulation and state estimation model is described in detail. Furthermore, the design of the state estimation module used by the system are explained with regards to object motion models and compensation for

the ego vehicle's motion, which are tuned to real world behaviour in as detailed in Section 7.5. The system model is described, followed by the explanation of the Kalman and extended Kalman filter.

### 7.4.1 System model

The underlying system model is based on various work reported in the literature (Bar-Shalom and Li, 1993; Brown, 2012; Kaempchen, 2007; Prat and Lemmer, 2011).

In-vehicle sensor systems provide discrete-time measurements or state estimation information to the environment perception module which computes the state information. Discrete-time systems, in a dynamic environment, include a representation of time which is cast in Equation 7.10 representing a measurement at an instant $i_k$ from a clock which has a time step $\Delta t$.

$$i_k = i_{k-1} + \Delta t \tag{7.10}$$

A system state vector $\boldsymbol{x}(i_k)$ with $n_x$ components represents the filtered information at every time instance $i_k$ with $k$ as an indication for constant time spans.

$$\boldsymbol{x}(i_k) = [x_1 \quad x_2 \quad ... \quad x_{n_x}]^T \tag{7.11}$$

The state vector is afflicted with an estimation error represented by

$$\boldsymbol{e}(i_k) = \tilde{\boldsymbol{x}}(i_k) - \hat{\boldsymbol{x}}(i_k) \tag{7.12}$$

with the true state vector $\tilde{\boldsymbol{x}}$ and the estimated vector $\hat{\boldsymbol{x}}$. Therefore, the uncertainty covariance matrix is estimated, for the state $\boldsymbol{x}(i_k)$, by

$$\boldsymbol{P}(i_k) = E[\boldsymbol{e}(i_k)\boldsymbol{e}^T(i_k)] \tag{7.13}$$

In the next step, the state space model is defined for a non-linear stochastic system for discrete-time measurements

$$\boldsymbol{x}(i_k) = \boldsymbol{f}[i_k, \boldsymbol{x}(i_{k-1}), \boldsymbol{u}(i_k), \boldsymbol{w}(i_k)] \tag{7.14}$$

with the state vector $\boldsymbol{x}(i_k)$ , the input vector $\boldsymbol{u}(i_k)$ , and the processed noise $\boldsymbol{w}(i_k)$ all providing the input data for the state transition function $\boldsymbol{f}$. For the case of a linear system, the equation is written as

$$\boldsymbol{x}(i_k) = \boldsymbol{F}(i_k)\boldsymbol{x}(i_{k-1}) + \boldsymbol{B}(i_k)\boldsymbol{u}(i_k) + \boldsymbol{w}(i_k), \tag{7.15}$$

with $\boldsymbol{B}$ and $\boldsymbol{u}$ representing the control input, and the time-varying state transition model is $\boldsymbol{F}(i_k)$. The uncorrelated, zero-mean process noise $\boldsymbol{w}(i_k)$ is normally distributed with a covariance matrix $\boldsymbol{Q}(i_k)$.

$$E[\boldsymbol{w}(i_k)] = 0; E[\boldsymbol{w}(i_k)\boldsymbol{w}(i_z)^T] = \boldsymbol{F_n} = \begin{cases} \boldsymbol{Q}(i_k) & \text{when k=z;} \\ 0 & \text{otherwise.} \end{cases} \tag{7.16}$$

Each sensor $s$ in a vehicle provides measurements relative to its position in the measurement space. Therefore, the measurement vector $\boldsymbol{z_s}(i_k)$ which contains the measurements, with $n_z$ components, is expressed as

$$\boldsymbol{z_s}(i_k) = [z_1 \quad z_2 \quad ... \quad z_{n_z}]^T \tag{7.17}$$

which allows the mapping of the measurement space to the true state space with the function $\boldsymbol{h_s}[i_k, \boldsymbol{x}(i_k), \boldsymbol{v}(i_k)]$ and $\boldsymbol{v}(i_k)$ being the measurement noise. This results in the equation for discrete-time measurements

$$\boldsymbol{z}_s(i_k) = \boldsymbol{h}[k,\boldsymbol{x}(i_k)] + \boldsymbol{n}_s(i_k) \tag{7.18}$$

and, in the case of linearity, it can be represented by the observation matrix $\boldsymbol{H_s}$ which has a size of $n_z \times n_x$:

$$\boldsymbol{z}_s(i_k) = \boldsymbol{H_s}(i_k)\boldsymbol{x}(i_k) + \boldsymbol{n_s}(i_k) \tag{7.19}$$

with $\boldsymbol{n_s}(i_k)$ as measurement noise. Both, the measurement and process noise, are modelled as white noise[1] with the covariance matrix $\boldsymbol{R_s}(i_k)$.

The system model for the offline simulation is limited by various assumptions with regards to the efficiency and power of simulation:

- The noise covariance of the measurements is known[2]
- The state of the ego vehicle is perfectly known.
- The pitch and roll angles are not considered, as well as the $z$ coordinate.
- Measurement and process noises are zero-mean, white[3], and mutually uncorrelated

The concept of the Kalman filtering technique and for non-linear systems the extended Kalman filter is explained in Appendix G.1 and Appendix G.2. The extended Kalman filter is used for the underlying research due to its capability of functioning in non-linear systems.

### 7.4.2 Motion model and object state prediction

In order to predict the motion of objects which are in the environment surrounding a vehicle, the behaviour of the tracked entity is modelled in a process model. The state estimation, which is described in this work utilises this process model and assumes that the state of an object changes over time. In this case, the process model is the motion model of the vehicle being tracked and it allows a prediction of its future state based on the current state, which contains the state vector and the corresponding uncertainty covariance matrix.

Modelling the behaviour of traffic participants or vehicles is very difficult and not feasible in real traffic. Therefore, the process model considers a variance between the actual state of an object and its state prediction, which is mostly assumed to be white noise. However, the motion model is approximated by a kinematic model of the first or second order, allowing a prediction according to the physics which

1 White noise: A random signal whose autocorrelation at any two arbitrary time steps is zero
2 In reality: Each sensor has its own measurement noise covariances which are provided in the sensor specification or need to be extracted out of offline measurements
3 Guaranteeing the correct processing of the Kalman filter

describes the motion of the vehicle. These models are often grouped into different model categories (Stellet et al., 2015).

- Constant velocity (CV) model - the deviation from a constant velocity is modelled as white process noise.
- Constant acceleration (CA) model - the change in acceleration is considered as a white process noise.

The modelled noise is described by the covariance matrix $\boldsymbol{Q}$ and recaptured later in Equation 7.23.

For the analysis regarding the extraction of the crash constellation, the pre-crash phase of two vehicles is simulated. The state of these vehicles consists of their

- Position
- Velocity
- Acceleration

The simulation is in 2D; it does not feature a movement or change in the vertical (z) axis of the vehicle.In the motion model used in this work, the state vector is represented by Equation 7.20a and 7.20b, respectively for the constant velocity model and the constant acceleration model.

$$\boldsymbol{x}_{CV} = [x \ y \ v_x \ v_y] \tag{7.20a}$$

$$\boldsymbol{x}_{CA} = [x \ y \ v_x \ v_y \ a_x \ a_y] \tag{7.20b}$$

As mentioned in G.2, the matrix $\boldsymbol{F}$ represents the transfer function for the state. For the constant velocity model and the constant acceleration model, $\boldsymbol{F}$ is expressed respectively as:

$$\boldsymbol{F_{CV}} = \begin{bmatrix} 1 & 0 & T & 0 \\ 0 & 1 & 0 & T \\ 0 & 0 & 1 & 0 \\ 0 & 0 & 0 & 1 \end{bmatrix} \qquad \boldsymbol{F_{CA}} = \begin{bmatrix} 1 & 0 & T & 0 & \frac{1}{2}T^2 & 0 \\ 0 & 1 & 0 & T & 0 & \frac{1}{2}T^2 \\ 0 & 0 & 1 & 0 & T & 0 \\ 0 & 0 & 0 & 1 & 0 & T \\ 0 & 0 & 0 & 0 & 1 & 0 \\ 0 & 0 & 0 & 0 & 0 & 1 \end{bmatrix} \tag{7.21}$$

with $\boldsymbol{T}$ describing the sampling period which is the sensor update time step defined in Section 7.2.4. In automotive sensor networks, different sensor types (monochrome camera, RADAR, or LIDAR) have different update rates; therefore, the fusion of sensor data varies in the time period and can be time variant accordingly.

A multiplication (shown in Equation 7.24 involving the noise gain $\boldsymbol{\Gamma}$ (illustrated in Equation 7.22) and the covariance of the process noise $\boldsymbol{Q_d}$ (depicted in Equation 7.23) gives the covariance matrix $\boldsymbol{Q}$.

$$\boldsymbol{\Gamma_{CV}} = \begin{bmatrix} T^2 & 0 \\ 0 & T^2 \\ T & 0 \\ 0 & T \end{bmatrix} \qquad \boldsymbol{\Gamma_{CA}} = \begin{bmatrix} T^2/2 & 0 \\ 0 & T^2/2 \\ T & 0 \\ 0 & T \\ 1 & 0 \\ 0 & 1 \end{bmatrix} \tag{7.22}$$

$$\boldsymbol{Q_d} = \begin{bmatrix} \sigma_{a_x}^2 & 0 \\ 0 & \sigma_{a_y}^2 \end{bmatrix} \tag{7.23}$$

with $\sigma_{a_x}^2$ and $\sigma_{a_y}^2$ describing the acceleration noise in the directions (x,y).

$$\boldsymbol{Q} = \boldsymbol{\Gamma} \boldsymbol{Q}_d \boldsymbol{\Gamma}^T \tag{7.24}$$

### 7.4.3 Compensating for the ego-motion

Sensor data is commonly measured relative to the sensor coordinate system. In real vehicle systems, the compensation for the motion of the ego-vehicle is handled by the sensor itself. For the simulation model, the ego motion needs to be compensated to avoid a wrong prediction of the state of the tracked vehicle by adding the movement of the ego vehicle to the velocity of the sensed vehicle, for example. This section justifies the need to deploy ego-motion compensation towards achieving accurate state prediction within this work.

Let the change in position (Equation 7.25a) and orientation (Equation 7.25b) of the ego vehicle over some time interval be defined as

$$[\Delta x_{ego} \quad \Delta y_{ego} \quad ]^T \tag{7.25a}$$

$$[\Delta \psi_{ego}]^T \tag{7.25b}$$

These variables can be combined into a matrix describing the motion of the ego vehicle over some time interval as

$$\boldsymbol{u}_{ego} = [\Delta x_{ego} \quad \Delta y_{ego} \quad \Delta \psi_{ego}]^T \tag{7.26}$$

According to Stüker (2004), the following fundamental components describing the motion of the ego vehicle are sufficient for the ego-motion compensation and they were used in the present work:

- Longitudinal movement $\Delta y_{ego}$
- Lateral movement $\Delta x_{ego}$
- Yaw rate $\Delta \psi_{ego}$

For a correct compensation for the ego-motion of a vehicle, the order in which the compensation operations are applied is important. Therefore, the change in position $[\Delta x_{ego}\ \Delta y_{ego}]$ is taken into account first, then follows the compensation for the orientation, using the rotation matrix $\boldsymbol{R}_{ego}^T$.

$$\boldsymbol{R}_{ego}^T = \begin{bmatrix} \cos\psi & -\sin\psi \\ \sin\psi & \cos\psi \end{bmatrix} \tag{7.27}$$

The formula given below transforms the estimated state (including the position, velocity and acceleration) of the sensed vehicle at time $i_k$, to compensate for the

motion of the ego-vehicle.

$$\hat{\boldsymbol{x}}\left(i_k|i_{k-1}\right) = \boldsymbol{f}_{ego}[\hat{\boldsymbol{x}}(i_k|i_{k-1}), \hat{\boldsymbol{u}}_{ego}(i_k)] = \begin{bmatrix} \boldsymbol{R}_{ego}^T \cdot \left( \begin{bmatrix} x_{i_k} \\ y_{i_k} \end{bmatrix} - \begin{bmatrix} \Delta x_{ego} \\ \Delta y_{ego} \end{bmatrix} \right) \\ \boldsymbol{R}_{ego}^T \cdot \begin{bmatrix} v_{x_{i_k}} \\ v_{y_{i_k}} \end{bmatrix} \\ \boldsymbol{R}_{ego}^T \cdot \begin{bmatrix} a_{x_{i_k}} \\ a_{y_{i_k}} \end{bmatrix} \end{bmatrix} \tag{7.28}$$

As aforementioned, sensors measure the speed relative to the vehicle; therefore, it is necessary initially to compensate for the ego-motion. The same applies to the estimated acceleration, if included in the simulation model. Furthermore, motion compensation is necessary for the covariance matrix; it is calculated using the predicted covariance $\boldsymbol{P}(i_k|i_{k-1})$ as

$$\boldsymbol{P}(i_k|i_{k-1}) = \boldsymbol{F}_{ego}\boldsymbol{P}(i_k|i_{k-1})\boldsymbol{F}_{ego}^T \tag{7.29}$$

where the Jacobian $\boldsymbol{F}_{ego}$ of $\boldsymbol{f}_{ego}$ is given as

$$\boldsymbol{F}_{ego} = \left[\nabla_x \boldsymbol{f}'_{ego}\right]' \Big|_{\boldsymbol{x}=[\hat{\boldsymbol{x}}'_{i_k} \;\; \hat{\boldsymbol{u}}'_{ego}]'} \tag{7.30}$$

Due to the assumption that the ego-state is known precisely for linear driving manoeuvres, no uncertainty is added to the covariance matrix during the initialisation.

The yaw angle of the ego vehicle in the automotive environment is directly measured by sensors linked to the steering wheel of the vehicle and it is afflicted with a rather constant measurement noise. In the simulation model, it is not afflicted with variances because it is assumed that the path of the vehicle is known. This leads to

a simplified Jacobian matrix[1] as follows:

$$\boldsymbol{F}_{ego} = \begin{bmatrix} \cos(\Delta\psi_{ego}) & \sin(\Delta\psi_{ego}) & 0 & 0 & 0 & 0 \\ -\sin(\Delta\psi_{ego}) & \cos(\Delta\psi_{ego}) & 0 & 0 & 0 & 0 \\ 0 & 0 & \cos(\Delta\psi_{ego}) & \sin(\Delta\psi_{ego}) & 0 & 0 \\ 0 & 0 & -\sin(\Delta\psi_{ego}) & \cos(\Delta\psi_{ego}) & 0 & 0 \\ 0 & 0 & 0 & 0 & \cos(\Delta\psi_{ego}) & \sin(\Delta\psi_{ego}) \\ 0 & 0 & 0 & 0 & -\sin(\Delta\psi_{ego}) & \cos(\Delta\psi_{ego}) \end{bmatrix} \tag{7.31}$$

## 7.5 Simulation model tuned to emulate real-world behaviour

This section describes the implementation of the extended Kalman filter, including the selection of uncertainty parameters associated with the performance of the sensor fusion system and how the sensor field of view is taken into account. Furthermore, the section presents the initialisation method for the simulation framework which aims to reproduce the behaviour of real-world sensor fusion, including the error in state estimation. For this work the EKF is used for the simulation model becauseBarth and Franke, 2008 the in-vehicle sensor fusion utilises the same principle for predicting the opponents state.

### 7.5.1 Implementation of the extended Kalman filter

Section 4.2.1 explained the basic principles of Kalman filtering. A more detailed presentation of the algorithmic side is given in Appendix G, Section G.2. In the first steps of this work, a simple Kalman filter was implemented. Due to the growing demand for vehicle motion scenarios which require a non-linear system, it was decided that the extended Kalman filter fulfils the requirements and it was therefore implemented in this work.

As an iterative filter (see Appendix G, Section G.2), the Kalman filter considers previous measurements and needs therefore an initialisation routine. Different options

1 The acceleration is also directly derived from the position over time

are available for this routine. Commonly, the measurement vector is initialised with reasonable values[1] and the covariance matrix is updated with slightly higher ones[2]. The second approach relies on initialising the state vector with the first measurement available; this is the approach used in this work.

Regarding the measurement principle[3], the measurement uncertainty covariance matrix $\mathbf{R}$ is used for initialising the covariance matrix for the prediction $\mathbf{P}$ (Equation 7.29), allowing a more robust and fast initialisation of the EKF.

The work presented in this thesis has considered two main motion models (detailed in Section 7.4.2); the constant velocity (**CV**) model and the constant acceleration (**CA**) model. For the CA model (which includes the estimation of the objects acceleration), the state vector, the covariance matrix, and other matrices involved differ in size and require an additional check to return the correct implementation for the motion model.

For the process noise, the acceleration is modelled with a standard deviation (longitudinal $\sigma_{a_x}$, lateral $\sigma_{a_y}$) set to

$$\sigma_{a_x} = 4 \ \frac{m}{s^2} \qquad \sigma_{a_y} = 4 \ \frac{m}{s^2} \tag{7.32}$$

This choice is based on the maximal deceleration of passenger vehicles, which is said to be 11m/s$^2$, according to Kaempchen (2007), nearly the 3 times the sigma values chosen in Equation 7.32 to represent the process noise. This includes the assumption, that the maximum deceleration can be achieved within a single measurement interval.

1 Observed via various experiments
2 Representing a higher confidence in the process model
3 The principle which underpins the operation of a sensor

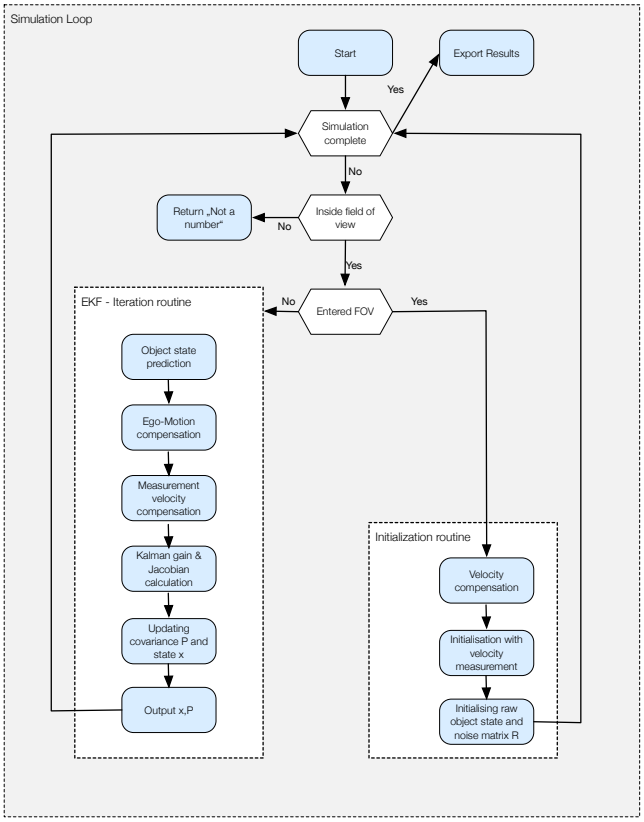


**Figure 7.2:** Flow chart for the extended Kalman filter implemented for estimating the state of the tracked vehicle

The state estimation and object tracking is implemented as specified in Section 7.4.2, which allows plausible tracking of objects, even if the objects are leaving or entering the FOV of the vehicle. Figure 7.2 depicts the flow chart for the extended Kalman filter. Furthermore, based on the EKF, the simulation model supports state estimation for scenarios which are not highly non-linear. In cases of a highly non-linear system which affects the state estimation system more than the EKF is able to correct, the estimation error accumulates over time. An example for this state of the system is a highly non-linear scenario which features two vehicles performing large non-linear manoeuvres combined with a low sensor update rate.

### 7.5.2 Tuning the state estimation output of the simulation model to real world behaviour

Assuming time invariant process noise and measurement noise, the uncertainty associated with the covariance matrix of the state estimation converges towards a definite value for linear and slightly non-linear systems. This effect is shown in Figure 7.3 which illustrates that the standard deviation for the estimated position converges towards a low value over time. This convergence is achieved in a short amount of time, for accurate initialisation routines assuming an unchanged covariance matrix:

$$\boldsymbol{P}_{i_{k-1}} = \boldsymbol{P}_{i_k} \tag{7.33}$$

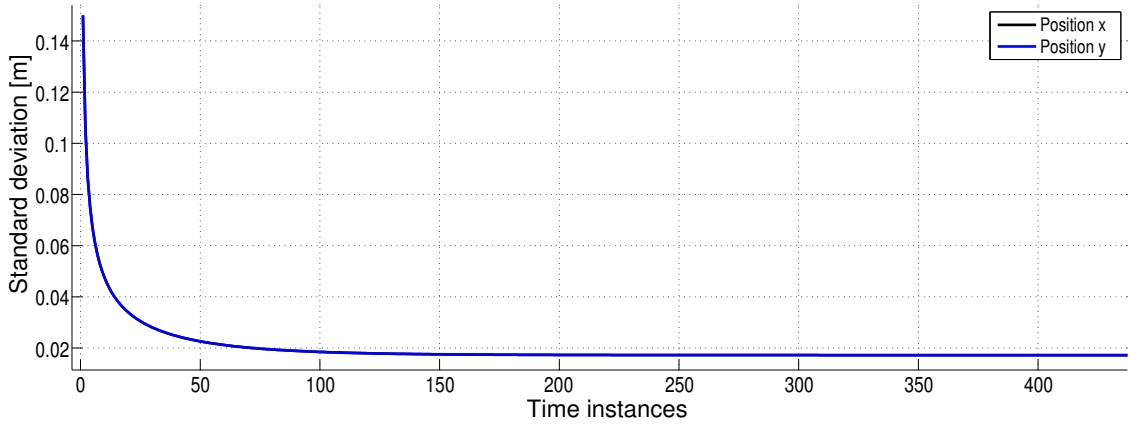


**Figure 7.3:** The standard deviation for the position estimation over time

The innovation covariance $\boldsymbol{S}_k$, as explained in Appendix G.1, is the sum of the predicted and actual measurement vector covariances (Equation 7.34). It is denoted with

$$\boldsymbol{S}(i_k) = \boldsymbol{H}(i_k)\boldsymbol{P}(i_k|i_{k-1})\boldsymbol{H}^T(i_k) + \boldsymbol{R}(i_k) \tag{7.34}$$

Combined with the Kalman gain formula (Equation 7.35)

$$\boldsymbol{K}(i_k) = \boldsymbol{P}(i_k|i_{k-1})\boldsymbol{H}^T(i_k)\boldsymbol{S}^{-1}(i_k) \tag{7.35}$$

it leads to the formula for estimating the covariance update (Equation 7.36)[1].

$$\boldsymbol{P}(i_k|i_k) = [\boldsymbol{I} - \boldsymbol{K}(i_k)\boldsymbol{H}(i_k)]\boldsymbol{P}(i_k|i_{k-1}) \tag{7.36}$$

Solving Equation 7.36 with respect to $\boldsymbol{R}$ relates the estimation covariance $\boldsymbol{P}$ to the measurement noise covariance $\boldsymbol{R}$, under the assumption of a converged and stable $\boldsymbol{P}$ with

$$\boldsymbol{P} = \boldsymbol{P}(i_k|i_{k-1}) = \boldsymbol{P}(i_k|i_k) \tag{7.37}$$

This allows a simplified denotation for $\boldsymbol{R}$ with

$$\boldsymbol{R} = \left(\left(\boldsymbol{I} - \frac{\boldsymbol{P}}{\boldsymbol{P}(i_k|i_{k-1})}\right)/\boldsymbol{H}\right) \backslash (\boldsymbol{P}(i_k|i_{k-1})\boldsymbol{H}^T) - \boldsymbol{H}\boldsymbol{P}(i_k|i_{k-1})\boldsymbol{H}^T \tag{7.38}$$

with $\boldsymbol{P}(i_k|i_{k-1})$ representing

$$\boldsymbol{P}(i_k|i_{k-1}) = \boldsymbol{F}(i_k)\boldsymbol{P}\boldsymbol{F}^T(i_k) + \boldsymbol{Q}(i_k) \tag{7.39}$$

In reality, the covariance of the measurement noise is influenced by many input parameters in a time variable manner. Equation 7.38 is still a good approximation, for reproducing the behaviour of a real in-vehicle state estimation system. However, if the motion models of the state estimation system are not known, it is difficult to derive the measurement covariance matrix out of the prediction covariance matrix $P$ even if it is recorded by real-world experiments.

Another opportunity to derive the measurement covariance matrix is to extract the variances out of test drives by using an expensive reference system in both the ego and object vehicles. Values extracted from various real-world test drives can be used to tune the simulation to achieve a near to real-world state estimation performance. To determine the measurement covariance matrix $R$ , using data collected from test drives of real vehicles, two vehicles were driven in 15 test runs of a front-to-front near-miss collision scenario. Figure 7.4 illustrates the vehicle configuration for the data collection.

1 For more detailed information about Kalman filtering, see Section G.1

- Two vehicles were equipped with dGPS to determine their exact location.
- The prototype vehicle featured a full sensor fusion and state estimation system.
- A head on collision scenario with a near miss use-case was executed.
- Three iterations per test run in which the speeds varied from 20 to 60 km/h for both vehicles in steps of 10 km/h.

The state estimation performance of the prototype vehicle was evaluated within these 15 test runs with regards to the following criteria:

- Error in lateral and longitudinal position estimation.
- Error in lateral and longitudinal velocity estimation.
- Histogram computed over the average error for the above mentioned test runs.

The covariance matrix $P$ was extracted out of the average error distributed over the test runs.

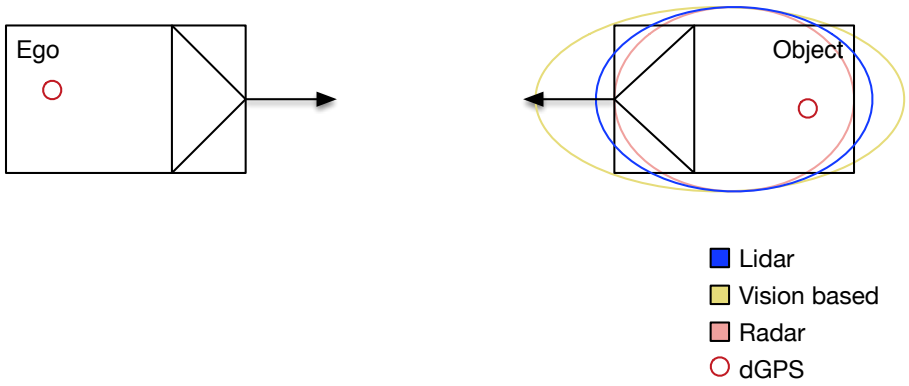


**Figure 7.4:** Real-world front-to-front near miss scenario for extracting sensor variances to be reproduced in the simulated state estimation model

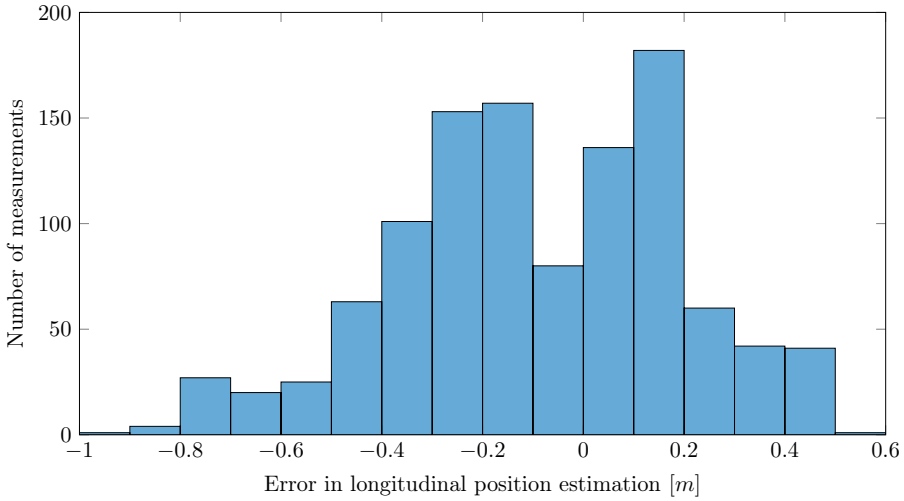


**Figure 7.5:** Average error in longitudinal position estimation of the in-vehicle state estimation system

Number of measurements: 1093

Range of values: -0.94733m ... 0.51494m

Standard deviation: 0.28146

Variance: 0.07922

Median: -0.10315

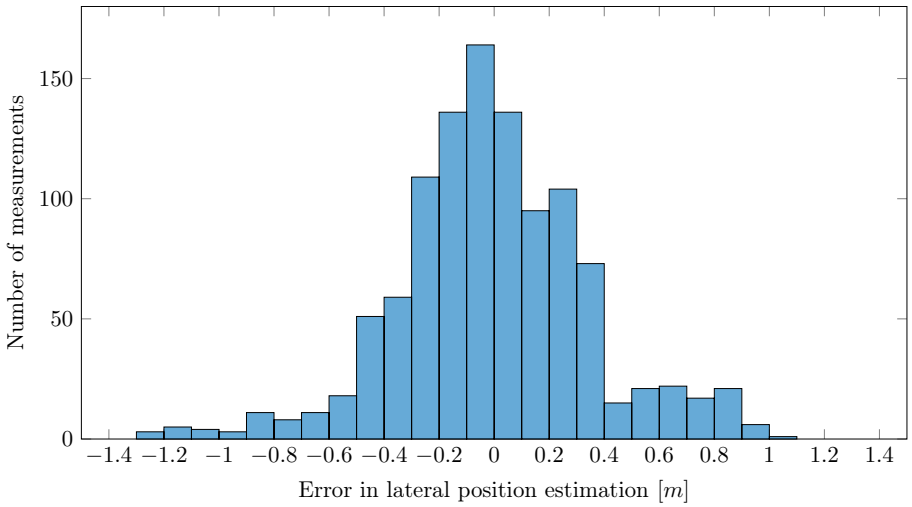


**Figure 7.6:** Average error in lateral position estimation of the in-vehicle state estimation system

Number of measurements: 1093

Range of values: -1.2496 ... 1.0394

Standard deviation: 0.3518

Variance: 0.12376

Median: -0.021019

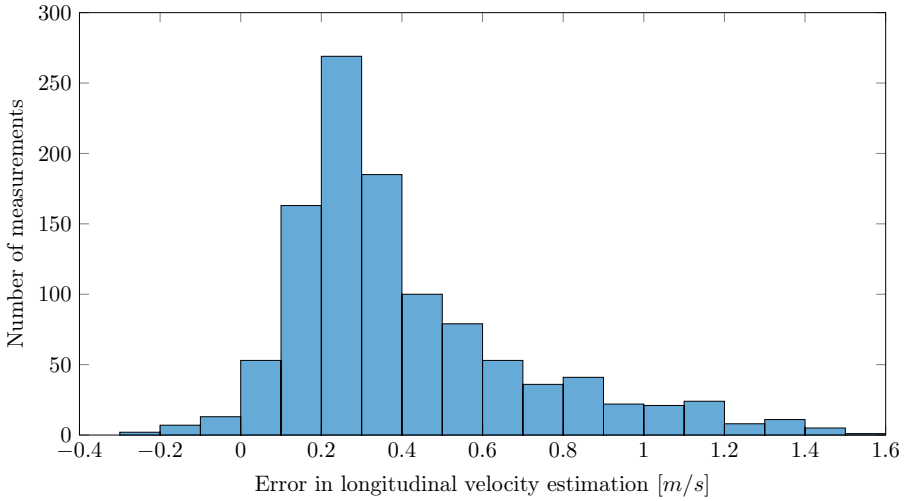


**Figure 7.7:** Average error in longitudinal velocity estimation of the in-vehicle state estimation system

Number of measurements: 1093

Range of values: -0.29717 ... 1.5223

Standard deviation: 0.29893

Variance: 0.089359

Median: 0.31594

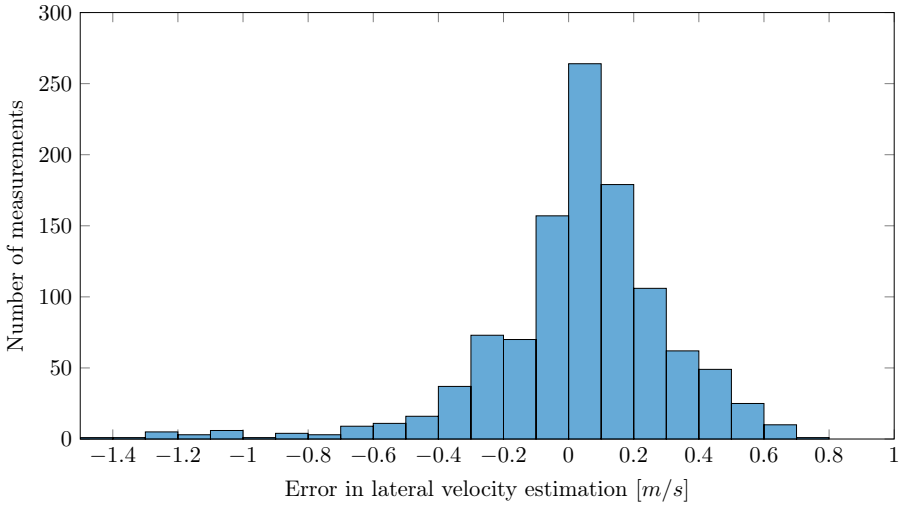


**Figure 7.8:** Average error in lateral velocity estimation of the in-vehicle state estimation system

Number of measurements: 1093
Range of values: -1.4694 ... 0.72295
Standard deviation: 0.28377
Variance: 0.080526
Median: 0.056365

The state estimation covariance matrix $R$ for the simulation model was set to

$$\boldsymbol{P}_{sim} = \begin{bmatrix} 0.3^2 & 0 & 0 & 0 \\ 0 & 0.3^2 & 0 & 0 \\ 0 & 0 & 0.2^2 & 0 \\ 0 & 0 & 0 & 0.2^2 \end{bmatrix} \tag{7.40}$$

The estimation variances for the velocities were improved due to the fact, that the conditions were not optimal on the day the experiments were conducted. The velocity estimations of the in-vehicle state estimation process are usually slightly better due to the fact that the RADAR sensor measures the velocity directly. This has a major impact on the current in-vehicle state estimation process.

## 7.6 Conclusion

This chapter presents the simulation model produced in this work. The model is for evaluating the performance of the crash constellation extraction algorithm developed in this research.

The simulation model has been devised to offer the following functionality:

- Ability to emulate the behaviour of the sensor system of a real self-driving vehicle prototype.
- Ability to define and simulate vehicle-to-vehicle collision scenarios.
- Ability to simulate various vehicle motion behaviours, based on different 2D models of vehicle dynamics.
- Ability to estimate the state of a tracked vehicle, using an extended Kalman filter which includes the above-mentioned motion models and emulation of the behaviour of a real vehicle sensor system.
- Ability to extract the constellation of a crash.

The main architectural components of the simulation model are connected sequentially. These modules are listed below, from first to last:

- Definition of a test run.
- Sensor simulation, and vehicle state estimation.
- Calculation of the ground-truth for vehicle state.
- Crash constellation extraction.
- Visualisation and storage of simulation results.

A manoeuvre editor enables the user to define various pre-crash and crash simulations, as part of the definition of test scenarios. Furthermore, different models of driving dynamics (a constant velocity model, and a constant acceleration model) are implemented into the simulation model, to allow a realistic simulation of vehicle trajectories. The extended Kalman filter included in the simulation model, uses

values of the measurement noise covariances recorded for a real self-driving vehicle prototype. This effectively allows the simulator to emulate the behaviour of a real-world sensor system.

# 8 Performance Assessment

This chapter presents and discusses the empirical evaluation of the performance of the crash constellation algorithm. The assessment was conducted using a simulator, and (as shown in Figure 7.1) the crash constellation extraction process receives its input from the simulation model which performs vehicle state estimation. Hence, the performance assessment methodology is divided into two main steps:

(i) Assessment of the soundness of the simulation model for vehicle state estimation: The assessment included a study which considered simulation data on its own, to analyse the error in the estimates of the position and velocity of the object vehicle. This simulation-only study was followed by another study which compared the position and velocity estimates from the simulator to those obtained from a real test drive.

(ii) Performance assessment of the crash constellation extraction algorithm: This assessment covered the main crash constellation parameters, namely: point of collision on the body of the ego vehicle and relative velocity between the vehicles.

The vehicle alignment offset (or vehicle overlap) was not considered explicitly in this performance assessment, as the collision scenarios are separated into a front-to-front collision scenario featuring a 100 % collision overlap and a front-to-side collision scenario in which the overlap cannot be estimated. The collision overlap is mainly important as an indicator of accident severity in head-on collisions, as weaker vehicle body parts can be hit for collision overlaps smaller than 30%. For collision overlaps of more than 70% the deformation architecture (passive vehicle construction elements) can be used for collision impact absorption. Importantly, the overlap between the colliding vehicles is directly related to the point of collision on the vehicle body, resulting in strong correlation between measurements of the two parameters. Hence, the uncertainty associated with the predicted point of collision is a good indicator of the uncertainty associated with the predicted vehicle overlap. Therefore, it is sufficient to assess only one of these two parameters; in light of the considerations discussed above, the parameter chosen in this research is the point of collision.

# 8.1 Assessment of the soundness of the simulation model for vehicle state estimation

## 8.1.1 General information about the assessment method

### 8.1.1.1 Methodological considerations for assessing the simulation model

The extended Kalman filter implemented in the simulation model (Chapter 7), which includes noise parameters of a real-world in-vehicle sensor fusion system needs to be validated. According to Murray-Smith (2015) a simulation model cannot be validated, rather the error of the model needs to stay in the specified ranges of operation. This means, that the performance of the model needs to work within the same boundaries of performance as the real-world behaviour, because models are approximations of real-world systems. Murray-Smith (2015) stated that:

"Anyone with modelling experience will know that what we are really interested in when we are assessing model quality is more related to a process of invalidation."

Figure 8.1 shows the modelling process of a simulation model according to Murray-Smith (2015). For this thesis the simulation model for the in-vehicle sensor fusion system was derived as follows:

The **requirements** were analysed in Section 7.4.1 including the analysis of different modelling options. The extended Kalman filter featuring a constant velocity or constant acceleration model were chosen as the **conceptional design**. This is the basis for the state estimation filtering technique used in the simulation **approach**. Furthermore, the chosen **model and its parameter** were tuned to emulate real world behaviour with regards to uncertainties associated with the sensor fusion system of a real vehicle, in Section 7.4. Chapter 7 shows the complete **simulation model** including the model for estimating the state of the object vehicle. Therefore, Section 8.1.1.2 evaluates the simulation model with an assessment of the state estimation model with or without a simualted vehicle-to-vehicle communication. Adopting the process mentioned by Murray-Smith (2015) the measurements gathered during a test drive of a real vehicle on a highway with a state-of-the art sensor fusion system are compared to a similar simulation scenario in Section 8.1.2.2.

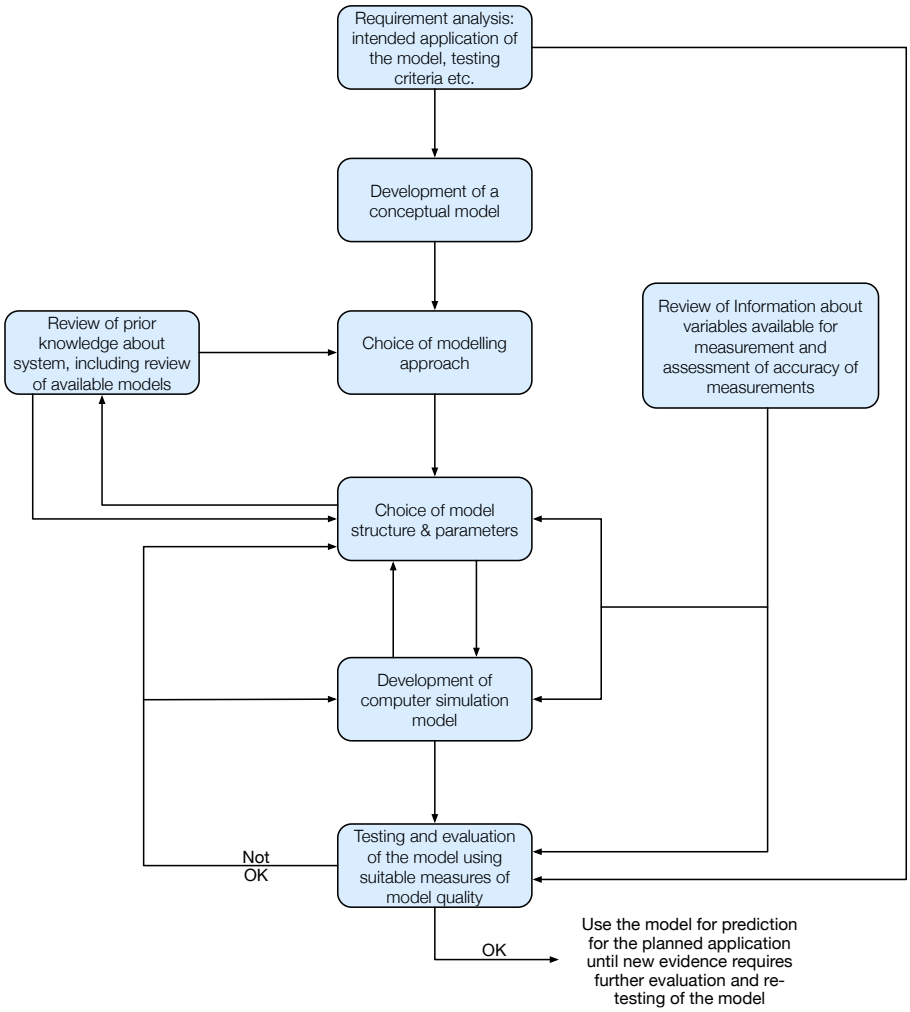


**Figure 8.1:** Block diagram showing the initial top-level representation of the modelling process (Murray-Smith, 2015)

#### 8.1.1.2 Implementation of the simulated V2V communication

This section describes the integration of a virtual vehicle-to-vehicle sensor as an additional data sensor. Experiments were conducted to assess the behaviour of the model with regards to errors in position and velocity estimation. The V2V data influence the motion model which is described in Section 7.4.2.

As already discussed in Section 3.2.5, V2V-communication enhances the field of view of the sensor and is able to provide additional information for perceiving the environment. Built on near field communication, vehicle data can be sent to another vehicle. The receiving vehicle can treat the incoming V2V stream as emanating from a virtual sensor which feeds into the sensor fusion system. The use of V2V enables a

higher accuracy in the acquisition of the velocity and acceleration of the surrounding objects. V2V is also able to transmit other data, such as driver intention, which is a very important parameter for pre-crash applications in general and the crash constellation extraction in particular.

As mentioned above the integration of the V2V communication into the model was implemented by including a more precise estimation of the velocity ($\sigma_v$ =0.1 m/s) and acceleration ($\sigma_a$ =0.1 m/s$^2$) of the tracked object. These values are based on the work of Khairnar and Kotecha (2013) who analysed the performance of the IEEE 802.11p standard for vehicle-to-vehicle ad-hoc communications. Furthermore, the cooperative awareness messages require an update rate of 10Hz and a maximum latency of 100 ms (ETSI, 2009, 2011; Shi and Sung, 2014). This latency was therefore chosen as uncertainty for the velocity and acceleration estimation in the Jacobian matrix (Equation 7.31).

Generally the position estimation provided by V2V is less accurate compared to the environment perception system used in vehicles nowadays. Consequently, it was decided that the virtual V2V channel must not provide position estimates to the simulation model. Nevertheless, as the velocity and acceleration information is included in the state estimation process, the filtered position is expected to be of higher quality with V2V than without.

#### 8.1.1.3 Assessment scenarios

As discussed in Section 5.2.2.3, the chosen scenarios are front-to-front and front-to-side collisions. The front-to-front collision scenario illustrated in Figure 8.2 is constrained by

- Straight motion starting from a 300m distance between the object vehicle and ego vehicle.
- The motion profile does not change in velocity (i.e. no acceleration is applied).
- The scenario is for a head-on collision (180°in angle between the two vehicles).
- The tracking and prediction starts when the object vehicle enters the field of view of the ego vehicle (i.e. 200m from the latter).

The front-to-side collision is constrained by

- Straight motion at a 90°angle between the object vehicle and ego vehicle.
- The motion profile does not change in velocity (i.e. no acceleration is applied).
- The tracking and prediction starts when the object vehicle enters the field of view of the ego vehicle.

The figure shows the **object vehicle**, which is the vehicle being tracked, the **ego vehicle**, the **measurement** output of the virtual fusion system and the aligned **position estimation**, which is the output of the extended Kalman filter. The **ground truth (GT)** gives the position at each time step without any process noise and is the reference position for assessing the position estimated by the simulation.

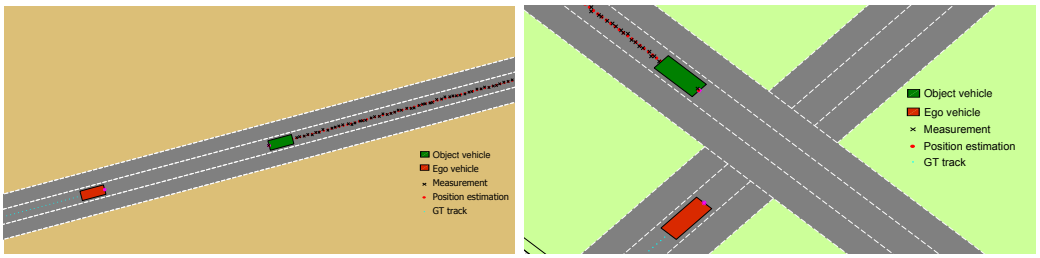


**Figure 8.2:** Front-to-front (left) collision scenario ($v_{obj} = v_{ego}$= 60 km/h) and front-to-side (right) collision scenario ($v_{obj} = v_{ego}$ = [30 km/h ... 60 km/h])

The following sections focus on the performance of the state estimation process and the prediction of the time-to-collision for the tracked object.

## 8.1.2 Assessment of the simulated vehicle state estimation

### 8.1.2.1 Assessment of simulation data on its own

**Aim:** To study the error in the estimates of the position and velocity of the object vehicle, with or without vehicle-to-vehicle (V2V) communication used to provide additional data on the driving environment.

**Method:** Position and velocity estimates were computed for a single object vehicle using the simulation model described earlier, with input data produced according to the scenarios described in Section 8.1.1.3 and field of view as described in Section 7.3.2. The EKF was implemented in line with Section 7.5.1; the covariance matrix for the measurement noise was tuned to emulate a real in-vehicle sensor data fusion system as described in Section 7.5.2. V2V communication was implemented as an enhancement to the state estimation process as presented in Section 8.1.1.2. The simulation was run over a length of 10 s, with a time step of 100ms.

The estimation error from the Kalman filtering technique was calculated for a sensor fusion system with or without V2V communication.

The calculation of the magnitude of the measurement error is described by the following equation:

$$e_{pos} = \sqrt{e_x^2 + e_y^2} \tag{8.1}$$

with $e_x$ and $e_y$ representing the offset between the actual and the estimated position of the object. The error in the position estimation is similar in both directions resulting from the chosen values for the transfer function matrix $\mathbf{F}$. Therefore, the covariance associated with the position estimation can be illustrated as a circle or ellipse in 2D space depending on $\sigma_x$ and $\sigma_y$.

**Results:** The error resulting from the estimation of the position of the object vehicle is illustrated in Figure 8.3 for the front-to-front collision scenario (and in Figure 8.4 for the front-to-side collision scenario) and for the error in the velocity estimation of the object in Figure 8.5 for the front-to-front collision scenario (analogous in Figure 8.6 for the front-to-side collision scenario). The two solid curves show the $3\sigma$ confidence interval of the covariance matrix of the Kalman filter, which includes 99.73% of the measurement error in each figure with or without V2V activated.

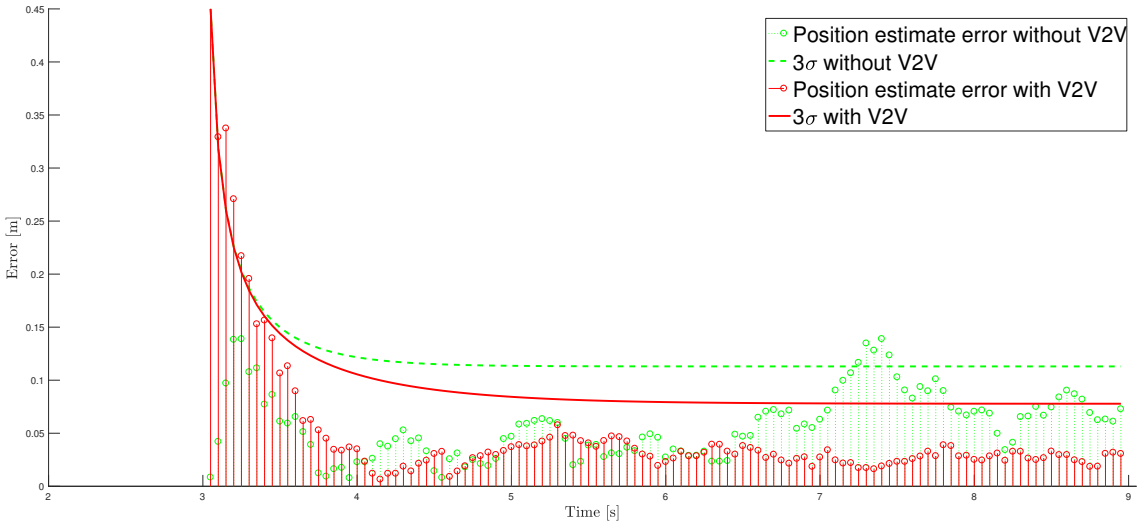


**Figure 8.3:** Front-to-front collision scenario: Position estimation error together with $3\sigma$ confidence interval for $v_{obj}$=$v_{ego}$=60 km/h; with or without V2V. The object vehicle enters the field of view of the ego vehicle after three seconds of the simulation run, hence the state estimation process is triggered at 3s as shown above.

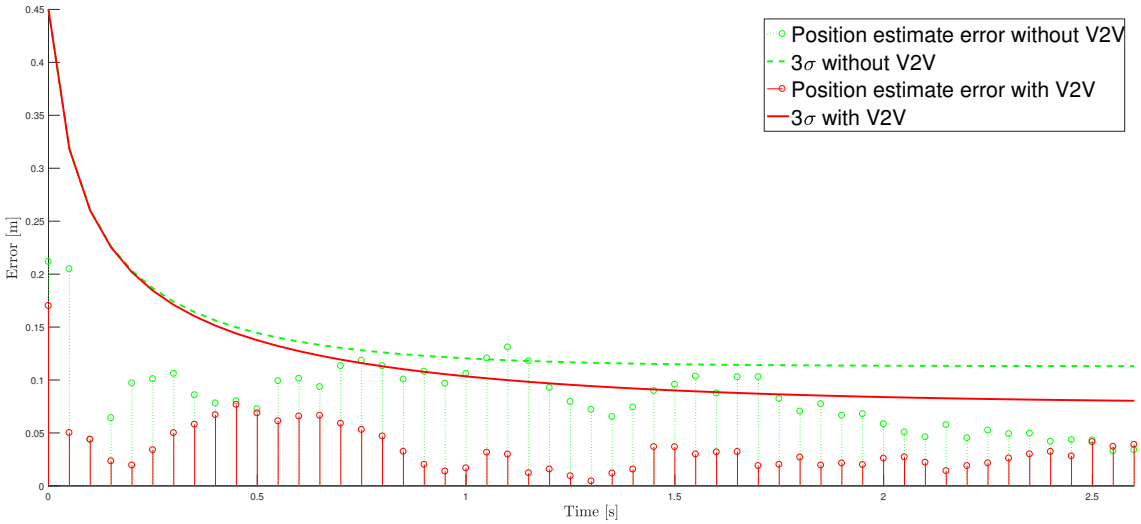


**Figure 8.4:** Front-to-side collision scenario: Position estimation error together with $3\sigma$ confidence interval for $v_{obj} = v_{ego}$=40 km/h; with or without V2V. The object vehicle is within the field of view of the ego vehicle already at simulation start, hence the state estimation process is triggered at simulation start.

**Discussion:** In the investigated front-to-front collision scenario, the object vehicle enters the field of view of the ego vehicle after three seconds, triggering the state estimation process. For the front-to-side collision scenario, the object vehicle is already in the field of view of the ego vehicle at simulation start. This is shown in

Figure 8.4 and 8.6 as measurement data is available at the beginning of the simulation run. As mentioned in Section 7.5.2 the noise covariance matrix converges towards a low value. The measurement matrix $\boldsymbol{R}$ is initialised in an identical manner for both fusion set ups, and it shows a lower error rate. For position estimation, slightly better performance was obtained for the system with V2V communication. This behaviour can be explained by the better precision of the velocity and acceleration measurements, which are directly transmitted from the tracked vehicle to the ego-vehicle, resulting in increased reliability and being therefore less error prone.

The covariances for the position estimation produce the expected behaviour, as illustrated in Figure 8.3 and Figure 8.4. Analogous behaviour is depicted for velocity in Figure 8.5 and 8.6 which (under the conditions of the reported experiment) implies an acceptable behaviour of the simulation model.

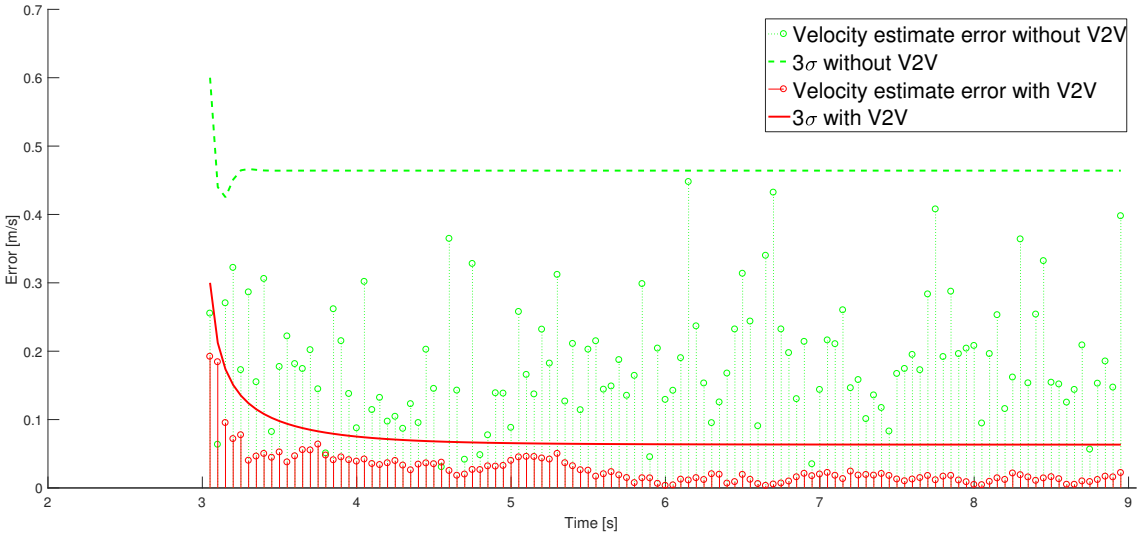


**Figure 8.5:** Front-to-front collision scenario: Velocity estimation error and $3\sigma$ confidence interval for $v_{obj} = v_{ego}$= 60 km/h; with or without V2V information

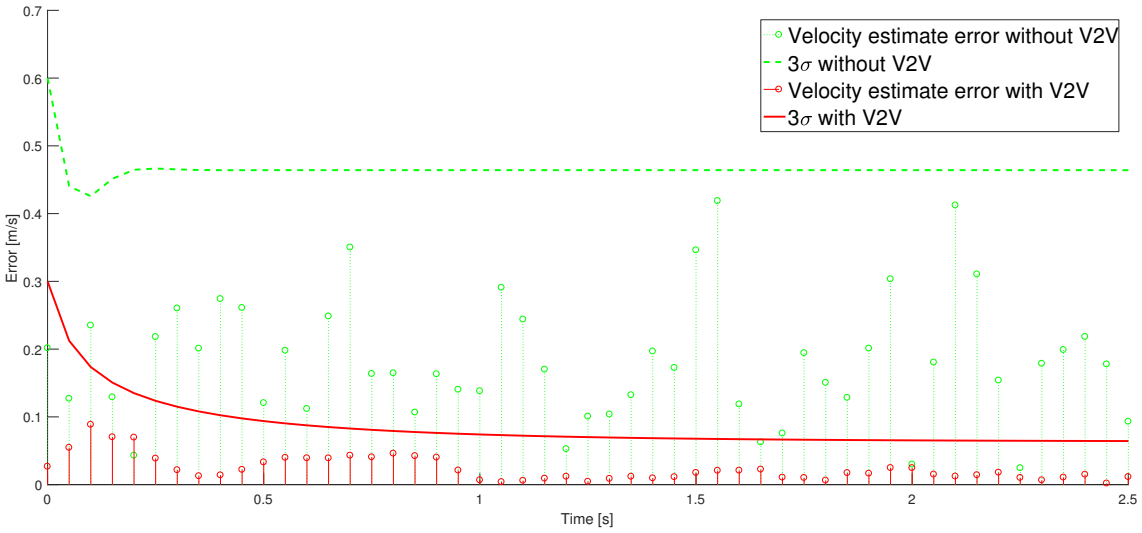


**Figure 8.6:** Front-to-side collision scenario: Velocity estimation error and $3\sigma$ confidence interval for $v_{obj} = v_{ego}$= 40 km/h; with or without V2V information

Accounting for the accurate acceleration measurements (where V2V communication was modelled with $\sigma_{a_x} = \sigma_{a_y} = 0.1$ m/s$^2$) the velocity estimation with V2V communication is considerably more robust and reliable than without. Focusing on the $3\sigma$ confidence interval, the magnitude of the error is up to four times smaller than without V2V communication.

Overall, the findings show that the simulation model performs in agreement with expectations. The distribution of errors observed in the experiments show that the covariances (built into the state estimation process) produce the expected level of estimation errors and behaviours, including the above observation of considerable improvement of the velocity estimation which accrues from V2V communication. The performance evaluation also corroborates the benefit of V2V communication (viewed as a virtual sensor) within a sensor data fusion architecture for pre-crash extraction of collision parameters. The results from experiments show that V2V increases the confidence level of the estimated position of the oncoming vehicle against which a collision is possible.

#### 8.1.2.2 Comparative assessment of simulation data against real data collected for a prototype vehicle

According to Hirsenkorn et al. (2016) it is not feasible to implement sensor models which can reproduce real world system behaviour at a microscopic level of detail.

However, it is possible to produce sensor noise which behaves in a comparable way to the real sensor fusion system. This is the approach adopted in this thesis to replicate the sensor behaviour of a real in-vehicle sensor fusion system. In this section the errors associated with vehicle position and velocity are compared, as they should be comparable in order to derive a correct model.

**Aim:** To evaluate the simulation model through a comparison against position and velocity measurements from a real test drive.

**Method:** To assess the reliability of estimates produced by the simulation model, errors associated with vehicle position and velocity computed by the simulation model were measured, and compared to similar measurements published in (Aeberhard et al., 2012) for the performance of a sensor data fusion system of a real vehicle subjected to a real test drive. An overtaking scenario, similar to the one in Aeberhard et al. (2012) was created using the simulation model.

In the real test drive reported in (Aeberhard et al., 2012), the overtaking manoeuvre, performed with the test vehicle, is shown in Figure 8.7. The target vehicle accelerated longitudinally with $a_x^{max} = 1.5$ m/s$^2$ to perform an overtaking manoeuvre. Then, the target vehicle performed a lane change manoeuvre, accelerating laterally with $a_y^{max} = 1$ m/s$^2$. After overtaking the host vehicle the target vehicle performed another lane change manoeuvre with $a_y^{max} = -1$ m/s$^2$. Afterwards, the target vehicle decelerated with $a_x^{max} = -2$m/s$^2$. The described longitudinal and lateral acceleration profiles for the target vehicle are shown in Figure 8.8. The test drive was performed with the following velocities: the host vehicle drove at 80 km/h, while the target vehicle overtook with a velocity of 90 km/h. Highly accurate differential GPS measurements served as ground truth data. A constant acceleration model was used. A fusion algorithm using information matrix fusion with a sensor-to-global fusion strategy was utilized (Aeberhard et al., 2012).

The test vehicle, which served as a host vehicle during the test drive, was equipped with the sensors shown in Figure 8.9.

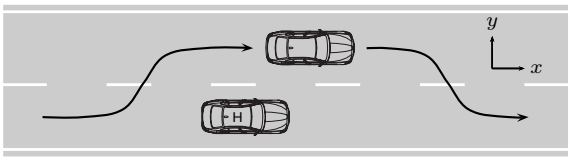


**Figure 8.7:** Overtaking manoeuvre performed in (Aeberhard et al., 2012)

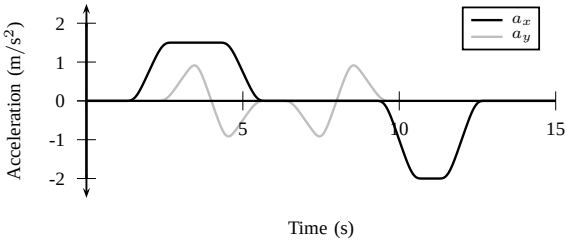


**Figure 8.8:** Longitudinal and lateral accelerations during the overtaking maneuver, performed in Aeberhard et al. (2012)

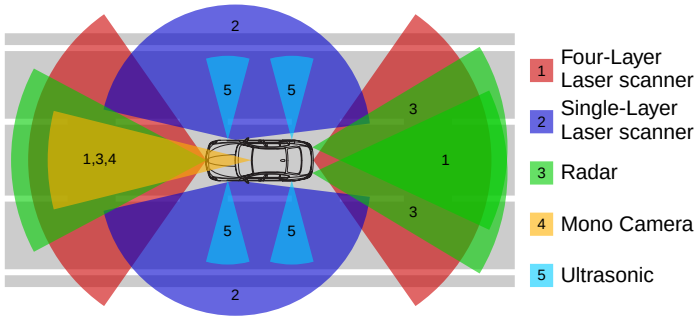


**Figure 8.9:** BMW 5 Series test vehicle surround with a sensor configuration (Aeberhard et al., 2012)

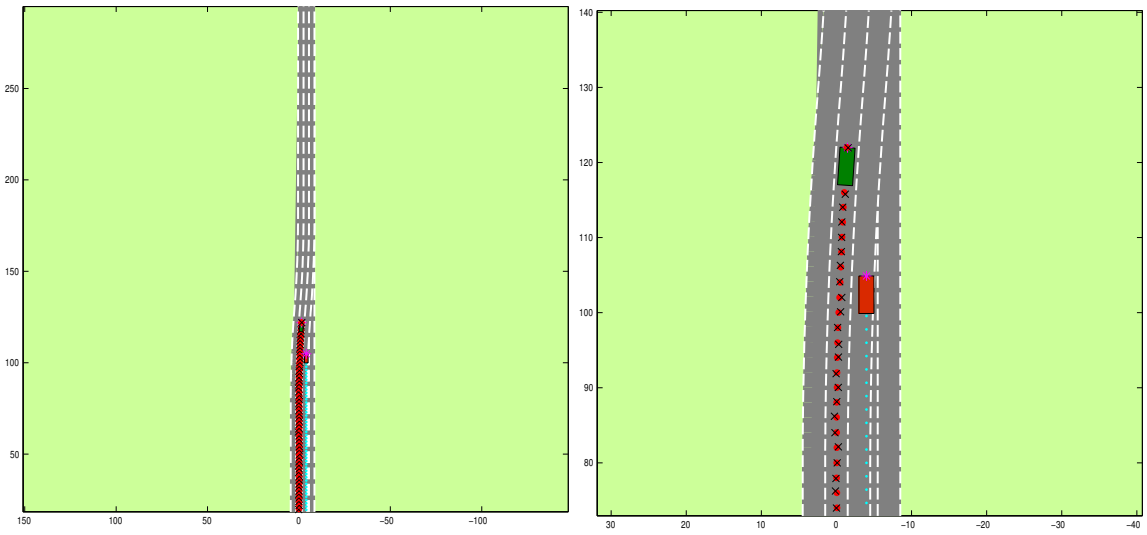

**Figure 8.10:** Visualisation of the overtaking scenario performed in the simulation framework (left – the whole scenario, right – a close look)

A similar overtaking scenario was performed in the simulation framework. In the simulation model, the host vehicle has a sensor field-of-view with a front-facing horizontal opening angle of 120°(as stated in Section 7.3.2). Hence, due to the target vehicle being outside the field of view of the host vehicle, the simulation results do not include the part of the overtaking manoeuvre when the target vehicle approaches the host vehicle from the rear. In effect, the simulation only considers a cut-in manoeuvre, instead of a full overtaking manoeuvre. At the start of the simulation the host vehicle is in the central lane, driving at 80 km/h, whereas the target vehicle is immediately on the left of the host vehicle, driving with a velocity of 90 km/h. Both vehicles keep moving for 3 seconds. The object vehicle overtakes the host vehicle and performs a lane change manoeuvre with an acceleration of $a_y^{max} = -1$ m/s$^2$. Afterwards, the target vehicle travels at a constant speed for 1 second, followed by a deceleration with $a_x^{max} = -2$ m/s$^2$ for 2 s. After one second of driving further with a constant velocity the simulation ends. The host vehicle remains in the central lane with a velocity of 80 km/h during the entire simulation. The scenario is demonstrated in Figure 8.10.

**Results:** Below, the estimation error for the components of the state vector from the simulation are compared to those from the real test drive.

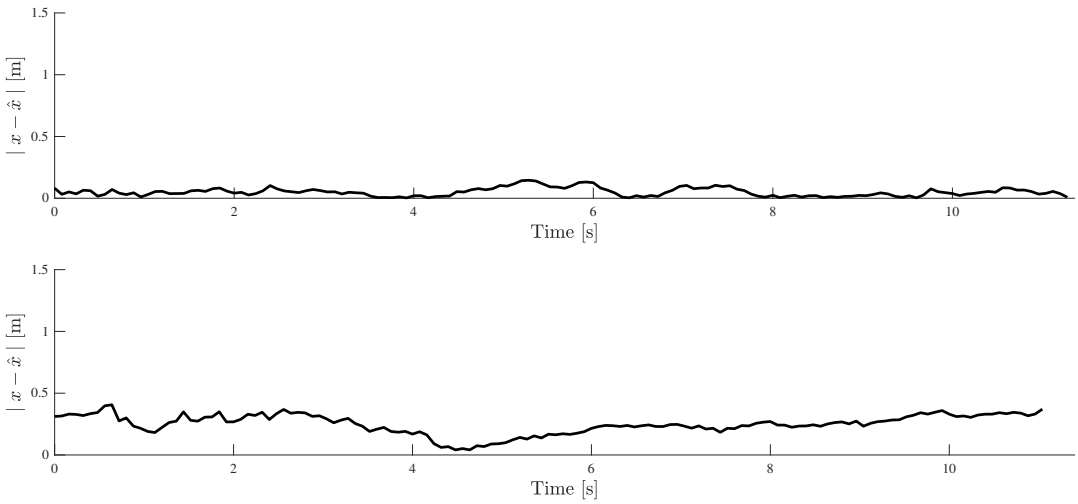


**Figure 8.11:** Absolute error in $x$ position estimation of the real test drive (bottom) (Aeberhard et al., 2012) and for the simulation (top ) during an overtaking manoeuvre, where the target vehicle overtakes the host vehicle with $v_{host} = 80$ km/h and $v_{target} = 90$ km/h.

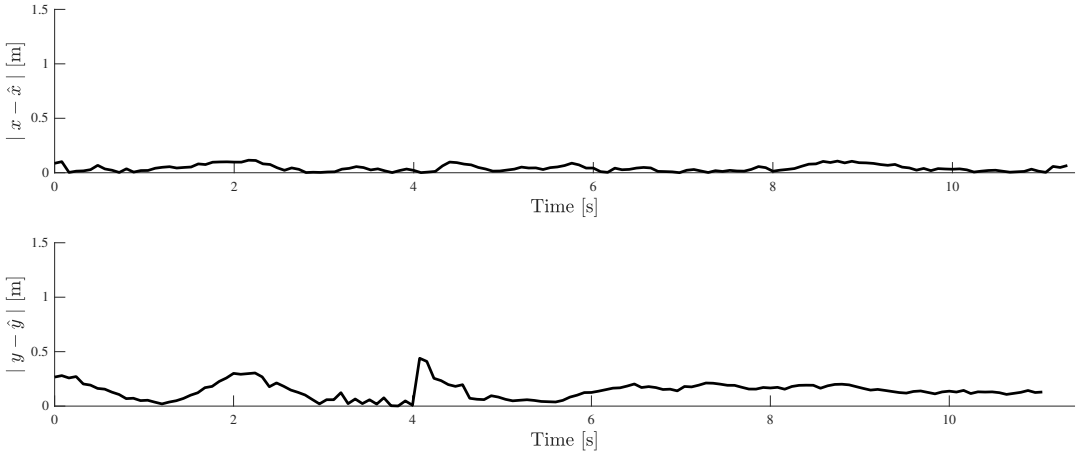


**Figure 8.12:** Absolute error in $y$ position estimation of the real test drive (bottom) (Aeberhard et al., 2012) and for the simulation (top) during an overtaking manoeuvre, where the target vehicle overtakes the host vehicle with $v_{host} = 80$ km/h and $v_{target} = 90$ km/h.

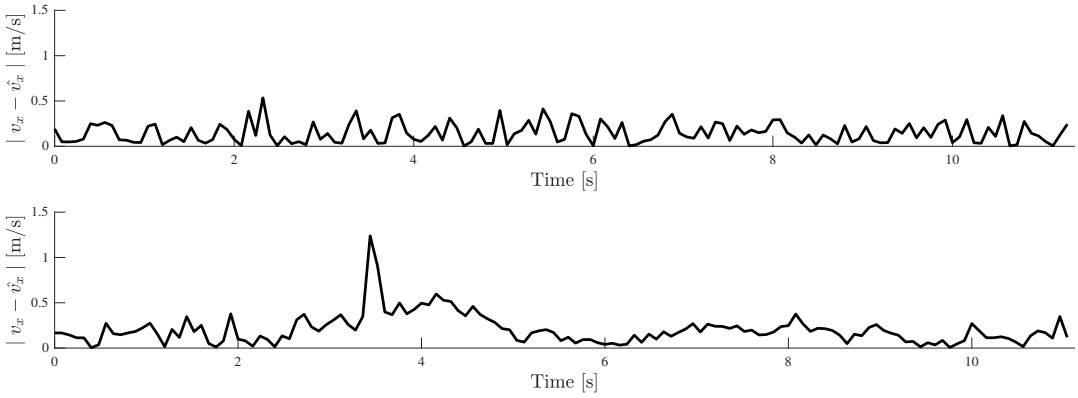


**Figure 8.13:** Absolute error in $v_x$ velocity estimation of the real test drive (bottom) (Aeberhard et al., 2012) and for the simulation (top) during an overtaking manoeuvre, where the target vehicle overtakes the host vehicle with $v_{host} = 80$ km/h and $v_{target} = 90$ km/h.

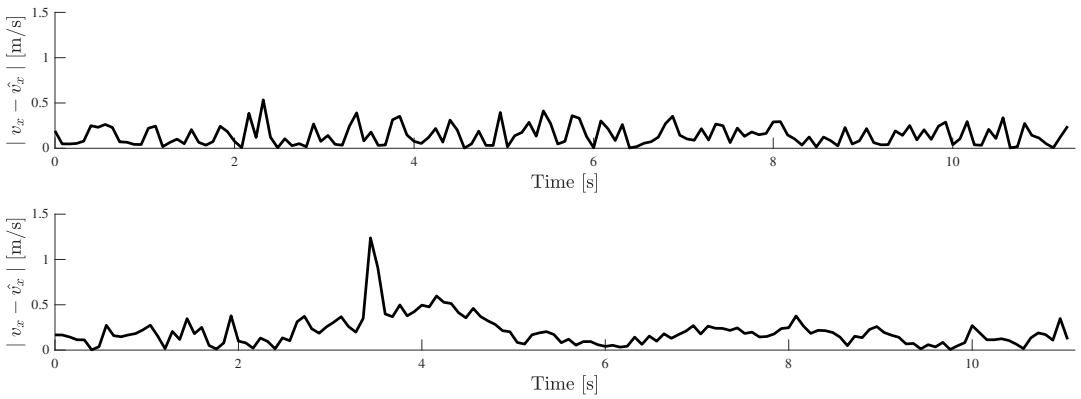


**Figure 8.14:** Absolute error in $v_y$ velocity estimation of the real test drive (bottom) (Aeberhard et al., 2012) and for the simulation (top) during an overtaking manoeuvre, where the target vehicle overtakes the host vehicle with $v_{host} = 80$ km/h and $v_{target} = 90$ km/h.

To verify the behaviour of the state estimation model at high speeds, real-world measurements from Aeberhard et al. (2012) of a test drive on a highway were used in the comparisons included in this thesis. This is because it was not possible to drive the prototype vehicle at high speeds at the BMW test ground because of speed restrictions which are in force at the ground.

**Discussion:** Figures 8.13 and 8.14 show that the velocity estimation error of the simulation model is very similar to that of the test vehicle in the overtaking scenario, reported in (Aeberhard et al., 2012), both in the x and y directions. Whereas the average error is 0.17 m/s and 0.15 m/s in the $x$ and $y$ directions respectively, in (Aeberhard et al., 2012), the simulation model has an estimation error of approximately 0.15 m/s in both directions. The position estimation however has a better accuracy in the simulation model , as shown in Figures 8.11 and 8.12. Contrary to the average estimation error of 0.19m and 0.09m in the $x$ and $y$ directions, the simulation model shows an average estimation error of 0.08m and 0.06m in the respective $x$ and $y$ directions. This difference can be explained by the abstractions applied to the simulation model. For example, the assumption that the ego state is perfectly known, leads to a higher accuracy in the estimations. Nevertheless, the use (in the simulation model) of virtual sensors with better performance than currently available sensors can be justified by the fact that the real life leverage of V2V communication and its integration to the sensor data fusion will probably be possible several years from now. Also, more accurate sensors will probably be available then.

## 8.2 Performance assessment of the crash constellation extraction algorithm

This section discusses the performance assessment of the constellation extraction algorithm and its accuracy for the two scenarios described in Section 5.2.2.3.

The investigation for each scenario includes the following analyses:

- For each scenario the time-to-collision estimation accuracy was studied with or without simulated vehicle-to-vehicle communication. The intervals between the maximum and minimum values (estimated by including state prediction uncertainty) were compared to the ground truth of the time-to-collision value to demonstrate the accuracy of the estimation of the time-to-collision.
- The uncertainty associated with the estimation of the point of collision on the body of the ego vehicle was examined. The position of the predicted collision point varies due to the different possible trajectories that an object vehicle is able to take, corresponding to different maximal accelerations, along the circumference of the modified Kamm's circle. Similarly, the experiments also examined the uncertainty associated with estimates of the relative velocity between the vehicles
- Furthermore, the effect of vehicle speed upon the uncertainty associated with the estimated time-to-collision was examined.
- Similarly, the uncertainty associated with the estimated position of the object vehicle, and with the estimated relative velocity between the vehicles, was investigated for different vehicle speeds and time-to-collision.

The simulated front-to-front collision scenario involves two vehicles ending in a head-on collision. The ego vehicle and object vehicle travelled with a constant speed towards each other. The simulation starting point was at a distance of 300m between the two motor vehicles. The velocity was varied from 30 to 130 km/h. The simulation of the input data into the sensor simulation and state estimation module was triggered by the object vehicle entering the field of view of the ego vehicle. The field of view of the modelled sensor is set to 200m and therefore, the tracking started after each vehicle covered 50m. The crash constellation algorithm was set to a maximum time-to collision of 500ms. The scenario is illustrated in Figure 8.2. Each

simulation run was executed with or without simulated vehicle-to-vehicle communication. Furthermore, as shown in Figure 8.2 the second scenario was configured as a front-to-side vehicle to vehicle collision. The ego vehicle travelled velocities of 40km/h and 50km/h. The object vehicle speed was increased in steps of 20km/h from 30km/h to 60km/h. Due to the close starting point the object vehicle was already in the field of view of the ego vehicle at the beginning of the simulation.

## 8.2.1 Assessment of supporting parameters

### 8.2.1.1 Assessment of time-to-collision estimates

#### 8.2.1.1.1 Effect of V2V information on time-to-collision estimates

**Aim:** To compare the accuracy of the time-to-collision estimates obtained with or without V2V communication.

**Method:** The simulation model explained in Section 7.1 was used to generate a front-to-front and front-to-side collision scenario. The simulation model provided the velocity and position of the object vehicle to the collision extraction algorithm. Tracking of the object vehicle was triggered after it entered the field of view of the ego vehicle. The time to collision is the time left until the collision occurs; under the assumption that both vehicles keep their velocities constant and the distance $d$ is known, it is computed as follows:

$$TTC = \frac{d}{v_{obj} - v_{ego}} = \frac{d}{v_{diff}} \tag{8.2}$$

The performance tests were conducted with both the object vehicle and ego vehicle travelling at a constant velocity set to $v_{obj} = v_{ego} = 60$km/h for the front-to-front collision scenario and with $v_{obj} = v_{ego} = 40$km/h for the front-to-side collision scenario. For comparison, the experiments were conducted with or without simulated V2V communication.

**Results:** Figure 8.15 compares the time-to-collision estimation with or without V2V communication for velocities $v_{obj} = v_{ego}$ =40 km/h. The main prediction represents the median of time-to-collision estimates for the possible trajectories represented by the modified Kamm's circle and it has been drawn with solid lines (green and red). The maximal variation along the modified Kamm's circle is illustrated with dashed lines for both test runs. For comparison, the ground-truth time-to-collision (GT TTC) is plotted as black line.

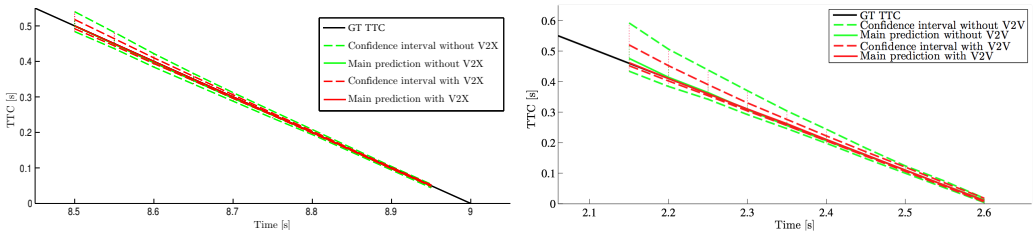


**Figure 8.15:** Time-to-collision estimates for a head-on collision scenario (left; with $v_{obj} = v_{ego}$=60 km/h) and a front-to-side collision scenario (right; $v_{obj} = v_{ego}$ =40 km/h) with constant speed for the ego vehicle and object vehicle. Shown are the estimate of the time-to-collision and its ground truth, and the confidence intervals corresponding to the maximum and minimum values estimated by including state prediction uncertainty, with or without a simulated V2V communication.

**Discussion:** As the figure shows, the variation of time-to-collision estimates, when V2V communication is included, is approximately twice as low as without V2V communication; thus showing that the extraction of the time-to-collision is more precise with V2V communication. This improvement results from increased accuracy in estimating the state of the object vehicle, which is due to the quality of the additional information provided by V2V communication. The figure also shows that the extraction of the time-to-collision is highly precise for both sensing options. This high precision is explained by the fact that the trajectory for each vehicle in the chosen head-to-head collision scenario is a motion along a straight line, which is exactly the main trajectory of the modified Kamm's circle. For the crossing scenario, the time-to-collision estimation with simulated V2V communication displays a variation which is about half of the variation observed without V2V. For this case, the difference is more significant.

#### 8.2.1.1.2 Effect of velocity and V2V information on time-to-collision estimates

**Aim:** To investigate the impact of vehicle velocity on the accuracy of time-to-collision estimates, with or without simulated V2V communication.

**Method:** For this analysis the scenarios described in Section 8.2.1.1.1 were enhanced by varying the velocity from 30 to 130 km/h in steps of 20 km/h for the front-to-front collision scenario. The speeds for the tracked vehicle and for the ego vehicle were increased at the same steps ($v_{obj} = v_{ego}$). For the front-to-side collision scenario the object vehicle speed was varied from 30 to 60 km/h in steps of 10 km/h and from $v_{ego} = 40$km/h to $v_{ego} = 50$km/h for the ego vehicle accordingly. To assess the effect of vehicle velocity, and of vehicle-to-vehicle communication, upon the accuracy of time-to-collision estimates, the collision point and its corresponding time-to-collision were computed for each velocity with accelerations bounded by the modified Kamm's circle, with or without V2V communication. Furthermore, the position estimation uncertainty was used to compute the maximum and minimum estimated time-to-collision for each velocity. In line with the update rate of the simulated sensor fusion system, the starting point of the collision parameter extraction ranges from 450ms to 500ms before collision.

**Results:** Figure 8.16 depicts the variation of time-to-collision estimates with or without simulated V2V communication input for different velocities for the front-to-front collision scenario. Figure 8.17 and 8.18 illustrate the estimation of the time-to-collision for the front-to-side collision scenario accordingly. All figures show the maximum variation of the values of time-to-collision plotted around 0 which represents the ground truth of time-to-collision values of the simulation.

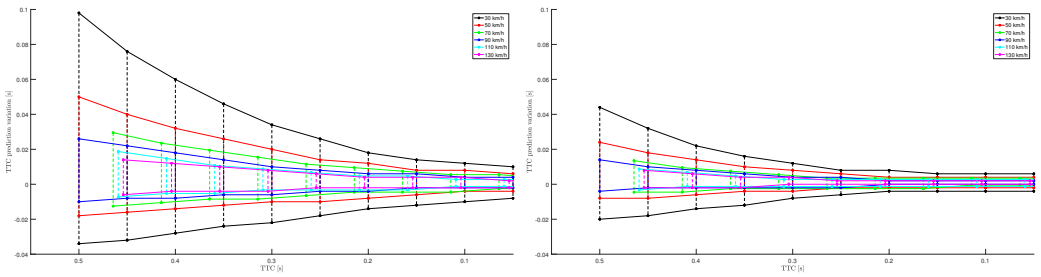

**Figure 8.16:** Variation of the time-to-collision estimates for front-to-front collision scenarios with velocities ranging from 30km/h to 130km/h with (right) and without (left) simulated V2V communication; $v_{obj} = v_{ego}$

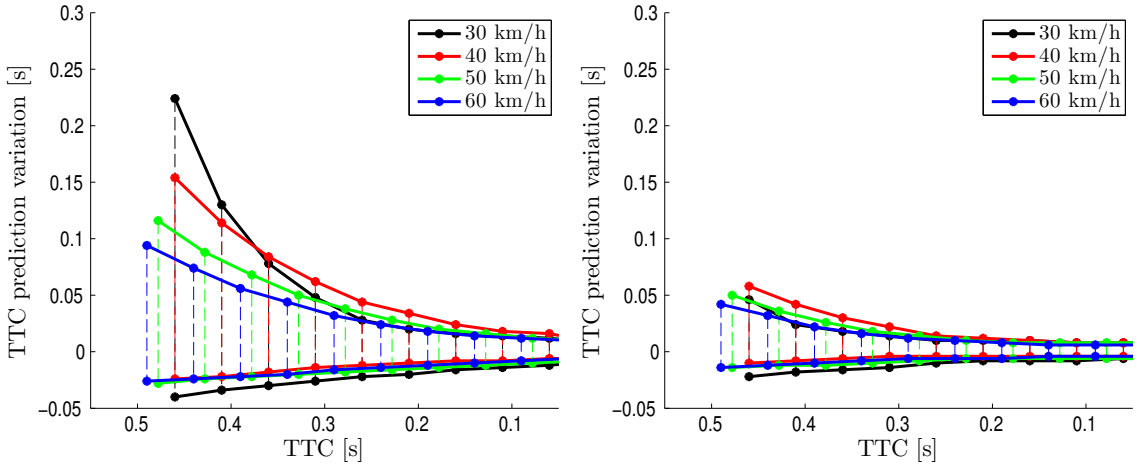


**Figure 8.17:** Variation of the time-to-collision estimates for front-to-side collision scenarios with velocities ranging from 30km/h to 60km/h with (right) and without (left) simulated V2V communication; $v_{ego} = 40$ km/h

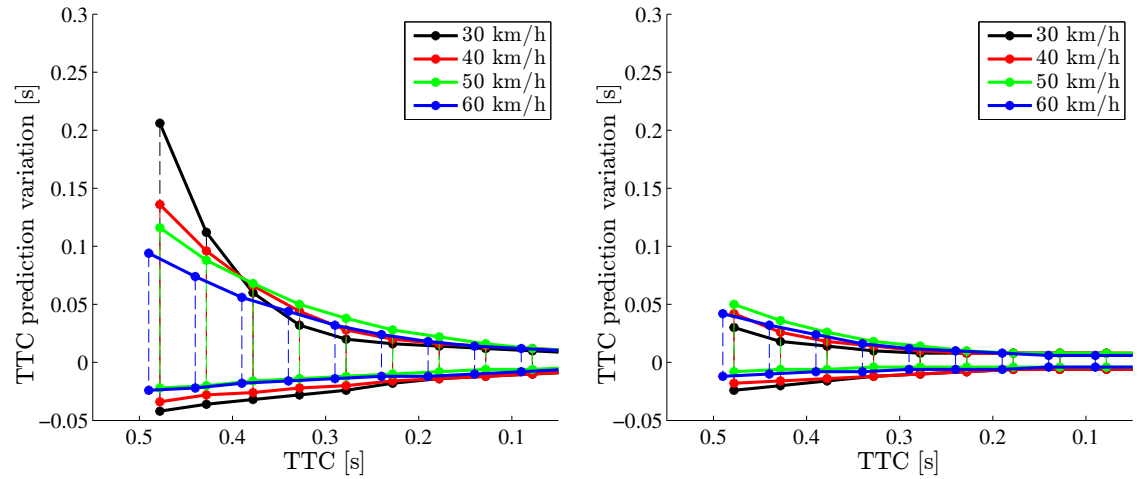


**Figure 8.18:** Variation of the time-to-collision estimates for front-to-side collision scenarios with velocities ranging from 30km/h to 60km/h with (right) and without (left) simulated V2V communication; $v_{ego} = 50$ km/h

**Discussion:** Figure 8.16 shows that for increasing velocities, the uncertainty associated with the calculated time-to-collision decreases as a function of velocity and of time-to-collision for both scenarios with or without simulated V2V information. Figure 8.17 and 8.18 show a similar behaviour regarding the effect of the presence or absence of simulated V2V information on the estimation of the time-to-collision for the front-to-side collision scenario. This effect can be explained by the fact that at higher speeds the driving manoeuvres are limited due to the friction of the vehicle.

This effect is modelled along the modified Kamm's circle and limits the minimal turn radius and therefore the possible trajectories accordingly. Nevertheless, the decrease in accuracy is overall smaller when V2V communication is present, as the enhanced quality of information about the motion parameters of the object vehicle allows a better estimation of its state and therefore its trajectory. This effect is shown in Figure 8.19.

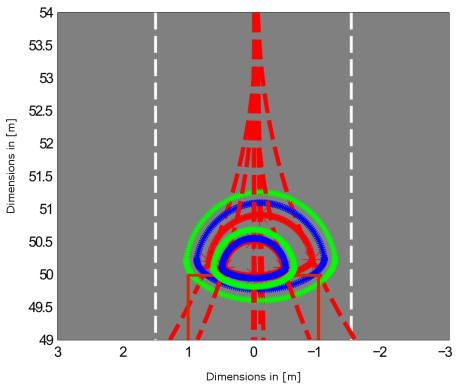


**Figure 8.19:** Illustration of the vehicle position bounding regions, including velocity (blue) or position (green) estimation errors for a front-to-front collision scenario. Each bounding region is computed for acceleration values within the modified Kamm's circle, and including state estimation uncertainties, if applicable. Shown in red are the boundaries for vehicle position estimated without the effect of state estimation uncertainties. The smaller bounding region in each colour corresponds to presence of V2V communication.

The variation for the time-to-collision estimates in scenarios with $v_{obj} = v_{ego}$=30 km/h ranges between +100ms and -30ms. Under such conditions, an extraction of the constellation is not feasible for use in the real world as the time of the collision cannot be localised accurately enough. The -30ms results from the limited acceleration that the object vehicle is able to perform. For higher speeds (for example $v_{obj} = v_{ego}$=130 km/h) in comparison, the variation of the time-to-collision estimates reduces by a factor of about one-fifth. Due to the better state estimation and therefore the decreased uncertainty for the bounding regions of vehicle position and velocity, the presence of V2V data cuts the variation of the time-to-collision estimates by about half for front-to-front collision scenarios.

With V2V as an additional data source, the simulation also showed that a given level of accuracy for the estimation of the time-to-collision (TTC) is achievable about 110 ms earlier for moderate velocities, when the time-to-collision is in the range [0.5s,

0.2s]. Furthermore, the simulation also showed that the uncertainty in the prediction of vehicle position at the time of collision can be reduced by about half when V2V communication is integrated into the sensor data fusion.

Front-to-side collisions which occur at lower speeds strengthen the effect of erroneous position prediction along the modified Kamm's circle and therefore decreases the time-to-collision estimation accuracy. Braking or steering in those cases can avoid or delay a collision. This leads to the effect that the estimation uncertainty in time-to-collision values decreases with increasing speeds of the collision opponents. However, as Figures 8.17 and 8.18 show, the time-to-collision estimation inaccuracies are decreased by available V2V information.

#### 8.2.1.1.3 Prediction uncertainty for the position of the object vehicle

**Aim:** To analyse the position prediction uncertainty for the centre point of the object vehicle, with or without simulated V2V information.

**Method:** In this experiment, the vehicle collision scenario and velocity range are as described in Section 8.2.2. The Kamm's circle bounds the space of possible values for the acceleration of the vehicle, at a given time. Hence, its perimeter can be mapped linearly (using equations of vehicle motion) onto the perimeter of the bounding region for the position of the vehicle. Thus, the diameter of the modified Kamm's circle (presented in Section 6.2.1) can be used to analyse the prediction uncertainty of vehicle motion parameters (i.e. positions), such as those for the centre point of the object vehicle. Half of the width of the modified Kamm's circle for the position of the object vehicle was measured, to estimate the position prediction uncertainty. This is because the bounding region for position estimates is symmetric along the width, relative to the middle of the region. Figure 8.20 illustrates the estimated width of the prediction uncertainty.

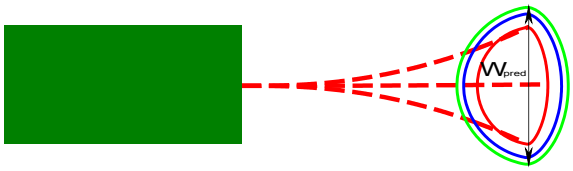


**Figure 8.20:** Width of the bounding region for vehicle position. The colour coding is same as in Figure 8.19.

**Results:** Figures 8.21 shows the half width of the prediction area measured for a range of values for the time-to-collision, with or without simulated V2V information. The uncertainty is based on three core elements:

- The possible trajectories of the object vehicle
- The uncertainty in the velocity estimation.
- The uncertainty in the position estimation.

These elements influence the overall estimation differently. As Figure 8.3 shows, the position estimation is only slightly improved by available vehicle-to-vehicle information. In contrast, Figure 8.5 illustrates the improvement of the velocity estimation with available V2V information included into the state estimation. Furthermore, a major advantage of the V2V communication is the early transmission of change in movement the object vehicle as explained in Section 6.2.1. The results for the front-to-front collision scenario are shown in Figure 8.21.

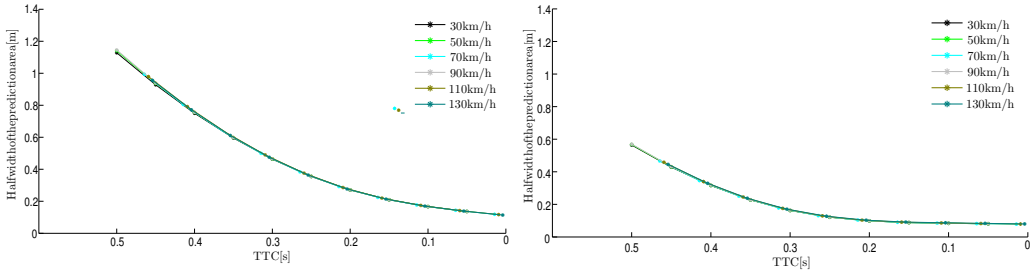


**Figure 8.21:** Half width of the prediction area estimated for various velocities with (left) and without (right) simulated V2V communication ($v_{obj} = v_{ego}$), for a front-to-front collision scenario

Figures 8.22 and 8.23 illustrate the prediction uncertainty for front-to-side collision scenarios.

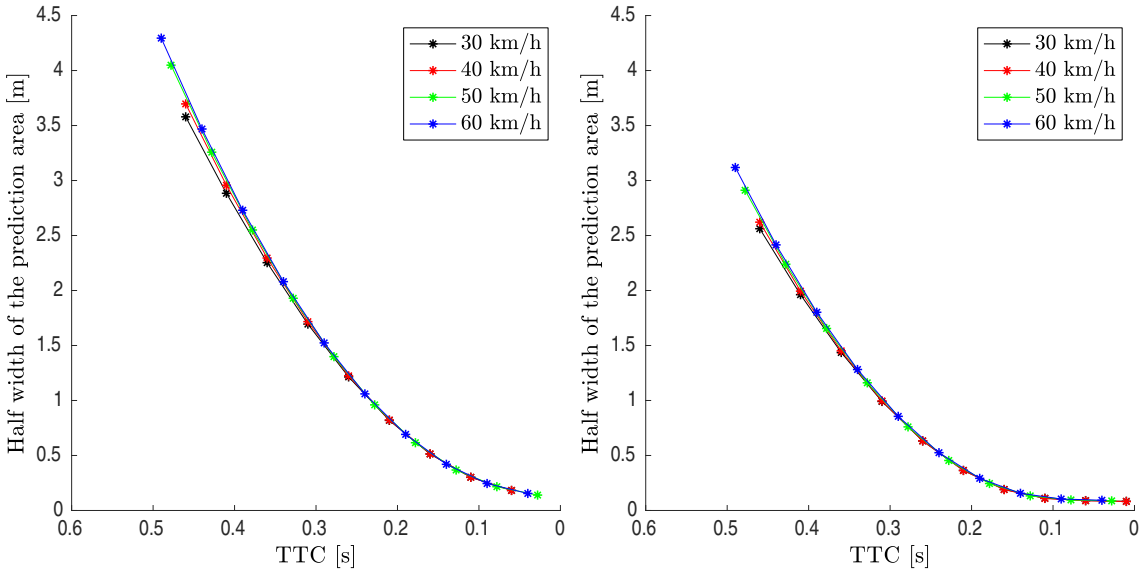


**Figure 8.22:** Half width of the prediction area estimated for various velocities with (left) and without (right) simulated V2V communication ($v_{ego}$ = 40 km/h; $v_{obj}$ = [30 ... 60] km/h), for a front-to-side collision scenario

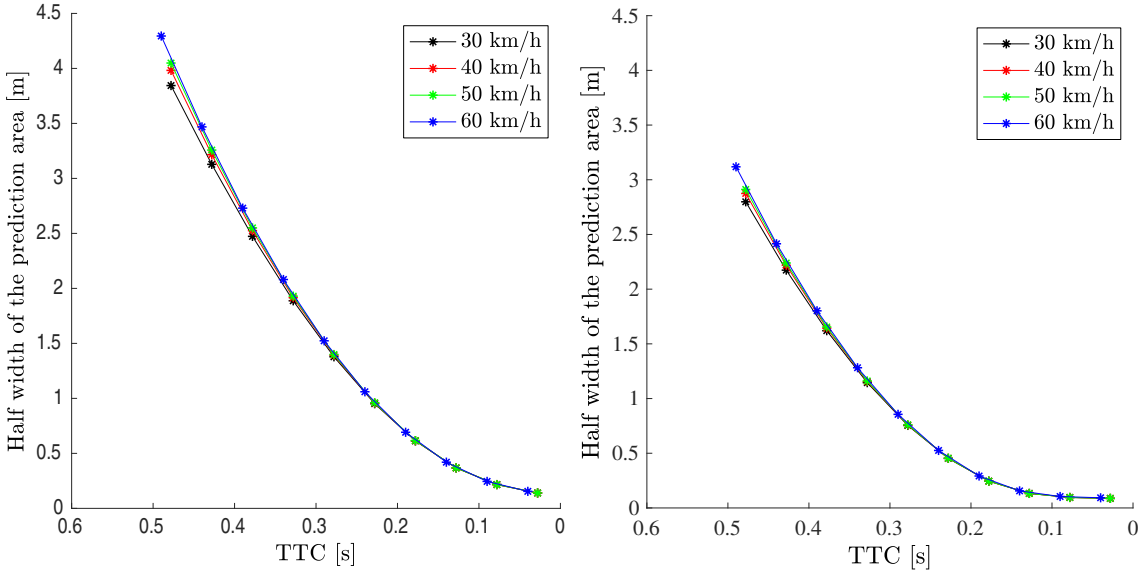


**Figure 8.23:** Half width of the prediction area estimated for various velocities with (left) and without (right) simulated V2V communication ($v_{ego}$ = 50 km/h; $v_{obj}$ = [30 ... 60] km/h), for a front-to-side collision scenario

**Discussion:** The presence of simulated V2V information lowers the prediction area almost by 25% when the time to collision is 500ms. Furthermore, Figure 8.21 illustrates that the prediction uncertainty corresponding to a time-to-collision of around

500ms is too high to enable a reliable extraction of the crash constellation. Hence, the crash constellation extraction would not be feasible for active safety measures when the time-to-collision is near 500ms, neither with nor without V2V communication. For smaller values of time-to-collision though, the estimation uncertainty shrinks to a meaningful size for further application of active safety measures. Estimation uncertainty is significantly insensitive to different velocities, as Figures 8.21, 8.22, and 8.23 show. This can be explained by the fact that the velocity error has little influence on the position estimation in the current implementation. The extraction of the crash constellation for front-to-side collisions for higher time-to-collisions is not reliable. Figure 8.22 and 8.23 show that a stable extraction of the crash constellation is feasible for time-to-collision values below 100ms which is too little for future active safety systems to react on upcoming collisions.

## 8.2.2 Assessment of crash constellation parameters

### 8.2.2.1 Assessment of the collision point on the ego vehicle

**Aim:** To analyse the estimation precision for the location of the initial contact point on the body of the ego vehicle, when involved in a head-on collision with the object vehicle.

**Method:** The scenario is similar to the one mentioned in Section 8.2.1.1.1 for a head-on collision for vehicle velocities set to $v_{obj} = v_{ego} = 60$ km/h. The width for each vehicle is set to 2 metre.

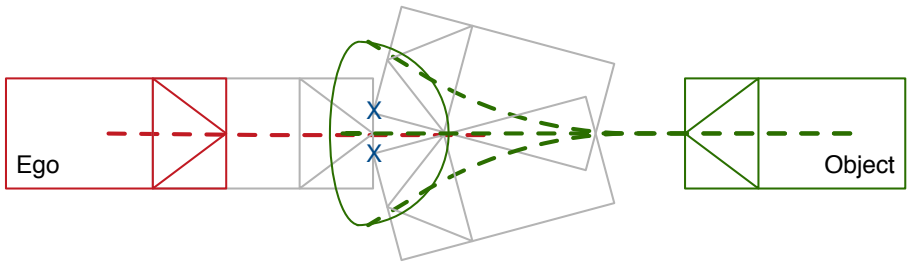


**Figure 8.24:** Extraction of the possible collision points (blue crosses) for a head-on collision scenario where the ego vehicle and object vehicle travel at constant speed ($v_{obj} = v_{ego}$=60 km/h).

As it can be seen in Figure 8.24 the straight-line trajectory of the ego vehicle and object vehicle leads to a front-to-front collision with 100% overlap between the two vehicle fronts, if it is assumed that both vehicles have the same width. However, if the driver of the object vehicle performs a steering manoeuvre then there is a single point of initial contact on the body of the ego vehicle; if it is assumed that both vehicles have a perfectly rectangular shape. In such a case, the collision detection algorithm would extract two possible contact points which are represented by the blue crosses in Figure 8.24. Figure 8.25 illustrates the distribution of (and hence, uncertainty associated with) the collision point estimates, computed using possible maximal acceleration values which lie on the circumference of the modified Kamm's circle. It is important to note that this experiment investigates the point of collision, not the overlap.

**Results:** Figure 8.25 shows the collision point estimates, plotted along the vertical axis, for values of time-to-collision ranging between [0 ... 500] ms with (left) or without simulated V2V communication (right) (for front-to-front collision scenarios). The time-to-collision is plotted along the horizontal axis, with labels shown at the bottom of the figure. The grey lines show the distribution of the point of collision for different values of the time-to-collision.

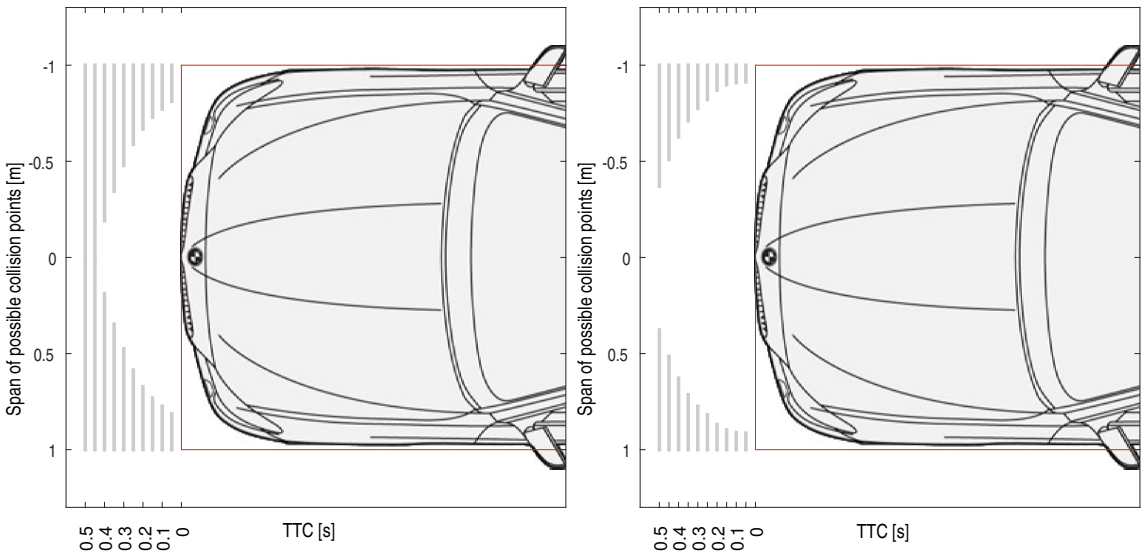


**Figure 8.25:** Distribution (shown as a vertical grey bar) of possible collision points on the front of the ego vehicle, in a head-on collision with the object vehicle, for a scenario where $v_{obj} = v_{ego}$=60 km/h and values of time-to-collision range from 0 to 500ms; with (left) or without (right) simulated V2V communication

Figure 8.26 illustrates the collision point estimations analogue to Figure 8.25 for front-to-side collision scenarios. Due to the possibility that the collision can occur on the side or front of the ego vehicle, the grey bars are distributed over the front and side of the ego vehicle.

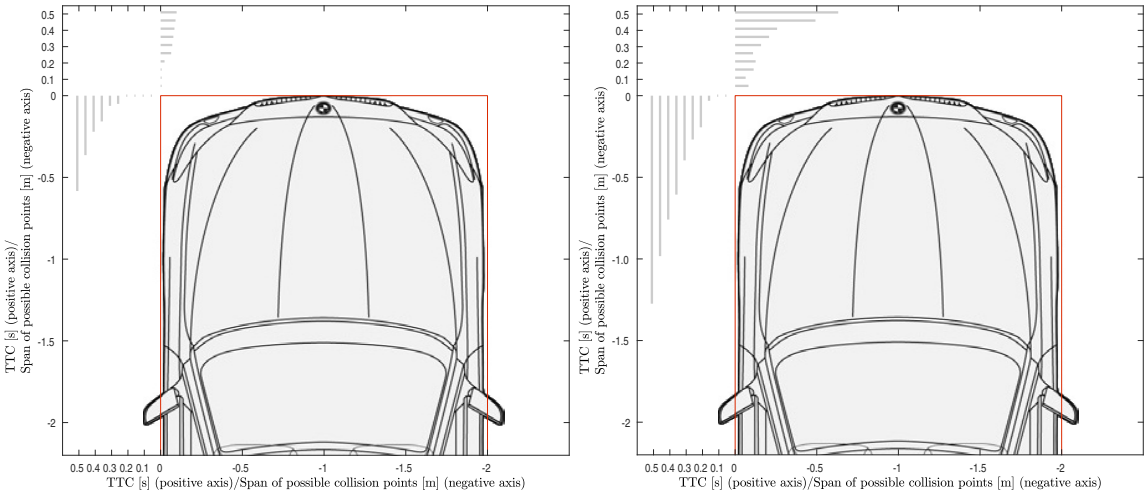


**Figure 8.26:** Extraction of the collision point with its uncertainties along the Kamm's circle for front-to-side scenarios with $v_{obj} = v_{ego} = 40$ km/h based on the TTCs ranging from 0 to 500ms; with (left) and without (right) modelled V2V communication

**Discussion:** For a time-to-collision of 500ms and no V2V information, the collision point, for a front-to-front collision, varies along the whole vehicle front and the accuracy of the collision point extraction increases as the time-to-collision decreases. With a decrease of the time left until the collision occurs, the area covered by possible points of collision shrinks. The important information derived from this analysis is that for a time-to-collision value of 0.05 seconds the uncertainty of the collision point extraction is about plus or minus 15cm, which is a total inaccuracy of about 30cm for the situation without V2V information. The major influences on the estimation uncertainty for the point of collision are the uncertainties in the position and velocity estimation. In comparison, the plot on the left (which includes the effect of V2V information, in Figure 8.15) shows that the uncertainty for the collision point estimates is about 15cm in total, which is twice as accurate as without V2V information. A major advantage of using V2V information is that at a time-to-collision of 500ms the uncertainty is already below 1.2m and the performance at 300ms before the collision has an estimation uncertainty of about 30cm, which is a good estimate for future advanced safety systems.

As shown in Figure 8.26, for a front-to-side collision, the collision side differs based on the interaction with the other vehicle. Furthermore, similar to the front-to-front collision scenario, the decrease in time-to-collision values shows a strong reduction of the extraction uncertainty of the point of collision. The plot on the left shows the strong influence of simulated V2V communication on the variation of the collision point extraction accuracy. For future active safety systems it will be inevitable to add V2V information to the fusion process to achieve the necessary performance at time-to-collision values of 300ms.

#### 8.2.2.2 Assessment of the delta velocities of the vehicles

**Aim:** To analyse the estimation precision for the difference (herein referred to as "delta") in velocity between the ego and object vehicle involved in a front-to-front and front-to-side collision.

**Method:** Similar to the scenarios in Section 8.2.1.1.2 velocities of the ego and object vehicle for the head-on-collision were varied from 30 to 130km/h in steps of 20 km/h for both vehicles ($v_{ego} = v_{obj}$). Similar to the front-to-side collision scenario described in Section 8.2.1.1.2 the velocities of the object vehicle range between 30 and 60km/h in steps of 10km/h while the velocity of the ego vehicle is kept constant at $v_{ego} = 40$ km/h or $v_{ego} = 50$ km/h. The delta in velocities for different times-to-collision were investigated to assess the impact of the state estimation process on the estimation accuracy of the delta in velocity before a collision occurs. To assess the impact of a simulated vehicle-to-vehicle communication each experiment was undertaken with or without a V2V communication.

**Results:** Figure 8.27 illustrates the different deltas in velocities for time-to-collisions between 0 and 500ms before a front-to-front collision with or without a simulated vehicle to vehicle communication. Similarly, Figure 8.28 and 8.29 show the change in delta velocities for time-to-collisions between 0 and 500ms for front-to-side collisions. Both figures illustrate the influence of a simulated vehicle-to-vehicle-communication. The plot of the estimated deltas in velocities are aligned around 0 as the velocity of the ground truth measurement was subtracted from the maximal predicted delta velocities along the modified Kamm's circle. This allows the comparison of the prediction uncertainty in delta velocities for different speeds.

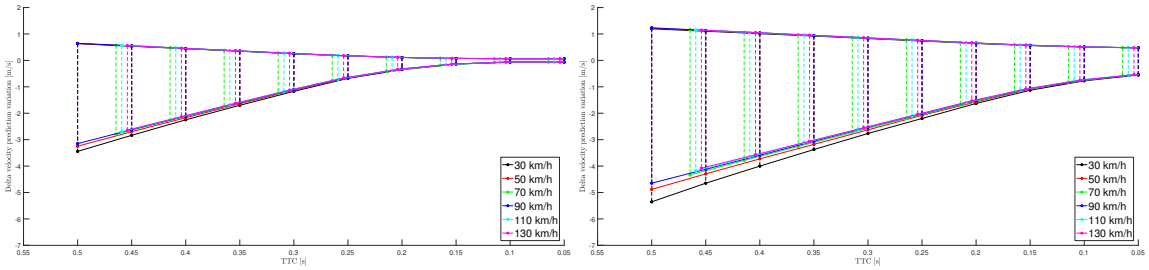


**Figure 8.27:** Estimated delta in velocities with its uncertainties for front-to-front collision scenarios with $v_{obj} = v_{ego} = [30 \text{ to } 130 \text{ km/h}]$ based on the TTCs ranging from 0 to 500ms; with (left) or without (right) modelled V2V communication

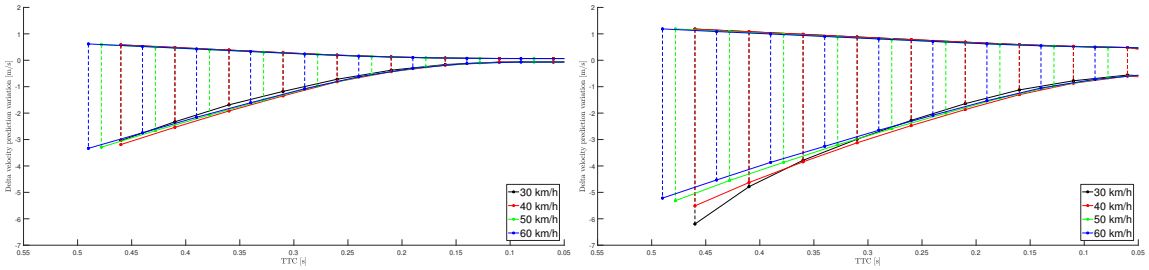


**Figure 8.28:** Estimated delta in velocities with its uncertainties for front-to-side collision scenarios with $v_{obj} = [30 \text{ to } 60\text{km/h}]$ and $v_{ego} = 40\text{km/h}$ based on the TTCs ranging from 0 to 500ms; with (left) or without (right) modelled V2V communication

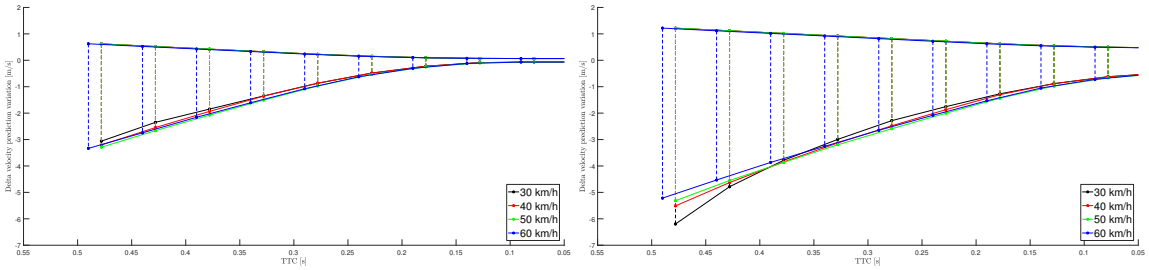


**Figure 8.29:** Estimated delta in velocities with its uncertainties for front-to-side collision scenarios with $v_{obj} = [30 \text{ to } 60\text{km/h}]$ and $v_{ego} = 50\text{km/h}$ based on the TTCs ranging from 0 to 500ms; with (left) or without (right) modelled V2V communication

**Discussion:** Figure 8.27 for front-to-front collision scenarios shows a similar behaviour as Figure 8.28 and 8.29 (front-to-side collision scenarios); increasing velocities results in a decreased uncertainty in the estimation of the delta velocity estimation for both use cases, with or without a simulated vehicle-to-vehicle communication. This effect was already explained in Section 8.2.1.1.2 and originates

from the fact that the manoeuvres are limited for the colliding vehicles at higher velocities. This effect is modelled along the modified Kamm's circle which is based on the friction between the road and tyres. However, the presence of simulated vehicle-to-vehicle communication has a strong impact onto the estimation uncertainty for both front-to-front and front-to-side collision scenarios. Vehicle-to-vehicle communication lowers the estimation error for delta velocities by 40% in cases of front-to-front collision scenarios and even by 50% for front-to-side collision scenarios at time-to-collisions of 500ms. This major decrease of estimation uncertainty when vehicle-to-vehicle communication is present is due to the more precise velocity and acceleration information of the object vehicle which are provided by the V2V information to the state estimation process. For front-to-front collision scenarios, a given level of accuracy of the delta in velocity estimation can be reached 150ms earlier with vehicle-to-vehicle information. For front-to-side collisions, a given level of accuracy of the delta in velocity estimation is reached even 200ms in advance.

## 8.3 Conclusion

This chapter discusses the correctness of the simulation model for vehicle state estimation, and the assessment of the collision extraction algorithm for a front-to-front collision scenario as described in Section 8.2.

*Correctness of the simulation model for vehicle state estimation:* The simulation model was evaluated with or without V2V communication in a front-to-front collision scenario by assessing the output of the simulation with regards to errors associated with position and velocity estimates. Overall, the findings show that the simulation model performs in agreement with expectations. The distribution of position and velocity errors observed in the experiments shows that the measurement covariances produce the expected level of estimation errors and behaviours. It was observed for instance, that velocity estimation with V2V communication is considerably more robust and reliable than without. The performance evaluation also corroborates the expectation that V2V communication increases the confidence level of the estimated position of the oncoming vehicle against which a collision is possible. V2V communication allows a given level of accuracy for the estimation of the time-to-collision to be achieved about 110 ms earlier for moderate velocities. Furthermore, the uncertainty in the vehicle position prediction at the time of collision can be reduced

by about half.

In a further step, a highway cut-in scenario was chosen for the comparison of a real in-vehicle state estimation system to the simulation model. For this use case the uncertainties in position and velocity are calculated for the real vehicle and for the simulation model. These outputs of the real and simulated world were compared and this investigation revealed that the velocity estimation of the simulation is very similar to the one for the test vehicle during the cut-in scenario. However, the position estimation displayed a better accuracy within the simulation which can be explained by the simplifications made in the simulation model.

*Performance assessment of the constellation extraction algorithm:* Simulation experiments, for the performance evaluation of the crash constellation extraction algorithm, show that the uncertainty associated with the estimated time-to-collision decreases as vehicle velocity increases or as the time-to-collision decreases. The results also show that a decreasing time-to-collision leads to a decreasing uncertainty associated with the estimated position of the tracked vehicle, the estimated collision point on the ego vehicle, and the estimated relative velocity between the two vehicles about to collide. The assessment showed that simulated V2V information has a beneficial influence on the constellation extraction accuracy. However, the simulated V2V information cannot be more accurate than the in-vehicle measurement systems of the object vehicle which senses its dynamic state. The position estimation was not provided through the simulated V2V communication due to its inaccuracy, as position measurements would require a highly accurate global positioning sensor. Nevertheless, the velocity and acceleration information can be directly derived from the in-vehicle inertia sensors and are more accurate than estimations made indirectly through the radar, lidar or camera systems of the ego vehicle. The simulated V2V information took the latency for the data transmission into account. The experiments showed that V2V information contributes towards a more accurate extraction of the collision constellation.

In cases of the mentioned front-to-front collision scenarios, V2V information improves the collision constellation extraction accuracy significantly:

- The prediction of the time-to-collision is cut by half with V2V information present. (Section 8.2.1.1.1,8.2.1.1.2)

- The predicted collision area is reduced by 25% at values of time-to-collision of 500ms. (Section 8.2.1.1.3)
- The prediction of the point representing the object vehicle is triggered 90ms earlier. (Section 8.2.2.1)
- The uncertainty associated with the prediction of delta in velocities is cut by half for scenarios with V2V information present. (Section 8.2.2.2)

Further outcomes of the investigation have shown that the velocity has minor influence on the collision area for low values of time-to-collision.

The next chapter presents the concluding remarks and offers avenues for further work.

# 9 Conclusions and Further Work

## 9.1 Conclusions

Extracting the crash constellation out of sensory data during the pre-crash phase is a crucial part of future active safety systems. Current research on crash detection algorithms and severity predictions modules is underway. These approaches are reviewed in Chapter 4. In this thesis, a novel algorithm for extracting the constellation of a crash is proposed and its extraction performance is assessed.

### 9.1.1 Achievement of the objectives

The thesis provides a review of the state-of-the art in the area of techniques for predicting collisions between motor vehicles; covering algorithms for state estimation, prediction of trajectories, collision and crash severity (Chapter 4).

The thesis also reports on its discovery of new facts, in the form of findings of a binary logistic regression which uncovered three crash constellation parameters which significantly influence the severity outcome of a motor vehicle collision (Chapter 5). The same chapter presents the performance assessment scenarios which were selected for this research; namely: front-to-front and front-to-side vehicle collisions.

A novel algorithm for extracting the constellation of a crash has been designed based on a combination and enhancement of existing algorithms. The algorithm takes into account physical constraints on the acceleration of a vehicle, with regards to the forces acting on the vehicle and to the timing of V2V communication (Chapter 6).

A simulation model was implemented for risk free testing of crash constellation extraction algorithms. It features a technique for integrating (into the simulation model) the uncertainties associated with the data captured by the sensors of a real vehicle, so as to emulate real-world state estimation behaviour. The thesis thus also reports on its discovery of another set of new facts, in the form of findings from simulation experiments, conducted using the simulation model mentioned above, which

assessed the performance of the crash constellation extraction algorithm devised in this research (Chapter 8).

## 9.1.2 Summary of the contribution to knowledge

The research reported in this thesis has proposed a new crash constellation extraction algorithm, and discovered new facts relating to parameters which significantly influence the severity of a crash and to findings from performance assessment experiments. Details are given bellow.

### 9.1.2.1 Significant parameters influencing crash severity

The first primary research question addressed by the thesis is:

- What are the most significant collision parameters which influence the injury severity for a frontal collision between two motor vehicles?

To answer this question, data for a limited parameter set, whose selection was guided by findings from the literature review reported in Section 5.1, were selected from the GIDAS database. Then, a binary logistic regression was applied to the data, to identify the parameters which significantly influence the severity of a frontal collision. The findings of the regression analysis yielded three crash constellation parameters: the point of collision on the vehicle body; the relative velocity between the vehicles; and the vehicle alignment offset (or vehicle overlap).

### 9.1.2.2 Crash constellation extraction algorithm

The second primary research question addressed by the thesis is:

- How to extract the constellation of a crash before the accident occurs?

To answer this question, a novel algorithm for extracting the constellation of a crash during the pre-crash phase, was devised as part of the primary research. Knowing the collision constellation beforehand allows the active safety system to deploy countermeasures which are better adapted to the crash constellation. The secondary research questions addressed by the thesis include:

- How to integrate physical constraints, imposed on the rate of acceleration of a real vehicle, together with data from vehicle-to-vehicle communication, into the crash constellation extraction algorithm?

To answer this question, the physical constraints on the acceleration of a vehicle were studied. There-from, the gradual rise and and eventual saturation of vehicle acceleration generated by forces controlled by the accelerator, brake or steering wheel were modelled, together with the acceleration lag relative to the timing of information received from V2V communication, to shape the data input into the crash constellation extraction algorithm.

#### 9.1.2.3 Simulation model for risk free testing

Another secondary research question addressed by the thesis is:

- How to integrate uncertainties, associated with the data captured by sensors of a real vehicle, into a simulation model devised for assessing the performance of crash constellation extraction algorithms?

To answer this question, the extended Kalman filter was studied and a mathematical formula was derived to transform covariance matrices computed for real-world test drives into the covariance matrices used by the extended Kalman filter deployed in the simulation model to perform vehicle state estimation. Thus, for the performance assessment a simulation model was devised and implemented, including the ability to import uncertainties associated with a real world sensor fusion behaviour. The uncertainty-related behaviour of the simulation model can be adjusted to fit any sensor fusion system and therefore, predictions can be made about future sensor performance in investigations of collision extractions algorithms. The simulation model was enhanced by simulated V2V communication.

#### 9.1.2.4 Performance assessment

The thesis includes a discussion of new facts discovered through experiments, conducted using the simulation model mentioned above, which assessed the performance of the crash constellation extraction algorithm devised in this research.

With regards to the soundness of the simulation model, it performed in agreement with expectations when considering the level of estimation errors associated with position and velocity estimation. Furthermore, the estimation of position or velocity was observed to be more robust and reliable with V2V communication than without; considerably more so for velocity than position. In addition, the uncertainties in position and velocity estimates were similar for a real vehicle and for the simulation model.

Simulation experiments, for the performance evaluation of the crash constellation extraction algorithm, show that the uncertainty associated with the estimated time-to-collision decreases as vehicle velocity increases or as the actual time-to-collision decreases. The results also show that a decreasing time-to-collision leads to a decreasing uncertainty associated with the estimated position of the tracked vehicle, estimated collision point on the ego vehicle, and estimated relative velocity between the two vehicles about to collide. The results of the performance assessment of the crash constellation extraction algorithm also show that V2V information has a beneficial influence on the precision of the constellation extraction, with regards to the predicted time-to-collision, the predicted position and velocity of the oncoming vehicle against which a collision is possible; the predicted relative velocity between the two vehicles about to collide, and the predicted point of collision on the body of the ego vehicle.

### 9.1.3 Limitations of the findings

The limitations of the findings are widely linked to the simulation model which was used in the primary research in place of a real motor vehicle because of safety and monetary cost considerations that are explained in the body of the thesis. The simulation model facilitates a 2D track model which limits the possibilities of the scenarios being simulated. Furthermore, the pitch and roll components of vehicle rotation are not covered by the simulation model which is also important for future works regarding collision extraction algorithms. The sensor behaviour is limited to the behavioural model reproducing real world sensor fusion behaviour. Current work in progress in the field of research on reproducing real world sensor behaviour through sensor model simulation has been undertaken by Hirsenkorn et al. (2016) who discussed major challenges with regards to devising sensor models which can reproduce the behaviour of real sensor systems. Furthermore, the vehicle motion

model for front-to-side collisions is difficult to derive because it is not easy to accurately model lateral motion due to unstable uncertainty matrices. This lowers the accuracy of the crash constellation extraction algorithm. Nevertheless, the trends can be derived allowing an assessment of the performance of pre-crash collision mitigation algorithms.

## 9.2 Further work

Due to the work undertaken in this thesis further research avenues have arisen. First, the simulation model needs to be enhanced with regards to the ability of virtual sensor integration. The area of simulation models for sensors is attracting an increasing amount of research interest, for instance the work reported by Hirsenkorn et al. (2016). Such work would allow better emulation of real world sensor fusion systems, resulting in more realistic state estimation uncertainties. Furthermore, the motion model for the vehicle should be replaced by a more sophisticated vehicle model. However, it is expected that a more realistic model would slow down the simulation speed and therefore should be used for only analysing specific scenarios. The simulation model with its enhancements need to allow the simulation of detailed collision scenarios using highly sophisticated sensor models tuned to different types of road traffic scenarios.

A second field of research strongly linked to the extraction of the crash constellation is the prediction of its severity outcome. The enhancement of the simulation of the collision prediction algorithm, to include the impulse force that the ego vehicle would receive during the crash phase would allow the prediction of the severity of prospective injury to vehicle occupant(s), as described in Fender, Duddeck, and Zimmermann (2014) and Song, Fender, and Duddeck (2015), for example. This method applied on several collision constellations would allow the estimation of a global severity distribution over these collision constellations. Thus, a crash mitigation system could actively reduce the severity of injuries sustained by the occupants by triggering manoeuvres which would minimise the local severity risk.

Another topic for future research is the investigation into methods for assessing the correctness of simulation models for automotive purposes. Current research collects field data using autonomous driving vehicles and replays these in a simulation model.

This method needs to be assessed with regards to its accuracy for active safety systems.

Due to its modularity, the simulation model can easily be extended through all the aforementioned research strands.

# References


Aaltonen, R. (1979). *Revolution am Steuer: die neue Fahrtechnik*. PC Moderner Verlag.

Aeberhard, M., S. Schlichtharle, N. Kaempchen, and T. Bertram (2012). 'Track-to-Track Fusion With Asynchronous Sensors Using Information Matrix Fusion for Surround Environment Perception'. In: *IEEE Transactions on Intelligent Transportation Systems* 13.4, pp. 1717–1726. ISSN: 1524-9050. DOI: 10.1109/TITS.2012.2202229.

Aeberhard, M. and N. Kaempchen (2011). 'High-level sensor data fusion architecture for vehicle surround environment perception'. In: *8th International Workshop on Intelligent Transportation - WIT*.

Aeberhard, M., T Kühbeck, B Seidl, M Friedl, J Thomas, and O Scheickl (2015). 'Automated Driving with ROS at BMW'. In: *ROSCon 2015 Hamburg, Germany*.

Agamennoni, G., J. I. Nieto, and E. M. Nebot (2011). 'A Bayesian approach for driving behavior inference'. In: *Intelligent Vehicles Symposium (IV), 2011 IEEE*. IEEE, pp. 595–600.

Agamennoni, G., J. I. Nieto, and E. M. Nebot (2012). 'Estimation of multivehicle dynamics by considering contextual information'. In: *IEEE Transactions on Robotics* 28.4, pp. 855–870.

Al-Ghamdi, A. S. (2002). 'Using logistic regression to estimate the influence of accident factors on accident severity'. In: *Accident Analysis & Prevention* 34.6, pp. 729 –741. ISSN: 0001-4575. DOI: 10.1016/S0001-4575(01)00073-2. URL: http://www.sciencedirect.com/science/article/pii/S0001457501000732.

Althoff, D., C. N. Brand, D. Wollherr, and M. Buss (2011). 'Computing unions of Inevitable Collision States and increasing safety to unexpected obstacles'. In: *2011 IEEE/RSJ International Conference on Intelligent Robots and Systems (IROS)*, pp. 3114–3119. DOI: 10.1109/IROS.2011.6094448.

Althoff, M. and A. Mergel (2011). 'Comparison of Markov chain abstraction and Monte Carlo simulation for the safety assessment of autonomous cars'. In: *IEEE Transactions on Intelligent Transportation Systems* 12.4, pp. 1237–1247.

Althoff, M., O. Stursberg, and M. Buss (2009). 'Model-based probabilistic collision detection in autonomous driving'. In: *IEEE Transactions on Intelligent Transportation Systems* 10.2, pp. 299–310.

Ameling, C. (2002). 'Steigerung der aktiven Sicherheit von Kraftfahrzeugen durch ein Kollisionsvermeidungssystem'. In: *FORTSCHRITT BERICHTE-VDI REIHE 12 VERKEHRSTECHNIK FAHRZEUGTECHNIK*.

Ammoun, S. and F. Nashashibi (2009). 'Real time trajectory prediction for collision risk estimation between vehicles'. In: *Intelligent Computer Communication and Processing, 2009. ICCP 2009. IEEE 5th International Conference on*. IEEE, pp. 417–422.

Aoude, G., J. Joseph, N. Roy, and J. How (2011). 'Mobile agent trajectory prediction using Bayesian nonparametric reachability trees'. In: *Proc. of AIAA Infotech@ Aerospace*, pp. 1587–1593.

Aoude, G. S., B. D. Luders, K. K. Lee, D. S. Levine, and J. P. How (2010). 'Threat assessment design for driver assistance system at intersections'. In: *Intelligent Transportation Systems (ITSC), 2010 13th International IEEE Conference on*. IEEE, pp. 1855–1862.

Aoude, G. S., V. R. Desaraju, L. H. Stephens, and J. P. How (2012). 'Driver behavior classification at intersections and validation on large naturalistic data set'. In: *IEEE Transactions on Intelligent Transportation Systems* 13.2, pp. 724–736.

Appel, H., G. Krabbel, and D. Vetter (2013). *Unfallforschung, Unfallmechanik und Unfallrekonstruktion*. Springer-Verlag.

Arulampalam, M., S. Maskell, N. Gordon, and T. Clapp (2002). 'A tutorial on particle filters for online nonlinear/non-Gaussian Bayesian tracking'. In: *IEEE Transactions on Signal Processing* 50.2, pp. 174–188. ISSN: 1053-587X. DOI: 10.1109/78.978374.

Aycard, O., Q. Baig, S. Bota, F. Nashashibi, S. Nedevschi, C. Pantilie, M. Parent, P. Resende, and T.-D. Vu (2011). 'Intersection safety using lidar and stereo vision sensors'. In: *Intelligent Vehicles Symposium (IV)*. IEEE, pp. 863–869.

Backhaus, K., B. Erichson, W. Plinke, and R. Weiber (2006). *Multivariate analysemethoden*. Springer, Berlin.

Bahouth, G. T., K. H. Digges, N. E. Bedewi, A. Kuznetsov, J. S. Augenstein, and E. Perdeck (2004). 'Development of URGENCY 2.1 for the prediction of crash injury severity'. In: *Advanced Emergency Nursing Journal* 26.2, pp. 157–165.

Baker, S. P. and B. O'neill (1976). 'The injury severity score: an update.' In: *Journal of Trauma and Acute Care Surgery* 16.11, pp. 882–885.

Baker, S. P., B. o'Neill, W. Haddon Jr, and W. B. Long (1974). 'The injury severity score: a method for describing patients with multiple injuries and evaluating

emergency care.' In: *Journal of Trauma and Acute Care Surgery* 14.3, pp. 187–196.

Bar-Shalom, Y. (1987). *Tracking and data association*. Academic Press Professional, Inc.

Bar-Shalom, Y. (1990). 'Multitarget-multisensor tracking: advanced applications'. In: *Norwood, MA, Artech House, 1990, 391 p.* 1.

Bar-Shalom, Y. and X.-R. Li (1993). 'Estimation and tracking- Principles, techniques, and software'. In: *Norwood, MA: Artech House, Inc, 1993.*

Barrios, C., Y. Motai, and D. Huston (2016). 'Intelligent forecasting using dead reckoning with dynamic errors'. In: *IEEE Transactions on Industrial Informatics* 12.6, pp. 2217–2227.

Barth, A. and U. Franke (2008). 'Where will the oncoming vehicle be the next second?' In: *Intelligent Vehicles Symposium*. IEEE, pp. 1068–1073.

Batz, T., K. Watson, and J. Beyerer (2009). 'Recognition of dangerous situations within a cooperative group of vehicles'. In: *Intelligent Vehicles Symposium, 2009 IEEE*. IEEE, pp. 907–912.

Bautin, A., L. Martinez-Gomez, and T. Fraichard (2010). 'Inevitable Collision States: A probabilistic perspective'. In: *Robotics and Automation (ICRA), 2010 IEEE International Conference on*, pp. 4022–4027. DOI: 10.1109/ROBOT.2010.5509233.

Behnood, A. and F. Mannering (2017). 'The effect of passengers on driver-injury severities in single-vehicle crashes: A random parameters heterogeneity-in-means approach'. In: *Analytic methods in accident research* 14, pp. 41–53.

Bener, A., T. Lajunen, T. Özkan, E. Yildirim, and K. S. Jadaan (2017). 'The Impact of Aggressive Behaviour, Sleeping, and Fatigue on Road Traffic Crashes as Comparison between Minibus/Van/Pick-up and Commercial Taxi Drivers'. In: *Journal of Traffic and Transportation Engineering* 5, pp. 21–31.

Berndt, H., J. Emmert, and K. Dietmayer (2008). 'Continuous driver intention recognition with hidden markov models'. In: *11th International IEEE Conference on Intelligent Transportation Systems*. IEEE, pp. 1189–1194.

Berthelot, A., A. Tamke, T. Dang, and G. Breuel (2011). 'Handling uncertainties in criticality assessment'. In: *Intelligent Vehicles Symposium (IV)*. IEEE, pp. 571–576.

Bishop, G. W. G. (1995). *An Introduction to the Kalman Filter*. Tech. rep. TR95-041. University of North Carolina at Chapel Hill, Department of Computer Science, Chapel Hill, NC, USA. URL: www.cs.unc.edu/~welch/media/pdf/kalman_intro.pdf.

Blackrnan, S. and A. House (1999). 'Design and analysis of modern tracking systems'. In: *Boston, MA: Artech House*.

Boufous, S., C. Finch, A. Hayen, and A. Williamson (2008). 'The impact of environmental, vehicle and driver characteristics on injury severity in older drivers hospitalized as a result of a traffic crash'. In: *Journal of Safety Research* 39.1, pp. 65–72.

Braess, H.-H. and U. Seiffert (2011). *Vieweg Handbuch Kraftfahrzeugtechnik*. Springer DE.

Braess, H. (1996). 'Aktive und passive Sicherheit im Strassenverkehr-Vorschlag einer ubergreifenden Gesamtbetrachtung'. In: *Zeitschrift fur Verkehrssicherheit* 42.2, pp. 50–51.

Brand, M., N. Oliver, and A. Pentland (1997). 'Coupled hidden Markov models for complex action recognition'. In: *Computer vision and pattern recognition, 1997. proceedings., 1997 ieee computer society conference on*. IEEE, pp. 994–999.

Brannstrom, M., E. Coelingh, and J. Sjoberg (2010). 'Model-based threat assessment for avoiding arbitrary vehicle collisions'. In: *IEEE Transactions on Intelligent Transportation Systems* 11.3, pp. 658–669.

Broadhurst, A., S. Baker, and T. Kanade (2005). 'Monte Carlo road safety reasoning'. In: *Intelligent Vehicles Symposium, 2005. Proceedings.* IEEE, pp. 319–324.

Brown, R. G. (2012). *Introduction to Random Signals and Applied Kalman Filtering with Matlab Exercises, 4th Edition*. 4th ed. Wiley.

Brown, T. L. (2005). 'Adjusted minimum time-to-collision (TTC): A robust approach to evaluating crash scenarios'. In: *Proceedings of the Driving Simulation Conference North America, 40*. Vol. 48.

Burg, H. and F. Zeidler (1980). 'EES-Ein Hilfsmittel zur Unfallrekonstruktion und dessen Auswirkungen auf die Unfallforschung'. In: *Verkehrsunfall* 18.4&5&6.

Busch, D. I. S. (2004). 'Entwicklung einer Bewertungsmethodik zur Prognose des Sicherheitsgewinns ausgewählter Fahrerassistenzsysteme [English: Development of an evaluation methodology to forecast the safety benefits of selected driver assistance systems]'. PhD thesis. Technische Universität München.

Busch, S. (2005). *Entwicklung einer Bewertungsmethodik zur Prognose des Sicherheitsgewinns ausgewählter Fahrerassistenzsysteme*. 588.

Böhmländer, D., V. Yano, T. Brandmeier, A. Zimmer, L. L. Ling, C. B. Wong, and T. Dirndorfer (2014). 'A novel approach for intelligent pre-crash threat assessment systems'. In: *17th International IEEE Conference on Intelligent Transportation Systems (ITSC)*, pp. 954–961. DOI: 10.1109/ITSC.2014.6957812.

Canary, J. D., L. Blizzard, R. P. Barry, D. W. Hosmer, and S. J. Quinn (2017). 'A comparison of the Hosmer–Lemeshow, Pigeon–Heyse, and Tsiatis goodness-of-fit tests for binary logistic regression under two grouping methods'. In: *Communications in Statistics-Simulation and Computation* 46.3, pp. 1871–1894.

CIVIL, I. D. and C. W. SCHWAB (1988). 'The Abbreviated Injury Scale, 1985 revision: a condensed chart for clinical use.' In: *Journal of Trauma and Acute Care Surgery* 28.1, pp. 87–90.

Conroy, C., G. T. Tominaga, S. Erwin, S. Pacyna, T. Velky, F. Kennedy, M. Sise, and R. Coimbra (2008). 'The influence of vehicle damage on injury severity of drivers in head-on motor vehicle crashes'. In: *Accident Analysis & Prevention* 40.4, pp. 1589–1594.

Continental (2016). *ARS 30X Datasheet*. URL: http://www.conti-online.com/www/download/industrial_sensors_de_de/themes/download/ars_300_datenblatt_de.pdf (visited on 07/13/2016).

Coué, C., C. Pradalier, C. Laugier, T. Fraichard, and P. Bessière (2006). 'Bayesian occupancy filtering for multitarget tracking: an automotive application'. In: *The International Journal of Robotics Research* 25.1, pp. 19–30.

Department of Defense (2014). *Global Positioning System Standard - Positioning Service Performance Standard*. URL: http://www.gps.gov/technical/ps/2008-SPS-performance-standard.pdf (visited on 07/19/2014).

DeStatis, ed. (2013). *Statistisches Bundesamt Deutschland: Verkehsunfälle*. URL: https://www.destatis.de/ (visited on 10/31/2013).

Dietmayer, K., A. Kirchner, and N. Kämpchen (2005). 'Fusionsarchitekturen zur Umfeldwahrnehmung für zukünftige Fahrerassistenzsysteme'. In: *Fahrerassistenzsysteme mit maschineller Wahrnehmung*. Springer, pp. 59–88.

Domsch, C. and W. Huber (2008). 'Integrale Sicherheit - ein ganzheitlicher Ansatz für die Fahrzeugsicherheit.' In: *17. Aachener Kolloquium Fahrzeug- und Motorentechnik*.

Donges, E. (1999). 'A conceptual framework for active safety in road traffic'. In: *Vehicle System Dynamics* 32.2-3, pp. 113–128.

Dyckmanns, H., R. Matthaei, M. Maurer, B. Lichte, J. Effertz, and D. Stüker (2011). 'Object tracking in urban intersections based on active use of a priori knowledge: Active interacting multi model filter'. In: *Intelligent Vehicles Symposium (IV), 2011 IEEE*. IEEE, pp. 625–630.

Ebner, A. (2014). 'Referenzszenarien als Grundlage für die Entwicklung und Bewertung von Systemen der Aktiven Sicherheit'. PhD thesis.

Ehmanns, D. and H. Spannheimer (2004). *ADASE technology road map*. [ONLINE]. D2D Roadmap Development. URL: http://www.adase2.net/.

Eichberger, A., D. Wallner, W. Hirschberg, and R. Cresnik (2009). 'A situation based method to adapt the vehicle restraint system in frontal crashes to the accident scenario'. In: *proceedings of the 21ST (ESV) international technical conference on the enhanced safety of vehicles, held June 2009*. Paper No. 09-0091. Stuttgart.

Eidehall, A., T. Schon, and F. Gustafsson (2005). 'The marginalized particle filter for automotive tracking applications'. In: *Intelligent Vehicles Symposium, 2005. Proceedings. IEEE*, pp. 370–375. DOI: 10.1109/IVS.2005.1505131.

Eidehall, A. and L. Petersson (2008). 'Statistical threat assessment for general road scenes using Monte Carlo sampling'. In: *IEEE Transactions on intelligent transportation systems* 9.1, pp. 137–147.

Elvik, R. (2017). 'Road safety effects of roundabouts: a meta-analysis'. In: *Accident Analysis & Prevention* 99, pp. 364–371.

ETSI, T. (2009). *Intelligent transport systems (ITS); vehicular communications; basic set of applications; definitions*. Tech. rep. Tech. Rep. ETSI TR 102 638.

ETSI, T. (2011). 'Intelligent transport systems (its); vehicular communications; basic set of applications; part 2: Specification of cooperative awareness basic service'. In: *Draft ETSI TS* 20.

European Commission (2013). *EU strategy to reduce injuries from road traffic accidents*. URL: http://ec.europa.eu/transport/road_safety/take-part/public-consultations/road_injuries_en.htm (visited on 09/18/2013).

European Commission (2018). *EU road fatalities*. URL: https://ec.europa.eu/transport/road_safety/sites/roadsafety/files/pdf/observatory/trends_figures.pdf (visited on 09/21/2017).

Fagerland, M. W. and D. W. Hosmer (2016). 'Tests for goodness of fit in ordinal logistic regression models'. In: *Journal of Statistical Computation and Simulation* 86.17, pp. 3398–3418.

Fender, J., F. Duddeck, and M. Zimmermann (2014). 'On the calibration of simplified vehicle crash models'. In: *Structural and Multidisciplinary Optimization* 49.3, pp. 455–469.

Floudas, N., A. Polychronopoulos, O. Aycard, J. Burlet, and M. Ahrholdt (2007). 'High level sensor data fusion approaches for object recognition in road environment'. In: *Intelligent Vehicles Symposium, 2007 IEEE*. IEEE, pp. 136–141.

Fraichard, T. and H. Asama (2003). 'Inevitable collision states. A step towards safer robots?' In: *Intelligent Robots and Systems, 2003. (IROS 2003). Proceedings. 2003*

*IEEE/RSJ International Conference on*. Vol. 1, 388–393 vol.1. DOI: 10.1109/IROS.2003.1250659.

Fraichard, T. and H. Asama (2004). 'Inevitable collision states-A step towards safer robots?' In: *Advanced Robotics* 18.10, pp. 1001–1024.

Freymann, R. (2004). 'Möglichkeiten und Grenzen von Fahrerassistenz-und aktiven Sicherheitssystemen [English: Possibilities and limitations of driver assistance and active safety systems]'. In: *Aktive Sicherheit durch Fahrerassistenz, Garching, Germany*. URL: http://www.ftm.mw.tum.de/uploads/media/01_freymann.pdf.

Fricke, N., C. Glaser, and M. De Filippis (2006). 'Passive und Aktive Sicher-heitsmaßnahmen im Kraftfahr-zeug'. In: *MMI-Interaktiv* 10.10, pp. 39–47.

Funkhouser, K. and F. Drews (2016). 'Reaction times when switching from autonomous to manual driving control: A pilot investigation'. In: *Proceedings of the Human Factors and Ergonomics Society Annual Meeting*. Vol. 60. 1. SAGE Publications Sage CA: Los Angeles, CA, pp. 1854–1858.

Gabauer, D. J. and H. C. Gabler (2008). 'Comparison of roadside crash injury metrics using event data recorders'. In: *Accident Analysis & Prevention* 40.2, pp. 548–558.

German Traffic Ministry (2016). *Traffic density*. Tech. rep. German federal ministry for traffic and infrastructure.

GIDAS (2014). *German In-Depth Accident Study*. URL: www.gidas.org (visited on 02/25/2012).

Gindele, T., S. Brechtel, and R. Dillmann (2010). 'A probabilistic model for estimating driver behaviors and vehicle trajectories in traffic environments'. In: *Intelligent Transportation Systems (ITSC), 2010 13th International IEEE Conference on*. IEEE, pp. 1625–1631.

Gordon, N. J., D. J. Salmond, and A. F. Smith (1993). 'Novel approach to nonlinear/non-Gaussian Bayesian state estimation'. In: *IEE Proceedings F (Radar and Signal Processing)*. Vol. 140. 2. IET, pp. 107–113.

Greene, D., J. Liu, J. Reich, Y. Hirokawa, A. Shinagawa, H. Ito, and T. Mikami (2011). 'An efficient computational architecture for a collision early-warning system for vehicles, pedestrians, and bicyclists'. In: *IEEE Transactions on Intelligent Transportation Systems* 12.4, pp. 942–953.

Gstalter, H. (1983). *Der verkehrskonflikt als kenngrosse zur beurteilung von verkehr...*

Gustafsson, F. (1998). 'Monitoring tire-road friction using the wheel slip'. In: *Control Systems, IEEE* 18.4, pp. 42–49. ISSN: 1066-033X. DOI: 10.1109/37.710877.

Haddon Jr, W. (1980). 'Advances in the epidemiology of injuries as a basis for public policy.' In: *Public health reports* 95.5, p. 411.

Harding, J., G. Powell, R. Yoon, J. Fikentscher, C. Doyle, D. Sade, M. Lukuc, J. Simons, and J. Wang (2014). *Vehicle-to-vehicle communications: Readiness of V2V technology for application*. Tech. rep.

He, M., E. Takeuchi, Y. Ninomiya, and S. Kato (2016). 'Precise and efficient model-based vehicle tracking method using Rao-Blackwellized and scaling series particle filters'. In: *Intelligent Robots and Systems (IROS), 2016 IEEE/RSJ International Conference on*. IEEE, pp. 117–124.

Helmer, T. (2013). *Development of a Methodology for the Evaluation of Active Safety using the Example of Preventive Pedestrian Protection*. Berlin.

Helmer, T., T. Kühbeck, C. Gruber, and R. Kates (2013). 'Development of an integrated test bed and virtual laboratory for safety performance prediction in active safety systems'. In: *Proceedings of the FISITA 2012 World Automotive Congress*. Springer, pp. 417–431.

Helmer, T., K. Kompaß, L. Wang, T. Kühbeck, and R. Kates (2017). 'Safety Performance Assessment of Assisted and Automated Driving in Traffic: Simulation as Knowledge Synthesis'. In: *Automated Driving*. Springer, pp. 473–494.

Hermes, C., C. Wohler, K. Schenk, and F. Kummert (2009). 'Long-term vehicle motion prediction'. In: *Intelligent Vehicles Symposium*. IEEE, pp. 652–657.

Herpel, T., C. Lauer, R. German, and J. Salzberger (2008). 'Multi-sensor data fusion in automotive applications'. In: *Sensing Technology, 2008. ICST 2008. 3rd International Conference on*. IEEE, pp. 206–211.

Hillenbrand, J., A. Spieker, and K. Kroschel (2006). 'A Multilevel Collision Mitigation Approach mdash;Its Situation Assessment, Decision Making, and Performance Tradeoffs'. In: *Intelligent Transportation Systems, IEEE Transactions on* 7.4, pp. 528 –540. ISSN: 1524-9050. DOI: 10.1109/TITS.2006.883115.

Hirsenkorn, N., T. Hanke, A. Rauch, B. Dehlink, R. Rasshofer, and E. Biebl (2016). 'Virtual sensor models for real-time applications'. In: *Advances in Radio Science* 14.B. Pp. 31–37.

Holt, V. von (2004). 'Integrale multisensorielle Fahrumgebungserfassung nach dem 4D-Ansatz'. In: *Universität der Bundeswehr München*.

Horst, R. van der and J. Hogema (1993). *Time-to-collision and collision avoidance systems*. na.

Hosmer, D. W. and S. Lemeshow (1980). 'Goodness of fit tests for the multiple logistic regression model'. In: *Communications in statistics-Theory and Methods* 9.10, pp. 1043–1069.

Hu, W., X. Xiao, Z. Fu, D. Xie, T. Tan, and S. Maybank (2006). 'A system for learning statistical motion patterns'. In: *IEEE transactions on pattern analysis and machine intelligence* 28.9, pp. 1450–1464.

Huang, J. and H.-S. Tan (2006). 'Vehicle future trajectory prediction with a DGPS/INS-based positioning system'. In: *American Control Conference, 2006*. IEEE, 6–pp.

Huber, K. N. W. (2007). 'Integration aspects of vehicle-communication based systems for driver assistance and active safety'. In: *$14^{th}$ Wolrd Congress on ITS* Beijing.

Ibeo (2010). *IBEO LUX (model 2010)*. URL: http://abott-mf.com/images/pdf/IbeoLUX2010.pdf (visited on 07/13/2016).

IBM (2012). *IBM SPSS Statistics*. Ed. by IBM.

Imprialou, M. and M. Quddus (2017). 'Crash data quality for road safety research: current state and future directions'. In: *Accident Analysis & Prevention*.

Jansson, J. (2004). 'Dealing with uncertainty in automotive collision avoidance'. In: *Advanced Microsystems for Automotive Applications 2004*. Springer, pp. 165–180.

Johnson, N. S. and H. C. Gabler (2012). 'Accuracy of a damage-based reconstruction method in NHTSA side crash tests'. In: *Traffic injury prevention* 13.1, pp. 72–80.

Joseph, J., F. Doshi-Velez, A. S. Huang, and N. Roy (2011). 'A Bayesian non-parametric approach to modeling motion patterns'. In: *Autonomous Robots* 31.4, p. 383.

Julier, S. and J. Uhlmann (2004). 'Unscented filtering and nonlinear estimation'. In: *Proceedings of the IEEE* 92.3, pp. 401–422. ISSN: 0018-9219. DOI: 10.1109/JPROC.2003.823141.

Kaempchen, N., B. Schiele, and K. Dietmayer (2009). 'Situation Assessment of an Autonomous Emergency Brake for Arbitrary Vehicle-to-Vehicle Collision Scenarios'. In: *Intelligent Transportation Systems, IEEE Transactions on* 10.4, pp. 678–687. ISSN: 1524-9050. DOI: 10.1109/TITS.2009.2026452.

Kaempchen, N. (2007). 'Feature level fusion of laser scanner and video data for advanced driver assistance systems'. PhD thesis. Univ., Fak. fuer Ingenieurwiss. und Informatik.

Kaempchen, N., M. Buehler, and K. Dietmayer (2005). 'Feature-level fusion for free-form object tracking using laserscanner and video'. In: *Intelligent Vehicles Symposium, 2005. Proceedings.* IEEE, pp. 453–458.

Kaempchen, N. and K. Dietmayer (2003). 'Data synchronization strategies for multi-sensor fusion'. In: *Proceedings of the IEEE Conference on Intelligent Transportation Systems*, pp. 1–9.

Kaempchen, N., K. Weiss, M. Schaefer, and K. C. Dietmayer (2004). 'IMM object tracking for high dynamic driving maneuvers'. In: *Intelligent Vehicles Symposium, 2004 IEEE*. IEEE, pp. 825–830.

Käfer, E., C. Hermes, C. Wöhler, H. Ritter, and F. Kummert (2010). 'Recognition of situation classes at road intersections'. In: *Robotics and Automation (ICRA), 2010 IEEE International Conference on*. IEEE, pp. 3960–3965.

Kalman, R. E. et al. (1960). 'A new approach to linear filtering and prediction problems'. In: *Journal of basic Engineering* 82.1, pp. 35–45.

Karrenberg, S. (2008). 'Zur Erkennung unvermeidbarer Kollisionen von Kraftfahrzeugen mit Hilfe von Stellvertretertrajektorien [English: Recognition of unavoidable collisions with motor vehicles by the help of representative trajectories]'. PhD thesis. Technischen Universität Carolo-Wilhelmina zu Braunschweig.

Kato, T., Y. Ninomiya, and I. Masaki (2002). 'An obstacle detection method by fusion of radar and motion stereo'. In: *Intelligent Transportation Systems, IEEE Transactions on* 3.3, pp. 182–188.

Khairnar, V. D. and K. Kotecha (2013). 'Performance of vehicle-to-vehicle communication using IEEE 802.11 p in vehicular ad-hoc network environment'. In: *arXiv preprint arXiv:1304.3357*.

Klanner, F., D. Ehmanns, and H. Winner (2006). 'ConnectedDrive: Vorausschauende Kreuz- ungsassistenz'. In: *15. Aachener Kolloquium Fahreug- und Motorentechnik* Aachen.

Klaus, F. (2006). 'Einführung in Techniken und Methoden der Multisensor-Datenfusion'. In:

Klingelschmitt, S., M. Platho, H.-M. Groß, V. Willert, and J. Eggert (2014). 'Combining behavior and situation information for reliably estimating multiple intentions'. In: *Intelligent Vehicles Symposium Proceedings*. IEEE, pp. 388–393.

Knapp, R. K. and J. J. Vardaman (1991). 'Response to an automated function failure cue: an operational measure of complacency'. In: *Proceedings of the Human Factors and Ergonomics Society Annual Meeting*. Vol. 35. 2. SAGE Publications, pp. 112–115.

Kompass, K, C. Gruber, and C. Domsch (2010). 'Der Beitrag von Fahrerassistenzsystemen zur Aktiven und Passiven Sicherheit – die Integrale Sicherheit als Antwort auf die wachsenden Anforderungen an die Fahrzeugsicherheit. [English: The con-

tribution of driver assistance systems for active and passive safety - the integrated safety as response to the growing demands on vehicle safety.]' In: *4. Tagung Fahrerassistenz*.

Kompass, K and W Huber (2009). 'Integrale Sicherheit-effektive Wertsteigerung in der Fahrzeugsicherheit/Integral safety-effective added value in vehicle safety'. In: *FAHRZEUGSICHERHEIT UND ELEKTRONIK, UMWELT UND ENERGIE. 11. TECHNISCHER KONGRESS DES VDA, 25. UND 26. MAERZ 2009, VOLKSWAGEN WOLFSBURG. TAGUNGSBAND*.

Kompass, K., C. Domsch, and R. E. Kates (2012). 'Integral Safety'. English. In: *Handbook of Intelligent Vehicles*. Ed. by A. Eskandarian. Springer London, pp. 709–727. ISBN: 978-0-85729-084-7. DOI: 10.1007/978-0-85729-085-4_27. URL: http://dx.doi.org/10.1007/978-0-85729-085-4_27.

Kononen, D. W., C. A. Flannagan, and S. C. Wang (2011). 'Identification and validation of a logistic regression model for predicting serious injuries associated with motor vehicle crashes'. In: *Accident Analysis & Prevention* 43.1, pp. 112–122.

Kopischke, S. (1999). 'Verfahren und Steuereinrichtung zur Minimierung von Unfallfolgen [English: Method and control device for minimizing the consequences of accidents]'. DE. Pat. DE 19828693 A1.

Kopischke, S. (2000). *Entwicklung einer Notbremsfunktion mit Rapid Prototyping Methoden [English: Development of an emergency brake with rapid prototyping methods]*. Mainz, G. ISBN: 9783896537829. URL: http://amazon.de/o/ASIN/3896537822/.

Kramer, F. (2008). *Passive Sicherheit von Kraftfahrzeugen: Biomechanik-Simulation-Sicherheit im Entwicklungsprozess [English: Passive safety of vehicles: biomechanics simulation safety in the development process]*. Springer DE.

Kuehbeck, T., G. Hakobyan, A. Sikora, C. Chibelushi, and M. Moniri (2014a). 'Evaluation of Performance Enhancement for Crash Constellation Prediction via Car-to-Car Communication'. In: *Communication Technologies for Vehicles*. Ed. by A. Sikora, M. Berbineau, A. Vinel, M. Jonsson, A. Pirovano, and M. Aguado. Vol. 8435. Lecture Notes in Computer Science. Springer International Publishing, pp. 57–68. ISBN: 978-3-319-06643-1. DOI: 10.1007/978-3-319-06644-8_6. URL: http://dx.doi.org/10.1007/978-3-319-06644-8_6.

Kuehbeck, T., G. Hakobyan, A. Sikora, C. C. Chibelushi, and M. Moniri (2014b). *Untersuchung der Effizienzsteigerung der Crashprädiktion mittels C2C Kommunikation*. Ed. by J. Sieck. Wireless Communication and Information. ISBN: 978-

3-86488-071-1. Verlag Werner Hülsbusch. URL: http://eprints.staffs.ac.uk/2446/.

Kumar, P., M. Perrollaz, S. Lefevre, and C. Laugier (2013). 'Learning-based approach for online lane change intention prediction'. In: *Intelligent Vehicles Symposium (IV), 2013 IEEE*. IEEE, pp. 797–802.

Lages, U. S. (2001). 'Untersuchungen zur aktiven Unfallvermeidung von Kraftfahrzeugen'. In: *FORTSCHRITT BERICHTE-VDI REIHE 12 VERKEHRSTECHNIK FAHRZEUGTECHNIK*.

Laugier, C., I. E. Paromtchik, M. Perrollaz, M. Yong, J.-D. Yoder, C. Tay, K. Mekhnacha, and A. Nègre (2011). 'Probabilistic analysis of dynamic scenes and collision risks assessment to improve driving safety'. In: *IEEE Intelligent Transportation Systems Magazine* 3.4, pp. 4–19.

Lawitzky, A., D. Althoff, C. F. Passenberg, G. Tanzmeister, D. Wollherr, and M. Buss (2013). 'Interactive scene prediction for automotive applications'. In: *Intelligent Vehicles Symposium (IV), 2013 IEEE*. IEEE, pp. 1028–1033.

Lee, C., K. Hedrick, and K. Yi (2004). 'Real-time slip-based estimation of maximum tire-road friction coefficient'. In: *Mechatronics, IEEE/ASME Transactions on* 9.2, pp. 454–458. ISSN: 1083-4435. DOI: 10.1109/TMECH.2004.828622.

Lefèvre, S., C. Laugier, and J. Ibañez-Guzmán (2012). 'Risk assessment at road intersections: Comparing intention and expectation'. In: *Intelligent Vehicles Symposium (IV), 2012 IEEE*. IEEE, pp. 165–171.

Lefèvre, S., D. Vasquez, and C. Laugier (2014). 'A survey on motion prediction and risk assessment for intelligent vehicles'. In: *Robomech Journal* 1.1, p. 1.

Li, X., Z. Sun, D. Cao, Z. He, and Q. Zhu (2016). 'Real-time trajectory planning for autonomous urban driving: Framework, Algorithms, and Verifications'. In: *IEEE/ASME Transactions on Mechatronics* 21.2, pp. 740–753.

Li, X., Z. Sun, D. Cao, D. Liu, and H. He (2017). 'Development of a new integrated local trajectory planning and tracking control framework for autonomous ground vehicles'. In: *Mechanical Systems and Signal Processing* 87, pp. 118–137.

Lin, C.-F., A. G. Ulsoy, and D. J. LeBlanc (2000). 'Vehicle dynamics and external disturbance estimation for vehicle path prediction'. In: *IEEE Transactions on Control Systems Technology* 8.3, pp. 508–518.

Liu, L.-C., C.-Y. Fang, and S.-W. Chen (2017). 'A Novel Distance Estimation Method Leading a Forward Collision Avoidance Assist System for Vehicles on Highways.' In: *IEEE Trans. Intelligent Transportation Systems* 18.4, pp. 937–949.

Lord, D. and F. Mannering (2010). 'The statistical analysis of crash-frequency data: a review and assessment of methodological alternatives'. In: *Transportation Research Part A: Policy and Practice* 44.5, pp. 291–305.

Lozano, R. et al. (2013). 'Global and regional mortality from 235 causes of death for 20 age groups in 1990 and 2010: a systematic analysis for the Global Burden of Disease Study 2010'. In: *The Lancet* 380.9859, pp. 2095 –2128. ISSN: 0140-6736. DOI: 10.1016/S0140-6736(12)61728-0. URL: http://www.sciencedirect.com/science/article/pii/S0140673612617280.

Lytrivis, P., G. Thomaidis, and A. Amditis (2008). 'Cooperative path prediction in vehicular environments'. In: *Intelligent Transportation Systems, 2008. ITSC 2008. 11th International IEEE Conference on*. IEEE, pp. 803–808.

Mages, M., M. Hopstock, and F. Klanner (2012). 'Kreuzungsassistenz [English: Intersection Assistance]'. In: *Handbuch Fahrerassistenzsysteme*. Springer, pp. 572–581.

Mandalia, H. M. and M. D. D. Salvucci (2005). 'Using support vector machines for lane-change detection'. In: *Proceedings of the human factors and ergonomics society annual meeting*. Vol. 49. 22. SAGE Publications Sage CA: Los Angeles, CA, pp. 1965–1969.

Mangel, T., M. Michl, O. Klemp, and H. Hartenstein (2011). 'Real-World Measurements of Non-Line-Of-Sight Reception Quality for 5.9GHz IEEE 802.11p at Intersections'. In: *Communication Technologies for Vehicles*. Ed. by T. Strang, A. Festag, A. Vinel, R. Mehmood, C. Rico Garcia, and M. Roeckl. Vol. 6596. Lecture Notes in Computer Science. Springer Berlin Heidelberg, pp. 189–202. ISBN: 978-3-642-19785-7. DOI: 10.1007/978-3-642-19786-4_17. URL: http://dx.doi.org/10.1007/978-3-642-19786-4_17.

Mannering, F. (2018). 'Temporal instability and the analysis of highway accident data'. In: *Analytic Methods in Accident Research* 17, pp. 1–13.

Mannering, F. L. and C. R. Bhat (2014). 'Analytic methods in accident research: Methodological frontier and future directions'. In: *Analytic methods in accident research* 1, pp. 1–22.

Martinez-Gomez, L. and T. Fraichard (2008). 'An efficient and generic 2D Inevitable Collision State-checker'. In: *Intelligent Robots and Systems, 2008. IROS 2008. IEEE/RSJ International Conference on*, pp. 234–241. DOI: 10.1109/IROS.2008.4650640.

Mehar, A., S. Chandra, and S. Velmurugan (2013). 'Speed and acceleration characteristics of different types of vehicles on multi-lane highways'. In: *European Transport* 55, pp. 1825–3997.

Michalaki, P., M. A. Quddus, D. Pitfield, and A. Huetson (2015). 'Exploring the factors affecting motorway accident severity in England using the generalised ordered logistic regression model'. In: *Journal of safety research* 55, pp. 89–97.

Miller, R. and Q. Huang (2002). 'An adaptive peer-to-peer collision warning system'. In: *Vehicular technology conference, 2002. VTC Spring 2002. IEEE 55th.* Vol. 1. IEEE, pp. 317–321.

Morris, B., A. Doshi, and M. Trivedi (2011). 'Lane change intent prediction for driver assistance: On-road design and evaluation'. In: *Intelligent Vehicles Symposium (IV), 2011 IEEE.* IEEE, pp. 895–901.

Murray-Smith, D. J. (2015). *Testing and Validation of Computer Simulation Models.* Springer.

Mählisch, M., R. Schweiger, W. Ritter, and K. Dietmayer (2006). 'Sensorfusion Using Spatio-Temporal Aligned Video and Lidar for Improved Vehicle Detection'. In: *Intelligent Vehicles Symposium, 2006 IEEE*, pp. 424–429. DOI: 10.1109/IVS.2006.1689665.

Müller, M., P. Nadarajan, M. Botsch, W. Utschick, D. Böhmländer, and S. Katzenbogen (2016). 'A statistical learning approach for estimating the reliability of crash severity predictions'. In: *2016 IEEE 19th International Conference on Intelligent Transportation Systems (ITSC)*, pp. 2199–2206. DOI: 10.1109/ITSC.2016.7795911.

Naab, K. (2004). 'Sensorik- und Signalverarbeitungsarchitekturen für Fahrerassistenz und Aktive Sicherheit [English: Sensors and signal processing architectures for driver assistance and active safety]'. In: *1. Tagung Aktive Sicherheit durch Fahrerassistenzsysteme.*

National Highway Traffic Safety Administration (2012). *Laboratory Test Procedure for New Car Assessment Program Frontal Impact Testing.*

Neubauer, M. (2014). 'Verfahren zur Analyse des Nutzens von Fahrerassistenzsystemen mit Hilfe stochastischer Simulationsmethoden'. In:

Neunzig, D (2004). 'Fahrerassistenz auf dem Weg zur aktiven Unfallvermeidung'. In: *FKA.*

NHTSA (2014). *U.S. Department of Transportation Announces Decision to Move Forward with Vehicle-to-Vehicle Communication Technology for Light Vehicles.* URL: http://www.nhtsa.gov/About+NHTSA/Press+Releases/2014/ci.USDOT+

to+Move+Forward+with+Vehicle-to-Vehicle+Communication+Technology+for+Light+Vehicles.print (visited on 02/24/2018).

Niehsen, W., R. Garnitz, M. Weilkes, and M. Stämpfle (2005). 'Informationsfusion für Fahrerassistenzsysteme'. In: *Fahrerassistenzsysteme mit maschineller Wahrnehmung*. Springer, pp. 43–57.

Niessen, B. (2011). 'Adaptive restraint systems: potential and effects of malfunctioning'. MA thesis.

Nitz, G. (2008). 'Entwicklung eines Systems zur aktiven Bremsung eines Fahrzeugs in Gefahrensituationen [English: Development of a system for active braking of a vehicle in dangerous situations]'. PhD thesis. Lehrstuhl für Messsystem- und Sensortechnik der Technischen Universität München.

OECD (2017). *Road Safety Annual Report 2017*. OECD Publishing.

Oliveira, P., F. Rodrigues, and P. R. Henriques (2005). 'A Formal Definition of Data Quality Problems.' In: *IQ*.

Oliver, N. and A. P. Pentland (2000). 'Graphical models for driver behavior recognition in a smartcar'. In: *Intelligent Vehicles Symposium, 2000. IV 2000. Proceedings of the IEEE*. IEEE, pp. 7–12.

Ortiz, M. G., J. Fritsch, F. Kummert, and A. Gepperth (2011). 'Behavior prediction at multiple time-scales in inner-city scenarios'. In: *Intelligent Vehicles Symposium (IV), 2011 IEEE*. IEEE, pp. 1068–1073.

Otte, D., C. Haasper, and C. Krettek (2006). 'Die neue Abbreviated Injury Scale (AIS) 2005-Nutzen einer standardisierten Klassifikation der Verletzungsschwere'. In: *VERKEHRSUNFALL UND FAHRZEUGTECHNIK* 44.10.

Parthasarathi, R. and T. Fraichard (2007). 'An Inevitable Collision State-Checker for a Car-Like Vehicle'. In: *Robotics and Automation, 2007 IEEE International Conference on*, pp. 3068–3073. DOI: 10.1109/ROBOT.2007.363938.

Pepy, R., A. Lambert, and H. Mounier (2006). 'Reducing navigation errors by planning with realistic vehicle model'. In: *Intelligent Vehicles Symposium, 2006 IEEE*. IEEE, pp. 300–307.

Polychronopoulos, A., M. Tsogas, A. J. Amditis, and L. Andreone (2007). 'Sensor fusion for predicting vehicles' path for collision avoidance systems'. In: *IEEE Transactions on Intelligent Transportation Systems* 8.3, pp. 549–562.

Prat, Á. C. and I. K. Lemmer (2011). 'Sensordatenfusion und Bildverarbeitung zur Objekt-und Gefahrenerkennung'. PhD thesis. Inst. für Verkehrssystemtechnik.

Putzinger, R (2005). 'Auswirkungen von Fahrerassistenzsystemen auf die Automobilproduktion/Impacts of driver assistance systems on the automotive production'. In: *VDI-Berichte* 1907.

Randler, M, U Wilhelm, and B Lucas (2003). 'Anforderungen von Komfort-und Sicherheitsfunktionen an die Umwelthypothese der Umfeldsensorik'. In: *Stiller, C., Maurer, M., Workshop Fahrerassistenzsysteme FAS2003*, pp. 42–44.

Rathgeber, C., F. Winkler, X. Kang, and S. Müller (2015). 'Optimal Trajectories for Highly Automated Driving'. In: *World Academy of Science, Engineering and Technology, International Journal of Mechanical, Aerospace, Industrial, Mechatronic and Manufacturing Engineering* 9.6, pp. 969–975.

Rauch, A., F. Klanner, R. Rasshofer, and K. Dietmayer (2012). 'Car2x-based perception in a high-level fusion architecture for cooperative perception systems'. In: *Intelligent Vehicles Symposium (IV)*. IEEE, pp. 270–275.

Reichardt, L., C. Sturm, F. Grunhaupt, and T. Zwick (2012). 'Demonstrating the use of the IEEE 802.11P Car-to-Car communication standard for automotive radar'. In: *Antennas and Propagation (EUCAP), 2012 6th European Conference on*, pp. 1576–1580. DOI: 10.1109/EuCAP.2012.6206084.

Risch, M. (2002). 'Der Kamm'sche Kreis - Wie start kann man beim Kurvenfahren Bremsen'. In: *Fahrphysik und Verkehr* PdN-Ph. 5/51. Jg.

Ristic, B., S. Arulampalm, and N. J. Gordon (2004). *Beyond the Kalman filter: Particle filters for tracking applications*. Artech House Publishers.

Röckl, M., J. Gacnik, and J. Schomerus (2008). 'Integration of Car-2-Car Communication as a Virtual Sensor in Automotive Sensor Fusion for Advanced Driver Assistance Systems'. In: *FISITA 2008*. Ed. by A. of German Engineers (VDI). Springer Automotive Media. URL: http://elib.dlr.de/55254/.

Ruser, H. and F. Puente León (2007). 'Informationsfusion-Eine Übersicht (Information Fusion-An Overview)'. In: *tm-Technisches Messen* 74.3, pp. 93–102.

Savolainen, P. T., F. L. Mannering, D. Lord, and M. A. Quddus (2011). 'The statistical analysis of highway crash-injury severities: a review and assessment of methodological alternatives'. In: *Accident Analysis & Prevention* 43.5, pp. 1666–1676.

Saxena, A. and M. Zawodniok (2014). 'Indoor positioning system using geo-magnetic field'. In: *Instrumentation and Measurement Technology Conference (I2MTC) Proceedings, 2014 IEEE International*. IEEE, pp. 572–577.

Schlögl, M. and R. Stütz (2017). 'Methodological considerations with data uncertainty in road safety analysis'. In: *Accident Analysis & Prevention*.

Schmidt, C, F Oechsle, and W Branz (2005). 'Untersuchungen zu letztmöglichen ausweichmanövern für stehende und bewegte hindernisse'. In: *FAS-Workshop. Walting*.

Schneider, U. (2006). 'Sensordatenfusion und Fehlerkalibrierung von umfelderkennenden Sensoren eines Straßenfahrzeuges [English: Sensor data fusion and error calibration of sensors recognising the environment of a road vehicle]'. PhD thesis. Ph. D thesis, Technische Universität Braunschweig, Institut für Regelungstechnik.

Segui-Gomez, M. and S. P. Baker (2002). 'Changes in injury patterns in frontal crashes: preliminary comparisons of drivers of vehicles model years 1993-1997 to drivers of vehicles 1998-2001.' In: *Annual proceedings/Association for the Advancement of Automotive Medicine. Association for the Advancement of Automotive Medicine* 46, p. 1.

Shao, X., B. Huang, and J. M. Lee (2010). 'Constrained Bayesian state estimation–A comparative study and a new particle filter based approach'. In: *Journal of Process Control* 20.2, pp. 143–157.

Shi, L. and K. W. Sung (2014). 'Spectrum requirement for vehicle-to-vehicle communication for traffic safety'. In: *2014 IEEE 79th Vehicular Technology Conference (VTC Spring)*. IEEE, pp. 1–5.

Shimomura, N., K. Fujimoto, T. Oki, and H. Muro (2002). 'An algorithm for distinguishing the types of objects on the road using laser radar and vision'. In: *Intelligent Transportation Systems, IEEE Transactions on* 3.3, pp. 189–195.

Sobhani, A., W. Young, D. Logan, and S. Bahrololoom (2011). 'A kinetic energy model of two-vehicle crash injury severity'. In: *Accident Analysis & Prevention* 43.3, pp. 741 –754. ISSN: 0001-4575. DOI: 10.1016/j.aap.2010.10.021. URL: http://www.sciencedirect.com/science/article/pii/S0001457510003143.

Song, L., J. Fender, and F. Duddeck (2015). 'A Semi-analytical Approach to Identify Solution Spaces for Crashworthiness in Vehicle Architectures'. In: *24th International Technical Conference on the Enhanced Safety of Vehicles (ESV)*. 15-0183.

Söntges, S. and M. Althoff (2015). 'Determining the nonexistence of evasive trajectories for collision avoidance systems'. In: *Intelligent Transportation Systems (ITSC), 2015 IEEE 18th International Conference on*. IEEE, pp. 956–961.

Steinberg, A. N., C. L. Bowman, and F. E. White (1999). 'Revisions to the JDL data fusion model'. In: *AeroSense'99*. International Society for Optics and Photonics, pp. 430–441.

Stellet, J. E., F. Straub, J. Schumacher, W. Branz, and J. M. Zöllner (2015). 'Estimating the Process Noise Variance for Vehicle Motion Models'. In: *2015 IEEE*

*18th International Conference on Intelligent Transportation Systems*, pp. 1512–1519. DOI: 10.1109/ITSC.2015.212.

Steux, B., C. Laurgeau, L. Salesse, and D. Wautier (2002). 'Fade: A vehicle detection and tracking system featuring monocular color vision and radar data fusion'. In: *Intelligent Vehicle Symposium, 2002. IEEE*. Vol. 2. IEEE, pp. 632–639.

Stevenson, M, M. Segui-Gomez, I Lescohier, C Di Scala, and G McDonald-Smith (2001). 'An overview of the injury severity score and the new injury severity score'. In: *Injury Prevention* 7.1, pp. 10–13.

Streubel, T. and K. H. Hoffmann (2014). 'Prediction of driver intended path at intersections'. In: *Intelligent Vehicles Symposium Proceedings*. IEEE, pp. 134–139.

Stüker, D. (2004). 'Heterogene Sensordatenfusion zur robusten Objektverfolgung im automobilen Straßenverkehr'. PhD thesis. Universität Oldenburg.

Takahama, T., T. Kimura, E. Iwasaki, and G. Naito (2003). 'Robust vehicle detection for collision avoidance systems by using a lidar sensor and a vision sensor'. In: *Proceedings. JSAE Annual Congress*. 68-03, pp. 11–14.

Takizawa, H., K. Yamada, and T. Ito (2004). 'Vehicles detection using sensor fusion'. In: *Intelligent Vehicles Symposium, 2004 IEEE*. IEEE, pp. 238–243.

Tamke, A., T. Dang, and G. Breuel (2011). 'A flexible method for criticality assessment in driver assistance systems'. In: *Intelligent Vehicles Symposium (IV), 2011 IEEE*. IEEE, pp. 697–702.

Tan, H.-S. and J. Huang (2006). 'DGPS-based vehicle-to-vehicle cooperative collision warning: Engineering feasibility viewpoints'. In: *IEEE Transactions on Intelligent Transportation Systems* 7.4, pp. 415–428.

The Defense Mapping Agency (1987). *supplement to department of defense world geodetic syssys 1984 technical report*. Tech. rep. URL: http://earth-info.nga.mil/GandG/publications/tr8350.2/TR8350.2-b/Introduction.pdf.

Theiler, P., K Schindler, et al. (2012). 'Automatic registration of terrestrial laser scanner point clouds using natural planar surfaces'. In: *ISPRS Annals of Photogrammetry, Remote Sensing and Spatial Information Sciences* 3, pp. 173–178.

Tran, Q. and J. Firl (2014). 'Online maneuver recognition and multimodal trajectory prediction for intersection assistance using non-parametric regression'. In: *Intelligent Vehicles Symposium Proceedings*. IEEE, pp. 918–923.

Umemura, Y. (2004). 'Driver behavior and active safety (overview)'. In: *R&D Review of Toyota CRDL* 39.2.

Vasquez, D. and T. Fraichard (2004). 'Motion prediction for moving objects: a statistical approach'. In: *Robotics and Automation, 2004. Proceedings. ICRA'04. 2004 IEEE International Conference on*. Vol. 4. IEEE, pp. 3931–3936.

Vasquez, D., T. Fraichard, and C. Laugier (2009). 'Growing hidden markov models: An incremental tool for learning and predicting human and vehicle motion'. In: *The International Journal of Robotics Research* 28.11-12, pp. 1486–1506.

Veeraraghavan, H., N. Papanikolopoulos, and P. Schrater (2006). 'Deterministic sampling-based switching Kalman filtering for vehicle tracking'. In: *Intelligent Transportation Systems Conference. ITSC'06*. IEEE, pp. 1340–1345.

Vukotich, A. and A. Kirchner (2001). 'Sensor fusion for driver-assistance-systems'. In: *Elektronik im Kraftfahrzeug,* Baden-Baden, Germany,

Wagner, M, L Hannawald, and H Liers (2015). 'Automated crash computation of passenger car accidents based on the GIDAS database'. In: *Berichte der Bundesanstalt fuer Strassenwesen. Unterreihe Fahrzeugtechnik* 102.

Ward, J., G. Agamennoni, S. Worrall, and E. Nebot (2014). 'Vehicle collision probability calculation for general traffic scenarios under uncertainty'. In: *Intelligent Vehicles Symposium Proceedings*. IEEE, pp. 986–992.

Ward, N., S Fairclough, and M Humphreys (1995). 'The effect of task automatisation in the automotive context: A field study of an Autonomous Intelligent Cruise Control system'. In: *Proceedings of the International Confeence on Experimental analysis and Measurement of Situation Awareness. Daytona Beach, FL. November*, pp. 1–3.

Wiest, J., F. Kunz, U. Kressel, and K. Dietmayer (2013). 'Incorporating categorical information for enhanced probabilistic trajectory prediction'. In: *Machine Learning and Applications (ICMLA), 2013 12th International Conference on*. Vol. 1. IEEE, pp. 402–407.

Winner, H., S. Hakuli, and G. Wolf, eds. (2011). *Handbuch Fahrerassistenzsysteme: Grundlagen, Komponenten und Systeme für aktive Sicherheit und Komfort (ATZ/MTZ-Fachbuch) (German Edition) [English: Manual for Driver Assistance Systems: Principles, components and systems for active safety and comfort]*. 2., korr. Aufl. 2012. Vieweg+Teubner Verlag. ISBN: 9783834814579. URL: http://amazon.com/o/ASIN/3834814571/.

Wisselmann, D, K Gresser, H Spannheimer, K Bengler, and A Huesmann (2004). 'ConnectedDrive-ein methodischer Ansatz für die Entwicklung zukünftiger Fahrerassistenzsysteme'. In: *Aktive Sicherheit durch Fahrerassistenzsysteme*.

Wood, D. P., N. Veyrat, C. Simms, and C. Glynn (2007). 'Limits for survivability in frontal collisions: Theory and real-life data combined'. In: *Accident Analysis & Prevention* 39.4, pp. 679–687.

World Health Organisation (2011). 'Global Plan for the Decade of Action for Road Safety 2011-2020'. In:

World Health Organisation (2013). *Global status report onroad safety 2013. Supporting a decade of action.*

World Health Organization (2017). *Global status report on road safety: time for action. Online-Dokument.* URL: whqlibdoc.who.int/publications/2009/9789241563840_eng.pdf (visited on 02/24/2018).

Xiong, X., L. Chen, and J. Liang (2017). 'A New Framework of Vehicle Collision Prediction by Combining SVM and HMM'. In: *IEEE Transactions on Intelligent Transportation Systems.*

Yan, X., E. Radwan, and M. Abdel-Aty (2005). 'Characteristics of rear-end accidents at signalized intersections using multiple logistic regression model'. In: *Accident Analysis & Prevention* 37.6, pp. 983–995.

# Publications

T. Helmer, T. Kühbeck, C. Gruber, and R. Kates (2013). 'Development of an integrated test bed and virtual laboratory for safety performance prediction in active safety systems'. In: *Proceedings of the FISITA 2012 World Automotive Congress*. Springer, pp. 417–431

T. Kuehbeck, G. Hakobyan, A. Sikora, C. Chibelushi, and M. Moniri (2014a). 'Evaluation of Performance Enhancement for Crash Constellation Prediction via Car-to-Car Communication'. In: *Communication Technologies for Vehicles*. Ed. by A. Sikora, M. Berbineau, A. Vinel, M. Jonsson, A. Pirovano, and M. Aguado. Vol. 8435. Lecture Notes in Computer Science. Springer International Publishing, pp. 57–68. ISBN: 978-3-319-06643-1. DOI: 10.1007/978-3-319-06644-8_6. URL: http://dx.doi.org/10.1007/978-3-319-06644-8_6

T. Kuehbeck, G. Hakobyan, A. Sikora, C. C. Chibelushi, and M. Moniri (2014b). *Untersuchung der Effizienzsteigerung der Crashprädiktion mittels C2C Kommunikation*. Ed. by J. Sieck. Wireless Communication and Information. ISBN: 978-3-86488-071-1. Verlag Werner Hülsbusch. URL: http://eprints.staffs.ac.uk/2446/

M. Aeberhard, T Kühbeck, B Seidl, M Friedl, J Thomas, and O Scheickl (2015). 'Automated Driving with ROS at BMW'. in: *ROSCon 2015 Hamburg, Germany*

T. Helmer, K. Kompaß, L. Wang, T. Kühbeck, and R. Kates (2017). 'Safety Performance Assessment of Assisted and Automated Driving in Traffic: Simulation as Knowledge Synthesis'. In: *Automated Driving*. Springer, pp. 473–494

# A Prototype Vehicle Used in the Primary Research

## A.1 Vehicle communication architecture and sensor integration

Figure A.1 1 depicts the in car communication set-up which provides an ADAS framework, including a state estimation algorithm, for fusing the different sensor technologies attached to the vehicle.

Different electronic control units (ECUs) are connected by automotive bus topologies which route the needed data to the ECUs. For instance, the vehicle velocity information is not only important for tracking algorithms, it is also needed for ego-motion compensation by a single sensor.

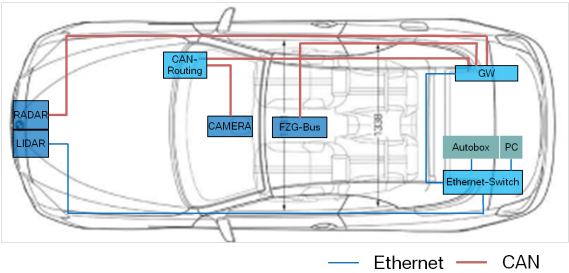


**Figure A.1:** Communication architecture for signal routing

The red lines represent automotive bus systems, such as the controller area network (CAN).

The gateway (GW) allows intelligent routing to and from the sensors (lidar, camera, and radar) and it is connected to the ADAS framework via an Ethernet which is located on the personal computer (PC) in the trunk of the vehicle. The autobox is a rapid prototyping environment which runs embedded Matlab code supporting real-time applications.

## A.2 Integrated data acquisition system

The integrated data acquisition system records data from each test drive onto a four-bay network allocated storage (NAS).

All sensor data, framework communication data, and reference system output are stored in a time synchronised order; this is important for evaluating the sensor fusion system, which is the basis for the evaluation of the whole system. Reference data collected while driving the vehicle under pre-defined scenarios will be compared to data from the simulation model.

The vehicle was driven under real-world near-miss scenarios, during which a record was kept of the sensor and data fusion variances of the outcome of the state estimation process. This record allows the adaptation of the simulation model to mimic the real-world sensor fusion behaviour. The real vehicle data is used for the evaluation of the simulation model in Section 7.1.

# B Theoretical Approximation for the Point of No Return

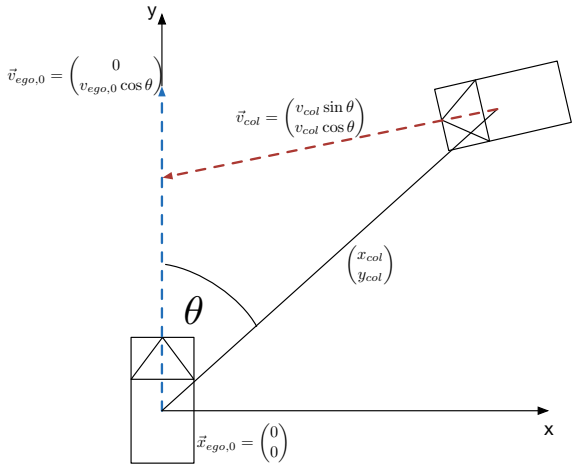


**Figure B.1:** Coordinate system and vectors for modelling the motion of two motor vehicles on a collision course. For the assumed scenario $\theta = 180°$ the collision object is stationary along the y axis.

In the following, the distance travelled and time needed until the ego-vehicle stops is calculated, assuming that brakes have been activated to avoid the collision. The following simplified scenario is considered. The collision-vehicle (i.e. obstacle to be avoided) is assumed to be stationary along the y-axis ($\theta = 180°$) and the ego vehicle is approaching the standing vehicle ($\vec{v}_{col} = \begin{pmatrix} 0 \\ 0 \end{pmatrix}$) at position $\vec{x}_{col,0} = \begin{pmatrix} x_{col} \\ y_{col} \end{pmatrix}$. With reference to Figure B.1, the modelling of more complex scenarios is also possible, using the appropriate coordinate transforms. Assuming that the ego vehicle moves at constant acceleration, the linear projected trajectory of the ego-vehicle is as follows:

$$\vec{x}_{ego} = \vec{x}_{ego,0} + \vec{v}_{ego,0} t + \frac{\vec{a}_{ego,0}}{2} t^2 \tag{B.1}$$

Therefore, the velocity of the ego vehicle is described on the basis of the uniform acceleration with

$$\vec{v}_{ego} = \begin{pmatrix} 0 \\ v_{ego,0} \cos\theta \end{pmatrix} + \begin{pmatrix} 0 \\ a_{ego} t \cos\theta \end{pmatrix} \tag{B.2}$$

leading to the time needed for a complete stand-still, as a result of braking which gives rise to a maximum deceleration of $\vec{a}_{y,min} = -\mu g$ (where $\mu$ is the coefficient of friction and g is the gravitational constant) being described with

$$t = \frac{v_{ego,0}}{\mu g} \tag{B.3}$$

Besides braking, the ego vehicle can swerve to avoid the obstacle. For simplicity, the collision vehicle is circumvented, if the ego vehicle swerves to avoid the width of the collision vehicle. The following formula is applied to the above mentioned scenario with

$$\vec{v}_{ego} = \begin{pmatrix} v_{ego,0} \sin\theta \\ 0 \end{pmatrix} + \begin{pmatrix} a_{ego} t \sin\theta \\ 0 \end{pmatrix} \tag{B.4}$$

Half of the cumulated width of the ego vehicle and collision object represent the needed distance to be reached.Regarding equation B.1 the formula is re-factored determining the time needed for circumventing an obstacle by adding the width of each vehicle with $w_{swerve} = \frac{1}{2}(2m + 2m) = 2m$ and $\mu$ as the friction coefficient to

$$s = \frac{\mu g}{2} t^2 = w_{swerve} \tag{B.5}$$

$$t_{swerve} = \sqrt{\frac{2 w_{swerve}}{yg}} \tag{B.6}$$

Figure B.4 shows the time needed for each manoeuvre under ideal conditions. The "point of no return" therefore resides below $t = 0.6s$ for velocities above 20 km/h. This ideal calculation gives a first impression on which time frame collision detection algorithms need to focus.

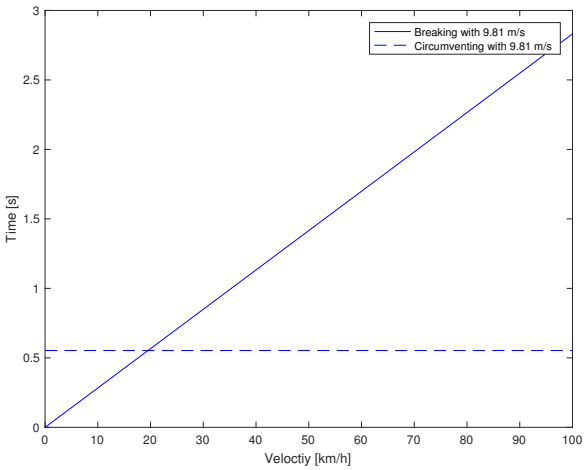


**Figure B.2:** Time needed avoiding a collision by circumventing or breaking

# C Expansion of the Reference Indices Used in Chapter 4

**Table C.1:** Harvard System referencing marks corresponding to the reference numbers shown in the classification diagrams given in Chapter 4

| Reference number | Havard System of Referencing |
|---|---|
| [1] | (Brannstrom, Coelingh, and Sjoberg, 2010) |
| [2] | (Lin, Ulsoy, and LeBlanc, 2000) |
| [3] | (Huang and Tan, 2006) |
| [4] | (Pepy, Lambert, and Mounier, 2006) |
| [5] | (Eidehall and Petersson, 2008) |
| [6] | (Kaempchen, Schiele, and Dietmayer, 2009) |
| [7] | (Miller and Huang, 2002) |
| [8] | (Polychronopoulos et al., 2007) |
| [9] | (Hillenbrand, Spieker, and Kroschel, 2006) |
| [10] | (Kaempchen et al., 2004) |
| [11] | (Ammoun and Nashashibi, 2009) |
| [12] | (Barth and Franke, 2008) |
| [13] | (Tan and Huang, 2006) |
| [14] | (Batz, Watson, and Beyerer, 2009) |
| [15] | (Lytrivis, Thomaidis, and Amditis, 2008) |
| [16] | (Joseph et al., 2011) |
| [17] | (Aoude et al., 2011) |
| [18] | (Tran and Firl, 2014) |
| [19] | (Lefèvre, Laugier, and Ibañez-Guzmán, 2012) |
| [20] | (Broadhurst, Baker, and Kanade, 2005) |
| [21] | (Althoff and Mergel, 2011) |
| [22] | (Greene et al., 2011) |
| [23] | (Aoude et al., 2010) |
| [24] | (Lawitzky et al., 2013) |
| [25] | (Käfer et al., 2010) |
| [26] | (Ward et al., 2014) |
| [27] | (Fraichard and Asama, 2004) |
| [28] | (Berthelot et al., 2011) |

**Table C.2:** Harvard System referencing marks corresponding to the reference numbers shown in the classification diagrams given in Chapter 4 (2)

| Reference number | Havard System of Referencing |
|---|---|
| [29] | (Xiong, Chen, and Liang, 2017) |
| [30] | (Veeraraghavan, Papanikolopoulos, and Schrater, 2006) |
| [31] | (Dyckmanns et al., 2011) |
| [32] | (He et al., 2016) |
| [33] | (Liu, Fang, and Chen, 2017) |
| [34] | (Hu et al., 2006) |
| [35] | (Hermes et al., 2009) |
| [36] | (Wiest et al., 2013) |
| [37] | (Tamke, Dang, and Breuel, 2011) |
| [38] | (Althoff, Stursberg, and Buss, 2009) |
| [39] | (Brand, Oliver, and Pentland, 1997) |
| [40] | (Klingelschmitt et al., 2014) |
| [41] | (Agamennoni, Nieto, and Nebot, 2011) |
| [42] | (Agamennoni, Nieto, and Nebot, 2012) |
| [43] | (Gindele, Brechtel, and Dillmann, 2010) |
| [44] | (Vasquez and Fraichard, 2004) |
| [45] | (Vasquez, Fraichard, and Laugier, 2009) |
| [46] | (Oliver and Pentland, 2000) |
| [47] | (Laugier et al., 2011) |
| [48] | (Ortiz et al., 2011) |
| [49] | (Morris, Doshi, and Trivedi, 2011) |
| [50] | (Kumar et al., 2013) |
| [51] | (Mandalia and Salvucci, 2005) |
| [52] | (Aoude et al., 2012) |
| [53] | (Berndt, Emmert, and Dietmayer, 2008) |
| [54] | (Streubel and Hoffmann, 2014) |
| [55] | (Lefèvre, Vasquez, and Laugier, 2014) |

# D Data Analysis to Identify Crash Constellation Parameters

## D.1 EES distribution for city, urban, and freeway areas

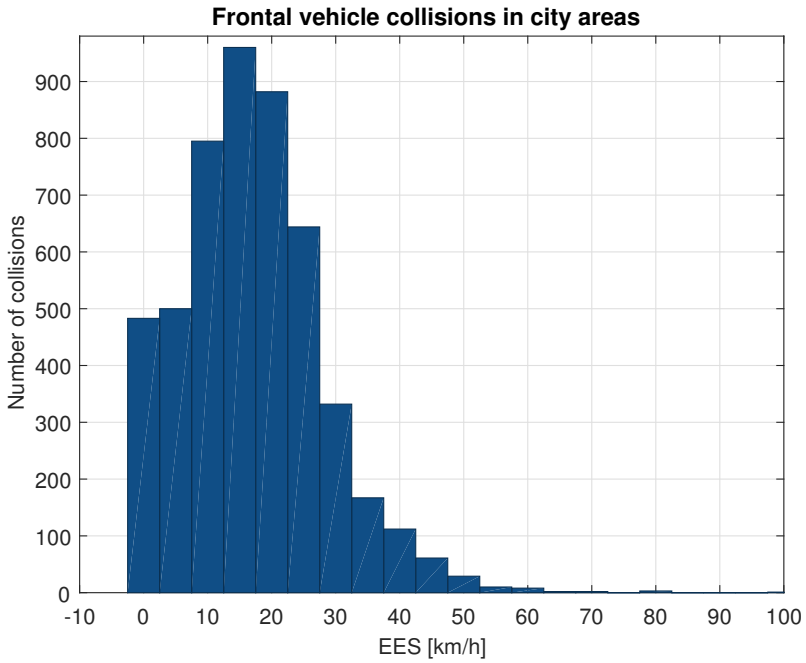


**Figure D.1:** EES distribution for 4043 frontal vehicle collisions in city areas (GIDAS, 2014)

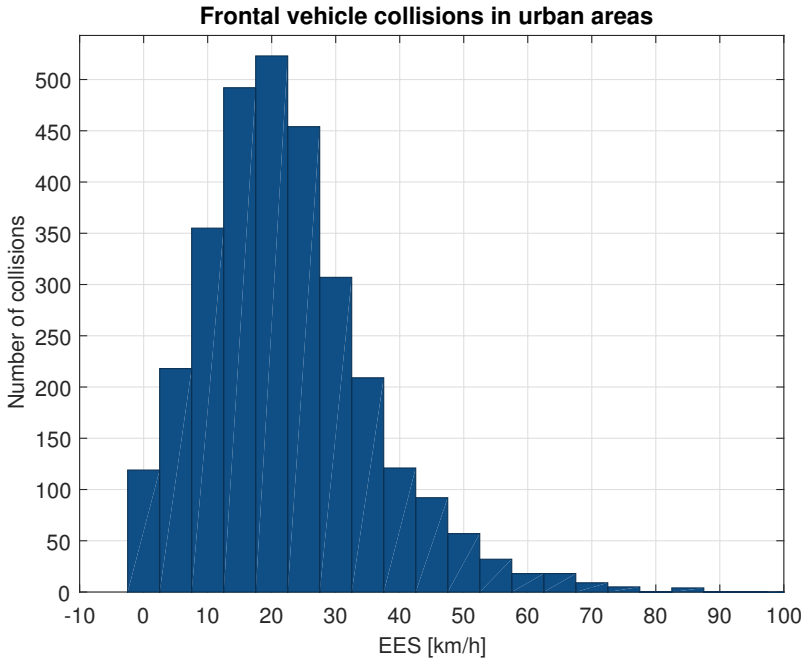


**Figure D.2:** EES distribution for 4176 frontal vehicle collisions in urban areas (GIDAS, 2014)

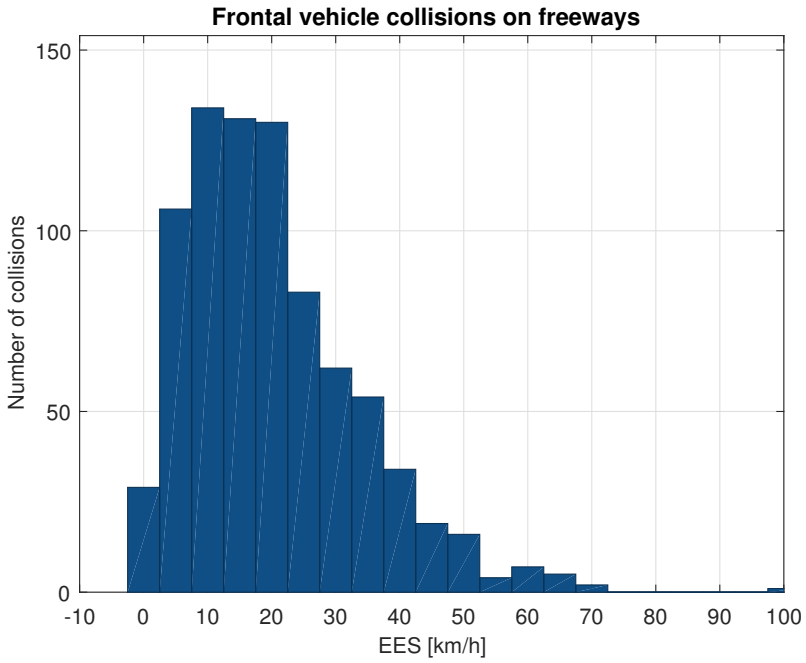


**Figure D.3:** EES distribution for 834 frontal vehicle collisions in freeway areas (GIDAS, 2014)

## D.2 EES distribution for city, urban, and freeway areas with injuries greater than MAIS three

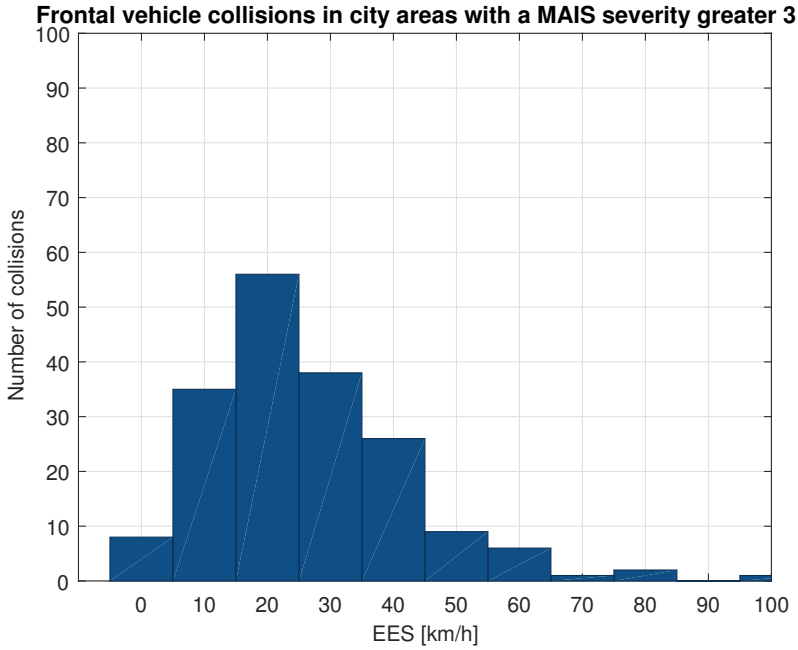


**Figure D.4:** EES distribution for 187 frontal vehicle collisions in city areas with injuries greater than MAIS 3(GIDAS, 2014)

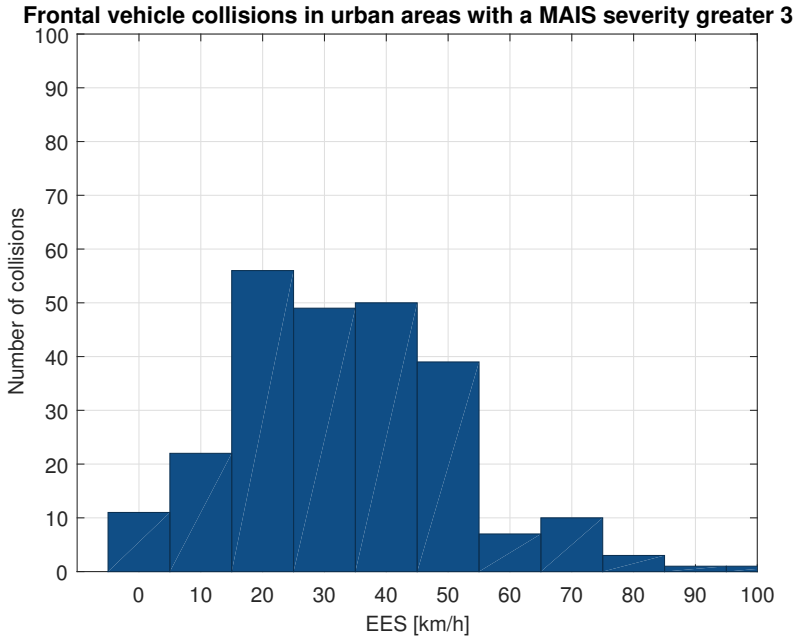


**Figure D.5:** EES distribution for 251 frontal vehicle collisions in urban areas with injuries greater than MAIS 3(GIDAS, 2014)

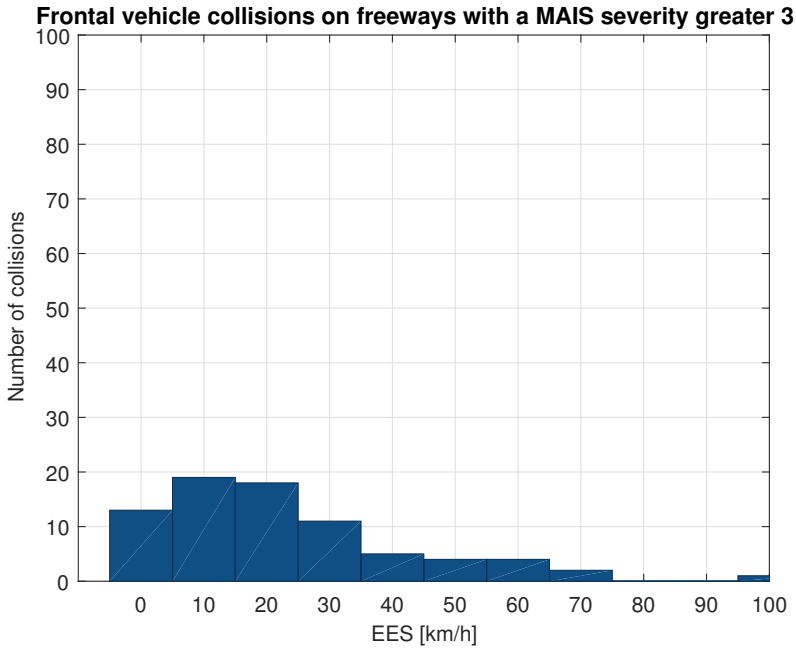


**Figure D.6:** EES distribution for 79 frontal vehicle collisions in freeway areas with injuries greater than MAIS 3(GIDAS, 2014)

## D.3 Explanation of GIDAS parameters and specifications

In the following the different GIDAS parameters are explained

### D.3.1 Grouping of deformation energy according to GIDAS specification (VDI1)

Figure D.7 illustrates the GIDAS coding for the direction of the deformation energy. The parameter in the GIDAS specification is VDI1.

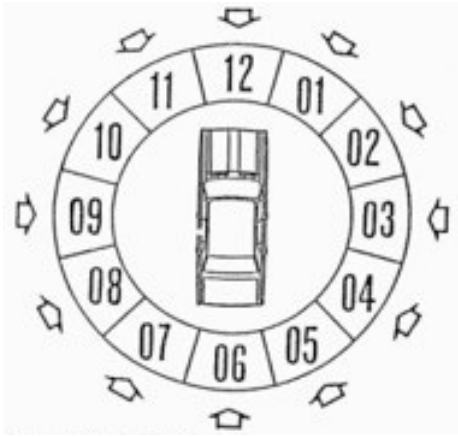


**Figure D.7:** Direction of the deformation energy according to GIDAS

### D.3.2 Grouping of damaged zones along the vertical axis of the vehicle

The following figure shows the specification of the GIDAS VDI4 parameter.


**Figure D.8:** Specification of the GIDAS VDI4 parameter

The complete list of variables is listed in the GIDAS (2014) manuals.

# E Binary Logistic Regression

## E.1 Coding independent and dependent variables using MS Excel

To code the variables into dependent and independent variables MS Excel can be used to generate the input scripts for SPSS. A input command for SPSS recoding a variable into its binary portions is separated as follows using the length of a vehicle as an example:

RECODE LAENGE (1500 thru 1999= 1 ) INTO LANEGE_bl2000. (E.1)

These instructions for the different ranges in which the variables are coded are produced by setting the ranges as shown in Table E.1

**Table E.1:** Setting the core elements of the instruction set

| Variable | Bereich (start) | Bereich (stop) | New Var | Dynamic_Var_part |
|---|---|---|---|---|
| LAENGE | 1500 | 1999 | LANEGE | bl2000 |
| LAENGE | 2000 | 2499 | LANEGE | bl2500 |
| LAENGE | 2500 | 2999 | LANEGE | bl3000 |
| LAENGE | 3000 | 3499 | LANEGE | bl3500 |
| LAENGE | 3500 | 3999 | LANEGE | bl4000 |
| LAENGE | 4000 | 4499 | LANEGE | bl4500 |
| LAENGE | 4500 | 4999 | LANEGE | bl5000 |
| LAENGE | 5000 | 5499 | LANEGE | bl5500 |
| LAENGE | 5500 | 5999 | LANEGE | bl6000 |
| LAENGE | 6000 | 6499 | LANEGE | bl6500 |
| LAENGE | 6500 | 6999 | LANEGE | bl7000 |

With simple concatenation commands the following table is generated automatically containing the instruction set for SPSS coding dummy variables for variable "LAENGE".

**Table E.2:** Auto generated instruction set to code dummy variables for specific ranges in SPSS

| Set of instructions |
|---|
| RECODE LAENGE (1500 thru 1999 = 1 ) INTO LANEGE_bl2000. |
| RECODE LAENGE (2000 thru 2499 = 1 ) INTO LANEGE_bl2500. |
| RECODE LAENGE (2500 thru 2999 = 1 ) INTO LANEGE_bl3000. |
| RECODE LAENGE (3000 thru 3499 = 1 ) INTO LANEGE_bl3500. |
| RECODE LAENGE (3500 thru 3999 = 1 ) INTO LANEGE_bl4000. |
| RECODE LAENGE (4000 thru 4499 = 1 ) INTO LANEGE_bl4500. |
| RECODE LAENGE (4500 thru 4999 = 1 ) INTO LANEGE_bl5000. |
| RECODE LAENGE (5000 thru 5499 = 1 ) INTO LANEGE_bl5500. |
| RECODE LAENGE (5500 thru 5999 = 1 ) INTO LANEGE_bl6000. |
| RECODE LAENGE (6000 thru 6499 = 1 ) INTO LANEGE_bl6500. |
| RECODE LAENGE (6500 thru 6999 = 1 ) INTO LANEGE_bl7000. |

## E.2 List of parameters for the binary logistic regression

The following tables contains the complete list of the parameters used in the binary logistic regression analysis.

**Table E.3:** Full parameter list for the binary logistic regression (part one)

| Parameter | Description |
|---|---|
| strkl | Separated into the different classes of the street. |
| strart | A bit more sophisticated representation of the classes of the street |
| uart | Describes the type of the accident |
| utyp | A more sophisticated view on the type of the accident. |
| AIRBF | Describes the front airbag if activated or not activated. |
| FART | Rough description of the class the vehicle belongs to. We only focus on car to car collisions. |
| FZGKLASS | A more detailed view describing the class of the vehicle under investigation |
| KLASSECE | Categorisation of the vehicle due to the EU norm. |
| ABF | Type of the car including cabrio, coupe, limousine, and more |
| LAENGE | Length of the vehicle |
| BREITE | Width of the vehicle |
| GEWGES | Total weight of the vehicle |
| LENKER | Left or right steered vehicle |
| RHSBEN | The usage of the belts. The analysis is limited to accidents with belts used. |
| GESCHL | The gender of the occupant |
| pverl | Severity of the injury the person suffered. |
| MAIS | The MAIS coded injury of the person in the vehicle. |
| VDI1 | Describing the direction of the collision impulse clockwise arround the vehicle. |
| VDI2 | Describes the direction of the impulse by front, left, right, rear, roof, bottom. |
| VDI3 | Describes the hoizontal zones the vehicle is damaged. A more sophisticated parameter. |
| VDI4 | Describes the vertical zones the vehicle is damaged. A more sophisticated parameter. |
| VDI5 | Gives a rough estimated of the collision opponends size |
| VDI6 | Indicates the degree of deformation regarding the different vehicle architectures |
| DV | Derives the vectorial speed difference between intake and outlet. |
| DECK | Provides the degree of overlap |
| EES | Illustrates the energy a vehicle absorbs in a collision compared to a vehicle crash to a rigid body. The energy equivalent speed is explained in Section 5.2.2.3 and (Burg and Zeidler, 1980) |
| V0 | Represents the inital velocity of each sequence. In this case the primary collisions are in focus and therefore, this parameter represents the initial velocity |
| VK | Provides the speed at the end of each sequence. |
| BV | Provides the average breaking force applied in the collision phase. |

**Table E.4:** Full parameter list for the binary logistic regression (part two)

| Parameter | Description |
|---|---|
| DWINK | Angle of deflection is the difference in degree between the angle at inlet to the angle at outlet. |
| KWINK | Describes the angle at collision time. |
| IMP | Delivers the angle of the momentum at collision time |
| STOSSPX | Provides the point of contact along the vehicle longitudinal axis and is resulted in cm. |
| STOSSPY | Respectively, quantifies the distance to the vehicles longitudinal axis. |
| GROESP | Delivers the height of an occupant |
| GEWP | Provides the weigth of the occupant |
| airbfb_1 | These are the generated dummy variables for the binary logistic regression analysis |
| airbfb_2 | |
| fartb_1 | |
| fartbzgclass_1 | |
| fartbzgclass_2 | |
| fartbzgclass_3 | |
| fartbzgclass_4 | |
| fartbzgclass_5 | |
| fartbzgclass_6 | |
| fartbzgclass_7 | |
| fartbzgclass_8 | |
| fartbzgclass_9 | |
| fartbzgclass_10 | |
| fartbzgclass_11 | |
| fartbzgclass_12 | |
| abfb_1 | |
| abfb_2 | |
| abfb_3 | |
| abfb_4 | |
| abfb_5 | |
| abfb_6 | |
| abfb_7 | |
| abfb_8 | |
| abfb_9 | |
| abfb_10 | |
| abfb_11 | |
| abfb_12 | |
| GEWGES_500_1500 | |
| GEWGES_1500_2500 | |
| GEWGES_2500_3500 | |
| RHSBEN_not_existend | |
| RHSBEN_activated | |
| RHSBEN_not_activated | |

**Table E.5:** Full parameter list for the binary logistic regression (part three)

| Parameter | Description |
|---|---|
| GESCHL_pregnant | These are the generated dummy variables for the binary logistic regression analysis (continued) |
| GESCHL_male | |
| GESCHL_female | |
| PVERL_not_injured | |
| PVERL_minor_injury | |
| PVERL_severe_injury | |
| PVERL_fatal_injury | |
| VDI1_nine | |
| VDI1_ten | |
| VDI1_eleven | |
| VDI1_tewlve | |
| VDI1_one | |
| VDI1_two | |
| VDI1_three | |
| VDI3_0 | |
| VDI3_10 | |
| VDI3_20 | |
| VDI3_21 | |
| VDI3_30 | |
| VDI3_40 | |
| VDI3_41 | |
| VDI3_80 | |
| VDI3_81 | |
| VDI3_90 | |
| VDI3_91 | |
| VDI4_0 | |
| VDI4_1 | |
| VDI4_2 | |
| VDI4_3 | |
| VDI4_4 | |
| VDI4_5 | |
| VDI4_6 | |
| VDI4_7 | |
| VDI4_8 | |
| VDI5_1 | |
| VDI5_2 | |
| VDI5_3 | |
| VDI5_4 | |
| VDI5_6 | |

**Table E.6:** Full parameter list for the binary logistic regression (part four)

| Parameter | Description |
|---|---|
| VDI6_0 | |
| VDI6_1 | |
| VDI6_2 | |
| VDI6_3 | |
| VDI6_4 | |
| VDI6_5 | |
| VDI6_6 | |
| VDI6_7 | |
| VDI6_8 | |
| VDI6_9 | |
| LAENGE_trans | These are the normed values regarding the following formular. This is important not to distort the outcome of the binary regression analysis. |
| BREITE_trans | |
| GEWGES_trans | |
| DV_trans | |
| DECK_trans | |
| EES_trans | |
| BV_trans | |
| V0_trans | |
| VK_trans | |
| DWINK_trans | |
| KWINK_trans | |
| IMP_trans | |
| STOSSPX_trans | |
| STOSSPY_trans | |
| MAIS_1_6 | These are the dependend variables coded into the dummy variables. The underlying research is focused on people injuries above the MAIS score three. Therefore, the dummy variable MAIS_3_6 is used as dependend variable for this binary logistic regression. |
| MAIS_2_6 | |
| MAIS_3_6 | |
| MAIS_4_6 | |
| MAIS_5_6 | |
| MAIS_6_6 | |

## E.3 Hosmer-Lemshow-Test

Table E.7 shows the results of the Hosmer-Lemshow-Test:

**Table E.7:** Hosmer-Lemeshow-Test for the regression analysis

| Parameter | Step | Chi-square | df | Sig. |
|---|---|---|---|---|
| VDI1 | 1 | 3.83 | 2 | 0.147 |
| VDI4 | 1 | 41.5847885 | 1 | 1.1287E-10 |
| VDI5 | 1 | 12.1121183 | 8 | 0.14627111 |
| VDI6 | 1 | 13.628 | 3 | 0.003 |
| DV | 1 | 12.112 | 8 | 0.146 |
| EES | 1 | 366.99242 | 8 | 2.1304E-74 |
| V0 | 1 | 37.006755 | 8 | 1.1476E-05 |
| VK | 1 | 24.9570869 | 8 | 0.0015808 |

# F Full list of the results of the univariate linear binary regression analysis

## F.1 - F.6: Binary logistic regression results for severe accidents with a MAIS score higher than three

**Table F.1:** Binary logistic regression results for severe accidents with a MAIS score higher than three (part 1)

| Variable | Number of cases | Significance (p value) | Odds ratio | 95% Confidence interval | |
|---|---|---|---|---|---|
| | | | | Lower value | Upper value |
| strkl | | not significant | | | |
| uart | | not significant | | | |
| utyp | | not significant | | | |
| BETNR | | not significant | | | |
| AIRBF | | not significant | | | |
| FART | | not significant | | | |
| FZGKLASS | 4323 | not significant | | | |
| KLASSECE | 4323 | not significant | | | |
| ABF | 4302 | not significant | | | |
| LAENGE | 4214 | not significant | | | |
| BREITE | 4223 | not significant | | | |
| GEWGES | 4091 | not significant | | | |
| LENKER | 4323 | not significant | | | |
| PSKZ | | not significant | | | |
| RHSBEN | 4125 | 0.017139224 | 1.933794956 | 1.12438279 | 3.325880623 |
| GESCHL | 4302 | not significant | | | |
| pverl | | not significant | | | |
| MAIS | | not significant | | | |
| VDI1 | 4323 | 0.000988805 | 1.08880026 | 1.035050636 | 1.145341074 |
| VDI2 | 4323 | not significant | | | |
| VDI3 | 4323 | not significant | | | |
| VDI2 | 4323 | not significant | | | |
| VDI3 | 4323 | not significant | | | |
| VDI4 | 4323 | 1.48973E-17 | 0.476916745 | 0.402290267 | 0.565386737 |
| VDI5 | 4323 | 0.025446189 | 1.426288025 | 1.044599846 | 1.947441921 |
| VDI6 | 4322 | 9.66623E-52 | 1.941863572 | 1.781936557 | 2.116143876 |

**Table F.2:** Binary logistic regression results for severe accidents with a MAIS score higher than three (part 2)

| Variable | Number of cases | Significance (p value) | Odds ratio | 95% Confidence interval | |
|---|---|---|---|---|---|
| | | | | Lower value | Upper value |
| DV | 4273 | 9.73738E-60 | 1.078052949 | 1.068354887 | 1.087839045 |
| DECK | 4298 | not significant | | | |
| EES | 4298 | 0.001839775 | 1.001931401 | 1.000715705 | 1.003148575 |
| BV | 3936 | not significant | | | |
| V0 | 3966 | 4.01152E-17 | 1.018657203 | 1.01427957 | 1.02305373 |
| VK | 4245 | 4.78686E-19 | 1.019564192 | 1.01523145 | 1.023915424 |
| DWINK | 4214 | not significant | | | |
| KWINK | 4299 | not significant | | | |
| IMP | 4256 | not significant | | | |
| STOSSPX | 4302 | 1.68889E-23 | 1.018832567 | 1.015109932 | 1.022568854 |
| STOSSPY | 4302 | 0.01851669 | 0.995731879 | 0.992193781 | 0.999282593 |
| GROESP | 3334 | not significant | | | |
| GEWP | 3275 | not significant | | | |
| airbfb_1 | 4323 | 1.84408E-11 | 7.628205128 | 4.216693712 | 13.79979611 |
| airbfb_2 | 4323 | 1.84408E-11 | 0.131092437 | 0.072464839 | 0.237152629 |
| fartb_1 | 4323 | not significant | | | |
| fartbzgclass_1 | 4323 | not significant | | | |
| fartbzgclass_2 | 4323 | not significant | | | |
| fartbzgclass_3 | 4323 | not significant | | | |
| fartbzgclass_4 | 4323 | not significant | | | |
| fartbzgclass_5 | 4323 | not significant | | | |
| fartbzgclass_6 | 4323 | not significant | | | |
| fartbzgclass_7 | 4323 | not significant | | | |
| fartbzgclass_8 | 4323 | not significant | | | |
| fartbzgclass_9 | 4323 | not significant | | | |
| fartbzgclass_10 | 4323 | not significant | | | |

**Table F.3:** Binary logistic regression results for severe accidents with a MAIS score higher than three (part 3)

| Variable | Number of cases | Significance (p value) | Odds ratio | 95% Confidence interval | |
|---|---|---|---|---|---|
| | | | | Lower value | Upper value |
| fartbzgclass_11 | 4323 | not significant | | | |
| fartbzgclass_12 | 4323 | not significant | | | |
| abfb_1 | 4302 | not significant | | | |
| abfb_2 | 4302 | not significant | | | |
| abfb_3 | 4302 | not significant | | | |
| abfb_4 | 4302 | not significant | | | |
| abfb_5 | 4302 | not significant | | | |
| abfb_6 | 4302 | not significant | | | |
| abfb_7 | 4302 | not significant | | | |
| abfb_8 | 4302 | not significant | | | |
| abfb_9 | 4302 | not significant | | | |
| abfb_10 | 4302 | not significant | | | |
| abfb_11 | 4302 | not significant | | | |
| abfb_12 | 4302 | not significant | | | |
| GEWGES_500_1500 | 4323 | not significant | | | |
| GEWGES_1500_2500 | 4323 | not significant | | | |
| GEWGES_2500_3500 | 4323 | not significant | | | |
| RHSBEN_not_existend | 4323 | not significant | | | |
| RHSBEN_activated | 4323 | not significant | | | |
| RHSBEN_not_activated | 4323 | 0.019146042 | 1.929255733 | 1.113326932 | 3.343157861 |
| GESCHL_pregnant | 4323 | not significant | | | |
| GESCHL_male | 4323 | not significant | | | |
| GESCHL_female | 4323 | not significant | | | |
| PVERL_not_injured | 4323 | not significant | | | |
| PVERL_minor_injury | 4323 | 1.2507E-23 | 0.020400339 | 0.009527498 | 0.043681333 |
| PVERL_severe_injury | 4323 | 1.02316E-52 | 20.53223979 | 13.93482652 | 30.25318399 |

**Table F.4:** Binary logistic regression results for severe accidents with a MAIS score higher than three (part 4)

| Variable | Number of cases | Significance (p value) | Odds ratio | 95% Confidence interval | |
|---|---|---|---|---|---|
| | | | | Lower value | Upper value |
| PVERL_fatal_injury | 4323 | 2.9172E-26 | 188.1419339 | 71.45075555 | 495.4095589 |
| VDI1_nine | 4323 | not significant | | | |
| VDI1_ten | 4323 | not significant | | | |
| VDI1_eleven | 4323 | not significant | | | |
| VDI1_tewlve | 4323 | 0.000142784 | 1.955160383 | 1.383969414 | 2.762092922 |
| VDI1_one | 4323 | 0.0036557 | 0.438965702 | 0.251943225 | 0.764818693 |
| VDI1_two | 4323 | not significant | | | |
| VDI1_three | 4323 | not significant | | | |
| VDI3_0 | 4323 | not significant | | | |
| VDI3_10 | 4323 | not significant | | | |
| VDI3_20 | 4323 | not significant | | | |
| VDI3_21 | 4323 | not significant | | | |
| VDI3_30 | 4323 | 0.000128102 | 3.212352149 | 1.767937357 | 5.836861972 |
| VDI3_40 | 4323 | 0.055823392 | 0.145988072 | 0.020316808 | 1.049009118 |
| VDI3_41 | 4323 | not significant | | | |
| VDI3_80 | 4323 | 0.02694628 | 1.688299593 | 1.06155514 | 2.685075328 |
| VDI3_81 | 4323 | not significant | | | |
| VDI3_90 | 4323 | not significant | | | |
| VDI3_91 | 4323 | not significant | | | |
| VDI4_0 | 4323 | not significant | | | |
| VDI4_1 | 4323 | 2.92093E-26 | 6.621439072 | 4.668562213 | 9.39121155 |
| VDI4_2 | 4323 | 0.014387659 | 2.914265468 | 1.237437765 | 6.863329581 |
| VDI4_3 | 4323 | 1.39488E-16 | 0.251285935 | 0.181103555 | 0.34866583 |
| VDI4_4 | 4323 | not significant | | | |
| VDI4_5 | 4323 | not significant | | | |
| VDI4_6 | 4323 | not significant | | | |

**Table F.5:** Binary logistic regression results for severe accidents with a MAIS score higher than three (part 5)

| Variable | Number of cases | Significance (p value) | Odds ratio | 95% Confidence interval | |
|---|---|---|---|---|---|
| | | | | Lower value | Upper value |
| VDI4_4 | 4323 | not significant | | | |
| VDI4_5 | 4323 | not significant | | | |
| VDI4_6 | 4323 | not significant | | | |
| VDI4_7 | 4323 | not significant | | | |
| VDI4_8 | 4323 | not significant | | | |
| VDI5_1 | 4323 | not significant | | | |
| VDI5_2 | 4323 | not significant | | | |
| VDI5_3 | 4323 | not significant | | | |
| VDI5_4 | 4323 | not significant | | | |
| VDI5_6 | 4323 | 0.032482574 | 13.80463576 | 1.244910873 | 153.0775998 |
| VDI6_0 | | not significant | | | |
| VDI6_1 | | not significant | | | |
| VDI6_2 | | not significant | | | |
| VDI6_3 | | not significant | | | |
| VDI6_4 | | not significant | | | |
| VDI6_5 | | not significant | | | |
| VDI6_6 | | not significant | | | |
| VDI6_7 | | not significant | | | |
| VDI6_8 | | not significant | | | |
| VDI6_9 | | not significant | | | |
| LAENGE_trans | 4214 | not significant | | | |
| BREITE_trans | 4223 | not significant | | | |
| GEWGES_trans | 4091 | not significant | | | |
| DV_trans | 4273 | 9.73738E-60 | 3.211235424 | 2.790945418 | 3.694817134 |
| DECK_trans | 4298 | not significant | | | |
| EES_trans | 4298 | 0.001839775 | 1.131930541 | 1.047021748 | 1.223725059 |

**Table F.6:** Binary logistic regression results for severe accidents with a MAIS score higher than three (part 6)

| **Variable** | **Number of cases** | **Significance (p value)** | **Odds ratio** | **95% Confidence interval** | |
|---|---|---|---|---|---|
| | | | | **Lower value** | **Upper value** |
| BV_trans | 3936 | not significant | | | |
| V0_trans | 3966 | 4.01152E-17 | 1.787217625 | 1.561079347 | 2.046114341 |
| VK_trans | 4245 | 4.78686E-19 | 1.731853304 | 1.534923422 | 1.954049187 |
| DWINK_trans | 4214 | not significant | | | |
| KWINK_trans | 4299 | not significant | | | |
| IMP_trans | 4256 | not significant | | | |
| STOSSPX_trans | 4302 | 1.68889E-23 | 1.695894791 | 1.528944525 | 1.881074882 |
| STOSSPY_trans | 4302 | 0.01851669 | 0.819690674 | 0.694685647 | 0.967189698 |
| MAIS_1_6 | | not significant | | | |
| MAIS_2_6 | | not significant | | | |
| MAIS_3_6 | | not significant | | | |
| MAIS_4_6 | | not significant | | | |
| MAIS_5_6 | | not significant | | | |
| MAIS_6_6 | | not significant | | | |

# G Vehicle State Estimation Using a Kalman Filter or its Extended Version

## G.1 Kalman filter

Building upon the system model given in 7.4.1, a linear Kalman filter explained in 4.2.1 features a recursive linear filtering process. This section explains the functionality of a Kalman filter (the filter is explained in more detail in (Brown, 2012).

Generally, the Kalman filter as a recursive filtering technique operates in two steps, the prediction of the state vector $\hat{\boldsymbol{x}}$ followed by the update correcting the innovation with the measurement. The innovation is subsequently weighted by the Kalman gain $\mathbf{K}$ as briefly described in Section 4.2.1.

**Prediction**

Assuming that the system is linear, the dynamic model allows the prediction of the state as mentioned in Equation 7.15.

As the Kalman filter assumes a linear system, the prediction is performed based on the dynamic model, presented in Equation 7.15. Furthermore, Equation 7.15 is modified with $(i_{k-1}|i_{k-1})$ indicating the last estimation and $(i_k|i_{k-1})$ representing the prediction with reference to the last estimation. The resulting equation G.1 shows, that the observations are considered until the time instance $i_k$ is reached.

$$\boldsymbol{x}(i_k|i_{k-1}) = \boldsymbol{F}(i_k)\boldsymbol{x}(i_{k-1}|i_{k-1}) + \boldsymbol{B}(i_k)\boldsymbol{u}(i_k) + \boldsymbol{w}(i_k) \tag{G.1}$$

Based on the estimation error (Equation 7.12), the prediction uncertainty is derived

as follows

$$\begin{aligned} \boldsymbol{e}(i_k|i_{k-1}) &= \tilde{\boldsymbol{x}}(i_k) - \hat{\boldsymbol{x}}(i_k|i_{k-1}) \\ &= \boldsymbol{F}(i_k)\tilde{\boldsymbol{x}}(i_{k-1}) + \boldsymbol{w}(i_k) - \boldsymbol{F}(i_k)\hat{\boldsymbol{x}}(i_k|i_{k-1}) \\ &= \boldsymbol{F}(i_k)\boldsymbol{e}(i_{k-1}) + \boldsymbol{w}(i_k) \end{aligned} \tag{G.2}$$

resulting in the following covariance matrix based on Equation 7.13:

$$\begin{aligned} \boldsymbol{P}(i_k|i_{k-1}) &= E[\boldsymbol{e}(i_k|i_{k-1})\boldsymbol{e}^T(i_k|i_{k-1})] \\ &= \boldsymbol{F}(i_k)\boldsymbol{P}(i_{k-1}|i_{k-1})\boldsymbol{F}^T(i_k) + \boldsymbol{Q}(i_k) \end{aligned} \tag{G.3}$$

### Update

Based on a linear system for the observation and measurement space, the state vector (in line with the calculated covariance matrix) is mapped to the measurement state by:

$$\hat{\boldsymbol{z}}(i_k|i_{k-1}) = \boldsymbol{H}(i_k)\hat{\boldsymbol{x}}(i_k|i_{k-1}) \tag{G.4}$$

$$\boldsymbol{P}_{\hat{\boldsymbol{z}}}(i_k|i_{k-1}) = \boldsymbol{H}(i_k)\boldsymbol{P}(i_k|i_{k-1})\boldsymbol{H}(i_k)^T \tag{G.5}$$

The covariance matrix and the state vector are processed during the update cycle. These components represent the offset between the measurement $z(i_k)$ and its prediction $\hat{\boldsymbol{z}}(i_k|i_{k-1})$. The offset is also named as prediction uncertainty $\tilde{\boldsymbol{y}}(i_k)$ and is calculated in the measurement space, as Equation G.6 shows.

$$\tilde{\boldsymbol{y}}(i_k) = \boldsymbol{z}(i_k) - \hat{\boldsymbol{z}}(i_k|i_{k-1}) = \boldsymbol{z}(i_k) - \boldsymbol{H}(i_k)\hat{\boldsymbol{x}}(i_k|i_{k-1}) \tag{G.6}$$

Summing up the covariances of the predicted $\hat{z}$ and actual measurement vector $z$ at time $i_k$ leads to the innovation covariance matrix $\boldsymbol{S}$.

$$\boldsymbol{S}(i_k) = \boldsymbol{P}_{\hat{\boldsymbol{z}}}(i_k) + \boldsymbol{P}_{\boldsymbol{z}(\boldsymbol{i_k})} = \boldsymbol{H}(i_k)\boldsymbol{P}(i_k|i_{k-1})\boldsymbol{H}^T(i_k) + \boldsymbol{R}(i_k) \tag{G.7}$$

In the next step, the prediction of the state vector is updated by new measurements weighted with the Kalman gain:

$$\begin{aligned}\hat{\boldsymbol{x}}(i_k|i_k) =& \hat{\boldsymbol{x}}(i_k|i_{k-1}) + \boldsymbol{K}(i_k)\tilde{\boldsymbol{y}}(i_k) \\ =& \hat{\boldsymbol{x}}(i_k|i_{k-1}) + \boldsymbol{K}(i_k)[\boldsymbol{z}(i_k) - \boldsymbol{H}(i_k)\hat{\boldsymbol{x}}(i_k|i_{k-1})]\end{aligned} \tag{G.8}$$

The Kalman gain is ideally picked to minimize the mean square error, supporting an optimal estimation of the system and is illustrated in the following equation. Brown (2012) provides the detailed derivation of this equation.

$$\boldsymbol{K}(i_k) = \boldsymbol{P}(i_k|i_{k-1})\boldsymbol{H}^T(i_k)\boldsymbol{S}^{-1}(i_k) \tag{G.9}$$

The covariance matrix is re-factored, using Equation G.3, for predicting the covariances.

$$\boldsymbol{P}(i_k|i_k) = [\boldsymbol{I} - \boldsymbol{K}(i_k)\boldsymbol{H}(i_k)]\boldsymbol{P}(i_k|i_{k-1}) \tag{G.10}$$

In summary, the Kalman filtering technique performs the following steps recursively at every measurement update:

1. Predicting the state (Equation 7.15)
2. Predicting the error covariance matrix (Equation G.3)
3. Calculating the Kalman gain(Equation G.9)
4. Updating the predicted state(Equation G.8)
5. Updating the predicted uncertainty covariance matrix(Equation G.10)

At every measurement update, the observation space is filled with new measurements using Equations G.4 and G.5.

Furthermore, the measurement is used to initialise the system, as the Kalman filter recursively computes a measurement update of the last received measurement, beginning with $\boldsymbol{x}(t_0)$ and $\boldsymbol{P}(t_0)$.

A more detailed description provided by Bishop, 1995 is shown below

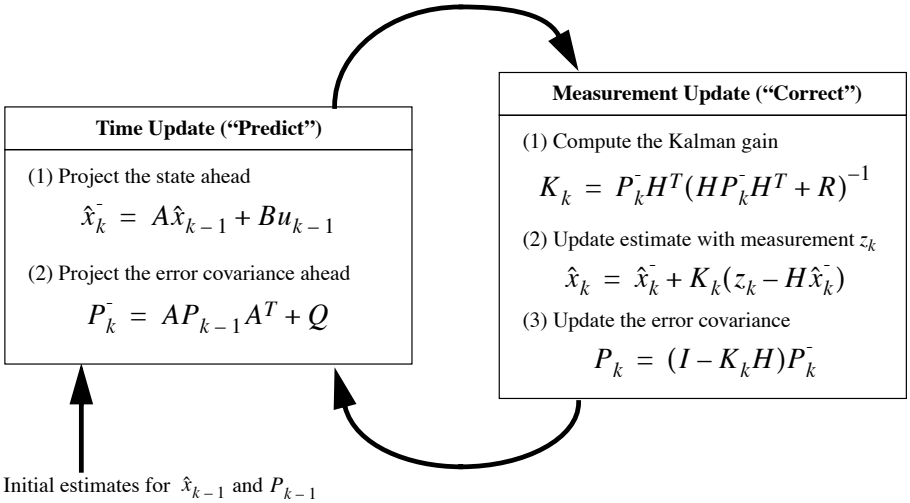


**Figure G.1:** The steps of the Kalman filter (Bishop, 1995)

## G.2 Extended Kalman filter

Section 4.2.1 highlighted the limited capabilities the Kalman filter with regards to estimating the state in highly non-linear environments. The Kalman filter uses linear process and measurement models, providing information about uncertainties in form of a Gaussian probability distribution.

In a highly non-linear environment, such as those found in the automotive area, the extended Kalman filtering technique needs to be applied (Bar-Shalom and Li, 1993; Kalman, 1960), it linearises the non-linear models during the current state estimation process. Equation G.13, given later, helps to describe this extension of the common Kalman filtering technique. The further assumptions being made in Section 4.2.1 are still relevant to the extended Kalman filter, especially with regards to the measurement and process noise[1].

The linearisation is realised by replacing the process and measurement model, in Equations 7.15 and G.4, with the state transition function $\boldsymbol{f}$ and the measurement function $\boldsymbol{h}$ for non-linearity during the filtering process.

1 The measurement and process noise is assumed to be uncorrelated, zero-mean, additive and white.

$$\boldsymbol{x}_{i_k} = \boldsymbol{f}(\boldsymbol{x}_{i_{k-1}}) + \boldsymbol{w}_{i_k}, \quad \boldsymbol{w}_{i_k} \sim \mathcal{N}(0, \boldsymbol{Q}_{\boldsymbol{i_k}}) \tag{G.11}$$

$$\boldsymbol{z}_{i_k} = \boldsymbol{h}(\boldsymbol{x}_{i_k}) + \boldsymbol{v}_{i_k}, \quad \boldsymbol{v}_{i_k} \sim \mathcal{N}(0, \boldsymbol{Q}_{\boldsymbol{i_k}}) \tag{G.12}$$

For the calculation of the uncertainty covariances (represented by Equations G.3, equation G.9, and G.10), the matrices $\boldsymbol{F}_{\boldsymbol{i_k}}$ and $\boldsymbol{H}_{\boldsymbol{i_k}}$ are substituted by the Jacobians of the transfer functions for the state $\boldsymbol{f}$ and the measurement function $\boldsymbol{h}$.

$$\boldsymbol{F}_{i_k} = J^{\boldsymbol{F}}_{i_k} = \frac{\partial}{\partial \boldsymbol{x}} \boldsymbol{f}(\boldsymbol{x}) \Big|_{\boldsymbol{x}=\hat{\boldsymbol{x}}_{i_{k-1}|i_{k-1}}} \qquad \boldsymbol{H}_{i_k} = J^{\boldsymbol{H}}_{i_k} = \frac{\partial}{\partial x} \boldsymbol{h}(\boldsymbol{x}) \Big|_{\boldsymbol{x}=\hat{\boldsymbol{x}}_{i_{k-1}|i_{k-1}}} \tag{G.13}$$

which equates to the first-order Taylor series for the functions $\boldsymbol{f}$ and $\boldsymbol{h}$ at the current state estimation. This truncation of the Taylor series approximation harms the accuracy of the prediction and measurement step. This allows a fast, sub-optimal filtering compared to a Bayesian filtering technique. Mählisch et al. (2006) presented an EKF filtering technique featuring a second order Taylor series approximation.